

**ALMA MATER STUDIORUM - UNIVERSITÀ DI BOLOGNA**

---

**FACOLTA' DI INGEGNERIA**

**CORSO DI LAUREA IN CIVIL ENGINEERING**

*DICAM– Dipartimento di Ingegneria Civile, Ambientale e dei Materiali*

**TESI DI LAUREA**

in  
Advanced Design of Structures

**FATIGUE LIFE ASSESSMENT OF A RAILWAY BRIDGE  
USING A DYNAMIC INTERACTION MODEL**

**CANDIDATO:**

Rossi Fabrizio

**RELATORE:**

Prof. Ing. Marco Savoia

**CORRELATORE:**

Prof. Ing. Loris Vincenzi

Anno Accademico 2010/11

Sessione III



# Index

<b>INTRODUCTION .....</b>	<b>1</b>
<b>1. BASIC OF DYNAMIC .....</b>	<b>5</b>
1.1 GENERAL REMARKS .....	5
1.2 SINGLE DEGREE OF FREEDOM SYSTEM .....	6
1.3 MULTI-DEGREE OF FREEDOM SYSTEM.....	9
1.4 DAMPING IN STRUCTURES.....	12
<b>2. METHODS FOR SOLVING THE EQUATIONS OF MOTION .....</b>	<b>15</b>
2.1 GENERAL OVERVIEW .....	15
2.2 CLASSICAL MODAL ANALYSIS.....	16
2.3 NUMERICAL TIME-STEPPING METHODS .....	18
<b>3. MOVING LOADS MODEL .....</b>	<b>21</b>
3.1 INTRODUCTION .....	21
3.2 SIMPLY-SUPPORTED BEAM SUBJECTED TO MOVING LOADS .....	22
3.3 ASSUMPTION AND LIMITATION OF THE MODEL .....	24
<b>4. VEHICLE-BRIDGE INTERACTION MODELS .....</b>	<b>25</b>
4.1 INTRODUCTION .....	25
4.2 TRAIN SUBSYSTEM.....	26
4.3 BRIDGE SUBSYSTEM.....	31
4.4 COMPUTATION OF THE COUPLED TRAIN-BRIDGE SYSTEM.....	34
<b>5. PONTELAGOSCURO RAILWAY BRIDGE.....</b>	<b>37</b>
5.1 DESCRIPTION OF THE BRIDGE.....	37
5.2 EXPERIMENTAL DATA .....	44
5.3 BRIDGE FINITE ELEMENTS MODEL.....	47
<b>6. OPTIMIZATION PROCESS .....</b>	<b>51</b>
6.1 INTRODUCTION .....	51
6.2 DIFFERENTIAL EVOLUTION ALGORITHM .....	52
6.3 THE RESPONSE SURFACE METHOD.....	57
6.4 DE ALGORITHM WITH A SECOND-ORDER APPROXIMATION .....	59
6.5 OPTIMIZATION ALGORITHM APPLICATION.....	62
6.6 OBTAINED RESULTS .....	64

<b>7.</b>	<b>2D MOVING LOADS VS. VBI MODELS APPLICATION.....</b>	<b>69</b>
	7.1 INTRODUCTION.....	69
	7.2 BRIDGE MODEL SETTING.....	70
	7.3 TRAIN DATA .....	73
	7.4 COMPARISON BETWEEN MOVING LOADS MODEL AND VBI MODEL .....	79
	7.5 PARAMETERS INVESTIGATION .....	101
<b>8.</b>	<b>3D VBI MODEL APPLICATION .....</b>	<b>105</b>
	8.1 INTRODUCTION.....	105
	8.2 THREE-DIMENSIONAL DYNAMIC ANALYSES.....	106
<b>9.</b>	<b>FATIGUE ASSESSMENT.....</b>	<b>125</b>
	9.1 GENERAL.....	125
	9.2 RAINFLOW CYCLE COUNTING .....	129
	9.3 PALMGREN-MINER RULE.....	131
	9.4 FATIGUE VERIFICATION .....	134
<b>10.</b>	<b>CONCLUSION AND FUTURE DEVELOPMENT .....</b>	<b>157</b>
	<b>APPENDIX .....</b>	<b>161</b>
	<b>REFERENCES.....</b>	<b>171</b>

# *INTRODUCTION*

With the end of the second world war, there was the need of rebuilding the decaying infrastructures of the country, as the railway lines and the bridges. In this historical period the most used material that allowed to build long span bridges was the steel, since prestressed concrete was just born in those years. Along with steel, the riveted systems, was the technique used to connect among each other the elements of the metallic structures. Nowadays this technique has been overcome by welding and high strength bolts systems that offer benefits in terms of costs and realization velocity.

However the study of the riveted connections is still a current issue, especially for those engineers that deal with maintenance and retrofitting of existent structures. In fact many of the bridges built at that time are nowadays still used, although traffic volumes, loads and speed are changed during these years. Therefore the service loads, the accumulated stress cycles due to traffic and aging, have been induced to the evaluation of the remaining fatigue life of these structures and to operations of maintenance and replacement.

The “discovery” of fatigue occurred in the 1800s when several researchers in Europe observed that bridge and railroad components were cracking when subjected to repeated loading. As the century progressed and the use of metals expanded with the increasing use of machines, more and more failures of components subjected to repeated loads were recorded. By the mid 1800s A. Wohler proposed a method by which the failure of elements from repeated loads could be mitigated, and in some cases eliminated. This method resulted in the stress-life response diagram and element test model approach to fatigue design and verification.

The aim of this research is to assess the fatigue life of an existent metallic railway bridge. In particular the investigated structure is a bridge on the railway line Bologna-Padova that crossing the Po river between Pontelagoscuro and Occhiobello. It was built in the years from 1946 to 1949, and it is a truss system, where the elements are connected by means of rivets.

The standard procedure given by the guidelines and therefore used by the designer to carry out dynamic analyses of bridges is to model the vehicles as a sequence of moving loads. Actually in this study in order to achieve more accurate results according to what really happens in the real case, a train-bridge dynamic interaction model is first set up and then used to perform dynamic analyses of the structure.

The dynamic interaction between a bridge and the moving vehicles represents a special discipline within the broad area of structural dynamics. The vehicles considered may be those constituting the traffic flow of a highway bridge, in general, or those that form a connected line of railroad cars, in particular.

In order to simulate the train-bridge interactive dynamics many kinds of two-dimensional and three-dimensional models for train carriages have been presented and adopted, in which the springs and damping are used to describe the interactive effects between wheels and primary suspensions as well as primary and secondary suspensions. Therefore from the theoretical point of view, the two subsystems, the bridge and the moving vehicles, can be simulated as two elastic structures. The two subsystems interact with each other through the *contact forces*, the forces induced at the contact points between the wheels and the rails surface (of the railway bridge) or the pavement surface (of the highway bridge). Such a problem is nonlinear and time-dependent due to the fact that the contact forces may move from time to time, while their magnitudes do not remain constant, as a result of the relative movement of the two subsystems.

Therefore this paper proposes in the first chapter some basic notions of dynamic for the single degree of freedom and multi degree of freedom systems, focusing the attention on the eigenvalue problem by which it is possible to obtain the eigenmodes and frequencies of an elastic system.

Since no analytical solution is possible for this kind of problems, in the second chapter, two possible ways to solve the equations of motion are presented. It is also discussed that if the system has classical damping, classical modal analysis can be used to uncoupled the equations of motion, otherwise numerical time-stepping methods are

needed. In this research only the Newmark's method is presented, because it is indeed the method used.

In the third chapter the classical way to represent a vehicle travelling on a bridge is presented. Usually this is done by means of a sequence of moving loads. This method is also the one proposed by the *Eurocode 1* [1] to carry out dynamic analysis of bridges, and it is the widespread method used by the researchers.

In the fourth chapter, other methods to model a vehicle crossing are discussed. These methods consider the dynamic interaction between the vehicle and the bridge. In this way the vehicle and the bridge are considered as two systems that exchange each other the interaction forces caused by the relative motion. Generally this problem is described by two sets of equations, one for the bridge and one for the vehicle, coupled by interactions conditions. It is shown that the solution can be obtained different methods, subdivided into two different group, which are iterative and non-iterative.

In the fifth chapter the railway bridge investigated is presented in details, not only in terms of material, geometry and structural topology, but also as regards the dynamic behavior of the structure. In fact from experimental modal analysis, natural frequencies and mode shapes are known. Furthermore the finite element model to perform the dynamic analyses is discussed.

Once the bridge has been modeled, in chapter six, an optimization algorithm is used to adjust the model to have modal parameters as closed as possible to the measured data. Therefore the *Differential Evolution Algorithm* used to solve the optimization problem of the significant mechanical parameters is described in detail, and the obtained results are presented.

Then in the seventh chapter a comparison between the moving loads and the vehicle-bridge interaction models is done, using an equivalent two dimensional model of the Pontelagoscuro bridge. Actually two dimensional analyses of the bridge are carried out using the trains models given by the Eurocode 1 for fatigue analyses, and as regard VBI analyses the data regarding the suspensions system of the train ETR 500Y [2], [3] have been used. Then the results obtained are compared with those obtained by another author [4], which has carry out dynamic analyses of the same bridge using the *Eurocode 1* approach, which is the moving loads method.

In chapter eight, three dimensional dynamic analyses of the bridge are computed using a more sophisticated 3D train model, used to involve and to take into account also lateral and torsional mode shapes of the structure.

Chapter nine is completely devoted to the assessment of the fatigue life of the bridge. First of all basic notion of fatigue theory are given along with the cycles counting Rainflow method used to reduce a spectrum of varying stress into a set of simple stress reversals, and Miner rule used to quantify the damage in the elements. Then the results obtained for the studied case are discussed and the critical elements that could be subjected to fatigue problem are identified using two different approaches, which are the Eurocode [5], and another method proposed by L. Georgiev [6].

In chapter ten, some conclusions and some proposal for future development are suggested.

# 1. BASIC OF DYNAMIC

## 1.1 General remarks

Any structure, or in general a system, may be described as a set of interconnected elements, that are able to react with the surrounding environment. The structure's behavior is studied through the use of suitable models able to simplify the real problem, which in general can be very complex. The models are appropriate only if the consequences derived from the assumptions are in agreement with the experimental results.

In studying the dynamic problem of a structure, *continuous* or *discrete* models can be used. Continuous systems have infinite number of degrees of freedom, in fact a generic configuration is fixed by infinite number of parameters or coordinates. The dynamic behavior of a continuous system is described by partial differential equations as the parameters defining the motion of the system depend both on time and space. A closed form solution is obtainable only in the particular case in which the mass and the elastic proprieties are uniformly distributed. This approach is rarely feasible if the flexural rigidity  $EI$  or mass  $m$  varies along the length of the beam, if complex constraint conditions are involved, or if the system is an assemblage of several members with distributed mass.

Discrete systems, instead, have a finite number of degrees of freedom, and the system's configuration is described by parameters that are only function of time. Therefore the differential equations of such systems are ordinary differential equations. However discrete systems can effectively idealize many classes of structures. Moreover effective methods that are ideal for computer implementation are available to solve the system of ordinary differential equations governing the motion of such systems.

---

## 1.2 Single degree of freedom system

Some structures, such as an elevated water tank or one-story frame structure or two-span bridge supported by a single column of figure (1.1), could be idealized as a concentrated mass  $m$  supported by a massless stem with stiffness  $k$ , when interested in understanding the structural dynamic in the horizontal direction.

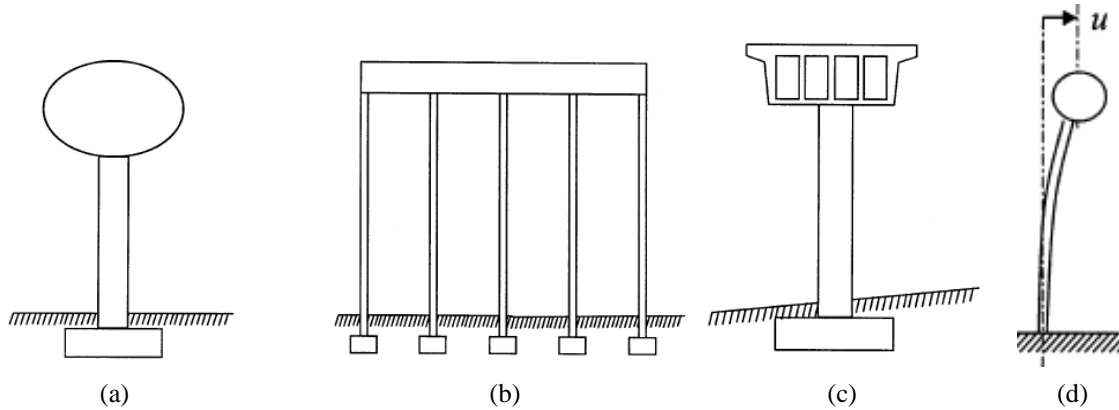


**Figure 1.1:** Example of SDOF structures: (a) Water tank supported by single column; (b) one-story frame building; (c) two-span bridge supported by single column; (d) induced motion of a SDOF.

In those models the number of independent displacements required to define the displaced positions of all the masses relative to their original position is just one. For that reason they are called *single degree of freedom system* (SDOF).

In a real structure each structural member (beam, column, wall, etc.) contributes to the inertial (mass), elastic (stiffness or flexibility), and energy dissipation (damping) properties of the structure. In the idealized system represented in figure (1.2), however, each of these properties is concentrated in three separate, pure components: mass component, stiffness component, and damping component.

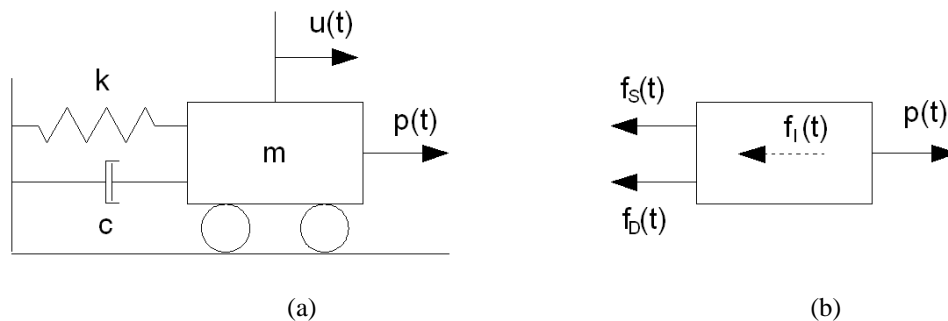


**Figure 1.2:** Idealized dynamic model (a) Damped SDOF system; (b) force equilibrium.

Therefore the response of a structure depends on its mass, stiffness, damping, and applied load  $p(t)$  or displacements. By applying Newton's law and D'Alembert's principle of dynamic equilibrium, it can be shown that

$$f_I + f_D + f_s = p(t) \quad (1.1)$$

where  $f_I$  is the inertial force of the single mass and is related to the acceleration of the mass by  $f_I = m\ddot{u}$ ;  $f_D$  is the damping force on the mass and related to the velocity across the viscous damper by  $f_D = c\dot{u}$ ;  $f_s$  is the elastic force exerted on the mass and related to the relative displacement between the mass and the ground by  $f_s = ku$ , where  $k$  is the spring constant;  $c$  is the damping ratio; and  $m$  is the mass of the dynamic system.

Substituting these expression for  $f_I$ ,  $f_D$ , and  $f_s$  into Eq. (1.1) gives

$$m\ddot{u} + c\dot{u} + ku = p(t) \quad (1.2)$$

The above equation of motion of a SDOF can be solved in closed form only for excitations that can be described analytically. If the excitation varies arbitrarily with time, closed form solution doesn't exist, and the equation can be solved by numerical time-step method.

The characteristics of the oscillations such as the time to complete one cycle of oscillation ( $T_n$ ) and the number of oscillation cycles per second ( $\omega_n$ ) are intrinsic properties of the system, and do not depend on the external applied force. Dividing the Equation (1.2) specialized for free vibration (right term equal to zero) by its mass  $m$  will result in

$$\ddot{u} + 2\nu\omega_n\dot{u} + \omega_n^2u = 0 \quad (1.3)$$

where  $\omega_n = \sqrt{k/m}$  the natural frequency of vibration of the undamped frequency;  $\nu = c/c_{cr}$  the damping ratio;  $c_{cr} = 2m\omega_n = 2\sqrt{km} = 2k/\omega_n$  the critical damping coefficient. The time required for the SDOF system to complete one cycle of vibration is called the natural period of vibration ( $T_n$ ) of the system and is given by

$$T_n = \frac{2\pi}{\omega_n} = 2\pi\sqrt{\frac{m}{k}} \quad (1.4)$$

Furthermore, the natural cyclic frequency of vibration  $f_n$  is given by

$$f_n = \frac{\omega_n}{2\pi} = \frac{1}{T_n} \quad (1.5)$$

The circular frequency of the vibration or the damped vibration frequency of the SDOF structure,  $\omega_d$ , is given by  $\omega_d = \omega_n \sqrt{1 - \nu^2}$ .

The damped period of vibration ( $T_d$ ) of the system is given by

$$T_d = \frac{2\pi}{\omega_d} = \frac{2\pi}{\omega_n \sqrt{1 - \nu^2}} \sqrt{\frac{m}{k}} \quad (1.6)$$

When  $\nu = 1$  or  $c = c_{cr}$  the structure returns to its equilibrium position without oscillating and is referred to as a critically damped structure. When  $\nu > 1$  or  $c > c_{cr}$ , the structure is overdamped and comes to rest without oscillating, but at a slower rate. When  $\nu < 1$  or  $c < c_{cr}$ , the structure is underdamped and oscillates about its equilibrium state with progressively decreasing amplitude, see figure (1.3).

For structure such as buildings, bridges, dams, and offshore structures, the damping ratio is less than 0.15 and thus can be categorized as underdamped structure. So the basic dynamic properties estimated using damped or undamped assumptions are approximately the same. Thus, the damping coefficient accounts for all energy-dissipating mechanisms of the structure and can be estimated only by experimental methods.

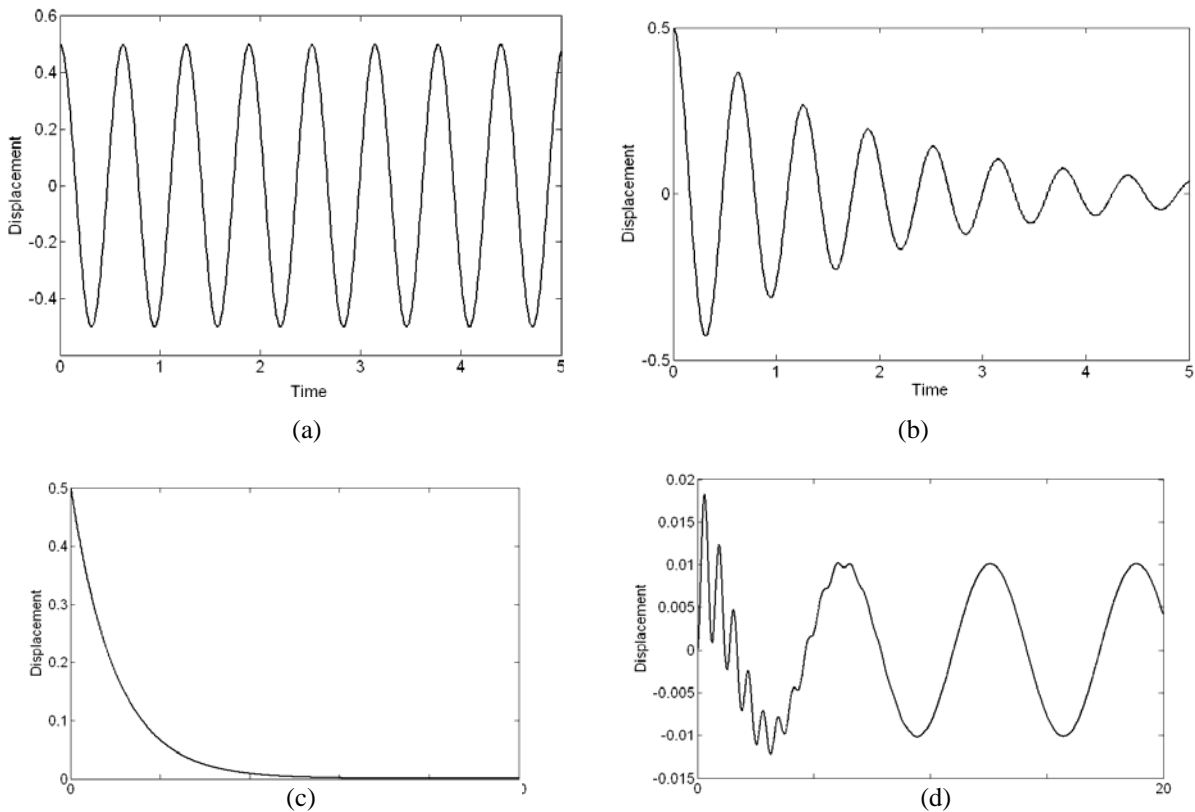


**Figure 1.3:** Example of SDOF systems responses: (a) Undamped free vibration; (b) Underdamped free vibration; (c) Overdamped free vibration; (d) Damped harmonic forced vibration.

### 1.3 Multi-degree of freedom system

The SDOF approach may not be applicable for complex structures such as multilevel frame structures and bridges with several supports. To predict the response of a complex structure, the structure is discretized with several members of lumped masses. As the number of lumped masses increases, the number of displacements required to define the displaced positions of all masses increases.

The equation of motion, of a *multi-degree of freedom* (MDOF) system represented in figure (1.4), is similar to that relative to the SDOF system, but the stiffness  $k$ , mass  $m$ , and damping  $c$  are matrices.

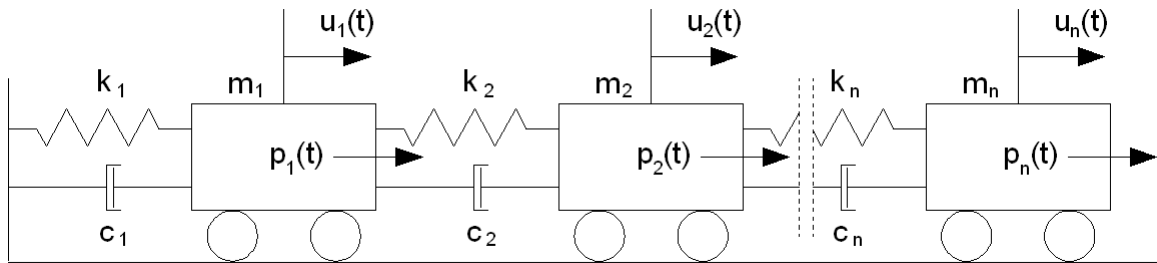


Figure 1.4: Idealized dynamic model of a MDOF system.

The most general equation of motion of an MDOF system can be written as

$$\mathbf{M}\ddot{\mathbf{u}} + \mathbf{C}\dot{\mathbf{u}} + \mathbf{K}\mathbf{u} = \mathbf{p}(t) \quad (1.7)$$

The stiffness matrix  $\mathbf{K}$  can be obtained from standard static displacement-based analysis models and may have off-diagonal terms. The mass matrix  $\mathbf{M}$  due to the negligible effect of mass coupling can best be expressed in the form of tributary lumped masses to the corresponding displacement degree of freedoms, resulting in a diagonal or uncoupled mass matrix. The damping matrix  $\mathbf{C}$  accounts for all the energy-dissipating mechanisms in the structure and may have off-diagonal terms. The right term  $\mathbf{p}(t)$  is the vector of the external forces acting on each degree of freedom.

To better understand the response of MDOF systems, we look first at the undamped, free vibrations. By setting  $\mathbf{C}$  and  $\mathbf{p}(t)$  to zero in the Eq. (1.7), the equation of motion of an  $N$ -DOF system can be shown as:

$$\mathbf{M}\ddot{\mathbf{u}} + \mathbf{K}\mathbf{u} = 0 \quad (1.8)$$

where  $\mathbf{M}$  and  $\mathbf{K}$  are  $n \times n$  square matrices.

The signal of a natural vibration mode can be described mathematically by:

$$\mathbf{u}_n(t) = \boldsymbol{\phi}_n(A_n \cos \omega_n t + B_n \sin \omega_n t) = \boldsymbol{\phi}_n q_n(t) \quad (1.9)$$

Where  $\boldsymbol{\phi}_n$  is the deflected shape of the structure, and the harmonic function describes the time variation of the displacement  $A_n$  and  $B_n$  constants determined using the initial conditions of the motion. Combining and simplifying equation (1.8) and (1.9) gives the eigenvalue problem, which is used to determine the eigenvector corresponding to the natural mode shapes,  $\boldsymbol{\phi}_n$ , and natural frequencies,  $\omega_n$ , of the structure.

$$\det[\mathbf{K} - \omega_n \mathbf{M}] = 0 \quad (1.10)$$

The  $N$  eigenvectors  $\boldsymbol{\phi}_n$  can be assembled in a single  $n \times n$  square modal matrix  $\boldsymbol{\Phi}$ . One of the important aspects of these mode shapes is that they are orthogonal to each other. This lead to

$$\mathbf{K}^* = \boldsymbol{\Phi}^T \mathbf{K} \boldsymbol{\Phi} \quad (1.11)$$

$$\mathbf{M}^* = \boldsymbol{\Phi}^T \mathbf{M} \boldsymbol{\Phi} \quad (1.12)$$

where  $\mathbf{K}^*$  and  $\mathbf{M}^*$  are diagonal matrices.

When damping of the MDOF system is included, the free vibration response of the damped system will be given by

$$\mathbf{M}\ddot{\mathbf{u}} + \mathbf{C}\dot{\mathbf{u}} + \mathbf{K}\mathbf{u} = 0 \quad (1.13)$$

The displacements are first expressed in terms of natural mode shapes, and later they are multiplied by the transformed natural mode matrix to obtain the following expression:

$$\mathbf{M}^* \ddot{\mathbf{q}} + \mathbf{C}^* \dot{\mathbf{q}} + \mathbf{K}^* \mathbf{q} = 0 \quad (1.14)$$

where,  $\mathbf{M}^*$  and  $\mathbf{C}^*$  are diagonal matrices given by Eqs. (1.11) and (1.12) and

$$\mathbf{C}^* = \boldsymbol{\Phi}^T \mathbf{C} \boldsymbol{\Phi} \quad (1.15)$$

While  $\mathbf{M}^*$  and  $\mathbf{K}^*$  are diagonal matrices,  $\mathbf{C}^*$  may have off-diagonal terms. When has off diagonal terms, the damping matrix is referred to as a *nonclassical* or *nonproportional* damping matrix. When is diagonal, it is referred to as a *classical* or *proportional* damping matrix. Classical damping is an appropriate idealization when similar damping mechanisms are distributed throughout the structure. Nonclassical damping idealization is appropriate for the analysis when the damping mechanisms differ considerably within a structural system. Since most civil structures have predominantly one type of construction

material, they could be idealized as a classical damping structural system. Thus, the damping matrix of Eq. (1.16) will be a diagonal matrix. Therefore the equation of  $n$ th mode shape or generalized  $n$ th modal equation is given by

$$\ddot{q}_n + 2\nu_n\omega_n\dot{q}_n + \omega_n^2q_n = 0 \quad (1.16)$$

Equation (1.16) is similar to the Eq. (1.3) of an SDOF system. Also, the vibration properties of each mode can be determined by solving the Eq. (1.16).

Methods for solving the equations of motions (1.3) or (1.17) and (1.7) are developed in detail in *chapter 2*.

In figure (2.5) the responses of some possible two degrees of freedom systems are shown.

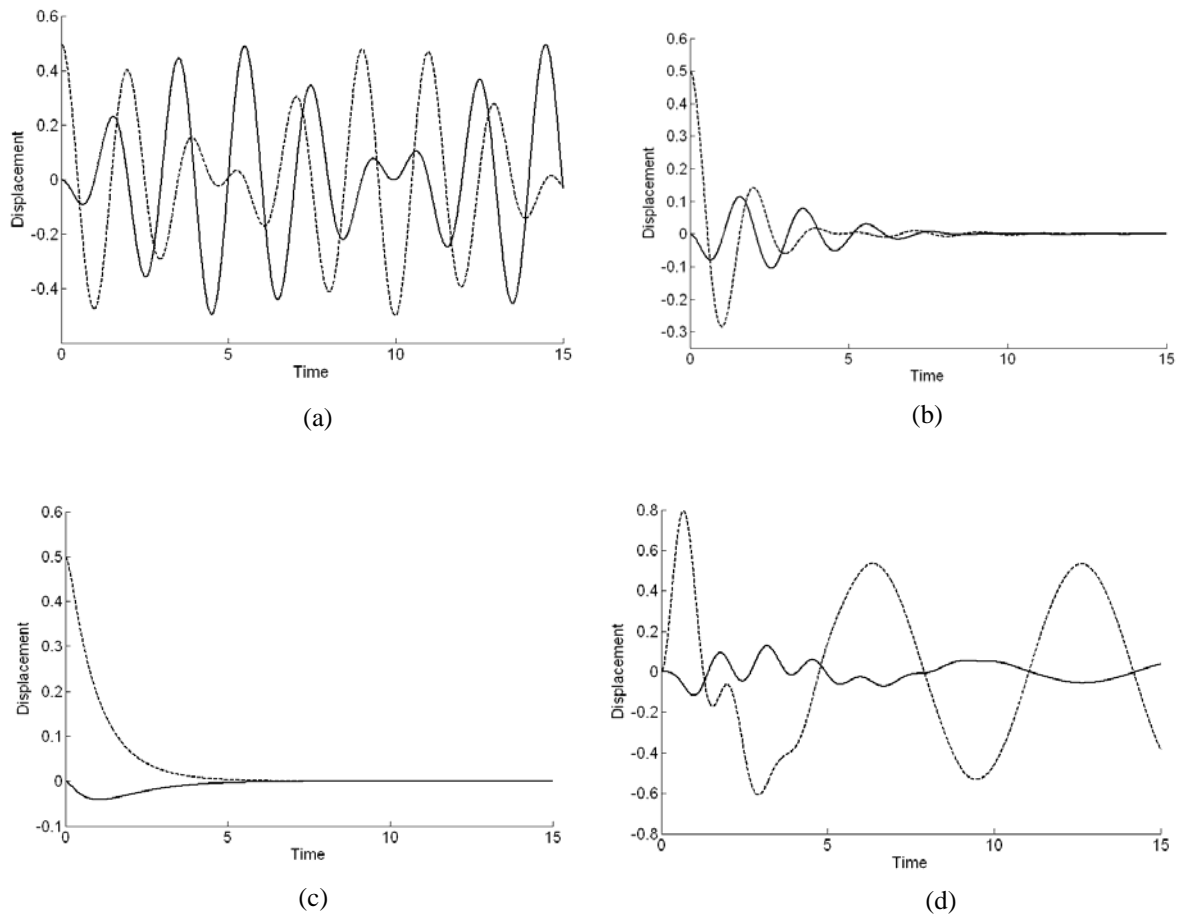


**Figure 2.5:** Example of 2-DOFs systems responses: (a) Undamped free vibration; (b) Underdamped free vibration; (c) Overdamped free vibration; (d) Damped harmonic forced vibration.

## 1.4 Damping in structures

The damping of a structure is related to the amount of energy dissipated during its motion. It could be assumed that a portion of the energy is lost due to the deformations, and thus damping could be idealized as proportional to the stiffness of the structure. Another mechanism of energy dissipation could be attributed to the mass of the structure, and thus damping idealized as proportional to the mass of the structure. In Rayleigh damping, it is assumed that the damping is proportional to the mass and stiffness of the structure.

$$\mathbf{C} = a_0\mathbf{M} + a_1\mathbf{K} \quad (1.17)$$

The generalized damping of the  $n$ th mode is then given by

$$C_n = a_0M_n + a_1K_n \quad (1.18)$$

$$C_n = a_0M_n + a_1\omega_nM_n \quad (1.19)$$

knowing that

$$v_n = \frac{C_n}{2\omega_nM_n} \quad (1.20)$$

therefore substituting Eq. (1.19) in (1.20) and simplifying results in

$$v_n = \frac{a_0}{2\omega_n} + \frac{a_1}{2}\omega_n \quad (1.21)$$

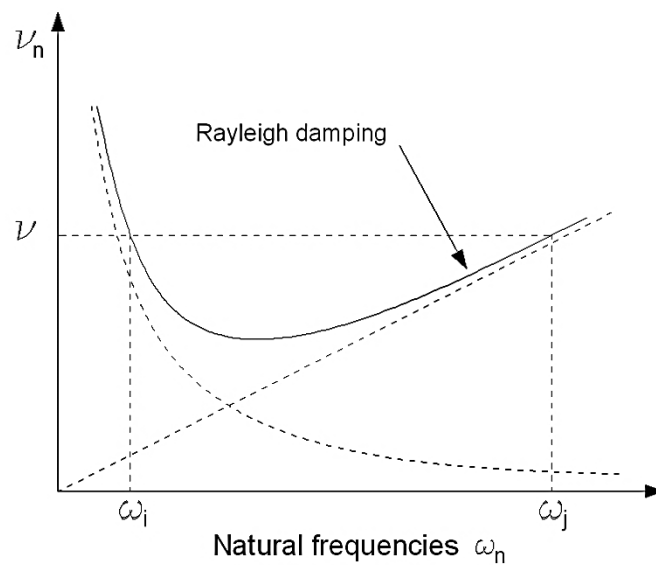


**Figure 1.6:** Rayleigh damping variation with natural frequency.

The coefficients  $a_0$  and  $a_1$  can be determined from specified damping ratios at two independent dominant modes (say,  $i$  and  $j$  modes). In figure (1.6) the Rayleigh damping variation with natural frequency is shown.

Expressing Eq. (1.21) for these two modes will lead to the following equations:

$$v_i = \frac{a_0}{2\omega_i} + \frac{a_1}{2}\omega_i \quad (1.22)$$

$$v_j = \frac{a_0}{2\omega_j} + \frac{a_1}{2}\omega_j \quad (1.23)$$

When the damping ratio at both the  $i$  and  $j$  modes is the same and equals  $v$ , it can be shown that

$$a_0 = v \frac{2\omega_i\omega_j}{\omega_i + \omega_j} \quad (1.24)$$

$$a_0 = v \frac{2\omega_i\omega_j}{\omega_i + \omega_j} \quad (1.25)$$

It is important to note that the damping ratio at a mode between the  $i$ th and  $j$ th mode is less than  $v$ . And, in practical problems the specified damping ratios should be chosen to ensure reasonable values in all the mode shapes that lie between the  $i$ th and  $j$ th mode shapes.



## 2. METHODS FOR SOLVING THE EQUATIONS OF MOTION

### 2.1 General overview

The dynamic response of linear systems with classical damping that is a reasonable model for many structures can be determined by classical modal analysis. Classical natural frequency and modes of vibration exist for such systems, and their equations of motion, when transformed to modal coordinates, become uncoupled (*chapter 1.3*). Thus the response in each natural vibration mode can be computed independently of the others, and modal response can be combined to determine the total response. Each mode responds with its own particular pattern of deformation, the mode shape, with its own frequency, the natural frequency, and with its own damping. Each modal response can be computed as a function of time by analysis of a SDOF system with the vibration properties of the particular mode. These SDOF equations can be solved in closed form for excitations that can be described analytically, or they can be solved by time stepping methods for complicated excitations.

For systems with nonclassical damping the equations of motion cannot be uncoupled by transforming to modal coordinates of the system without damping. Therefore such systems can be analyzed by direct solutions of the coupled system of differential equations. This approach requires numerical methods because closed-form analytical solutions are not possible even if the dynamic excitation is a simple function described analytically.

## 2.2 Classical modal analysis

For MDOF systems, the general form of the equations of motion are given by Eq. (1.7) repeated here for convenience:

$$\mathbf{M}\ddot{\mathbf{u}} + \mathbf{C}\dot{\mathbf{u}} + \mathbf{K}\mathbf{u} = \mathbf{p}(t)$$

which in modal coordinates can be rewritten as

$$\mathbf{M}^*\ddot{\mathbf{q}} + \mathbf{C}^*\dot{\mathbf{q}} + \mathbf{K}^*\mathbf{q} = \mathbf{p}^*(t) \quad (2.1)$$

where  $\mathbf{M}^*$ ,  $\mathbf{K}^*$  and  $\mathbf{C}^*$  are already introduced in Eq. (1.11) (1.12) and (1.15), while the right term is given by

$$\mathbf{p}^* = \mathbf{\Phi}^T \mathbf{p} \quad (2.2)$$

The expression (2.1) represents a set of  $N$  uncoupled equations in modal coordinates  $q_n(t)$ , if the system has classical damping. For such systems, the generic equation can be written as

$$M_n^*\ddot{q}_n + C_n^*\dot{q}_n + K_n^*q_n = p_n^*(t) \quad (2.3)$$

This equation governs the response of the SDOF. Dividing Eq. (2.3) by  $M_n^*$  gives

$$\ddot{q}_n + 2\nu_n\omega_n\dot{q}_n + \omega_n^2q_n = \frac{p_n^*(t)}{M_n^*} \quad (2.4)$$

Thus we have  $N$  uncoupled equations like Eq. (2.3) or (2.4) one for each natural mode. In summary, the set of  $N$  coupled differential equations (2.1) in nodal displacements  $\mathbf{u}(t)$  has been transformed to the set of  $N$  uncoupled equations (2.3) in modal coordinates  $\mathbf{q}(t)$ .

As already mentioned each modal equation is of the same form as the equation of motion of a SDOF system. Thus solution methods and results available for SDOF systems can be adapted to obtain solutions  $q_n(t)$  for the modal equations. So if the external forces are analytical functions, closed-form solutions are available, otherwise numerical methods are needed (*chapter 2.3*). Once  $q_n(t)$  is established, the displacement due to the  $n$ th mode will be given by  $\mathbf{u}_n(t) = \boldsymbol{\phi}_n q_n(t)$ . The total displacement due to combination of all mode shapes can then be determined by summing up all displacements for each mode, and is given by

$$\mathbf{u}(t) = \sum_{n=1}^N \mathbf{u}_n(t) = \sum_{n=1}^N \boldsymbol{\phi}_n q_n(t) = \mathbf{\Phi} \mathbf{q} \quad (2.5)$$

This procedure is known as *classical modal analysis* or the *classical superposition method* because individual modal equations are solved to determine the modal coordinates  $q_n(t)$ .

This analysis method is restricted to linear systems with classical damping. Linearity of the system is implicit in using the principle of superposition. Damping must be of the classical form in order to obtain modal equations that are uncoupled, a central feature of modal analysis.

It is shown that for MDOF system, the equations of motion can be transformed in modal coordinates to obtain Eq. (2.1). But this transformation is not advantageous when dealing with systems with many degrees of freedom excited by complicated expressions of the external forces. In fact in these cases solving  $N$  coupled equation of the type (1.7) or  $N$  equations of the type (2.3) is almost the same, because in both cases a numerical time-stepping method is needed.

Actually for many practical problems only the few first modes contribute significantly to the response. This means that for systems with classical or nonclassical damping it is necessary to solve the uncoupled modal equations for only the significant modes. If only the first  $J$  modes contribute significantly to the response, the size of Eq. (3.1) can be reduced accordingly;  $\Phi$  is now an  $N \times J$  matrix;  $\mathbf{M}^*$ ,  $\mathbf{K}^*$  and  $\mathbf{C}^*$  are  $J \times J$  matrices; and  $\mathbf{p}^*(t)$  is a  $J \times 1$  vector. Thus the problem reduces to solving these  $J$  uncoupled equations for  $q_n(t)$ ,  $n = 1, 2, \dots, J$  with a numerical method. Once  $q_n(t)$  have been determined at each time instant,  $\mathbf{u}(t)$  is computed from Eq. (2.5) with its summation truncated at  $N = J$ .

## 2.3 Numerical time-stepping methods

A vast body of literature exists about numerical time-stepping methods for integration of differential equations. However in this section only the Newmark's method is treated as, with appropriate choices of the parameters this scheme ensures convergence, stability and accuracy. The method is developed for the equation of motion of the SDOF, however the extension to the equations of the MDOF is straightforward.

In 1959, N. M. Newmark developed a family of time-stepping methods based on the following equations:

$$\dot{u}_{i+1} = \dot{u}_i + [(1 - \gamma)\Delta t]\ddot{u}_i + (\gamma\Delta t)\ddot{u}_{i+1} \quad (2.6.a)$$

$$u_{i+1} = u_i + (\Delta t)\dot{u}_i + [(0.5 - \beta)(\Delta t)^2]\ddot{u}_i + [\beta(\Delta t)^2]\ddot{u}_{i+1} \quad (2.6.b)$$

Typical selection for  $\gamma$  is  $1/2$  and  $\beta = 1/4$  is satisfactory from all points of view, including that of accuracy, as it possible to see in figure (2.1). For linear systems these two equations, combined with the equilibrium equation

$$m\ddot{u}_{i+1} + c\dot{u}_{i+1} + ku_{i+1} = p_{i+1} \quad (2.7)$$

at the end of time step, provide the basis for computing  $u_{i+1}$ ,  $\dot{u}_{i+1}$  and  $\ddot{u}_{i+1}$  from the known  $u_i$ ,  $\dot{u}_i$  and  $\ddot{u}_i$  at time  $i$ . Defining the following quantities

$$\Delta u_i = u_{i+1} - u_i \quad \Delta \dot{u}_i = \dot{u}_{i+1} - \dot{u}_i \quad \Delta \ddot{u}_i = \ddot{u}_{i+1} - \ddot{u}_i \quad (2.8)$$

$$\Delta p_i = p_{i+1} - p_i \quad (2.9)$$

the Eq. (2.6) can be rewritten as

$$\Delta \dot{u}_i = (\Delta t)\ddot{u}_i + (\gamma\Delta t)\Delta \ddot{u}_i \quad (2.10.a)$$

$$\Delta u_i = (\Delta t)\dot{u}_i + \frac{(\Delta t)^2}{2}\ddot{u}_i + \beta(\Delta t)^2\Delta \ddot{u}_i \quad (2.10.b)$$

The Eq. (2.10.b) can be solved for  $\Delta \ddot{u}_i$  and substituted in the Eq. (2.10.a). The two expression just founded are then substituted in the incremental equation of motion

$$m\Delta \ddot{u}_i + c\Delta \dot{u}_i + k\Delta u_i = \Delta p_i \quad (2.11)$$

This substitution gives

$$\hat{k}\Delta u_i = \Delta \hat{p}_i \quad (2.12)$$

where

$$\hat{k} = k + \frac{\gamma}{\beta \Delta t} c + \frac{1}{\beta (\Delta t)^2} m \quad (2.13)$$

and

$$\Delta \hat{p}_{i+1} = \Delta p_i + \left( \frac{1}{\beta \Delta t} m + \frac{\gamma}{\beta} c \right) \dot{u}_i + \left[ \frac{1}{2\beta} m + \Delta t \left( \frac{\gamma}{2\beta} - 1 \right) c \right] \ddot{u}_i \quad (2.14)$$

With  $\hat{k}$  and  $\Delta \hat{p}_i$  known from the system properties  $m$ ,  $k$  and  $c$ , algorithm parameters  $\gamma$  and  $\beta$ , and the  $\dot{u}_i$  and  $\ddot{u}_i$  at the beginning of the time step, the incremental displacement is computed from

$$\Delta u_i = \frac{\Delta \hat{p}_i}{\hat{k}} \quad (2.15)$$

Once  $\Delta u_i$  is known  $\Delta \dot{u}_i$  and  $\Delta \ddot{u}_i$  can be computed from Eqs. (2.10.a) and (2.10.b) then  $u_{i+1}$ ,  $\dot{u}_{i+1}$  and  $\ddot{u}_{i+1}$  from Eq. (2.8). The acceleration can also be obtained from the equation of motion  $t_{i+1}$ :

$$\ddot{u}_{i+1} = \frac{p_{i+1} - c\dot{u}_{i+1} - ku_{i+1}}{m} \quad (2.16)$$

Actually Eq. (2.16) is needed to obtain  $\ddot{u}_0$  to start the computations.

This procedure can readily be extended to MDOF systems. The scalar equations (2.10.a) and (2.10.b) that relate the response (displacement, velocity, and acceleration) increments over time step  $i$  to  $i + 1$  to each other and the response values at time  $i$ , and the scalar equation (2.11) of incremental equilibrium, all now become matrix equations.

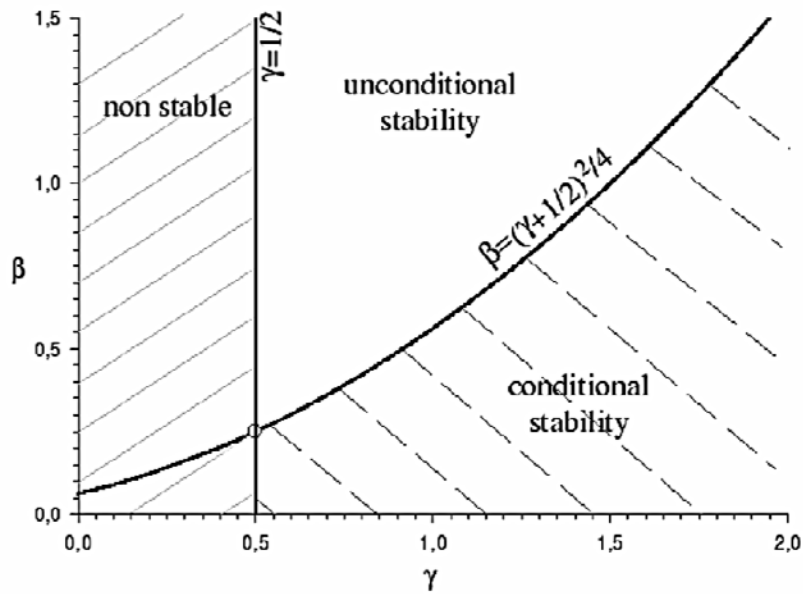


Figure 2.1: Newmark's parameters selection.



## 3. MOVING LOADS MODEL

### 3.1 Introduction

The simplest case that can be conceived of a moving vehicle is when it is represented as concentrated loads. This is the so called *moving loads* model.

The most basic problem in the study of vehicle-induced vibrations on bridges is the dynamic response of a simply-supported beam subjected to a single moving load. This problem is important in that the solution can be given in closed form. By the principle of superposition the solution obtained for a single moving load could be expanded to deal with a series of identical equi-distant moving loads. Research on the vibration of bridges traveled by moving loads is abundant. The most related ones are the works by Timoshenko [7] and Fryba [8].

In the dynamic analysis of a railway bridge, a moving train is traditionally represented as a series of moving axle loads. This approach is the one adopted by many researchers and also by many design codes, as for example the Eurocode 1. With this model, the global dynamic characteristics of the bridge caused by the moving action of the vehicle can be captured with a sufficient degree of accuracy. However, the effect of interaction between the bridge and the moving load is ignored. For this reason, the moving load model is good only for the case where the mass of the vehicle is small relative to that of the bridge, and only when the vehicle response is not of interest.

In this section the moving loads model will be treated in a general way within the framework of the finite elements method, leaving the reader who is interested in the analytical solution to others books and authors, [9].

---

### 3.2 Simply-supported beam subjected to moving loads

In this section, the general method to perform a dynamic analysis of railway bridges subjected to moving loads is given by means of reduced model of train bridges. The problem is illustrated in figure (3.1).

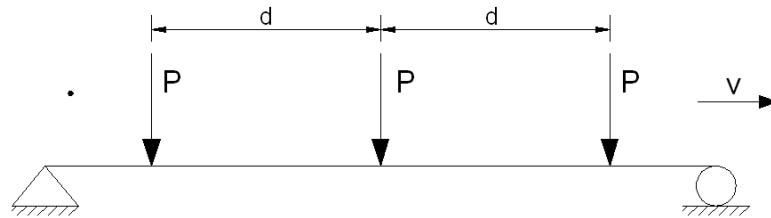


Figure 3.1: Moving loads model.

The model is based on the fact that the fundamental dynamic behavior of certain type of bridges may be described by the dynamic behavior of two-dimensional Bernoulli beams. The Bernoulli beam is modeled using several numbers of beam elements. A schematic illustration of the transformation of a railway bridge to a beam element model is shown in Figure (3.2). However, the whole following procedure is easily extended also to three-dimensional models, if more sophisticated analyses are needed.

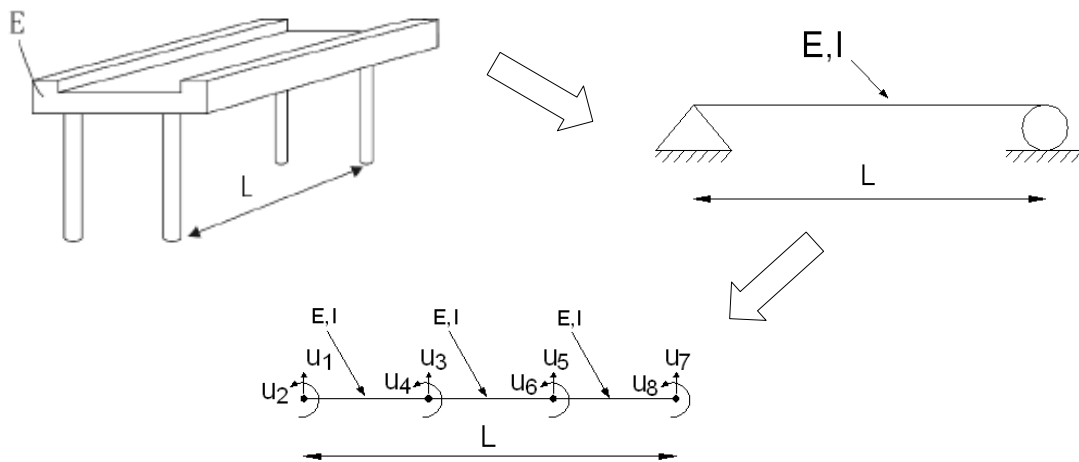
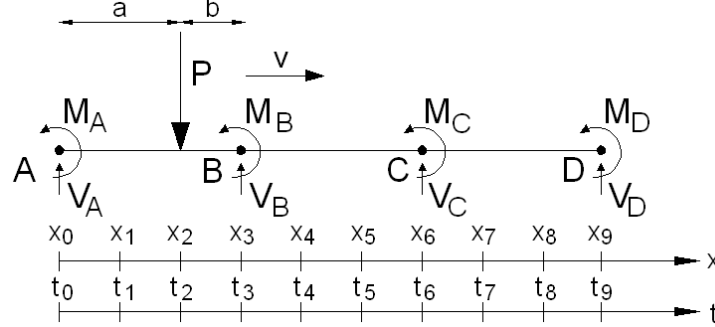


Figure 3.2: Transformation of a bridge to a reduced beam element model.

The model can be implemented given as input the properties of the beam elements such as the damping value, Young's modulus, moment of inertia and mass per unit length. Then the following steps could be performed in order to set-up the bridge model:

- Creating the matrices  $\mathbf{K}_e$ ,  $\mathbf{M}_e$  and  $\mathbf{C}_e$  for a 2D elastic Bernoulli beam element.
- Assemble the element matrices  $\mathbf{K}_e$ ,  $\mathbf{M}_e$  and  $\mathbf{C}_e$  in the global matrices  $\mathbf{K}$ ,  $\mathbf{M}$  and  $\mathbf{C}$ .

After that the load vector has to be constructed. Figure (3.3) illustrates a point load  $P$  that moves over a bridge consisting of three beam elements.



**Figure 3.3:** The equivalent nodal forces of a point load on a beam element.

The force moves with the velocity  $v$  between and over the nodes of the model. In a finite elements model all loads are applied at the element nodes. The load  $P$  is therefore assigned as equivalent nodal forces, when is situated between the nodes of a beam element. The equivalent shear forces  $V$  and moments  $M$  are computed as:

$$V_A = \frac{Pb^2}{L^2} + (1 + \frac{2a}{L}) \quad (3.1)$$

$$M_A = \frac{Pab^2}{L^2} \quad (3.2)$$

$$V_B = \frac{Pa^2}{L^2} + (1 + \frac{2b}{L}) \quad (3.3)$$

$$M_B = -\frac{Pa^2b}{L^2} \quad (3.4)$$

In this way a  $\mathbf{P}_b$  matrix can be generated which describes the load history at each node of the model for the whole time period of the analysis. The matrix is constructed by calculating the equivalent node loads using Eqs. (3.1)-(3.4) every time the load  $P$  moves a distance  $\Delta x$ . The size of the distance depends on the velocity  $v$  and the size of a time step  $\Delta t$  according to:

$$\Delta x = v \cdot \Delta t \quad (3.5)$$

After constructing the  $\mathbf{K}$ ,  $\mathbf{M}$ ,  $\mathbf{C}$  and  $\mathbf{P}_b$  matrices the dynamic responses in the bridge could be calculated by solving the equations of motion (1.7). This can be performed by using Newmark's time-step method, described in *chapter 2.3*.

### 3.3 Assumption and limitation of the model

Actually two-dimensional beam models can only calculate vertical bending modes. A key assumption in this model is that vertical modes of vibration contributes to the vertical accelerations of the bridge, which implies that it is assumed that accurate results may be achieved even though torsional and horizontal bending modes are neglected. This is a limitation of the model since all bridges have torsional bending modes and, if they are excited, they often increase the vertically acceleration of the bridge. Torsional bending modes are mainly excited when a bridge is subjected to eccentric dynamic loads, as on two-rail bridges, and the reduced model is therefore more accurate for bridges with a centric track.

Also it must be ensure that the frequencies and shapes of the modes that are calculated using the reduced model are nearly the same as the frequency and eigenmodes of the real bridge.

In this procedure the bridge is modeled using Bernoulli beams, which implies that shear deformation is neglected. When modeling truss bridges shear deformations cannot be neglected. Therefore, the reduced model introduces more approximations when truss bridges are considered.

Another limitation of the model is that the beams all have the same properties. To make benefit of the result using the reduced model, it may be limited to railway bridges that have constant stiffness and weight along the length.

A last assumption is that columns and foundations were assumed to have a neglected vertical deformation and are therefore modeled as simple supports.

Actually all this assumptions and limitations can be easily overcome with some devices. In fact as already said the model could be expanded in a three-dimensional model for instance, in order to have more sophisticated model, and models which take into account shear deformation can be built up. Therefore the bridge can be modeled in a finite elements software and performing a dynamic analysis assigning the load history at each node of the track.

# 4. VEHICLE-BRIDGE INTERACTION

## MODELS

### 4.1 Introduction

The dynamic response of railway bridges under moving trains has been a topic of research interest for many years, especially in last decades that has seen a worldwide development of high-speed railways.

In *chapter 3* the problem of a train passing over a bridge it is treated as a sequence of travelling loads.

Considerable experimental and theoretical research has recently been performed on train-bridge interaction. For this aim different vehicle models with different degree of sophistication have been developed to account for the dynamic properties of the vehicle. The simplest model for a train is a series of 1 degree-of-freedom (DOF) mass-spring-damper systems that account for the suspension of the vehicle. Liu et al. [2] studied train-bridge interaction with a 3-DOF vehicle model consisting of the car body and wheel-axle sets and proposed a 15-DOF vehicle model and analyzed the passage of the ETR 500Y high speed train on the Sesia viaduct [10].

In this section a review of this models and methods, for solve the train-bridge dynamic interaction problem, are given.

## 4.2 Train subsystem

Vehicle model with a varying degree of sophistication can be found in literature to account for the dynamic effect of the train on the bridge. Possible planar models consisting in masses supported by springs and dashpots that could be used in the two-dimensional analyses are those represented in figure (4.1). The simplest model in this case is a SDOF moving mass supported by spring-dashpot unit, the so called *sprung mass* model (figure (4.1 a)). Vehicle model (c) consist in a car body, assumed to be rigid, resting on the front and rear bogies, each of which in turn is supported by two wheel sets; while vehicle (b) is an intermediate model.

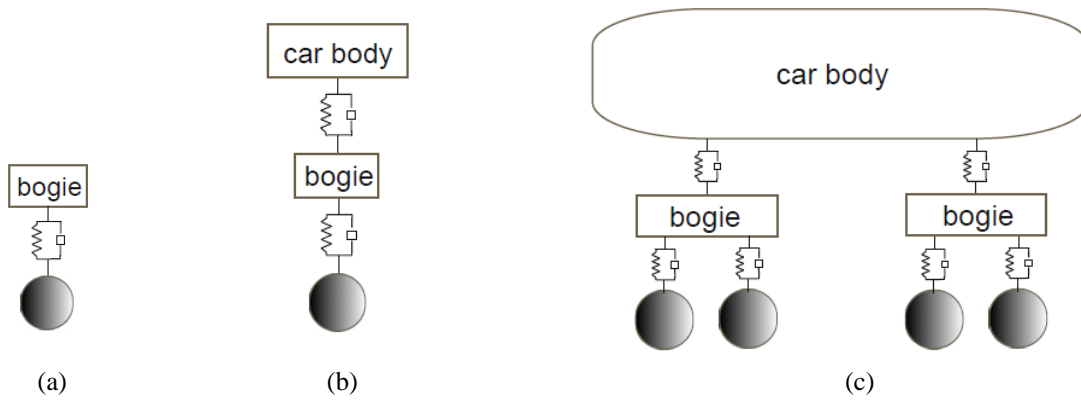


**Figure 4.1:** (a) a 1-DOF (b) a 2-DOF and (c) a 3-DOF vehicle models for dynamic train-bridge interaction analysis [2].

In order to study the train-bridge interaction, a train composed of a sequence of one of the three models just presented can be used.

In a similar way as for the bridge, the equation of motion of the vehicle can be rewritten as

$$\mathbf{M}_v \ddot{\mathbf{V}}_v + \mathbf{C}_v \dot{\mathbf{V}}_v + \mathbf{K}_v \mathbf{V}_v = \mathbf{P}_v \quad (4.1)$$

where  $\mathbf{M}_v$ ,  $\mathbf{C}_v$  and  $\mathbf{K}_v$ , are the mass, damping and stiffness matrices;  $\mathbf{V}_v$ ,  $\dot{\mathbf{V}}_v$  and  $\ddot{\mathbf{V}}_v$  are the displacement, velocity and acceleration vectors of the vehicle system; and  $\mathbf{P}_v$  is the force vector that collects the dynamic force on the vehicle. Without loss of generality, the terms in Eq. (4.1) specialized for the vehicle model (c) are given in the following. The mass matrix of the vehicle can be expressed as

$$\mathbf{M}_v = \begin{bmatrix} M_1 & 0 & 0 \\ 0 & M_2 & 0 \\ 0 & 0 & M_1 \end{bmatrix} \quad (4.2)$$

where  $M_1$  and  $M_2$  are the mass of the bogie and the car body, respectively.

The stiffness matrix of the vehicle system is expressed as

$$\mathbf{K}_v = \begin{bmatrix} 2K_V + K_{VV} & -K_{VV} & 0 \\ -K_{VV} & 2K_{VV} & -K_{VV} \\ 0 & -K_{VV} & 2K_V + K_{VV} \end{bmatrix} \quad (4.3)$$

where  $K_V$  and  $K_{VV}$  are the spring stiffness coefficients of the primary and secondary suspension system, respectively.

The damping matrix can be derived from the stiffness matrix by replacing the stiffness coefficients ( $K_V$ ,  $K_{VV}$ ) by the damping coefficients ( $C_V$ ,  $C_{VV}$ ) of the primary and secondary suspension system obtaining

$$\mathbf{C}_v = \begin{bmatrix} 2C_V + C_{VV} & -C_{VV} & 0 \\ -C_{VV} & 2C_{VV} & -C_{VV} \\ 0 & -C_{VV} & 2C_V + C_{VV} \end{bmatrix} \quad (4.4)$$

The displacement, velocity and acceleration vectors  $\mathbf{V}_v$ ,  $\dot{\mathbf{V}}_v$  and  $\ddot{\mathbf{V}}_v$  are expressed as

$$\mathbf{V}_v = [V_1 \quad V_2 \quad V_3]^T \quad (4.5)$$

$$\dot{\mathbf{V}}_v = [\dot{V}_1 \quad \dot{V}_2 \quad \dot{V}_3]^T \quad (4.6)$$

$$\ddot{\mathbf{V}}_v = [\ddot{V}_1 \quad \ddot{V}_2 \quad \ddot{V}_3]^T \quad (4.7)$$

where the subscript 1 and 3 indicate the vertical displacement, velocity and acceleration of the front and back bogie, respectively, while with the subscript 2 those of the car body.

The force vector  $\mathbf{P}_v$  is expressed in terms of the displacements and velocities of the wheel sets as follow

$$\mathbf{P}_v = \begin{bmatrix} K_V(V_{W1} + V_{W2}) + C_V(\dot{V}_{W1} + \dot{V}_{W2}) \\ 0 \\ K_V(V_{W3} + V_{W4}) + C_V(\dot{V}_{W3} + \dot{V}_{W4}) \end{bmatrix} \quad (4.8)$$

where  $V_{Wi}$  and  $\dot{V}_{Wi}$  (with  $i = 1,2,3,4$ ) represent the displacement and velocity of the  $i$ th wheel set, respectively.

More sophisticated three-dimensional models are available in order to perform more accurate train-bridge dynamic analyses [3]; a possible model is showed in figure (4.2). The equation of motion of this kind of model can still be represented by the Eq. (4.1). In this model the bogies and the wheel sets are linked by horizontal and vertical springs and dampers. There are horizontal and vertical springs ( $K_H$ ,  $K_V$ ) and dampers ( $C_H$ ,  $C_V$ ) at each side of each wheel set, also horizontal and vertical springs ( $K_{HH}$ ,  $K_{VV}$ ) and dampers ( $C_{HH}$ ,

$C_{VV}$ ) at each side of each bogie. Each car body and each bogie has 5 DOFs: the displacement in vertical direction ( $Z$ ) and longitudinal direction ( $Y$ ), and rotations around the  $X$ -axis ( $R_X$ ),  $Y$ -axis ( $R_Y$ ) and  $Z$ -axis ( $R_Z$ ). Each wheel set has 3 DOFs: the displacement in vertical direction ( $Z$ ) and longitudinal direction ( $Y$ ), and rotation around the  $X$ -axis ( $R_X$ ). In this way, the vehicle model has a degree of 27 DOFs.

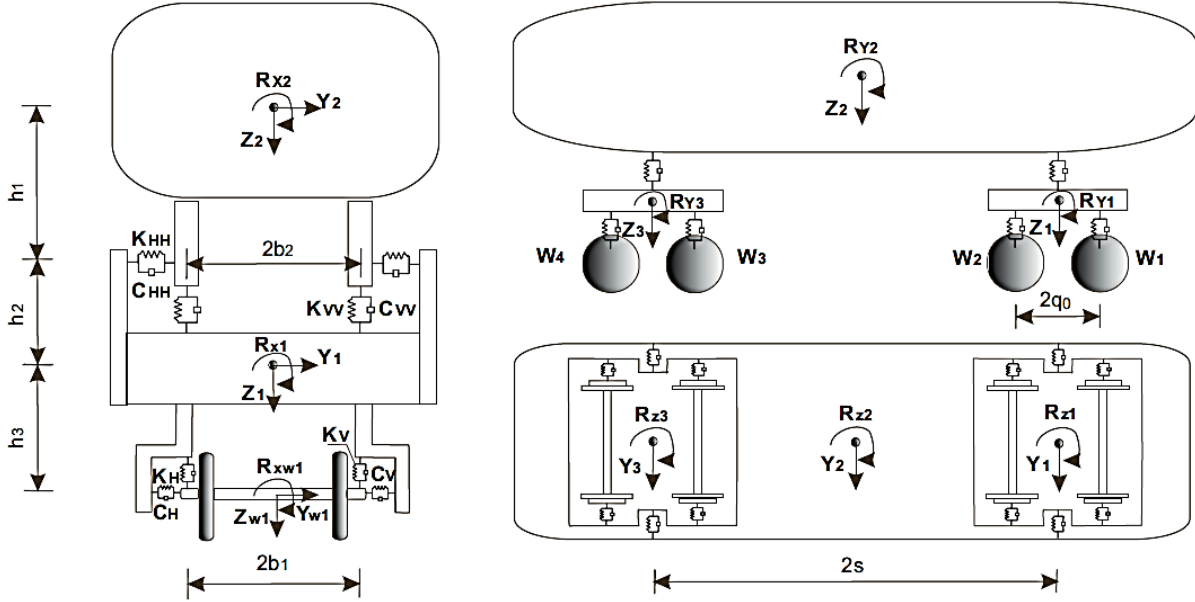


**Figure 4.2:** 27-DOF vehicle model for three dimensional dynamic interaction analysis [3].

The displacement as well as the velocity and acceleration vectors of the Eq. (4.1), of this model vehicle, assume the following form

$$\mathbf{V}_v = [Y_1, R_{X1}, R_{Z1}, Z_1, R_{Y1}, Y_2, R_{X2}, R_{Z2}, Z_2, R_{Y2}, Y_3, R_{X3}, R_{Z3}, Z_3, R_{Y3}] \quad (4.9)$$

where subscript 1 stands for the front bogie, subscript 2 stands for the car body, and subscript 3 stands for the rear bogie. The mass matrix of the vehicle system is given by

$$\mathbf{M}_v = \text{diag}[M_1, I_{X1}, I_{Z1}, M_1, I_{Y1}, M_2, I_{X2}, I_{Z2}, M_2, I_{Y2}, M_1, I_{X1}, I_{Z1}, M_1, I_{Y1}] \quad (4.10)$$

where  $M_1$  is the mass of the bogie,  $I_{X1}, I_{Y1}, I_{Z1}$  are the mass moments of inertia of the bogie around the  $X$ -axis,  $Y$ -axis and  $Z$ -axis; with the subscript 2 are indicated the same quantities for the car body  $M_2$  is the mass of the car body,  $I_{X2}, I_{Y2}, I_{Z2}$  are the mass moments of inertia of car body around the  $X$ -axis,  $Y$ -axis and  $Z$ -axis. The stiffness matrix of the vehicle system is expressed as [10]:

$$\mathbf{K}_v = \begin{bmatrix} \mathbf{K}_{11}^H & & & \\ & \mathbf{K}_{11}^V & & \text{sym} \\ \mathbf{K}_{21}^H & & \mathbf{K}_{22}^H & \\ & \mathbf{K}_{21}^V & & \mathbf{K}_{22}^V \\ & & \mathbf{K}_{32}^H & \mathbf{K}_{33}^H \\ & & \mathbf{K}_{32}^V & \mathbf{K}_{33}^V \end{bmatrix} \quad (4.11)$$

where

$$\mathbf{K}_{11}^H = \begin{bmatrix} 4K_H + 2K_{HH} & -4K_H h_3 + 2K_{HH} h_2 & 0 \\ -4K_H h_3 + 2K_{HH} h_2 & 4K_H h_3^2 + 4K_V b_1^2 + 2K_{HH} h_2^2 + 2K_{VV} b_2^2 & 0 \\ 0 & 0 & 4K_H q_0^2 \end{bmatrix}$$

$$\mathbf{K}_{11}^V = \begin{bmatrix} 4K_V + 2K_{VV} & 0 \\ 0 & 4K_V q_0^2 \end{bmatrix}$$

$$\mathbf{K}_{21}^H = \begin{bmatrix} -2K_{HH} & -2K_{HH} h_2 & 0 \\ 2K_{HH} h_1 & 2K_{HH} h_1 h_2 - 2K_{VV} b_2^2 & 0 \\ -2K_{HH} s & -2K_{HH} s h_2 & 0 \end{bmatrix}$$

$$\mathbf{K}_{22}^H = \begin{bmatrix} 4K_{HH} & -4K_{HH} h_1 & 0 \\ -4K_{HH} h_1 & 4K_{HH} h_1 + 4K_{VV} b_2^2 & 0 \\ 0 & 0 & 4K_{HH} s^2 \end{bmatrix}$$

$$\mathbf{K}_{21}^V = \begin{bmatrix} -2K_{VV} & 0 \\ 2K_{VV} s & 0 \end{bmatrix}$$

$$\mathbf{K}_{22}^V = \begin{bmatrix} 4K_{VV} & 0 \\ 0 & 4K_{VV} s^2 \end{bmatrix}$$

$$\mathbf{K}_{32}^H = \begin{bmatrix} -2K_{HH} & 2K_{HH} h_1 & 2K_{HH} s \\ -2K_{HH} h_2 & 2K_{HH} h_1 h_2 - 2K_{VV} b_2^2 & 2K_{HH} s h_2 \\ 0 & 0 & 0 \end{bmatrix}$$

$$\mathbf{K}_{33}^H = \begin{bmatrix} 4K_H + 2K_{HH} & -4K_H h_3 + 2K_{HH} h_2 & 0 \\ -4K_H h_3 + 2K_H h_2 & 4K_H h_3^2 + 4K_V b_1^2 + 2K_{HH} h_2^2 + 2K_{VV} b_2^2 & 0 \\ 0 & 0 & 4K_H q_0^2 \end{bmatrix}$$

$$\mathbf{K}_{21}^V = \begin{bmatrix} -2K_{VV} & -2K_{VV}s \\ 0 & 0 \end{bmatrix}$$

$$\mathbf{K}_{33}^V = \begin{bmatrix} 4K_V + 2K_{VV} & 0 \\ 0 & 4K_V q_0^2 \end{bmatrix}$$

Where the meaning of all the terms that appears in the above matrices is specified in the figure (4.2).

Also in this case the damping matrix can be derived from the stiffness matrix replacing the stiffness coefficients ( $K_V$ ,  $K_H$ ,  $K_{VV}$ ,  $K_{HH}$ ) by damping coefficients ( $C_V$ ,  $C_H$ ,  $C_{VV}$ ,  $C_{HH}$ ), in which  $C_V$  and  $C_H$  are vertical and horizontal damping coefficients at each side of bogie in the first suspension system,  $C_{VV}$  and  $C_{HH}$  are vertical and horizontal damping coefficients at each side of car body in the second suspension system.

The terms of the vector  $\mathbf{P}_v$  that are the interaction forces transferred to the bogies by the first suspension system can be expressed in terms of the displacements and velocities of the wheel sets as

$$\mathbf{P}_v = \begin{bmatrix} 2C_H(\dot{Y}_{W1} + \dot{Y}_{W2}) + 2K_H(Y_{W1} + Y_{W2}) \\ 2C_H[b_1^2(\dot{R}_{XW1} + \dot{R}_{XW2}) - h_3(\dot{Y}_{W1} + \dot{Y}_{W2})] + 2K_H[b_1^2(R_{XW1} + R_{XW2}) - h_3(Y_{W1} + Y_{W2})] \\ 2C_H q_0(\dot{Y}_{W1} - \dot{Y}_{W2}) + 2K_H q_0(Y_{W1} - Y_{W2}) \\ 2C_V(\dot{Z}_{W1} + \dot{Z}_{W2}) + 2K_V(Z_{W1} + Z_{W2}) \\ 2C_V q_0(-\dot{Z}_{W1} + \dot{Z}_{W2}) + 2K_V q_0(-Z_{W1} + Z_{W2}) \\ 0 \\ 0 \\ 0 \\ 0 \\ 0 \\ 0 \\ 2C_H(\dot{Y}_{W3} + \dot{Y}_{W4}) + 2K_H(Y_{W3} + Y_{W4}) \\ 2C_H[b_1^2(\dot{R}_{XW3} + \dot{R}_{XW4}) - h_3(\dot{Y}_{W3} + \dot{Y}_{W4})] + 2K_H[b_1^2(R_{XW3} + R_{XW4}) - h_3(Y_{W3} + Y_{W4})] \\ 2C_H q_0(\dot{Y}_{W1} - \dot{Y}_{W2}) + 2K_H q_0(Y_{W1} - Y_{W2}) \\ 2C_V(\dot{Z}_{W3} + \dot{Z}_{W4}) + 2K_V(Z_{W3} + Z_{W4}) \\ 2C_V q_0(-\dot{Z}_{W3} + \dot{Z}_{W4}) + 2K_V q_0(-Z_{W3} + Z_{W4}) \end{bmatrix} \quad (4.12)$$

### 4.3 Bridge subsystem

As shown in *chapter 3*, when a finite element model of the bridge is used to study its dynamic behavior, the equation of motion of the bridge can be expressed as

$$\mathbf{M}_b \ddot{\mathbf{V}}_b + \mathbf{C}_b \dot{\mathbf{V}}_b + \mathbf{K}_b \mathbf{V}_b = \mathbf{P}_b \quad (4.13)$$

where  $\mathbf{M}_b$ ,  $\mathbf{C}_b$  and  $\mathbf{K}_b$  are the mass matrix, damping matrix and stiffness matrix of the bridge, respectively;  $\mathbf{V}_b$ ,  $\dot{\mathbf{V}}_b$  and  $\ddot{\mathbf{V}}_b$  represent the displacement, velocity and acceleration vectors of the bridge DOFs; and  $\mathbf{P}_b$  is the force vector transferred to the bridge.

In some finite element model thousands of nodes and elements are used, therefore the Eq. (4.13) could be a system of thousands equations. Due to the fact that it is often possible to describe an approximate dynamic response with just a few eigenmodes the system equations can often be substantially reduced. In large finite element models a reduction of the system equations saves a lot of computer time. However, excluding modes is a crucial action. It is necessary to select the eigenmodes that have the largest influence on the result. This could be done using the modal superposition methods assuming that only the first  $N_0$  modes of the bridge are contributing to the response. The equation of motion of the bridge can be now rewritten as follow:

$$\ddot{\mathbf{q}} + \mathbf{C}_b^* \dot{\mathbf{q}} + \mathbf{K}_b^* \mathbf{q} = \mathbf{P}_b^* \quad (4.14)$$

where it has been assumed that the eigenvectors are normalized with respect to the mass matrix  $\mathbf{M}_b$ . The vector  $\mathbf{q}$  collects the modal coordinates. The matrices  $\mathbf{C}_b^*$ ,  $\mathbf{K}_b^*$  and the vector  $\mathbf{P}_b^*$  are defined as follows:

$$\mathbf{C}_b^* = 2\nu\mathbf{\Omega}$$

$$\mathbf{K}_b^* = \mathbf{\Omega}^2$$

$$\mathbf{P}_b^* = \mathbf{\Phi}^T \mathbf{P}_b$$

where  $\mathbf{\Phi}$  is the  $N_{DOF} \times N_0$  matrix of eigenvectors and  $\mathbf{\Omega}$  is the  $N_0 \times N_0$  diagonal matrix of eigenvalues of the considered modes.

As regard  $\mathbf{P}_b$ , it is determined by position, movement status and mass of the wheel sets. As described in *chapter 3.2* knowing the position of the  $i$ th axle of the train it is possible to obtain the nodal forces vector by applying the Eqs. (3.1)-(3.4). Actually  $\mathbf{P}_b$  is composed of two terms,  $\mathbf{P}_b^{qs}$  refers to the quasi-static part of the force that is related to the weight of the  $i$ th axle of the train, and  $\mathbf{P}_b^{dy}$  related to the dynamic part of the force.

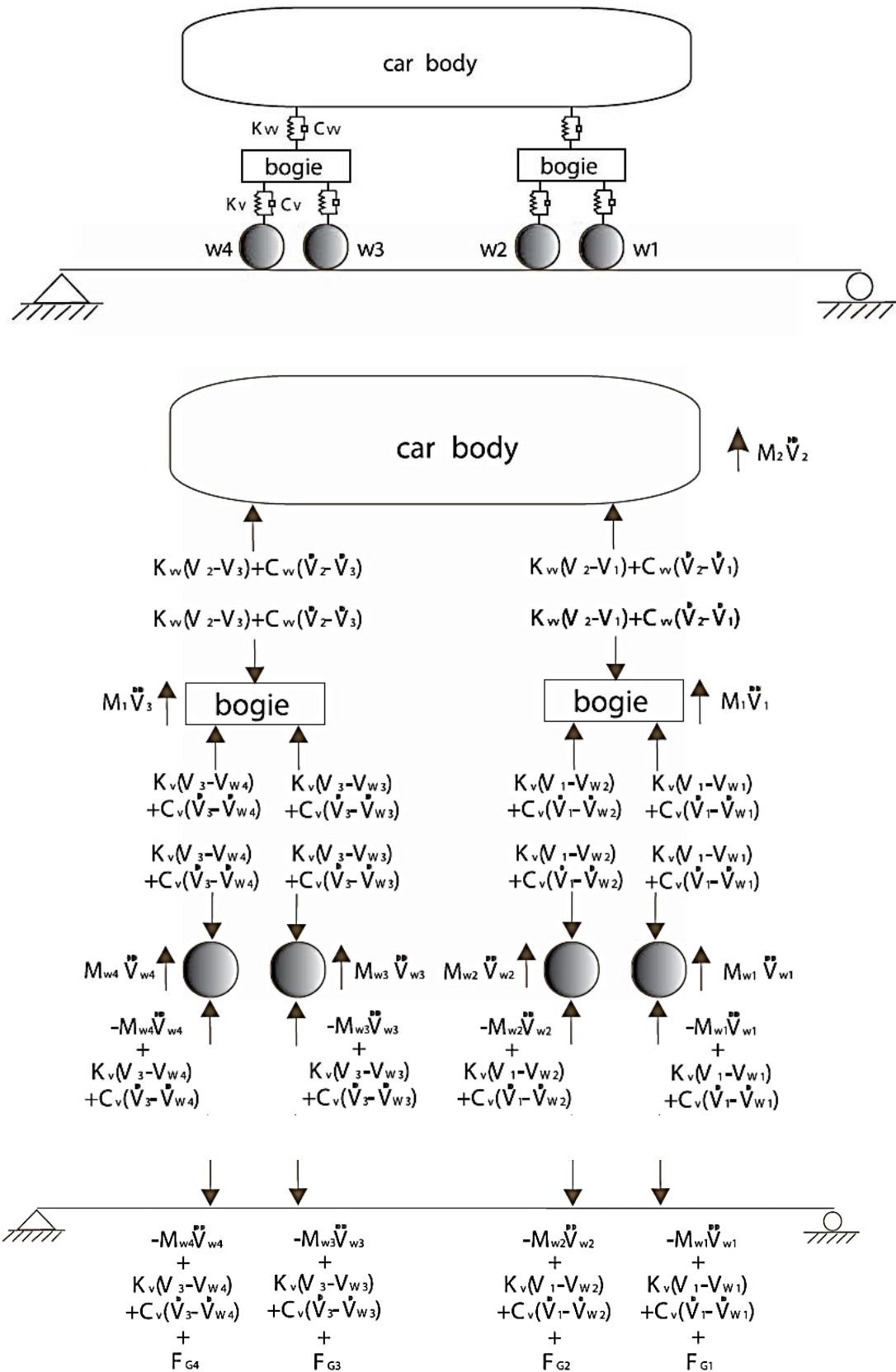


Figure 4.3: A simply supported beam subjected to a 3-DOF moving vehicle [2].

When considering a 3-DOF vehicle model of figure (4.3) the force  $\mathbf{P}_b$  transferred to the bridge can be written as

$$\mathbf{P}_b(t) = \sum_{i=1}^4 \mathbf{y}_i(t) F_{Gi} + \sum_{i=1}^4 \mathbf{y}_i(t) \left( -M_{Wi} \ddot{V}_{Wi} + K_V (V_j - V_{Wi}) + C_V (\dot{V}_j - \dot{V}_{Wi}) \right) \quad (4.15)$$

where  $\ddot{V}_{Wi}$  represents the acceleration of the  $i$ th wheel set;  $M_{Wi}$  and  $F_{Gi}$  represent the mass and the axle load of the  $i$ th wheel set, respectively, and  $V_j$  ( $j = 1|_{i=1,2}, j = 3|_{i=3,4}$ ) represents the displacement of the bogie, which is related to the first and second wheel axle displacement when considering the first boogie and to the third and fourth wheel axle displacement when considering the second boogie. The vector  $\mathbf{y}_i(t)$  is the  $N_{DOF} \times 1$  vector that transfers a moving unit load to nodal loads according to the position of the  $i$ th axle.

## 4.4 Computation of the coupled train-bridge system

In studying the dynamic response of the vehicle-bridge interaction system, two sets of equations of motion can be written, one for the bridge Eq. (4.13) and the other for the vehicles Eq. (4.1). It is the interaction or *contact forces* existing at the contact points of the two subsystems that make the two sets of equations coupled. The algorithms to carry out this calculation can be classified in two main groups: (a) those based on an *uncoupled iterative procedure* and (b) those based on the solution of the *coupled system*.

Algorithms based on an *uncoupled iterative procedure* treat the equations of motion of the vehicle and the bridge as two subsystems and solve them separately using a direct integration scheme. The compatibility conditions and equilibrium equations at the interface between the vehicle wheels and railway track are satisfied by an iterative procedure. One possible algorithm is illustrated in figure (4.4). In the first step of the iterative procedure, the bridge response given by the Eq. (4.13) is computed with only  $\mathbf{P}_b^{qs}$ , because the vehicle is not yet excited. Assuming that there is no jumping between the wheels and the railway track, the wheels displacements and velocities can be computed, knowing the nodal displacements and velocities of the bridge, using the following beam shape functions

$$N_1 = 1 - 3\frac{x^2}{L^2} + 2\frac{x^3}{L^3} \quad (4.16)$$

$$N_2 = 3\frac{x^2}{L^2} - 2\frac{x^3}{L^3} \quad (4.17)$$

$$N_3 = -x + 2\frac{x^2}{L} - \frac{x^3}{L^3} \quad (4.18)$$

$$N_4 = \frac{x^2}{L} - \frac{x^3}{L^3} \quad (4.19)$$

where  $x$  represents the generic position of the  $i$ th axle in between two successive nodes of the bridge. Then the right term of Eq. (4.1) can be computed and Eq. (4.1) can be solved for the displacement, velocity and acceleration of the vehicle DOFs. Then Eq. (4.13) is solved again considering also  $\mathbf{P}_b^{dy}$ , obtaining the bridge response. This procedure is repeated for a number of iterations at each time step, until some convergence criterion is met (for example, until the difference between the bridge deflection of two successive iterations is sufficiently small).

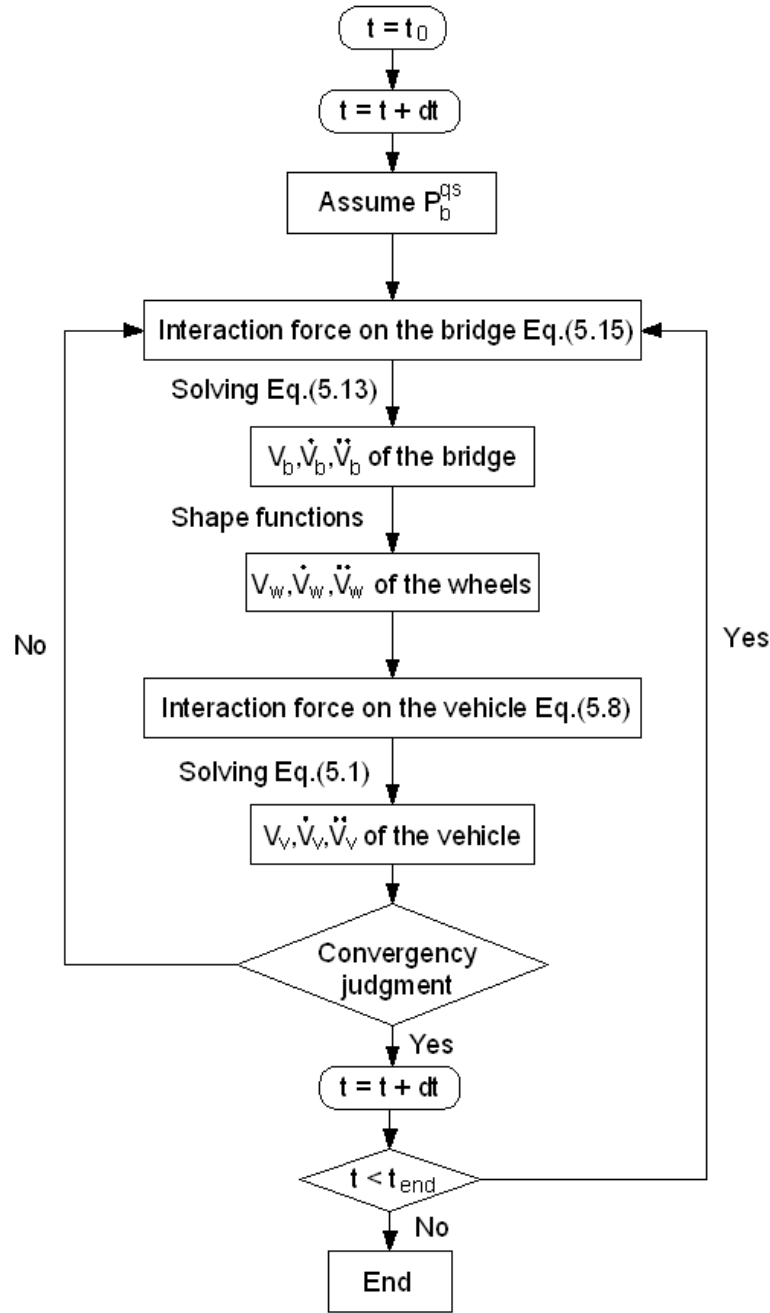


Figure 4.4: Flowchart of the iterative solution procedure [3].

Algorithms based on the solution of the *coupled system* are based on the solution of a unique system matrix at each point in time. The system matrix changes as the vehicle moves and is time-dependent. This procedure can be carried without any iteration solving the system given below for example with Newmark method

$$\begin{bmatrix} \mathbf{M}_b & \mathbf{0} \\ \mathbf{0} & \mathbf{M}_v \end{bmatrix} \begin{bmatrix} \ddot{\mathbf{V}}_b \\ \ddot{\mathbf{V}}_v \end{bmatrix} + \begin{bmatrix} \mathbf{C}_b & \mathbf{C}_{vb} \\ \mathbf{C}_{bv} & \mathbf{C}_v \end{bmatrix} \begin{bmatrix} \dot{\mathbf{V}}_b \\ \dot{\mathbf{V}}_v \end{bmatrix} + \begin{bmatrix} \mathbf{K}_b & \mathbf{K}_{vb} \\ \mathbf{K}_{bv} & \mathbf{K}_v \end{bmatrix} \begin{bmatrix} \mathbf{V}_b \\ \mathbf{V}_v \end{bmatrix} = \begin{bmatrix} \mathbf{P}_b \\ \mathbf{P}_v \end{bmatrix} \quad (4.20)$$

where  $\mathbf{C}_{vb}$ ,  $\mathbf{C}_{bv}$ ,  $\mathbf{K}_{vb}$  and  $\mathbf{K}_{bv}$  are coupled matrices attributed to the interaction between the bridge and train. More details of this method are given in [11] and [12].

An alternative approach that leads to considerable savings in computational time is to implement the interaction on an element level rather than on a global level [9]. An interaction element is defined as that bridge element in contact with a vehicle wheel. Those bridge elements that are not directly under the action of vehicle wheels remain unaltered in the global matrixes of the system. The interaction element is characterized by two sets of equations: those of the bridge element and those of the moving vehicle above the bridge element. The DOFs of the moving vehicle can be solved in time domain using Newmark method, and then, the DOFs of the vehicle that are not in direct contact with the bridge are eliminated and condensed to the DOFs of the associated bridge element via the method of dynamic condensation. The interaction element has the same number of DOFs as the original bridge element and it can be directly assembled with the other bridge elements into the global matrix, while retaining symmetry property that is lost when condensation takes place on a global level.

# 5. PONTELAGOSCURO RAILWAY BRIDGE

## 5.1 Description of the bridge

In this section a brief description of the structure that will be used to carry out the dynamic analyses is given.

The structure considered is the steel bridge on the Bologna-Padova railway line that crosses the Po river and connects the areas of Pontelagoscuro and Occhiobello nearby Ferrara and Rovigo, respectively.



**Figure 5.1:** Pontelagoscuro side bridge view.

The Bologna-Padova railway line is an important link between the Nord-East area of Italy and the Nord-South national line Milano-Roma. For this reason in recent years significant infrastructural and technological investments have been planned upon this railway line in order to supply the transport demand in terms of passengers and freight trains.



**Figure 5.2:** View of the oldest bridge on the left and the most recent on the right.

The viaduct is composed of 9 truss girder bridges; the total length is about 610 m; seven 75.60 m long bridges compose the inner part of the viaduct, while two 59.4 m long bridges are located at the ends of the viaduct. The longest bridges are 9.60 m high, it is composed by 7 panels of 10.80 m. The shorter bridge is composed by 6 panels of 9.90 m and it is 7.50 m high.; in the following, all the analyses will performed with reference to only this kind of structure.



**Figure 5.3:** Lateral span bridge view.

The bridge and each of its element was realized by connecting different kinds of hot-rolled profiles, obtained by the combination of thin plates with variable geometry along with L and I cross section shape elements.

The structure is composed by two main truss girders oriented in the longitudinal direction connected by transversal elements which form a closed cage sections as in figure (5.4).

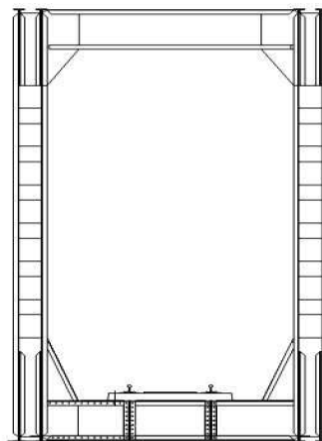


**Figure 5.4:** Internal elevation of the bridge.

The truss girders are delimited at the top by an upper chord which are obtained combining by means of rivets four plates with four L angular profiles forming a box shaped beam as in figure (5.5).



**Figure 5.5:** Detail of the upper chords.

This kind of cross section shape allows easy connections between elements and it guarantees an high moment of inertia in both directions in order to prevent instability phenomena.

In the lower part the vertical trusses are delimited by a lower chord, shown in figure (5.6) that are very similar to the upper chord



**Figure 5.6:** Detail of the lower chords.

Then the upper and lower chords are linked together by vertical and diagonal elements.

The diagonal elements, as it is possible to see in figure (5.7), have a cross section composed by four L-shaped profile connected by means of plates. Actually it can be

distinguished different kinds of diagonal elements, in fact the outer diagonals have connecting plates along all the length of the elements, instead the inner diagonals have connecting plates at regular intervals.



**Figure 5.7:** Detail of the diagonal elements.

The vertical elements exhibit a double T cross section made by L profile coupled two by two and connected by means of plates as in figure (5.8). Also in this case there is difference between the outer vertical elements, which have a full web, and the inner ones which have lightened web done by plates at regular intervals.



**Figure 5.8:** Detail of the vertical elements.

As already said in the upper and lower zone, there are struts and floor beams, respectively, which connect the truss girders, in order to create a closed box-shaped profile. There are struts and floor beams each 4.95 meters, in this way transversal elements and web elements are connected at the same time at the same node. The struts are consisting of two angular profile coupled two by two, with a web consisting of plates riveted with the profile as in figure (5.9).



**Figure 5.9:** Detail of the struts elements.

Actually the floor beams have a full web cross section while the struts have empty webs at regular intervals.

Also there are an upper and a lower braced systems, which connect the two truss girders, and create a sort of horizontal truss system to face the horizontal loads.



**Figure 5.10:** Detail of the braced systems.

The braced systems elements consist of four L cross section profiles riveted together, figure (5.10).

As in figure (5.11) in each node are connected the lower or the upper chord, three wall elements (diagonals and verticals), a struts or roof beam, and at regular intervals, the braced elements. In order to create the link between the various elements gusset plates are needed.



**Figure 5.11:** Detail of the nodes.

Each span of the entire bridge rests at the two ends on pillars that transfer the loads to the soil. The connection between the bridge structure and the pillar is done by support devices shown in figure (5.12). At one end the support device is fix and it can be schematized as an hinge, while at the other end the support is amenable to a roller constraint.



**Figure 5.12:** Detail of the support devices.

Moreover, along with the structural elements just described, there are also non structural or secondary elements as sleepers, railway tracks, platforms and parapets.

## 5.2 Experimental data

Dynamic analysis of structure are usually performed using suitable finite elements models. When dealing with existing structures it is possible to obtain their dynamic properties in terms of vibration frequencies and mode shapes, so that the numerical models can describe as much as possible the real structure. In this regard the bridge has been monitored. In particular some accelerometers have been positioned on the bridge in eight points. The scheme of the measuring points is depicted in figure (5.13).

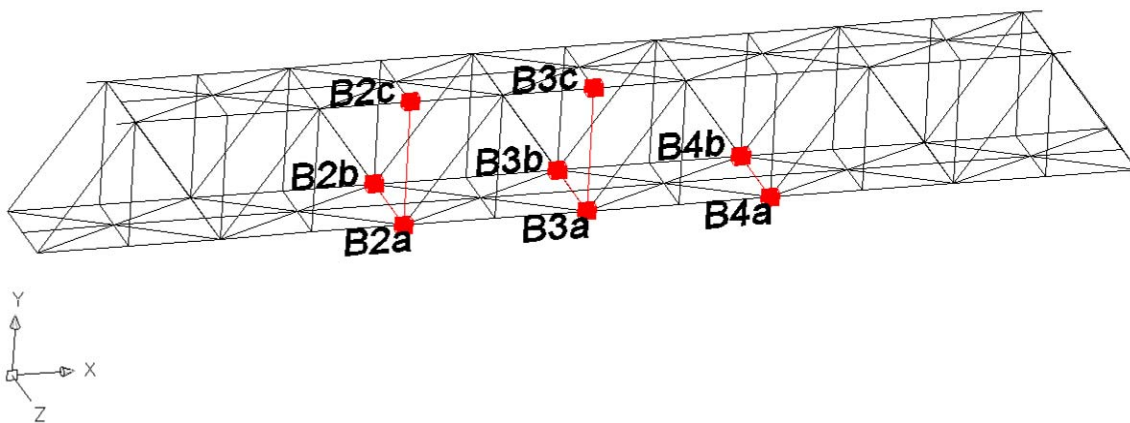


Figure 5.13: Measuring points scheme.

Recording the accelerations of the ambient free vibration of the bridge it has been possible to obtain by means of dynamic identification technique the vibration frequencies and modes as well as the damping ratio of each mode.

In table (5.1) are reported the first four frequencies of vibration that will be taken into account.

<i>Experimental data</i>			
	<b>Frequency</b>	<b>Damping ratio</b>	<b>Mode type</b>
<b>1<sup>st</sup></b>	2.143 Hz	0.65 %	First Lateral
<b>2<sup>nd</sup></b>	3.857 Hz	0.87 %	Vertical
<b>3<sup>rd</sup></b>	4.307 Hz	0.54 %	Torsional
<b>4<sup>th</sup></b>	4.700 Hz	1.90 %	Second Lateral

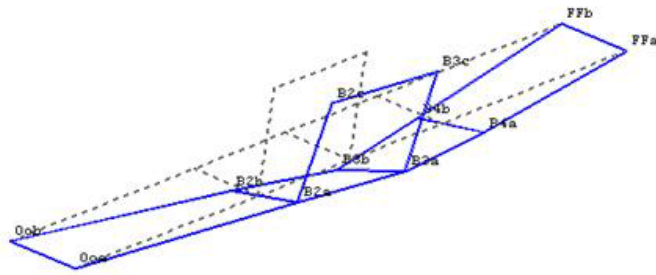
Table 5.1: Experimental frequencies and damping ratios.

In table (5.2) the experimental eigenvectors that describe the modal shapes of vibration associated with the first four frequencies are reported, the  $z$  and  $y$  axis are in agreement to that showed in figure (5.13).

<i>Experimental mode shapes</i>				
	<b>1<sup>st</sup> Mode</b>	<b>2<sup>nd</sup> Mode</b>	<b>3<sup>rd</sup> Mode</b>	<b>4<sup>th</sup> Mode</b>
<b>B2a (z)</b>	25.2	1.57	18.7	-11.4
<b>B2a (y)</b>	-5.77	9.99	7.08	3.42
<b>B2b (y)</b>	3.09	8.04	-22.3	-2.03
<b>B2c (z)</b>	37.1	-0.65	-28.7	-18.6
<b>B3a (z)</b>	34.7	2.26	30.2	0.64
<b>B3a (y)</b>	-6.32	14.4	8.14E	1.04
<b>B3b (y)</b>	8.33	11.8	-26.4E	0.19
<b>B3c (z)</b>	46.0	-1.50	-28.6	-0.82
<b>B4a (z)</b>	26.8	0.87	15.9	12.1
<b>B4a (y)</b>	-4.35	9.55	1.55	-0.76
<b>B4b (y)</b>	3.35	8.06	-23.4	2.03

**Table 5.2:** Experimental mode shapes.

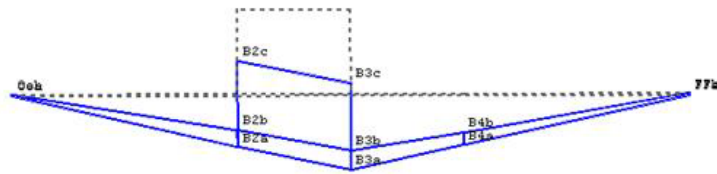
In figure (5.14) the configuration assumed by the bridge in each of the first four modal shapes are reported. The dashed lines represent the undeformed configuration while the continues lines the deformed one.



*1<sup>st</sup> mode*

*First Lateral*

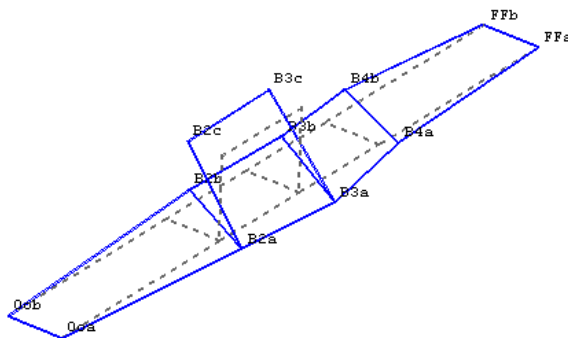
*Frequency 2.143 Hz*



*2<sup>nd</sup> mode*

*Flexural*

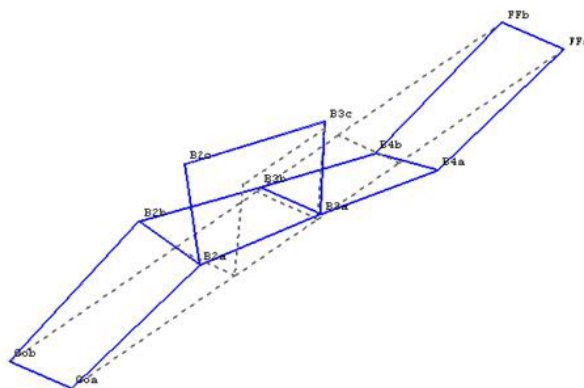
*Frequency 2.857 Hz*



*3<sup>rd</sup> mode*

*Torsional*

*Frequency 4.307 Hz*



*4<sup>th</sup> mode*

*Second Lateral*

*Frequency 4.700 Hz*

**Figure 5.14:** Deformed configuration in the first 4 modals shapes.

### 5.3 Bridge finite elements model

In *section 5.1* the bridge, object of the present study, has been widely described. In order to carry out dynamic analysis of the bridge subjected to crossing trains, a finite elements model that well represents the real structure is needed.

In order to set up a numerical model of the bridge it is been useful to analyze in detail the role of each element in the whole state, figure(5.15), as well as the geometry and the section dimensions of each member, figures (5.16) (5.17).

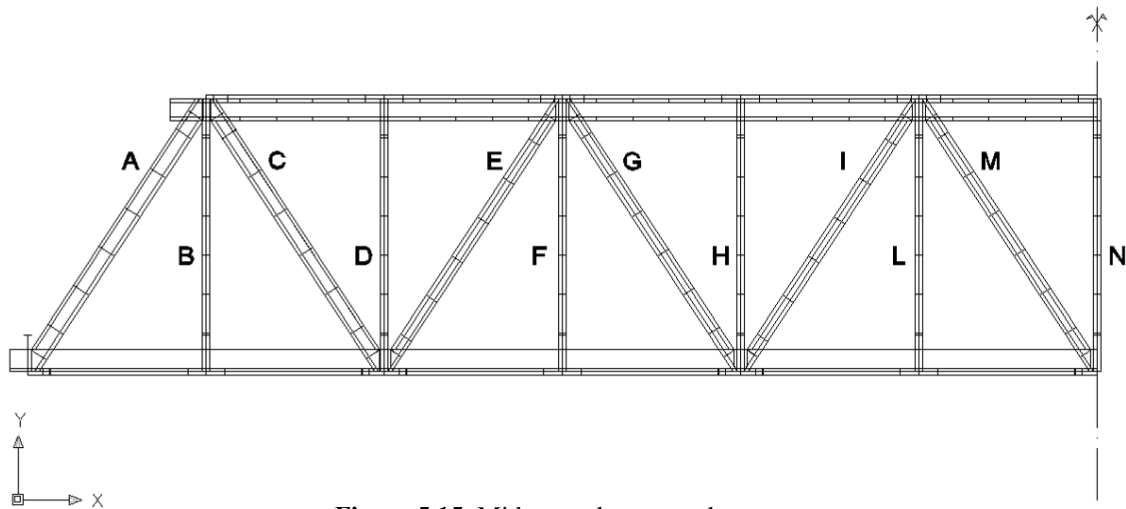


**Figure 5.15:** Mid span elements scheme.

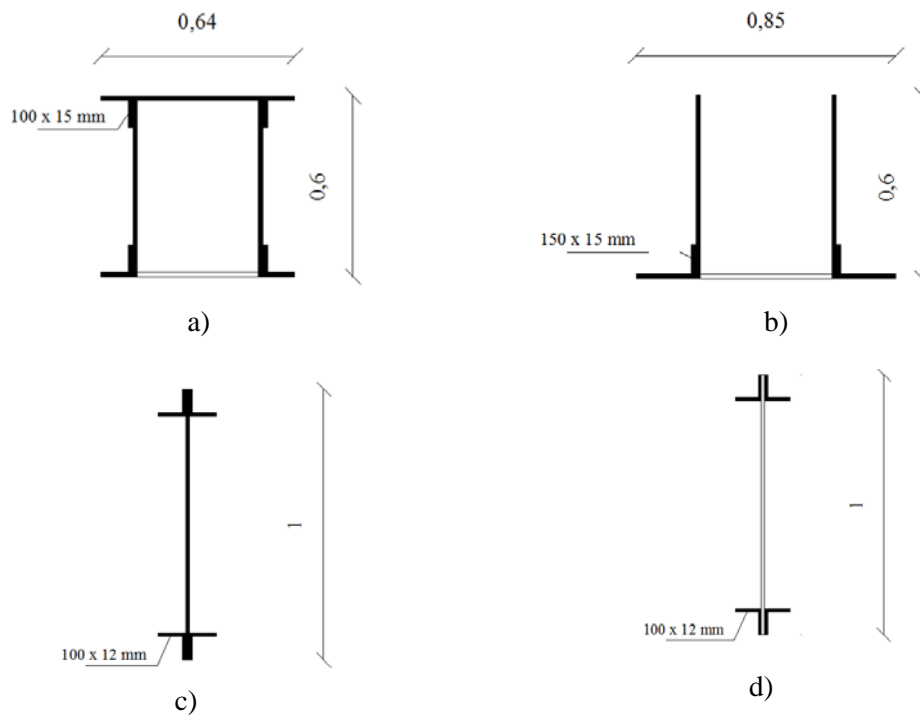


**Figure 5.16:** a), b) Upper, lower chord; c), d) Struts, roof beams.

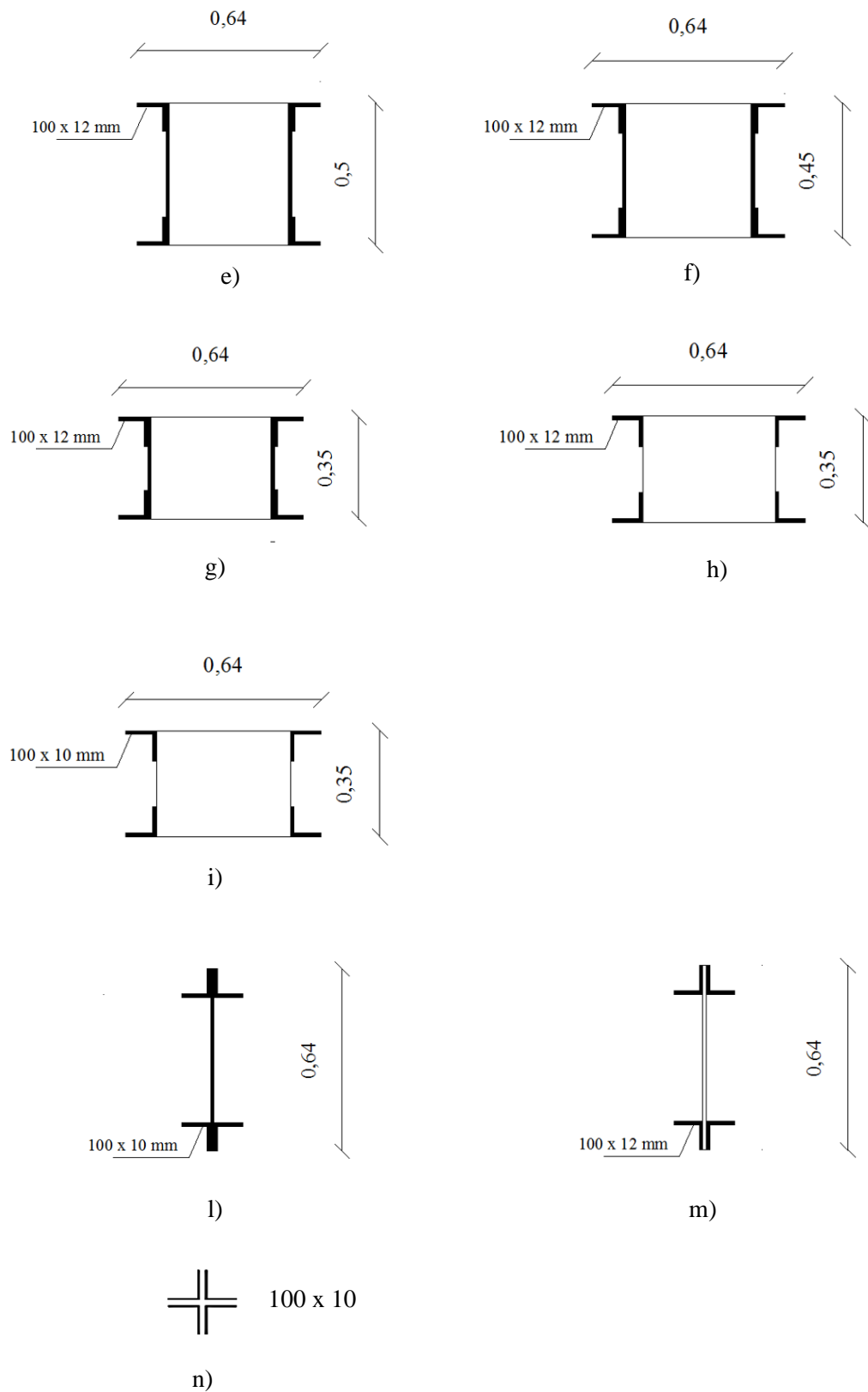


**Figure 5.17:** e) Diagonals A; f) Diagonals C; g) Diagonals E; h) Diagonals G, I; i) Diagonals M; l) Verticals B; m) Verticals D, F, H, L, N; n) Upper, bottom bracing system elements

As regards the material properties, the elastic properties listed in table (5.3) are assumed.

Structural steel	Elastic modulus $E$ [N/mm <sup>2</sup> ]	Poisson's ratio $\nu$	Density $\rho$ [Kg/m <sup>3</sup> ]
S 235	200000	0.25	7850

**Table 5.3:** Elastic properties of the structural steel.

Given the mechanical and geometrical characteristics of the several elements, as well as the bridge's layout, it has been possible to create a finite elements model. The model has been done using four nodes *shell* elements, except for the bracing elements done by *beam* elements. In this way a very sophisticated model closer to the real structure is been obtained.

In figure (5.18) a general view of the model realized with the finite elements software is shown.

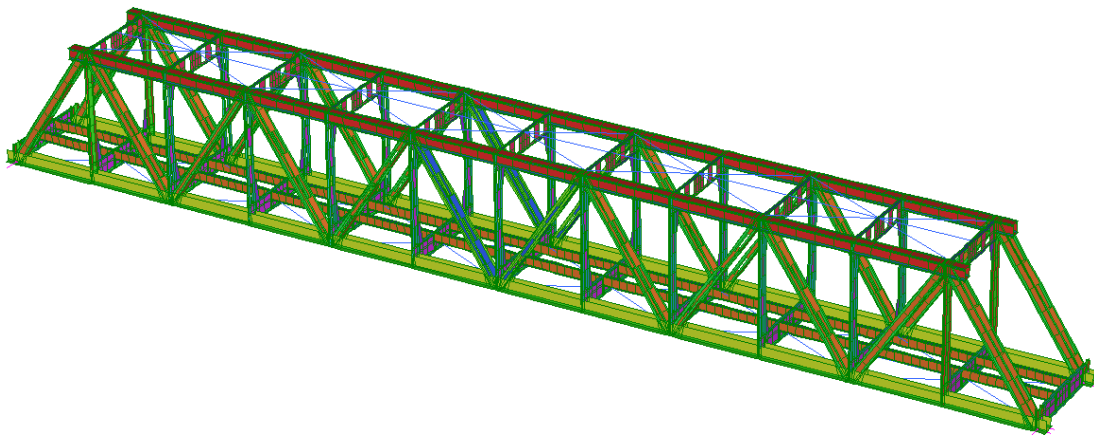


**Figure 5.18:** Bridge finite elements model.

Actually at this state of the art the finite elements model is not yet accurate and able to represent the real structure. In fact computing the frequencies and the deformed modal shapes of the modeled structure it can be possible to see that they are not in agreement to those of the real one. In fact can be seen in table (5.4) the frequencies of the model are higher in respect to those of the real structure. The reason lies in the fact that in the model the masses of all the non-structural elements are not considered resulting in a stiffer model.

Other details can influence the dynamic properties of the model, as for example the boundary conditions.

Mode	Experimental frequency	FEM frequency	Error
1 <sup>st</sup> First Lateral	2.143 Hz	3.306 Hz	~ 54 %
2 <sup>nd</sup> Vertical	3.857 Hz	5.564 Hz	~ 44%
3 <sup>rd</sup> Torsional	4.307 Hz	5.766 Hz	~ 34%
4 <sup>th</sup> Second Lateral	4.700 Hz	6.134 Hz	~ 31%

**Table 5.4:** Experimental and model frequencies difference.

Therefore the model must be calibrated through a suitable process so that it will reflect almost the same dynamic behavior of the real structure. This optimization algorithm is explained in detail in *chapter 6*.

## 6. OPTIMIZATION PROCESS

### 6.1 Introduction

As it has been possible to see in *Section 5* often the finite elements models don't fit correctly the dynamic behavior of the real structure. Therefore the model has to be adjusted performing an optimization process of those system parameters that mainly influence the structural behavior. Actually the optimization problem is based on an objective function to be minimized (cost function). In modal identification problems, the objective function to be minimized is the distance between modal parameters obtained from experimental tests and those given by a numerical model of the structure.

When the cost function is non differentiable or not explicitly defined, direct search approaches are very effective methods. Between them, genetic algorithms and evolution strategies are considered very promising numerical methods both in terms of efficiency and robustness, [13] and[14].

In *Section 6.2* the process used to solve the identification problem is described in details. Among all the evolution and genetic algorithms, the so called *Differential Evolution Algorithm* (DE) has been chosen.

Differential evolution algorithms are parallel direct search methods where  $N$  different vectors collecting the unknown parameters of the system are used in the minimization process. The vector population is chosen randomly or by adding weighted differences between vectors obtained from the old population.

## 6.2 Differential evolution algorithm

Differential Evolution is a heuristic direct search approach where NP vectors indicated by

$$\mathbf{x}_{i,G}, \quad i = 1, 2, \dots, NP$$

are used at the same time. Subscript  $G$  indicates the  $G^{\text{th}}$  generation of parameter vectors, called population. Vectors  $\mathbf{x}_{i,G}$  have  $D$  components, being  $D$  the number of optimization parameters.

The algorithmic scheme of the DE approach is shown in figure (6.1).

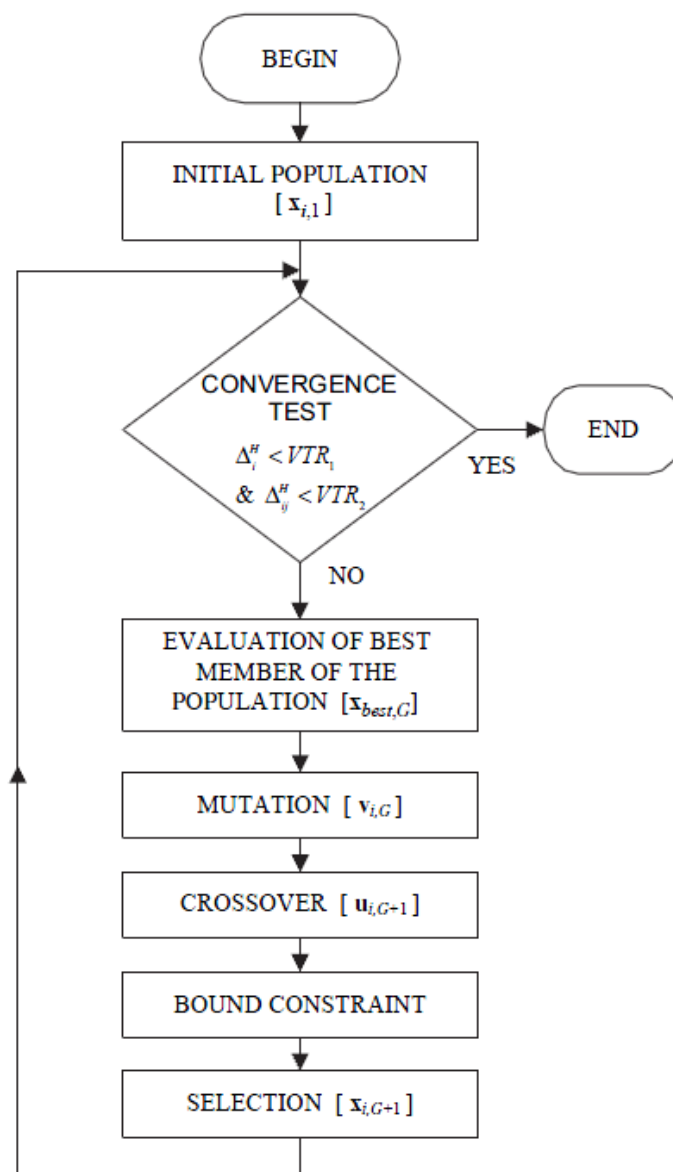


**Figure 6.1:** Flowchart of Differential Evolution Algorithm.

First of all, the initial population ( $NP$  vectors) is chosen randomly over the definition domain of identification parameters.

Then, DE generates a new set of parameter vectors (called *mutant vectors*) by the *Mutation* operation, in fact for each vector of  $G^{th}$  population

$$\mathbf{x}_{i,G}, \quad i = 1, 2, \dots, NP$$

a new trial vector  $\mathbf{v}_{i,G}$  is generated by adding to  $\mathbf{x}_{i,G}$  the difference between two other vectors of the same population. Actually three different combination strategies can be used for the mutation process: the “random” combination, the “best” combination, and an intermediate combination called “best-to-rand”.

In the random combination, figure (6.2), the mutant vector is generated according to the following expression

$$\mathbf{v}_{i,G+1} = \mathbf{x}_{r_1,G} + F \cdot (\mathbf{x}_{r_2,G} - \mathbf{x}_{r_3,G}) \quad (6.1)$$

where

$$r_1, r_2, r_3 \in \{1, 2, \dots, NP\}$$

are mutually different integer numbers. Moreover,  $F$  is a positive constant (scale parameter) controlling the amplitude of the mutation. Usually the scale parameter  $F$  is taken equal to 0.8.

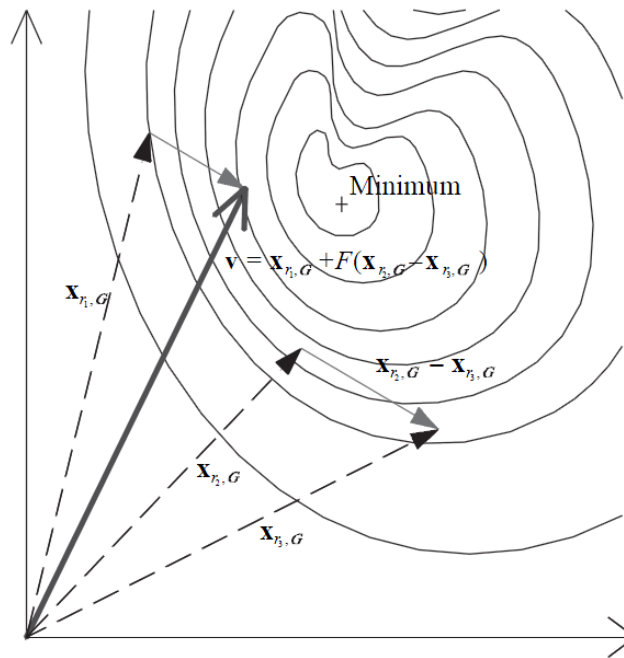


**Figure 6.2:** Mutation operation (random combination).

“Best” combination is similar to random combination, but the mutant vector is defined as:

$$\mathbf{v}_{i,G+1} = \mathbf{x}_{best,G} + F \cdot (\mathbf{x}_{r_1,G} - \mathbf{x}_{r_2,G}) \quad (6.2)$$

where  $\mathbf{x}_{best,G}$  is the vector giving the minimum value of the objective function (best vector) of  $G^{th}$  population. Finally, in the “best-to-rand” combination, the mutant vector is generated according to the expression:

$$\mathbf{v}_{i,G+1} = \mathbf{x}_{i,G} + F \cdot (\mathbf{x}_{best,G} - \mathbf{x}_{i,G}) + F \cdot (\mathbf{x}_{r_1,G} - \mathbf{x}_{r_2,G}) \quad (6.3)$$

The effectiveness of one method depends on the regularity of the objective function. For regular functions with only one (global) minimum, “best” combination converges more rapidly, because the best vector obtained from the previous generation is taken as the basic vector. In the presence of local minima, “random” or “best-to-rand” combinations are best choices, because convergence to local minima can be avoided.

Then, in the *Crossover* operation, a new set of trial vectors is generated by selecting some components of mutant vectors and some of original vectors. This is done in order to increase the diversity of the vectors. The *trial vector*  $\mathbf{u}_{i,G+1}$  is obtained by randomly exchanging the values of optimization parameters between the original vectors of the population  $\mathbf{x}_{i,G}$  and those of mutant population  $\mathbf{v}_{i,G+1}$ , figure (6.3):

$$\mathbf{u}_{i,G+1} = (u_{1i,G+1}, u_{2i,G+1}, \dots, u_{Di,G+1})$$

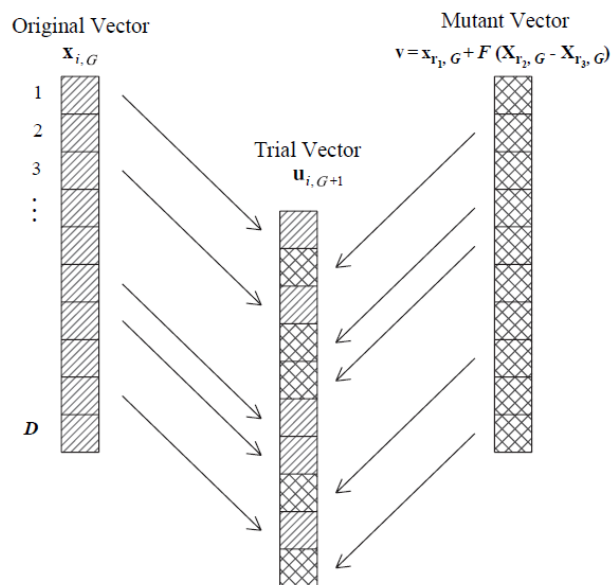


**Figure 6.3:** Crossover operation.

where

$$\mathbf{u}_{ji,G+1} = \begin{cases} v_{1i,G+1} & \text{if } rand(j) \leq CR \\ x_{ji,G} & \text{if } rand(j) > CR \end{cases}$$

The subscript  $j=1,2,\dots,D$ , where  $D$  is the number of optimization parameters, and  $u_{ji}$  is the  $j^{th}$  component of vector  $\mathbf{u}_i$ . Moreover,  $rand(j)$  is the  $j^{th}$  value of a vector of uniformly distributed random numbers, and  $CR$  is the crossover constant, with  $0 < CR < 1$ . Constant  $CR$  indicates the percentage of mutations considered in the trial vector.

*Selection* operation is then used to decide if a vector  $\mathbf{u}_i$  may be element of new population of generation  $G+1$ , each vector  $\mathbf{u}_{i,G+1}$  is compared with the previous vector  $\mathbf{x}_{i,G}$ . If vector  $\mathbf{u}_{i,G+1}$  gives a smaller value of objective function  $H$  than  $\mathbf{x}_{i,G}$ ,  $\mathbf{u}_{i,G+1}$  is selected as the new vector of population  $G+1$ ; otherwise, the old vector  $\mathbf{x}_{i,G}$  is retained:

$$\mathbf{x}_{i,G+1} = \begin{cases} \mathbf{u}_{i,G+1} & \text{if } H(\mathbf{u}_{i,G+1}) < H(\mathbf{x}_{i,G}) \\ \mathbf{x}_{i,G} & \text{if } H(\mathbf{u}_{i,G+1}) \geq H(\mathbf{x}_{i,G}) \end{cases}$$

with  $i=1,2,\dots,NP$ .

In the *convergence rule*, values of the objective function obtained from the population  $G+1$  are compared. Vectors are ordered depending on values of objective function as:

$$\tilde{\mathbf{x}}_{1,G+1} < \tilde{\mathbf{x}}_{2,G+1} < \dots < \tilde{\mathbf{x}}_{NP,G+1}$$

such that:

$$H(\tilde{\mathbf{x}}_{1,G+1}) < H(\tilde{\mathbf{x}}_{2,G+1}) < \dots < H(\tilde{\mathbf{x}}_{NP,G+1})$$

Convergence rule is then based on the difference of values  $H$  of the objective function of the first  $NC$  vectors and the distances between the same vectors,  $NC$  being the number of controlled vectors. The first, convergence test can be expressed as:

$$\Delta_i^H = \frac{|H(\tilde{\mathbf{x}}_{i,G+1}) - H(\tilde{\mathbf{x}}_{i+1,G+1})|}{|H(\tilde{\mathbf{x}}_{i,G+1})|} < VTR_1 \quad (6.4a)$$

where  $i=1,\dots,NC$  and  $VTR_1$  is the prescribed precision.

Control of values of objective function  $H$  only can be insufficient when the object function has a low gradient close to the minimum solution. For this reason, convergence requires also that the relative distance between the components of the first  $NC$  vectors is small, i.e.:

$$\Delta_{ij}^x = \frac{|\tilde{x}_{ji,G+1} < \tilde{x}_{ji+1,G+1}|}{|\tilde{x}_{ji,G+1}|} < VTR_2 \quad (6.4b)$$

*Bound constraint* usually is used in engineering applications, so that the optimization parameters are constrained to belong in given intervals, i.e.,

$$x_{j,G} \in [x_{j,min}, x_{j,max}]$$

where  $j = 1, 2, \dots, D$  and  $D$  is the number of the optimization parameters.

Introducing bound constraints is useful in order to restrain the analysis to ranges of identification parameters which are meaningful from the physical point of view. To this purpose, a projection algorithm is introduced. When a vector out of range after the mutant operation is obtained, its projection on the prescribed interval of parameters is considered, figure (6.4).

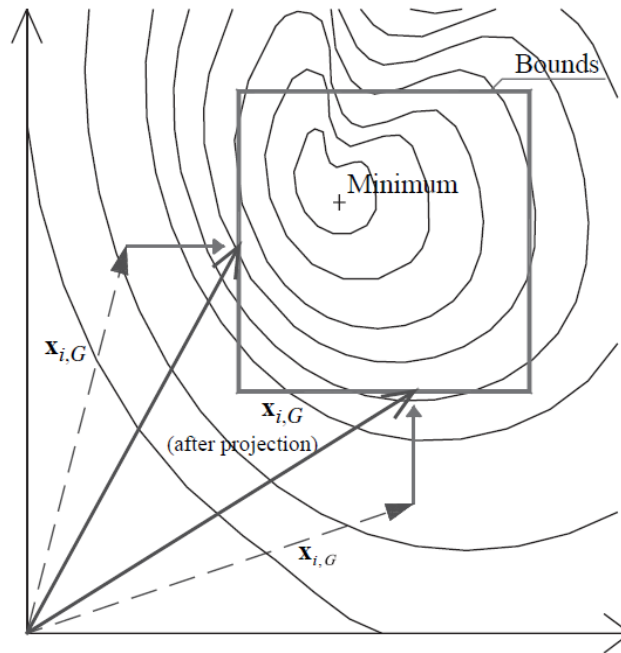


**Figure 6.4:** Bound constraint procedure.

### 6.3 The response surface method

The basic concept of the response surface method is to approximate the original complex or implicit cost function using a simple and explicit interpolation function. The idea of the surface response method (RSM) is that a cost function can be defined, such as:

$$\mathbf{H} = g(\mathbf{x}) \quad (6.5)$$

where  $\mathbf{x}$  denotes the  $D$ -dimensional vector of design parameters and  $g(\mathbf{x})$  is called response function. If  $g(\mathbf{x})$  is a continuous and differentiable function, it can be locally represented with a Taylor series expansion from an arbitrary point  $\mathbf{x}_k$ :

$$H = g(\mathbf{x}_k) + \nabla g(\mathbf{x}_k)^T \mathbf{p} + \frac{1}{2} \mathbf{p} \nabla^2 g(\mathbf{x}_k) \mathbf{p} \quad (6.6)$$

where  $\nabla g(\mathbf{x}_k)$  and  $\nabla^2 g(\mathbf{x}_k)$  are, respectively, the gradient vector which contains the first-order partial derivatives of function  $g$  and the Hessian matrix (second-order partial derivatives) evaluated at  $\mathbf{x}_k$ . Many practical evaluation techniques are available to define  $g(\mathbf{x})$ . Among those methods, reduction of Eq. (6.6) to a polynomial expression is the idea of RSM.

In classical RSM, the response surface is obtained by combining first or second order polynomials fitting the objective function defined in a set of sampling points. Second order approximations are commonly used in structural problems due to the computational efficiency with acceptable accuracy. Higher order polynomials are rarely used because the number of coefficients to be determined strongly increases with the order. Furthermore, some authors used quadratic polynomials without the cross terms, originating incomplete polynomials.

Adopting a second-order approximation function, Eq. (6.6) can be written as follows:

$$H = \frac{1}{2} \mathbf{x}^T \mathbf{Q} \mathbf{x} + \mathbf{L}^T \mathbf{x} + \beta_0 \quad (6.7)$$

where  $\mathbf{Q}$  is a  $D \times D$  coefficient matrix collecting the quadratic terms,  $\mathbf{L}$  is a  $D$ -dimension vector of linear terms and  $\beta_0$  is a constant. Without loss of generality and for the sake of simplicity, in the following only 2 parameters ( $x_1, x_2$ ) will be considered. Therefore, Eq.(6.7) can be written as follows:

$$H = \beta_0 + \beta_1 x_1 + \beta_2 x_2 + \beta_3 x_1^2 + \beta_4 x_2^2 + \beta_5 x_1 x_2 \quad (6.8)$$

where coefficients  $\beta$  are unknowns. In this method, response surface function includes the first and second order terms.

If  $NS$  observations are available, Eq. (6.8) can be expressed in a linear matrix notation as:

$$\mathbf{H} = \mathbf{Z} \cdot \boldsymbol{\beta} \quad (6.9)$$

where:

$$\mathbf{Z} = \begin{bmatrix} 1 & x_{1,1} & x_{2,1} & x_{1,1}^2 & x_{2,1}^2 & x_{1,1}x_{2,1} \\ 1 & x_{1,2} & x_{2,2} & x_{1,2}^2 & x_{2,2}^2 & x_{1,2}x_{2,2} \\ \dots & \dots & \dots & \dots & \dots & \dots \\ 1 & x_{1,NS} & x_{2,NS} & x_{1,NS}^2 & x_{2,NS}^2 & x_{1,NS}x_{2,NS} \end{bmatrix} \quad (6.10)$$

and

$$\mathbf{H} = \begin{bmatrix} H_1(x_{1,1}, x_{2,1}) \\ H_2(x_{1,2}, x_{2,2}) \\ \vdots \\ H_{NS}(x_{1,NS}, x_{2,NS}) \end{bmatrix} \quad (6.11)$$

And the vector  $\boldsymbol{\beta}$  collects the unknown parameters of the response surface determined by applying the least square estimates method:

$$\boldsymbol{\beta} = (\mathbf{Z}^T \mathbf{Z})^{-1} \mathbf{Z}^T \mathbf{H} \quad (6.12)$$

In Eq.(6.12), all coefficients  $\boldsymbol{\beta}$  have equal weight. However, a good RSM must be generated such that it describes the cost function well close to the solution point. The following weighted regression method is proposed to determine the coefficients of the RSM:

$$\boldsymbol{\beta} = (\mathbf{Z}^T \mathbf{W} \mathbf{Z})^{-1} \mathbf{Z}^T \mathbf{W} \mathbf{H} \quad (6.13)$$

where  $\mathbf{W}$  is an  $NS \times NS$  diagonal matrix of weight coefficients. For them, the following expression can be used:

$$w_i = \exp\left(-\frac{g(\mathbf{x}_i) - H_{best}}{H_{best}}\right) \quad (6.14)$$

where

$$H_{best} = \min(g(\mathbf{x}_i)) \quad (6.15)$$

Many algorithms have been proposed to select appropriate set of sampling points  $\mathbf{x}_k$ , in order to obtain better fitting of response function, [17].

## 6.4 DE algorithm with a second-order approximation

The RSM methodology is introduced in Differential Evolution algorithm to improve performance in term of speed rate and to obtain higher precision of results. The algorithmic scheme of the modified DE algorithm by the use of a quadratic response function (called in the following DE-Q) is shown in figure (6.5).

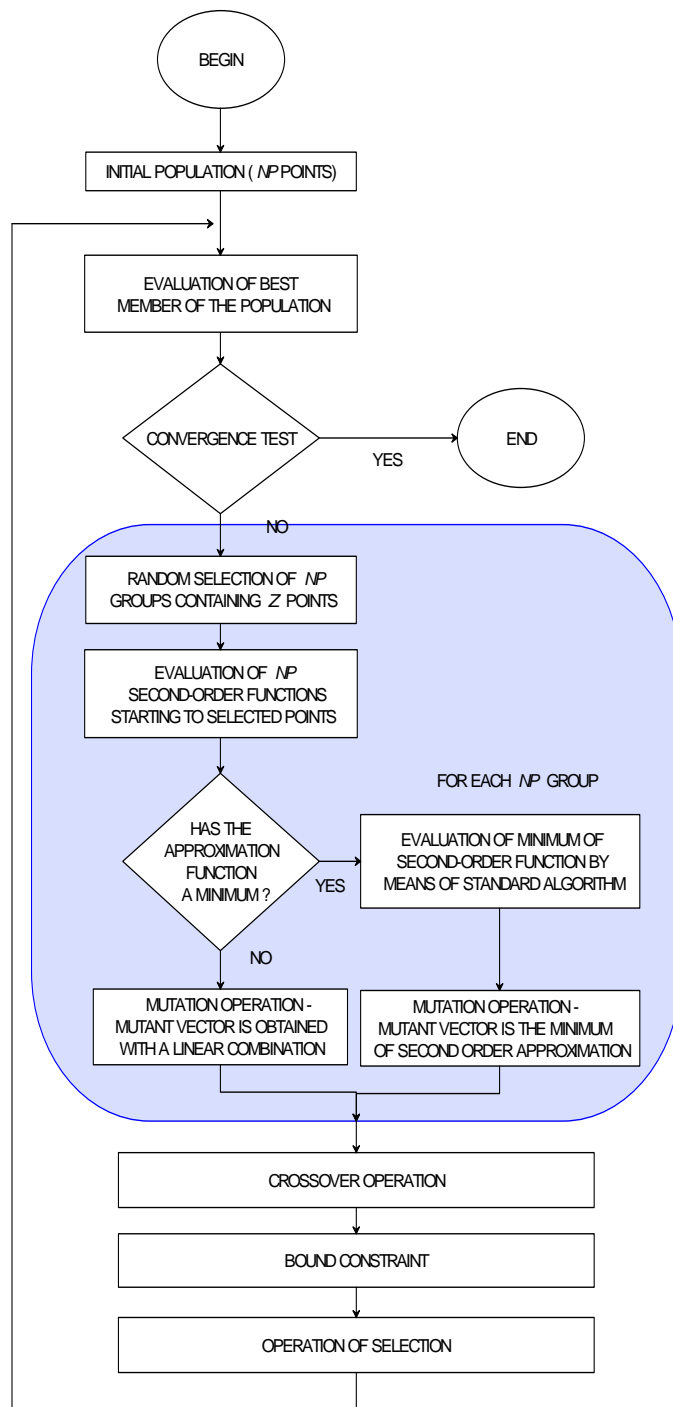


**Figure 6.5:** DE-Q algorithm flowchart.

First, the initial population is selected randomly. At each iteration,  $NP$  sets containing  $NS$  vectors are chosen (with  $NS < NP$ ). Starting from the  $NS$  sampling points, a RS is calibrated to fit the cost function  $H$ , Eq.(6.7). Solving the linear system of Eq.(6.13), coefficients  $\beta$  can be obtained and, from them, it can be checked if the RS function has a convex shape evaluating the  $Q$  matrix eigenvectors. If it is the case of figure (6.6a), the new parameter vector is defined as the minimum of a second-order polynomial approximation as:

$$\mathbf{v}_{i,G+1} = \mathbf{x}^* | H(\mathbf{x}^*) = \min g(\mathbf{x}) \quad (6.16)$$

Otherwise, figure (6.6b), classical Mutation operation based on linear combination is performed to obtain the trial vector  $\mathbf{v}_{i,G+1}$ . Crossover and Selection operations are then defined as in the original DE algorithm.

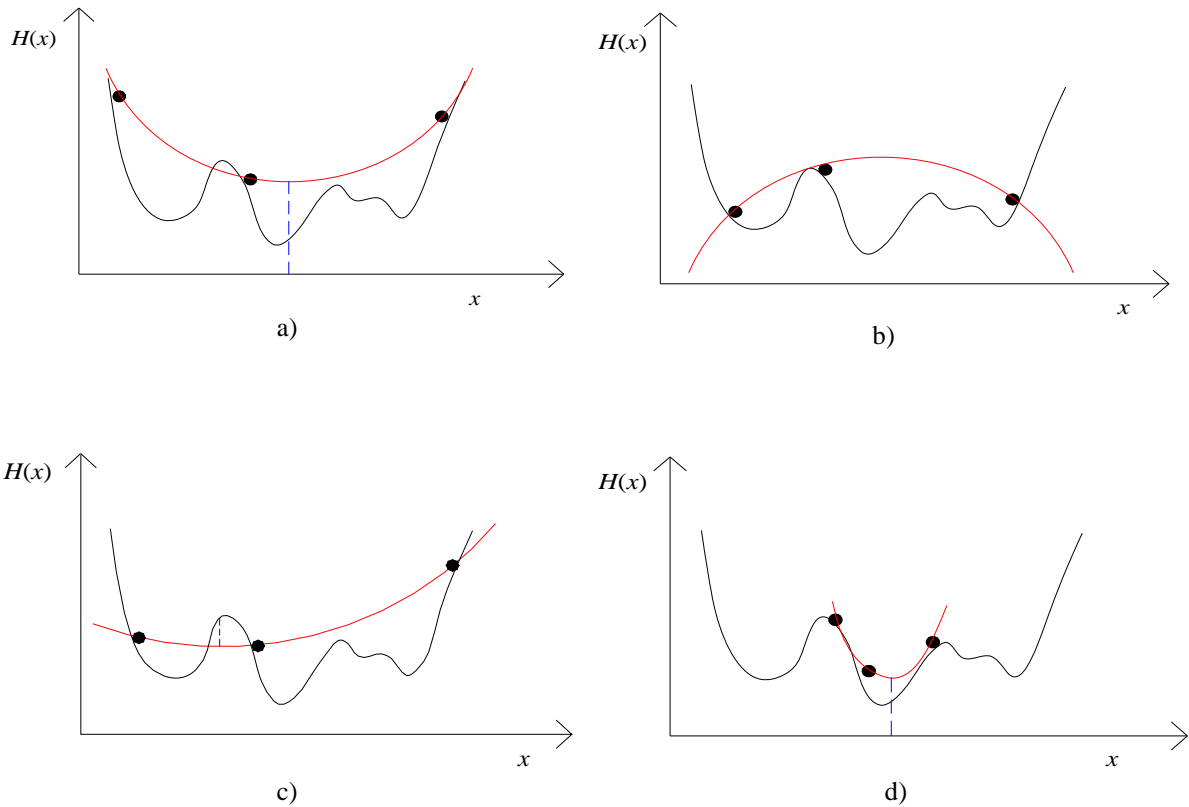


**Figure 6.6:** Approximation of cost function by quadratic response surface: a) positive convex shape, b) negative convex shape, c) response surface minimum gives an higher value of the cost function d) approximation of the cost function near the solution.

It is worth noting that the shape of objective function is usually unknown. If it presents only one (global) minimum, second-order approximation provides for the solution in a very low number of iterations. On the other hand, even if local minima are present,

global minimum is expected to be reached since multiple search points are used simultaneously. Moreover, if the minimum of second order approximation gives a higher values of cost function as in figure (6.6c), it can be rejected in the Selection operation (the old vector  $\mathbf{x}_{i,G}$  is retained). Finally, in order to detect the global minimum, several evaluations must be performed by using Genetic and Evolutionary algorithms, in order to obtain the prescribed precision. Close to the solution figure (6.6d), the second-order approximation gives very good performance in term of speed rate and higher accuracy with respect to the original algorithm.

For these reasons, global performance in term of speed rate is strongly improved by introducing the second order approximation by RSM and high precision of results of the original DE algorithm is preserved.

## 6.5 Optimization algorithm application

In this section the application of DE-Q algorithm to the Pontelagoscuo railway bridge, object of the present study, is described. More details concerning the algorithm are given in [15].

The aim of the updating procedure is to obtain vibration frequencies and modal shapes of the model as close as possible to those of the real structure.

First, the parameters to be optimize must be chosen. There are many parameter that may influence the dynamic behavior of the structure such as masses, elastic moduli, stiffness of external constraints, etc.

Analyzing the situation of the real structure has been chosen to formulate an optimization process leaving as unknown the two following mechanical parameters:

- density of the lower elements ( $M_{inf}$ )
- density of the upper elements ( $M_{sup}$ )

In fact by varying the density of the material and consequently the mass it is possible to vary also the frequencies of the system. Moreover varying the density of the material has a physical meaning, in fact in the model are taken into account only the masses of the structural elements, and so all the masses of the other elements as rivets, bolts, gusset plates, sleepers and all the other non-structural elements mainly located at the railway tracks level have been neglected.

Furthermore in the first model the supports at the two ends are treated as fixed hinges, but indeed looking at figure (6.12) it can be more truthful to consider at one side a double pendulum supports or roller supports. This aspect is confirmed also by the non-symmetrical experimental modal shapes.

Therefore the unknown parameters have been searched in limited significant intervals from a physical point of view:

- $M_{inf} = [12150 \div 27850 \text{ Kg/m}^3]$
- $M_{sup} = [7850 \div 15850 \text{ Kg/m}^3]$

In fact the relation inserted in the code are the following:

- $M_{inf} = 20000 + 7850 * \text{Corr}_1$
- $M_{sup} = 11850 + 4000 * \text{Corr}_2$

where the correct factors ( $\text{Corr}_1$  and  $\text{Corr}_2$ ) may assume values from -1 to 1. In this way the components of the population vectors are the correction factors (1, 2) that optimize the above expressions.

Actually in DE-Q algorithm are used 15 vectors ( $NP = 15$ ) that form the population, and each of them is done by 2 components (the two unknown parameters). The convergence test is imposed by the control of the relative error among 3 elements of the population ( $NC = 3$ ), and the convergence is satisfied when the results are lower than the constants  $VTR_1 = 10^{-3}$  and  $VTR_2 = 10^{-2}$ , [13].

The numerical tests are performed by adopting, as input data, frequencies and mode shape vectors; first, the experimental and the numerical modes are coupled by using the *MAC* (Modal Assurance Criterion) defined as

$$MAC = \frac{(\boldsymbol{\phi}_{exp}^T \boldsymbol{\phi}_{num})^2}{(\boldsymbol{\phi}_{exp}^T \boldsymbol{\phi}_{exp})(\boldsymbol{\phi}_{num}^T \boldsymbol{\phi}_{num})} \quad (6.17)$$

*MAC* is a correlation coefficient between two set of parameters. It assumes values from 0 to 1: zero is obtained when the two modes are completely uncorrelated and so orthogonal, while one is obtained when the two modes coincide.

Then, the objective function to be minimized during the identification procedure is defined as the relative error between modal frequencies and mode shapes obtained adopting a given set of identification parameters ( $\omega_{i,num}, \boldsymbol{\phi}_{i,num}$ ) and the reference solution ( $\omega_{i,exp}, \boldsymbol{\phi}_{i,exp}$ ), as

$$H = \sum_{i=1}^N \left[ w_1 \left( \frac{\omega_{i,num} - \omega_{i,exp}}{\omega_{i,exp}} \right)^2 + w_2 NMD_i^2 \right] \quad (6.18)$$

where *NMD* is the so called “*Normalized Modal Difference*” defined as:

$$NMD_i = \sqrt{\frac{1 - MAC(\boldsymbol{\phi}_{i,num}, \boldsymbol{\phi}_{i,exp})}{MAC(\boldsymbol{\phi}_{i,num}, \boldsymbol{\phi}_{i,exp})}} \quad (6.19)$$

In Eq. (6.19),  $N = 4$  first mode shapes are considered, and  $w_1$  and  $w_2$  are weight constants.

## 6.6 Obtained results

Running the analysis, the results obtained from the optimization process are:

- $M_{inf} = 14378 \text{ Kg/m}^3$
- $M_{sup} = 11224 \text{ Kg/m}^3$

Therefore in agreement to what already said, the algorithm try to associate a higher value of the density to the bottom elements and lower value, but still higher in respect to the nominal steel density, to the upper elements.

Performing a modal analysis, the first four new computed frequencies are very close to those of the real structure. In fact, now the first mode, that is the first lateral mode, has a frequency of 2.166 Hz; the second mode, that is vertical mode, has a frequency of 3.638 Hz; the third mode, that is torsional, has a frequency of 4.409 Hz; and the fourth mode, that is the second lateral, has a frequency of 4.749 Hz.

The first four mode shapes of the bridge are shown in figure (6.7) - (6.10).

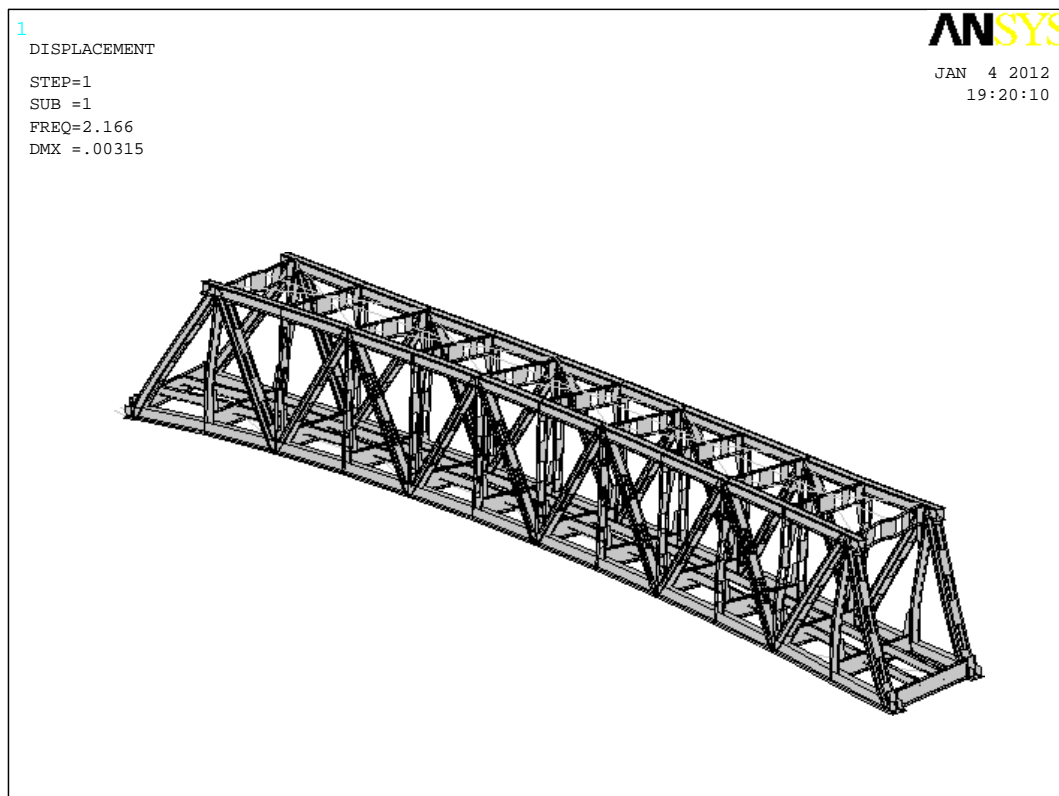


Figure 6.7: 1<sup>st</sup> mode shape at 2.166 Hz..

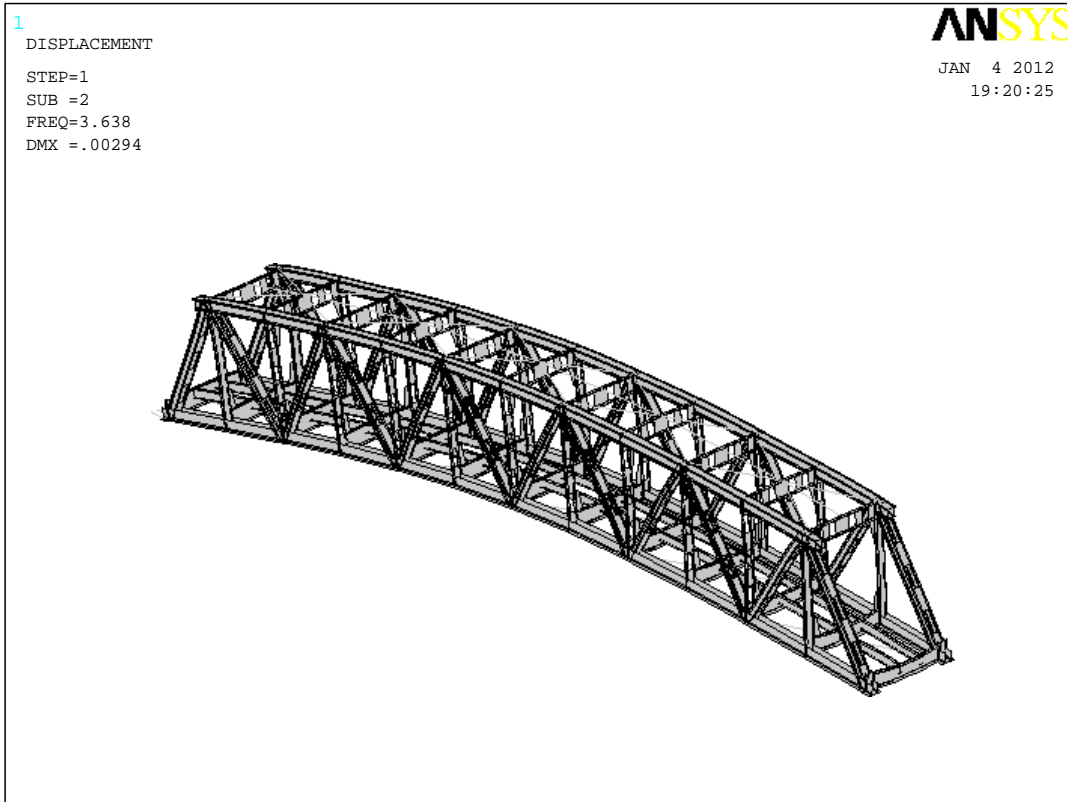


Figure 6.8: 2<sup>nd</sup> mode shape at 3.638 Hz..

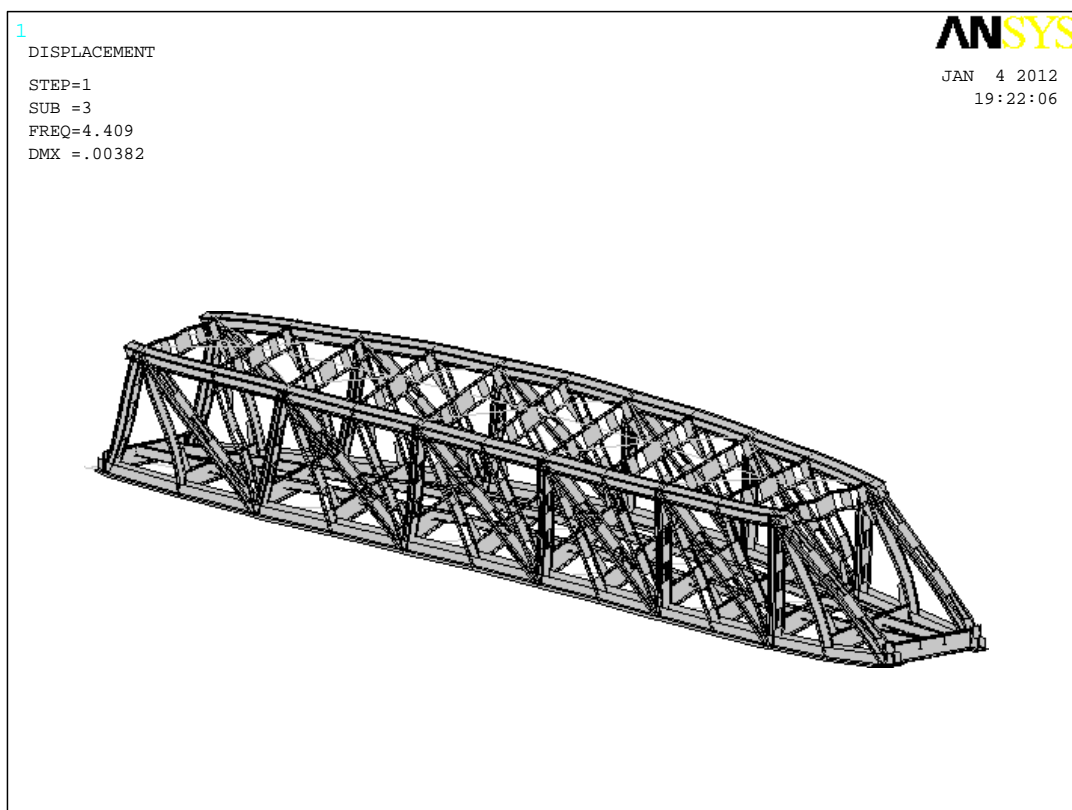
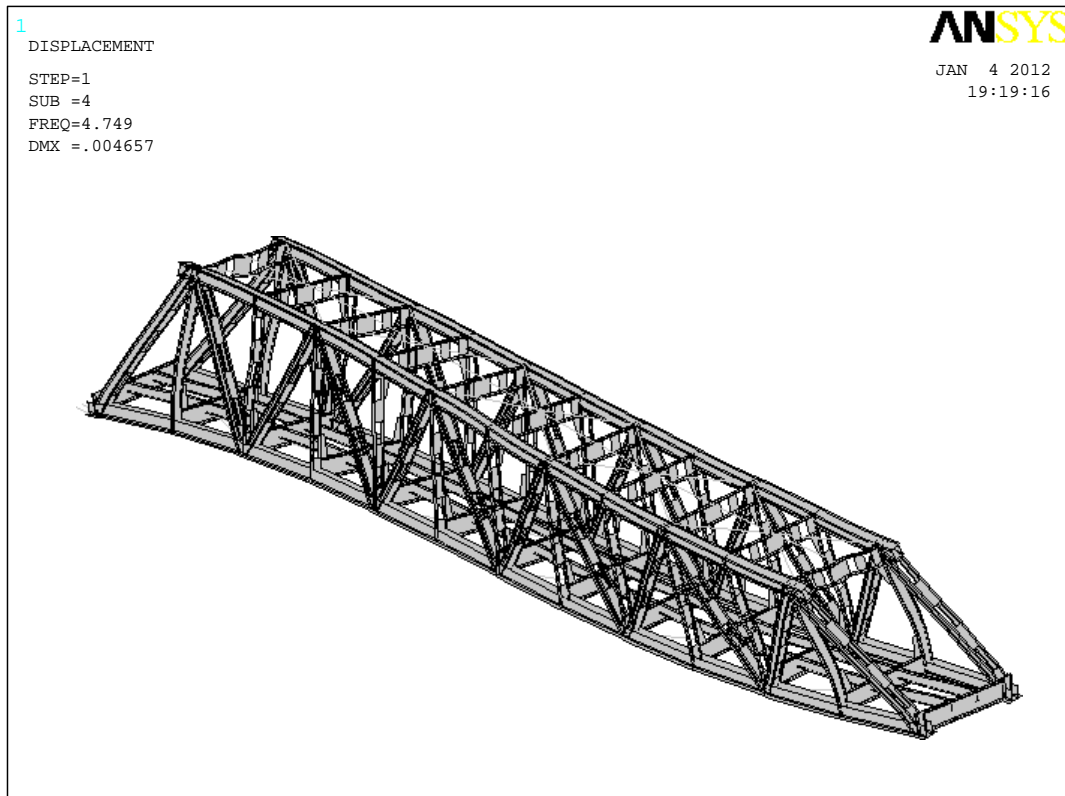


Figure 6.9: 3<sup>rd</sup> mode shape at 4.409 Hz.



**Figure 6.10:** 4<sup>th</sup> mode shape at 4.749 Hz.

At this point it is interesting to evaluate the goodness of the obtained results computing the relative errors between the numerical and experimental frequencies and modal shapes.

As for the frequencies they are compared in table (6.1), where the errors are computed simply as:

$$Error = \frac{\omega_{num} - \omega_{exp}}{\omega_{exp}} \quad (6.20)$$

Mode	Experimental frequency	Numerical frequency	Error
1 <sup>st</sup>	2.143 Hz	2.166 Hz	1,07 %
2 <sup>nd</sup>	3.857 Hz	3.638 Hz	5.68 %
3 <sup>rd</sup>	4.307 Hz	4.409 HZ	2.37 %
4 <sup>th</sup>	4.700 Hz	4.749 Hz	1.04 %

**Table 6.1:** Comparison between experimental and optimized numerical frequencies.

As regards the modal shapes the comparison is performed using the already discussed *MAC* coefficient computed through the Eq. (6.17). The two set of parameters in correlation are the experimental mode shapes of table (5.3) and the acquired numerical mode shapes, table (6.2), which values are taken directly from the model, in points representative of those monitored in situ.

<i>Numerical mode shapes</i>				
<i>Node</i>	<b>1<sup>st</sup> Mode</b>	<b>2<sup>nd</sup> Mode</b>	<b>3<sup>rd</sup> Mode</b>	<b>4<sup>th</sup> Mode</b>
<b>B2a (z) 260</b>	1.6106	-0.01350	2.3368	-1.5953
<b>B2a (y) 260</b>	0.46489	2.4068	1.4612	0.21681
<b>B2b (y) 656</b>	0.45401	2.4358	-1.4172	-0.22332
<b>B2c (z) 185</b>	2.8339	0.01646	-1.4250	-2.2408
<b>B3a (z) 232</b>	1.9474	-0.01522	3.1013	-0.47760
<b>B3a (y) 232</b>	-0.51560	2.7792	1.5616	-0.17035
<b>B3b (y) 606</b>	0.50345	2.8119	-1.5120	0.15547
<b>B3c (z) 195</b>	3.0845	0.01672	-0.82267	-0.05436
<b>B4a (z) 2576</b>	1.8596	-0.01001	2.6964	0.84255
<b>B4a (y) 2576</b>	-0.50954	2.3757	1.3749	-0.53048
<b>B4b (y) 2687</b>	0.49903	2.4056	-1.3320	0.51122

**Table 6.2:** Optimized numerical mode shapes.

Therefore, looking at table (6.1) and figure (6.11), it is possible to say that the first numerical mode is very well representative of that of the real structure with very minimal error differences both in frequencies and in mode shapes. The second mode has the higher error regarding the frequencies but is still acceptable since it has in any case about ninety-four percent of frequency accuracy, and it is very well representative regarding the mode shape. Concerning the third mode it has great frequencies accuracy, but it exhibits the lower correlation coefficient as regards the mode shape. Looking at the experimental data it is clear that this is a little bit strangely deformed shape, and it is very difficult to understand which parameters govern this mode shape. The fourth mode has an optimal frequencies correlation, and a worse but still acceptable *MAC* coefficient.

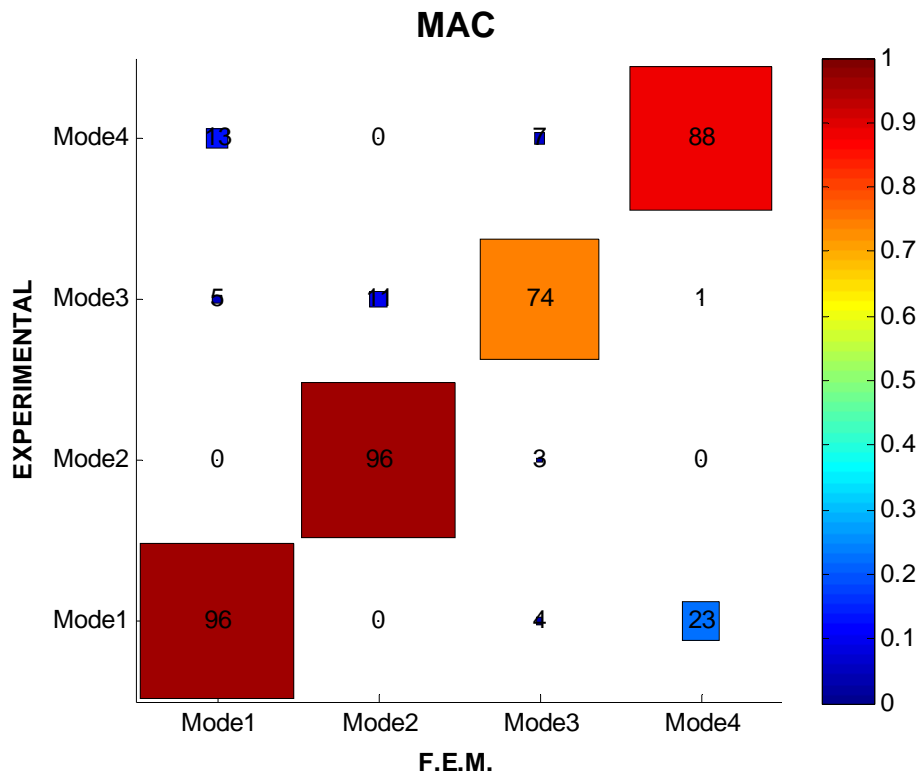


**Figure 6.11:** MAC correlation coefficients.

In conclusion a very fine and accurate model, that very well fit the dynamic behavior of the real structure, is been obtained though the use of this optimization process.

# 7. 2D MOVING LOADS VS. VBI MODELS

## APPLICATION

### 7.1 Introduction

In this section some preliminaries two-dimensional dynamic analyses of the Pontelagoscuro railway bridge using two way of representing the traveling trains are carried out. The first way is to represent the trains as a sequence of moving loads as explained in *chapter 3*, whereas the second way is to represent the trains as a sequence of two-dimensional car in which the vehicle-bridge dynamic interaction is taken into account, as explained in *chapter 4*.

The aim of these first dynamic analyses is to understand the differences that can be obtained using moving loads model and VBI model. Moreover it will be investigated the main parameters that govern this kind of problem, especially in the case of vehicle-bridge interaction.

In lack of information regarding the actual trains that daily cross the bridge, those given by the *Eurocode 1* to perform fatigue analyses will be used. Furthermore for VBI analyses the train parameter given in [2] will be used.

## 7.2 Bridge model setting

As already said the objective of this section is to perform some preliminaries dynamic analysis of the bridge solving the 2D problem of a train crossing as described in *chapter 3*, when the train is represented as a sequence of moving loads, or as in *chapter 4* when more sophisticated models are used.

It is underlined that the equations of motion solved to perform the dynamic analysis are those in real coordinates as in Eq. (1.7) rewritten in the following for clarity:

$$\mathbf{M}\ddot{\mathbf{u}} + \mathbf{C}\dot{\mathbf{u}} + \mathbf{K}\mathbf{u} = \mathbf{p}(t)$$

where  $\mathbf{M}$ ,  $\mathbf{C}$  and  $\mathbf{K}$  are the mass, damping and stiffness matrices of an equivalent beam-bridge model discretized in some number of elements as described in *chapter 3.2*, and figure (3.2). For this reason to compute  $\mathbf{M}$ ,  $\mathbf{C}$  and  $\mathbf{K}$  an equivalent mass per meter of bridge length and stiffness  $EI$  is needed.

The procedure to obtain those quantities is very simple. In fact running a static analysis of the model with only the self-weight of the structure it is possible to obtain the reaction forces as in figure (7.1). The sum of the reaction forces divided by the gravity acceleration and the length of the bridge gives the mass per meter of length of the bridge.

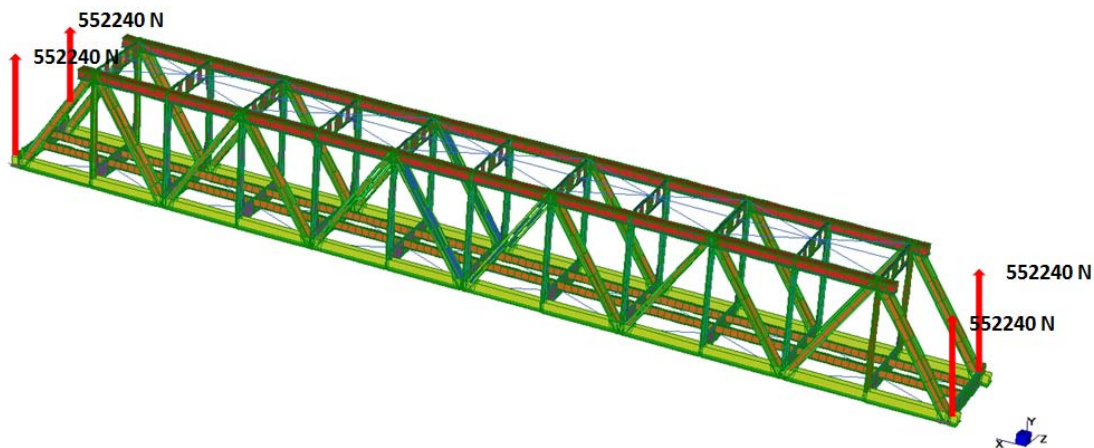


**Figure 7.1:** Reaction forces due to the self weight of the bridge.

Knowing that the bridge is 59.40 m long, the mass per meter of length is obtainable as

$$m = \frac{4 \cdot 552240}{g \cdot L} = \frac{4 \cdot 552240}{9.81 \cdot 59.40} = 3790.81 \text{ Kg/m} \quad (7.1)$$

In order to get an equivalent stiffness  $EI$ , and in particular fixing  $E$  get an equivalent  $I$ , a known force can be applied at the mid-span of the model and the relative displacement measured. Then this displacement should be equal to the displacement of a simply supported beam loaded by the same force as shown in figure (7.2).

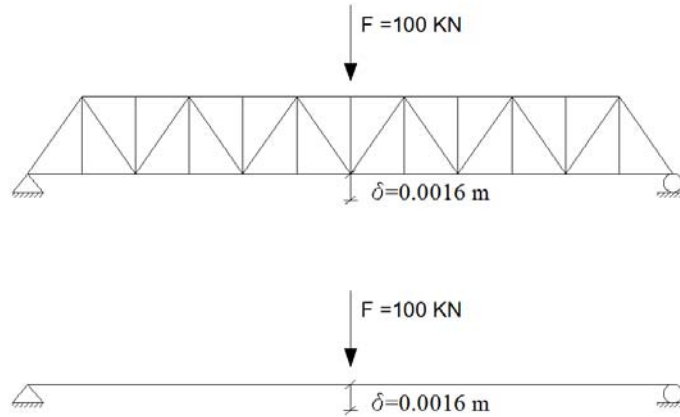


**Figure 7.2:** Procedure to get an equivalent stiffness  $EI$ .

The deflection of a simply supported beam subjected to a point load located at the half span is

$$\delta = \frac{F \cdot L^3}{48 \cdot E \cdot I} \quad (7.2)$$

Therefore inverting the formula and fixing  $E = 200000 \text{ MPa}$  as in table (5.4), it is possible to obtain an equivalent moment of inertia

$$I = \frac{F \cdot L^3}{48 \cdot E \cdot \delta} = \frac{100000 \cdot 59.40^3}{48 \cdot 2 \cdot 10^{11} \cdot 0.00160} = 1.3645 \text{ m}^4 \quad (7.3)$$

Finally, inserting all the parameters in the 2D beam-bridge model, presented in *chapter 3.2*, as the length, the number of elements used to discretize it, the mass per meter length, the elastic modulus and the inertia moment, allows to compute the frequencies of the simplified system and compare them with the real and the finite elements model as in table (7.1).

Mode	Frequency <i>real structure</i>	Frequency <i>2D beam-bridge model</i>
1 <sup>st</sup> Vertical	3.857 Hz	3.778 Hz
2 <sup>nd</sup> Vertical	9.804 Hz	15.106 Hz

**Table 7.1:** Comparison between experimental and models frequencies.

Hence the 2D beam-bridge model has the first vertical frequency that is very close to the real and the 3D FEM structures, while the second is not so close. However this approximation can be accepted because is the first mode that governs mainly the motion of the system.

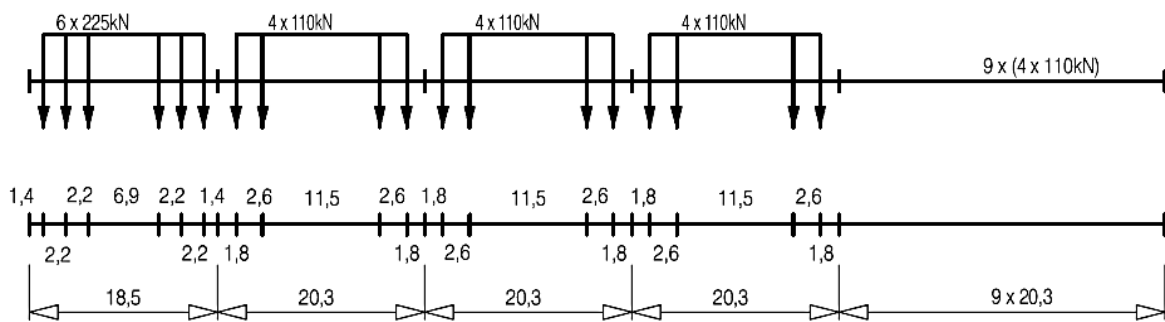
### 7.3 Train data

In this section will be illustrated the characteristics of the trains used to make a comparison between two ways for representing the train passing over the 2D beam-bridge; that are the moving loads and the vehicle-bridge interaction (VBI) models. Since there are no data about the actual trains that cross the bridge, some trains' models given by the *Eurocode 1* to perform fatigue analyses will be used.

In the following, for each train, are reported its characteristics in terms of sum of the loads of the overall train  $\Sigma Q$ , crossing speed  $v$ , total length  $L$  and distributed load per unit length  $q$ , with also a scheme from which the distribution of the concentrated axel loads can be deduced.

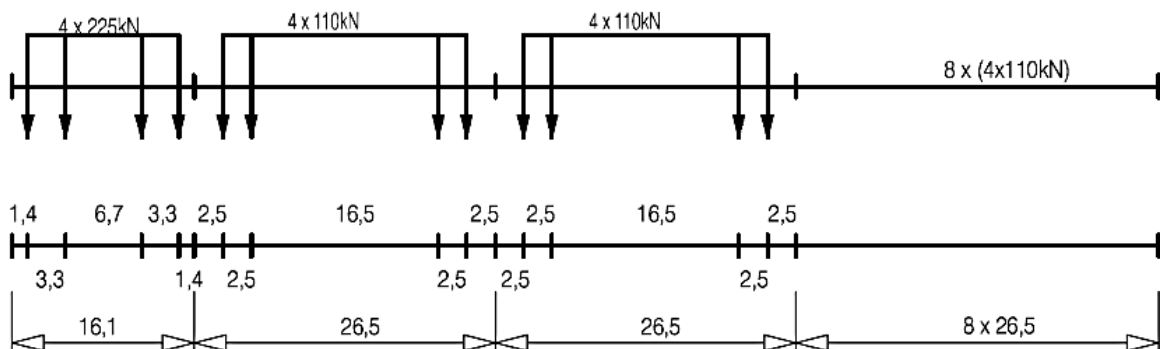
#### *Type 1*: Locomotive-hauled passenger train

$$\Sigma Q = 6630 \text{ KN} \quad v = 200 \text{ Km/h} \quad L = 262.10 \text{ m} \quad q = 25.30 \text{ KN/m}$$



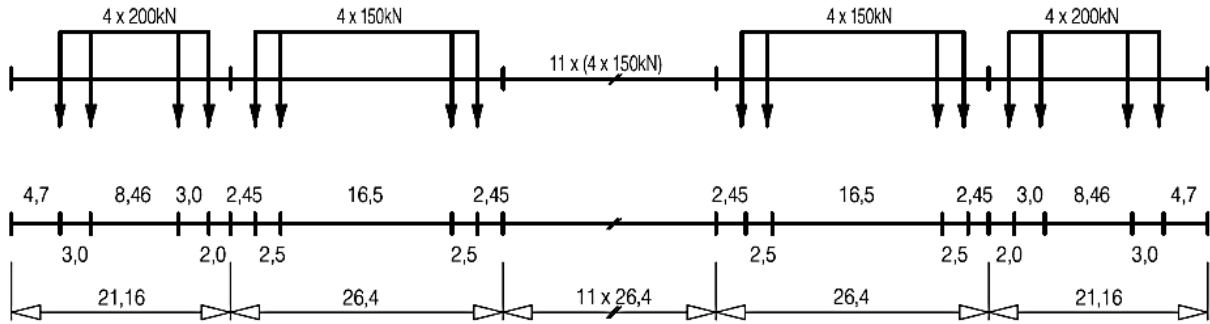
#### *Type 2*: Locomotive-hauled passenger train

$$\Sigma Q = 5300 \text{ KN} \quad v = 160 \text{ Km/h} \quad L = 281.10 \text{ m} \quad q = 18.90 \text{ KN/m}$$



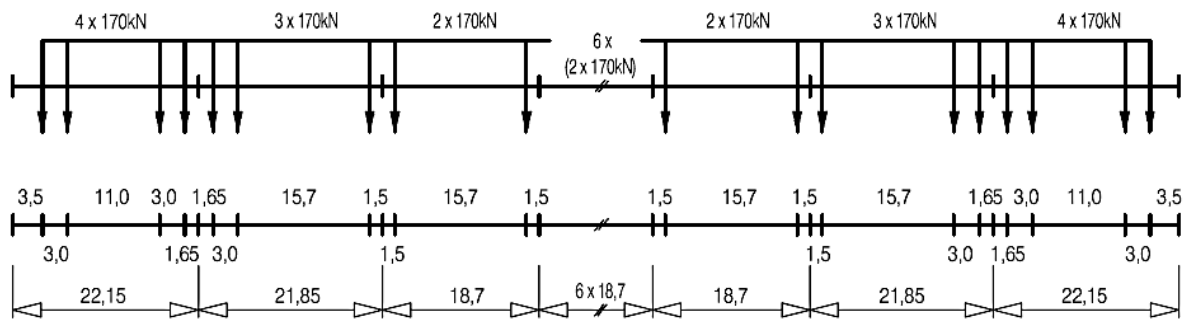
**Type 3:** High speed passenger train

$\Sigma Q = 9400 \text{ KN}$      $v = 250 \text{ Km/h}$      $L = 385.52 \text{ m}$      $q = 24.40 \text{ KN/m}$



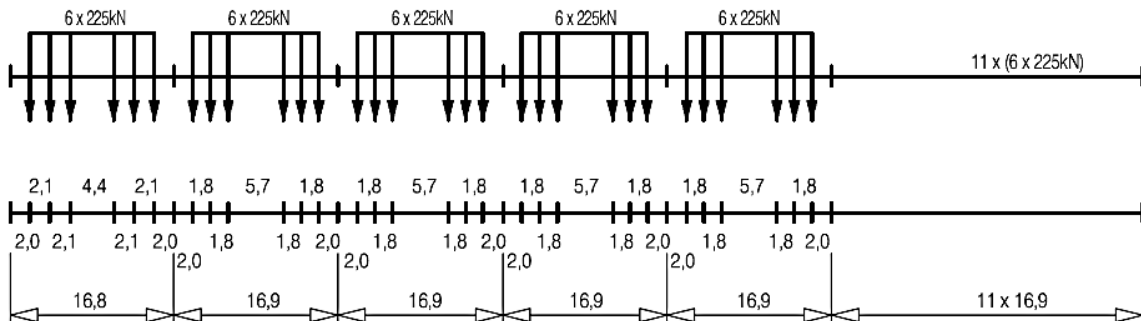
**Type 4:** High speed passenger train

$\Sigma Q = 5100 \text{ KN}$      $v = 250 \text{ Km/h}$      $L = 237.60 \text{ m}$      $q = 21.50 \text{ KN/m}$



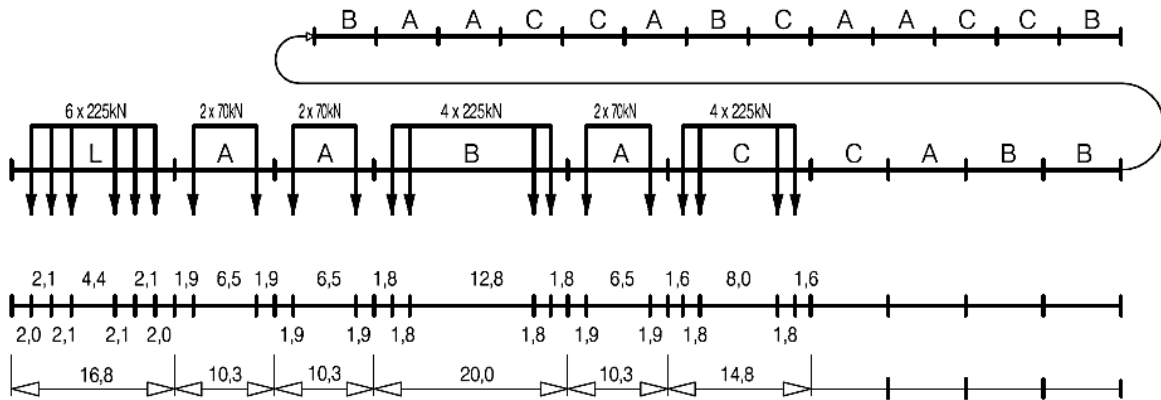
**Type 5:** Locomotive-hauled freight train

$\Sigma Q = 21600 \text{ KN}$      $v = 80 \text{ Km/h}$      $L = 270.30 \text{ m}$      $q = 80.0 \text{ KN/m}$



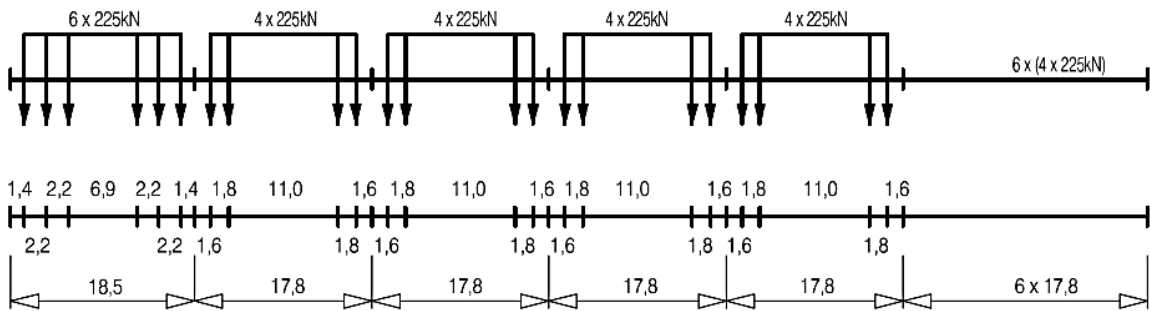
**Type 6:** Locomotive-hauled freight train

$\Sigma Q = 14310 \text{ KN}$      $v = 100 \text{ Km/h}$      $L = 333.10 \text{ m}$      $q = 43.0 \text{ KN/m}$



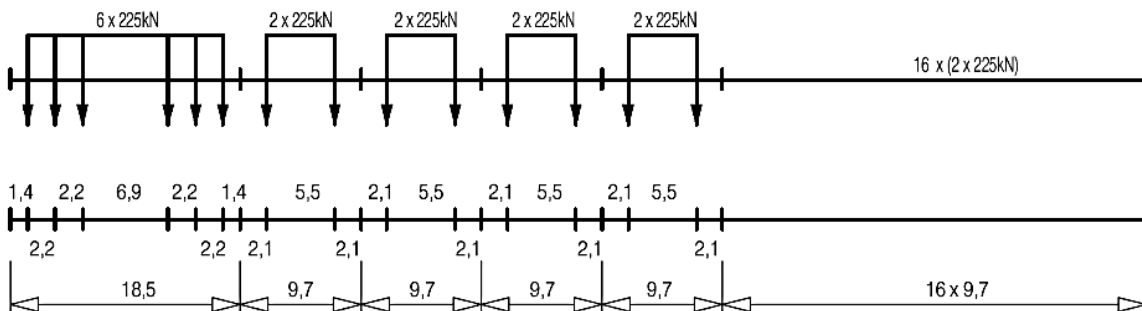
**Type 7:** Locomotive-hauled freight train

$\Sigma Q = 10350 \text{ KN}$      $v = 120 \text{ Km/h}$      $L = 196.50 \text{ m}$      $q = 52.70 \text{ KN/m}$



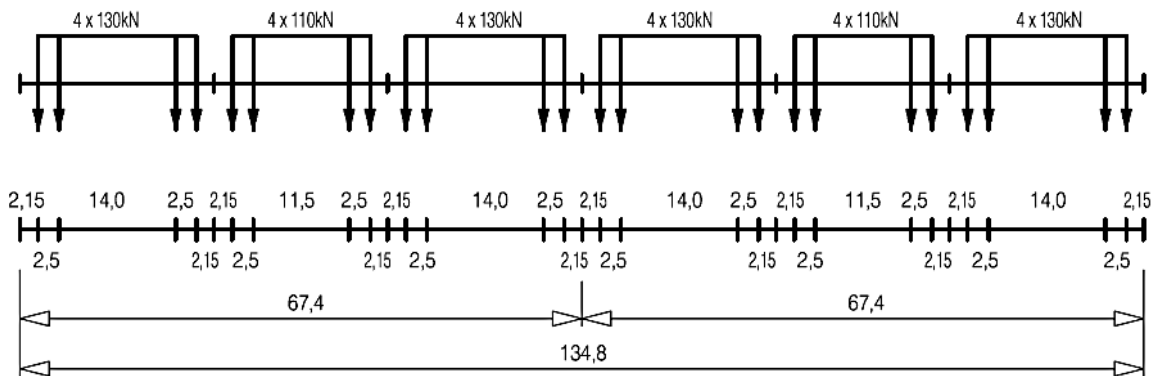
**Type 8:** Locomotive-hauled freight train

$\Sigma Q = 10350 \text{ KN}$      $v = 100 \text{ Km/h}$      $L = 212.50 \text{ m}$      $q = 48.70 \text{ KN/m}$



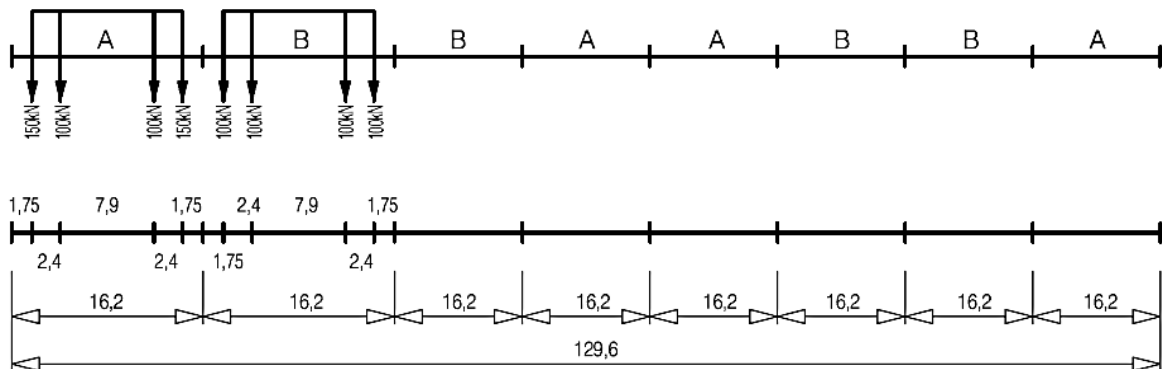
**Type 9:** Surburban multiple unit train

$\Sigma Q = 2960 \text{ KN}$      $v = 120 \text{ Km/h}$      $L = 134.80 \text{ m}$      $q = 22.0 \text{ KN/m}$



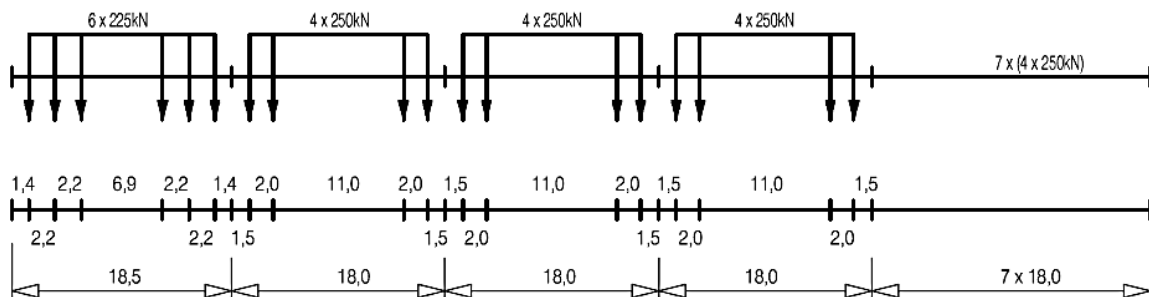
**Type 10:** Underground

$\Sigma Q = 3600 \text{ KN}$      $v = 120 \text{ Km/h}$      $L = 129.60 \text{ m}$      $q = 27.80 \text{ KN/m}$



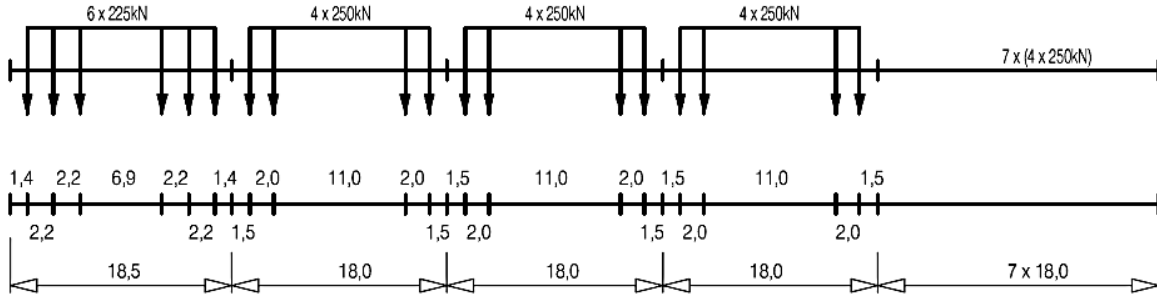
**Type 11:** Locomotive-hauled freight train

$\Sigma Q = 11350 \text{ KN}$      $v = 120 \text{ Km/h}$      $L = 198.50 \text{ m}$      $q = 57.2 \text{ KN/m}$



**Type 12:** Locomotive-hauled freight train

$$\Sigma Q = 11350 \text{ KN} \quad v = 100 \text{ Km/h} \quad L = 212.50 \text{ m} \quad q = 53.4 \text{ KN/m}$$



From the above trains models it has been possible to obtain the vector that collects the distances of the axels relative to the first one, and the vector of the concentrated loads as well as the velocity for each train. This data are important because allow to compute the nodal reaction forces for each time step. In this way a load history for each node can be obtained, and the structural response can be computed for each time step.

In order to perform VBI analysis the values of the vertical stiffness and vertical damping of the primary and secondary suspension systems are needed. In literature there are very poor data about the values of these devices and most of them are not reliable because refer to Chinese or Japanese trains that in Europe are not used. Moreover the trains' manufacturers do not spread information due to professional secret and copyrights. Therefore in the absence of informations the data about the Italian ETR500Y high speed train given in [2] will be used for each type of train; the main characteristics are reported in table (7.2).

Item	Unit	Locomotive	Passenger car
Mass of the bogie ( $M_1$ )	Kg	3896	2760
Mass of the wheel set ( $M_W$ )	Kg	2059	1583
Vertical stiffness of the primary suspension system ( $K_V$ )	N/m	1792200	808740
Vertical damping of the primary suspension system ( $C_V$ )	N s/m	15250	7500
Vertical stiffness of the secondary suspension system ( $K_{VV}$ )	N/m	472060	180554
Vertical damping of the secondary suspension system ( $C_{VV}$ )	N s/m	36250	16250

**Table 7.2:** Dynamic characteristics of the Italian ETR500Y high speed train.

It is pointed out that in the following VBI analysis, for passenger and high-speed trains it will be used respectively the data for the locomotive and the cars, while for freight trains it will be used only the data of the locomotive also for the other wagons..

## 7.4 Comparison between moving loads model and VBI model

In this section the dynamic analyses of the bridge will be compared using two ways of representing the crossing train; the first one is when the train is modeled as a loads sequence (*moving loads model*), while the second one is when the train is modeled as a sequence of 3-DOFs cars as in figure (4.1) (*VBI model*), for some trains type given in *chapter 7.3*.

As regards the bridge model, it will be subdivided into 25 beam elements, and so 26 nodes. Also in the analysis it has been assumed a time step of 0.02 seconds and a Rayleigh damping assigning a damping ratio of 2% for the first frequency and the last frequency of vibration, as explained in *chapter 1.4*.

The results obtained are reported in the following, where for each considered train, the displacement of the half span node in time are shown for both moving loads and VBI models. Furthermore to better understand the dynamic behavior of the bridge first the effects in terms of forces, on a generic node, will be reported.

As regards the train type 1, the force variation in time on the mid span node using both moving loads and VBI models are shown in figure (7.3)(7.4), respectively.

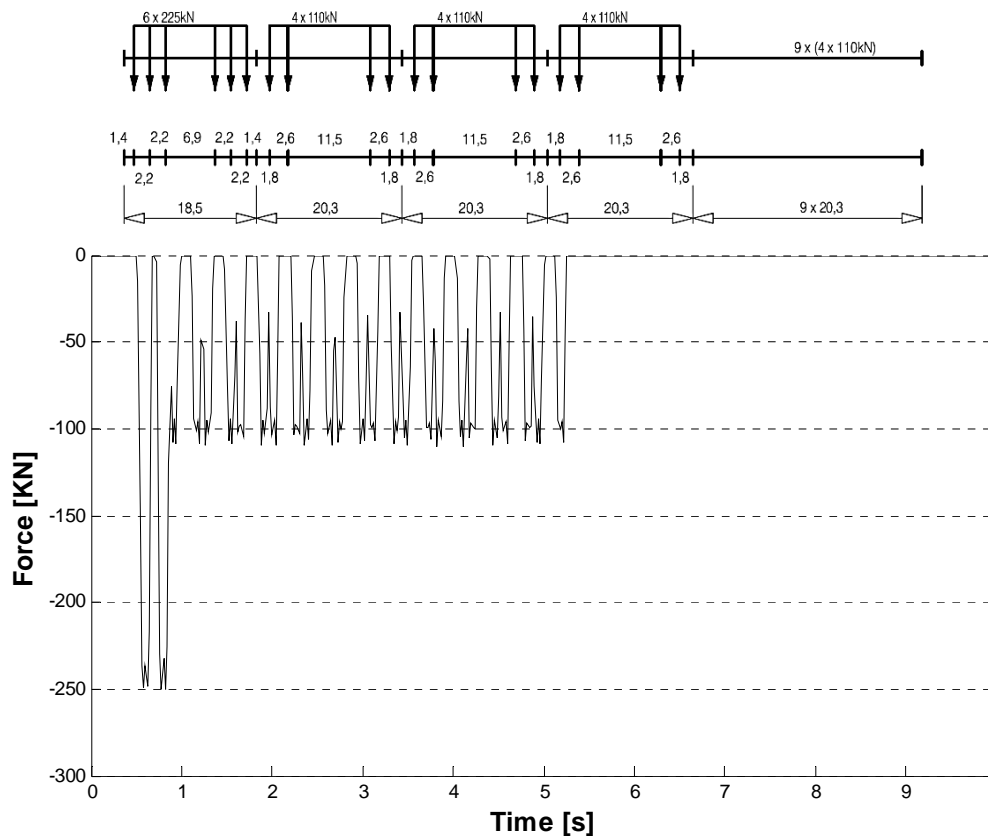


**Figure 7.3:** Mid span node force variation due to the passage of train type 1 using moving loads model.

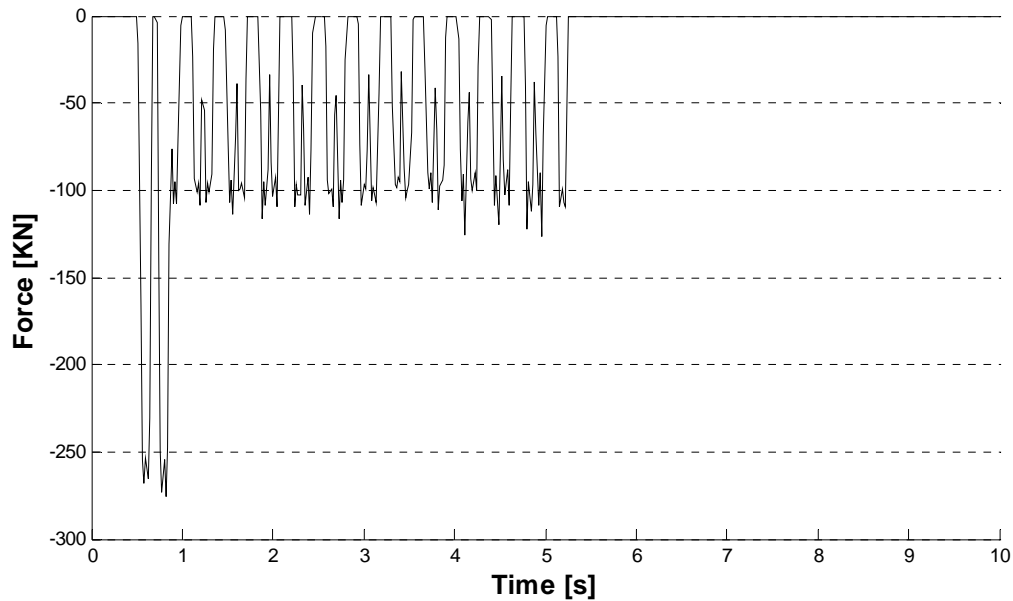


**Figure 7.4:** Mid span node force variation due to the passage of train type 1 using VBI model.

The above figures show the equivalent vertical nodal forces caused by a passenger train on the mid span node. In most of those kinds of trains the locomotive has a bigger weight in comparison to the passenger cars, therefore the force peaks are observed in correspondence to the passing of the locomotive.

The main difference is that the peak values are not constant in the VBI model, whereas they are constant in the moving loads model. The values difference between the two above plots is nothing more than the dynamic part of the force transmitted. The dynamic part of the force can be negative as in the initial part of figure (7.4) where the peaks are higher in respect to those of figure (7.3) getting an amplification of the total force, or positive as in the case of some peaks in the central part of figure (7.4) having a reduction of the transmitted total force.

Another interesting difference is that the first two peaks which are relative to the locomotive, in the VBI model have a higher value in respect to those regarding the moving loads model. However this is only a local observation, this means that in other nodes the transmitted force on the bridge can have different values from node to node when VBI model is used.

Figures (7.5) (7.6) show the displacement in time of the mid span node due to the passage of the train type 1 using both moving loads and VBI models, respectively.

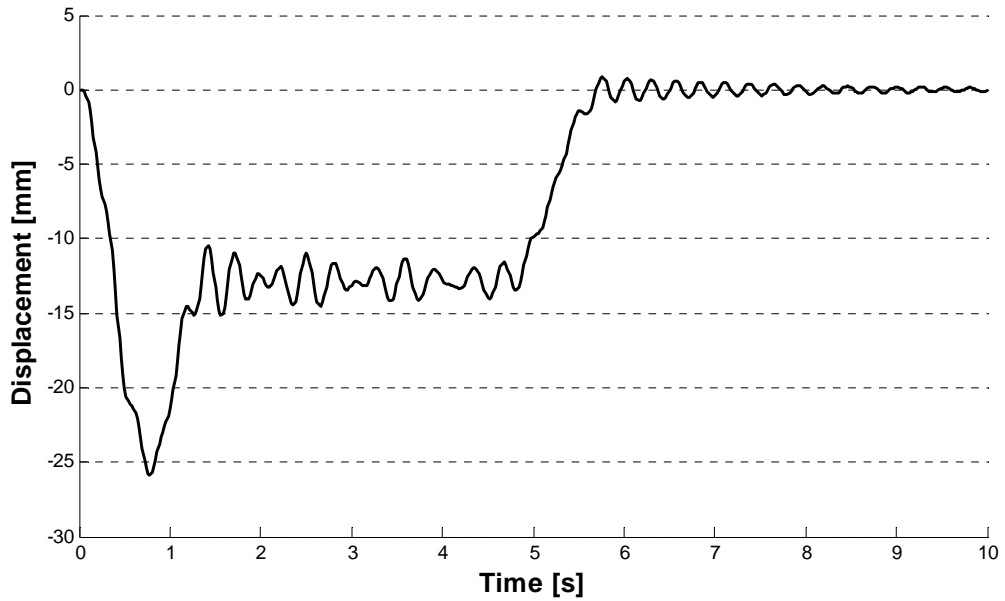


Figure 7.5: Mid span node displacement due to the passage of train type 1 using moving loads model.

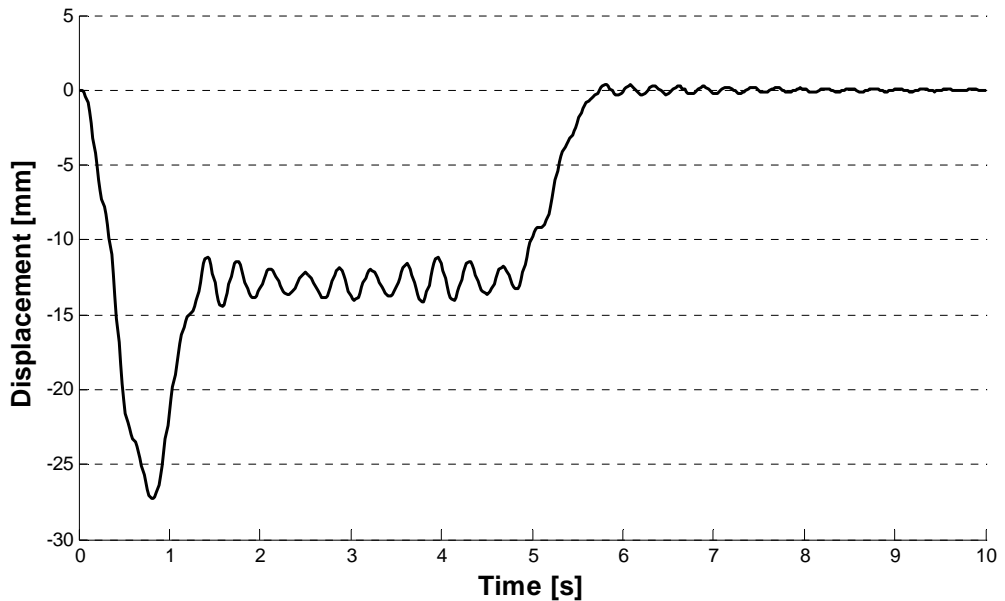


Figure 7.6: Mid span node displacement due to the passage of train type 1 using VBI model.

The maximum displacement of the bridge is about 2.5 cm and 2.7 cm for the moving loads model and VBI model respectively. The little differences between the two patterns are the amplitude of the oscillations in the central part of the plots and the residual oscillation when the train leave the bridge, that are more marked in the moving loads model.

In figure (7.7) the two plots are compared to better understand the differences between the two results obtained.

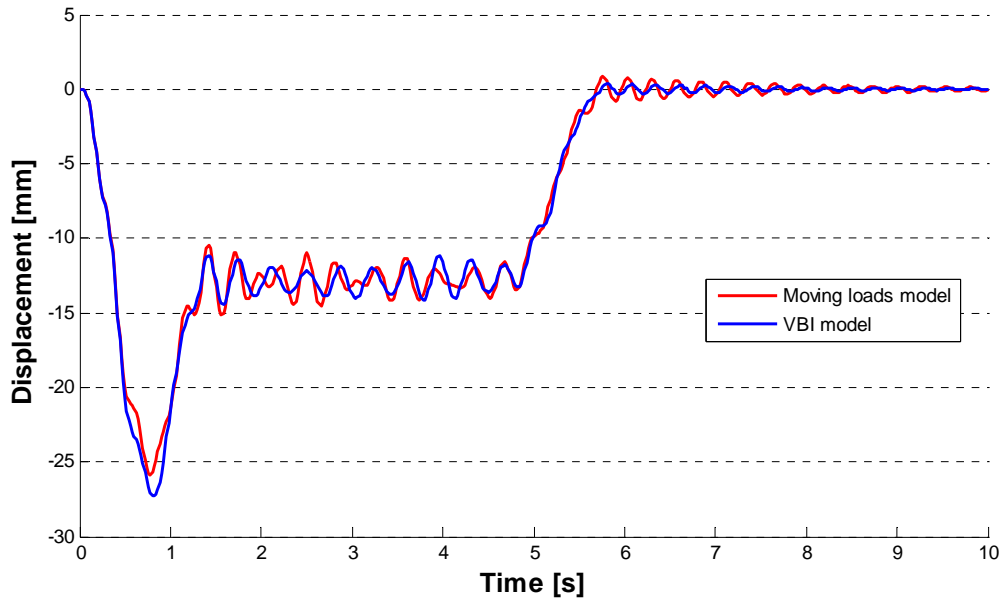


Figure 7.7: Comparison between moving loads and VBI models for train type 1.

Figures (7.8) (7.9) show the force variation in time on the mid span node due to the passage of the train type 2 using both moving loads and VBI models, respectively.

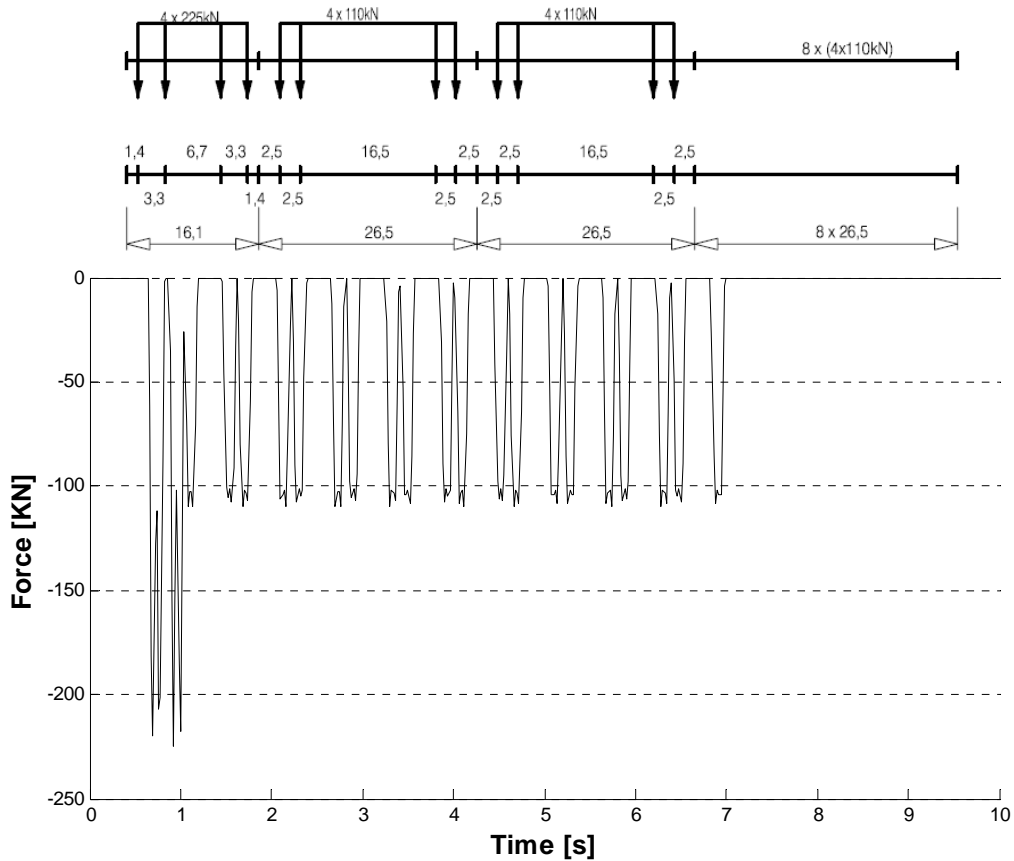
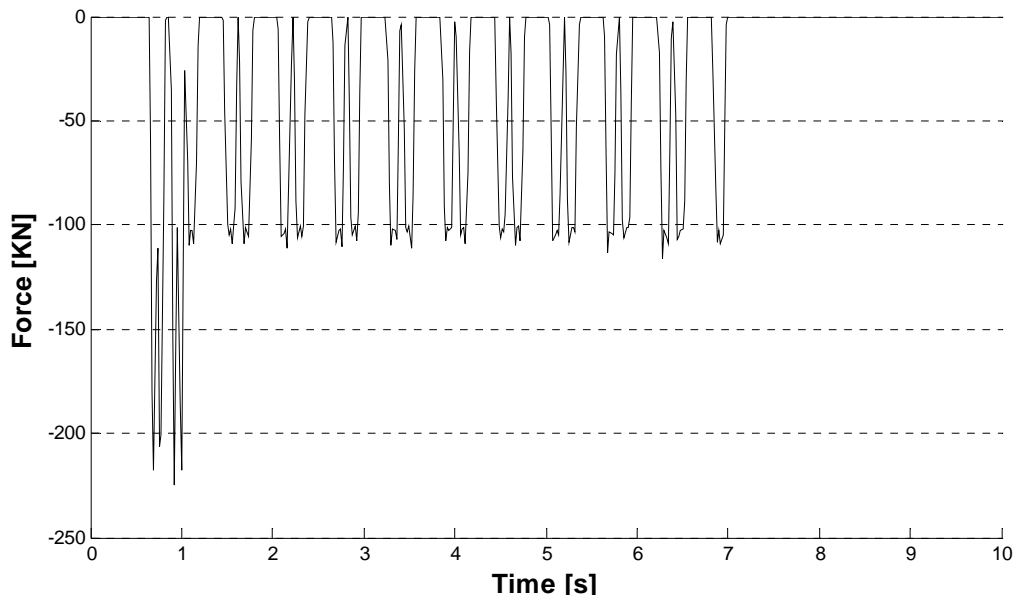


Figure 7.8: Mid span node force variation due to the passage of train type 2 using moving loads model.



**Figure 7.9:** Mid span node force variation due to the passage of train type 2 using VBI model.

For the two models the above plots show that the transmitted forces are almost the same, suggesting that for this train type may not be a strong dynamic interaction.

Figures (7.10) (7.11) show the displacement in time of the mid span node due to the passage of the train type 2 using both moving loads and VBI models, respectively.

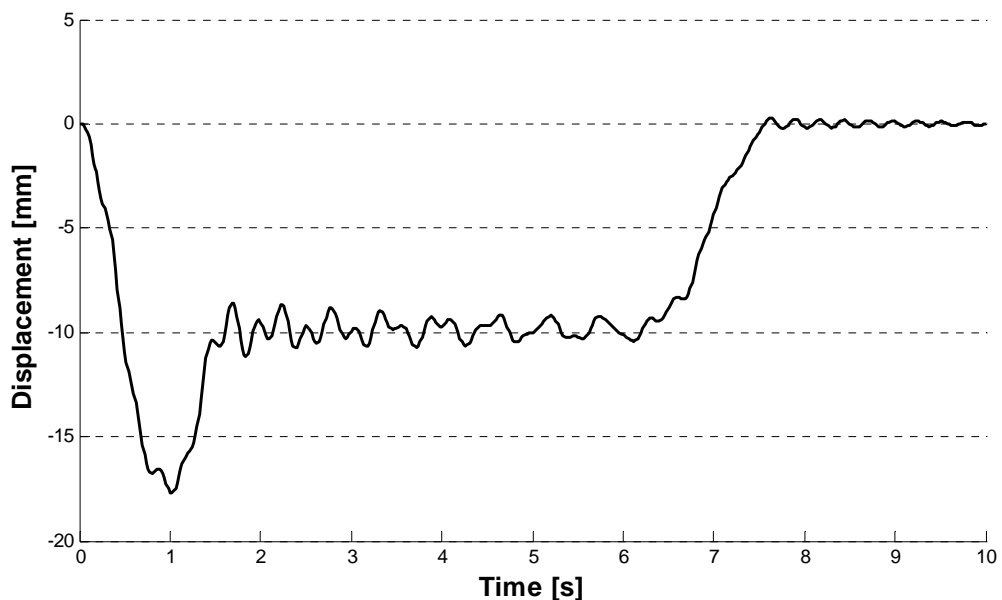


**Figure 7.10:** Mid span node displacement due to the passage of train type 2 using moving loads model.

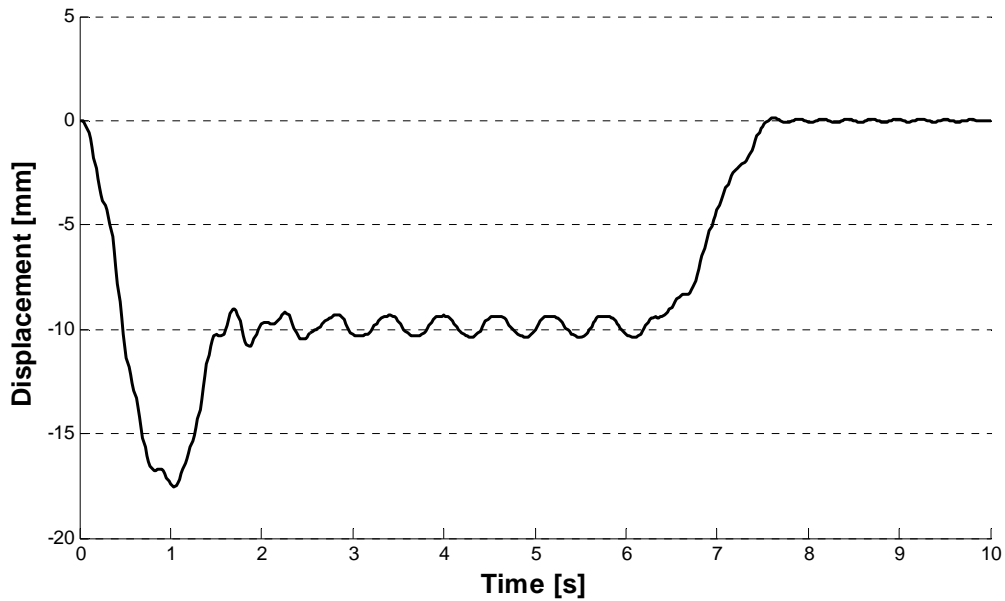


**Figure 7.11:** Mid span node displacement due to the passage of train type 2 using VBI model.

In the next plot, figure (7.12) the two figures (7.10) (7.11) are compared to better understand the differences between the two.

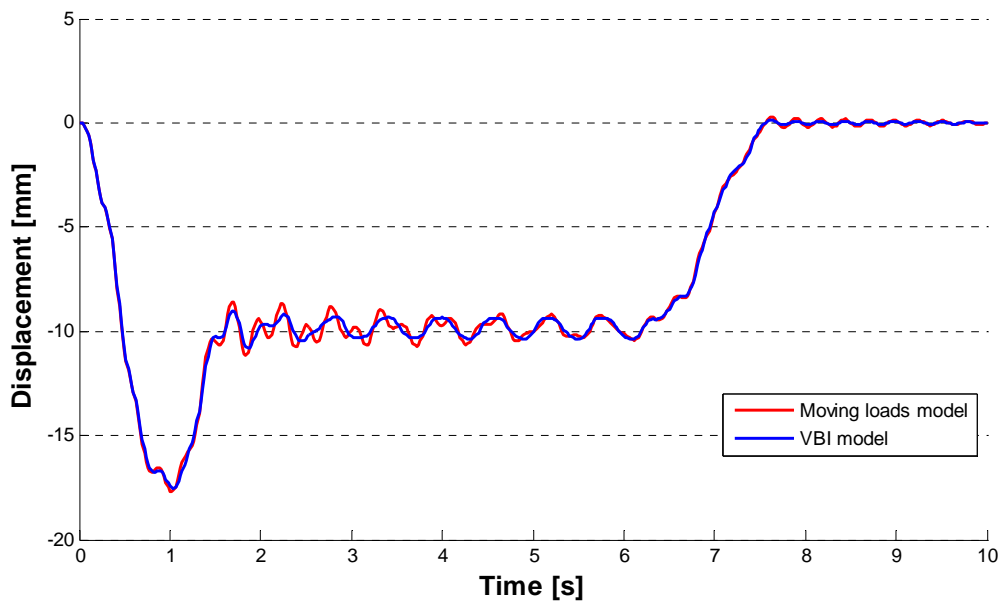


**Figure 7.12:** Comparison between moving loads and VBI models for train type 2.

Indeed figure (7.12) confirms that in this case there is not strong dynamic interaction, in fact the two shapes are almost coincident. Also the final residual oscillations are very similar in amplitude. The maximum displacement reached for both the model is about  $1.7\text{ cm}$  at more or less one second of the observation time.

As regards the train type 3, the force variation in time on the mid span node using both moving loads and VBI models are shown in figure (7.13)(7.14), respectively.

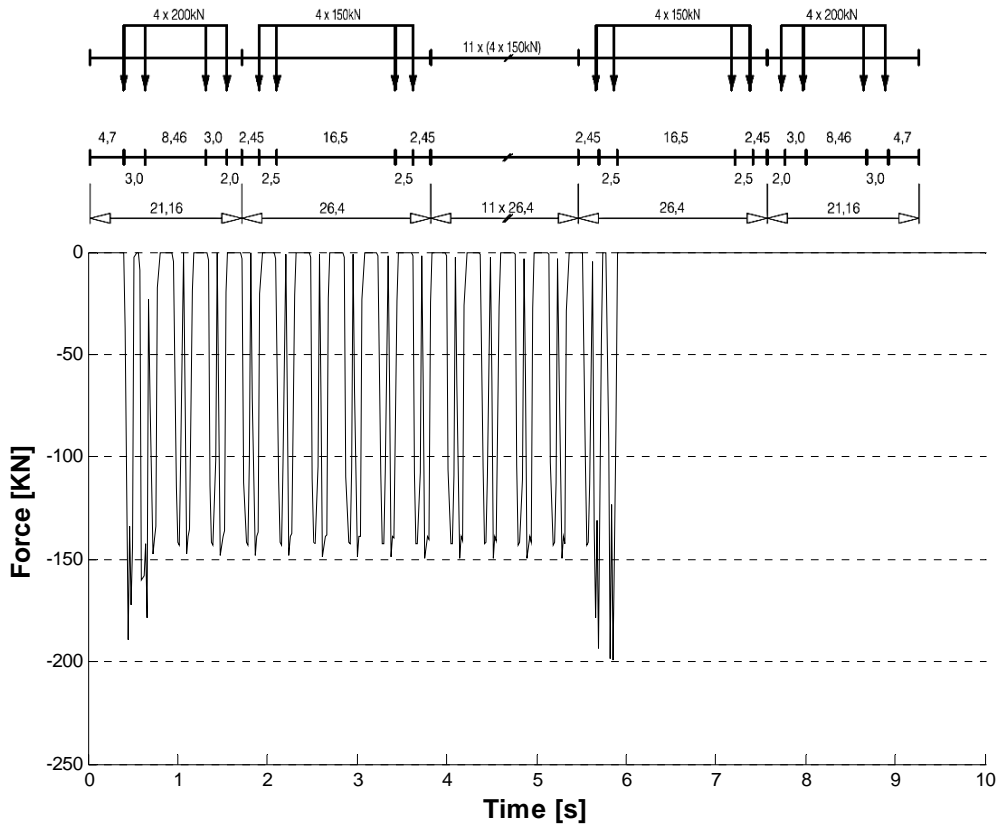


Figure 7.13: Mid span node force variation due to the passage of train type 3 using moving loads model.

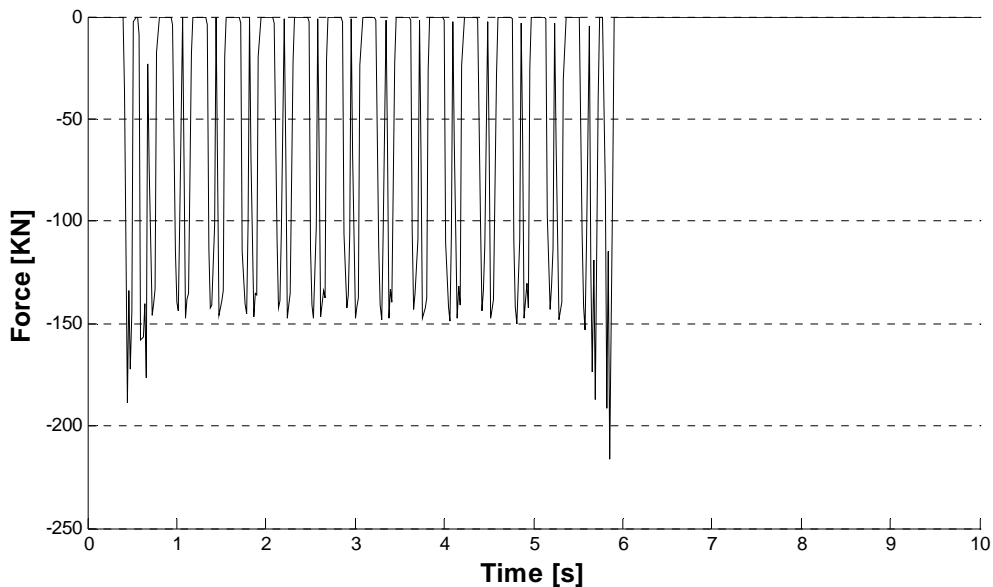


Figure 7.14: Mid span node force variation due to the passage of train type 3 using VBI model.

In this case there are some differences of the transmitted forces, in particular moving loads model exhibits higher peak values in the central part of the plot.

Figures (7.15) (7.16) show the displacement in time of the mid span node due to the passage of the train type 3 using both moving loads and VBI models, respectively.

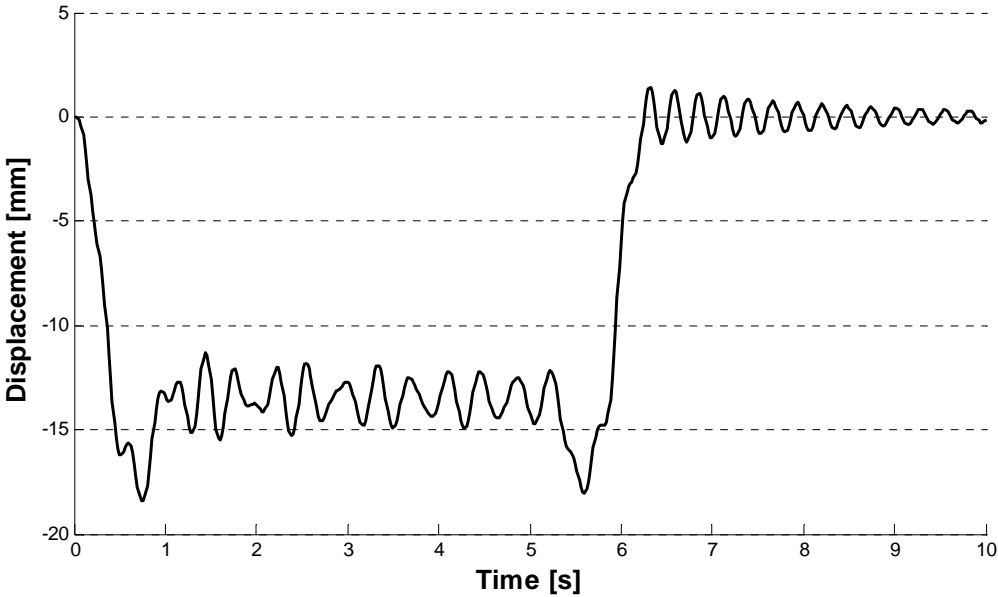


Figure 7.15: Mid span node displacement due to the passage of train type 3 using moving loads model.

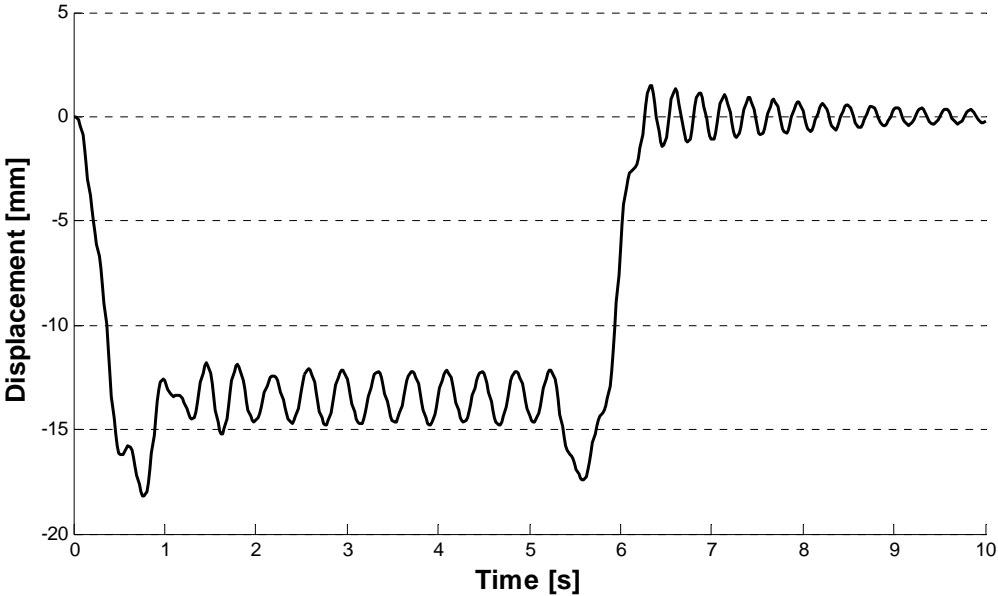


Figure 7.16: Mid span node displacement due to the passage of train type 3 using VBI model.

Also in this case the dynamic behavior of the bridge is almost similar when moving loads or VBI models are considered, as it is possible to see also in figure (7.17). In fact both the models give a maximum displacement of about 1.8 cm at 0.8 seconds and 5.6 seconds, which is the moment in which the initial and final locomotive pass at the mid span point of the bridge.

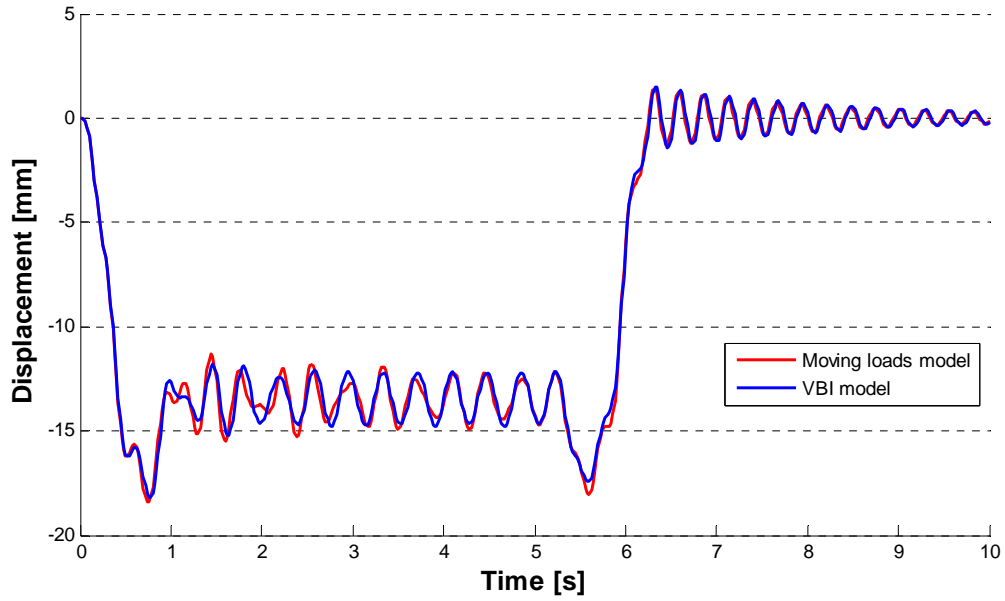


Figure 7.17: Comparison between moving loads and VBI models for train type 3.

As regard the train type 5, the force variation in time on the mid span node using both moving loads and VBI models are shown in figure (7.18)(7.19), respectively.

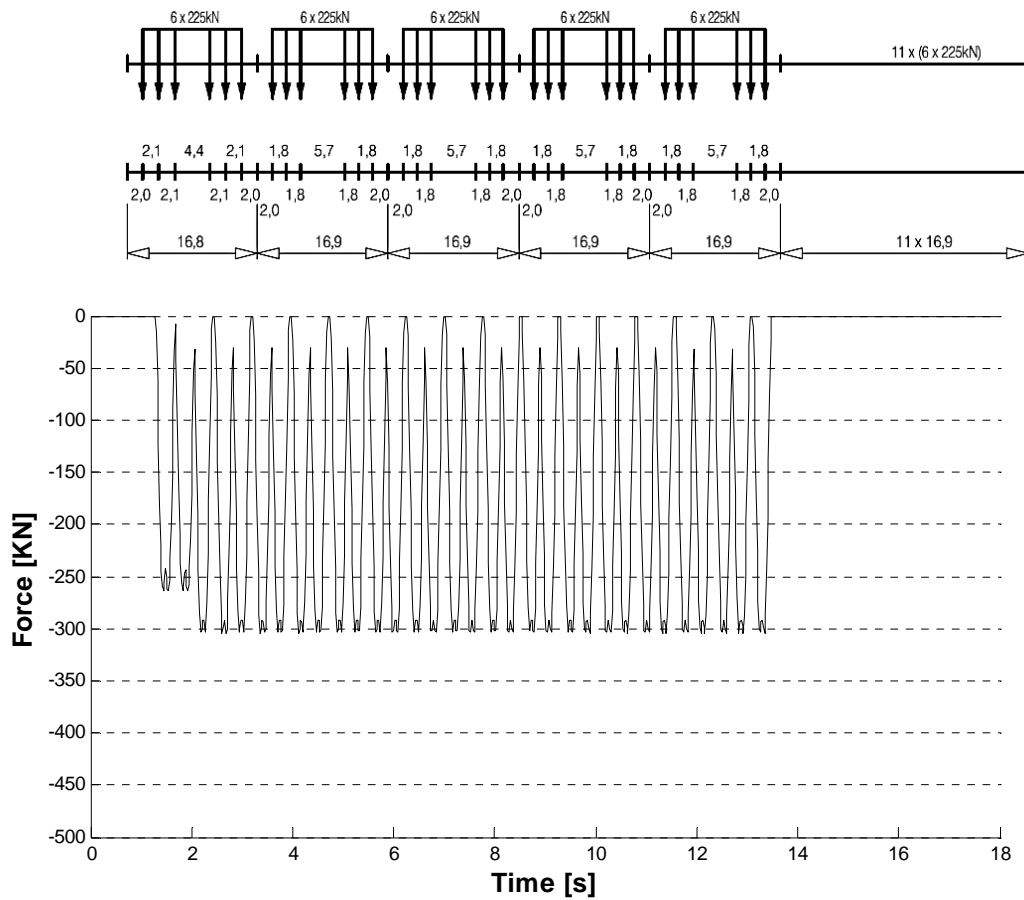
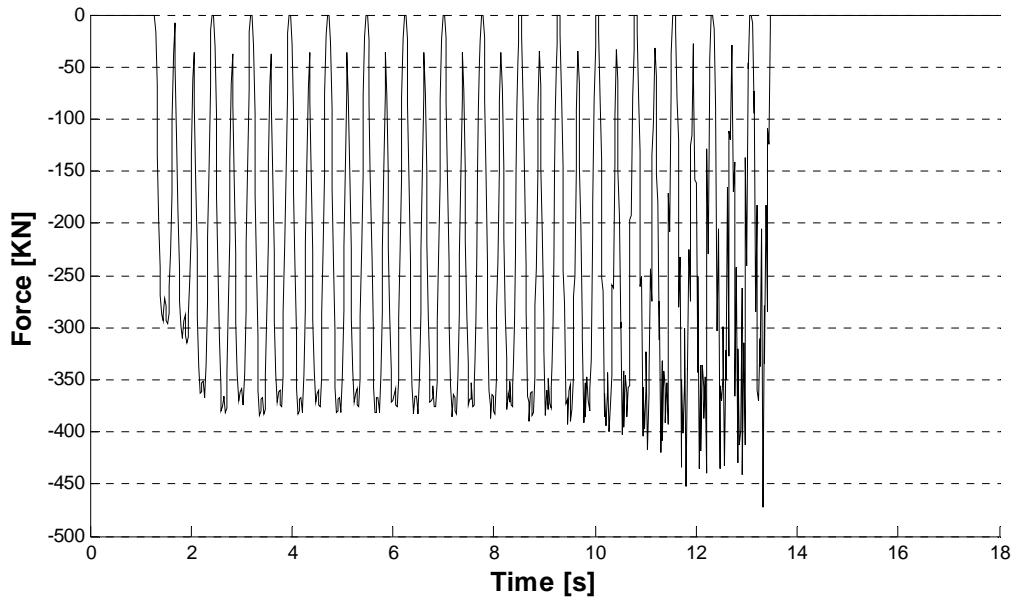


Figure 7.18: Mid span node force variation due to the passage of train type 5 using moving loads model.



**Figure 7.19:** Mid span node force variation due to the passage of train type 5 using VBI model.

The above figures show the trend of the force transmitted by a freight train on the mid span node of the bridge. In these kinds of trains the locomotive and the wagons have the same weight. The VBI model in this case exhibits substantial higher values of the forces transmitted.

Figures (7.20) (7.21) show the displacement in time of the mid span node due to the passage of the train type 5 using both moving loads and VBI models, respectively.

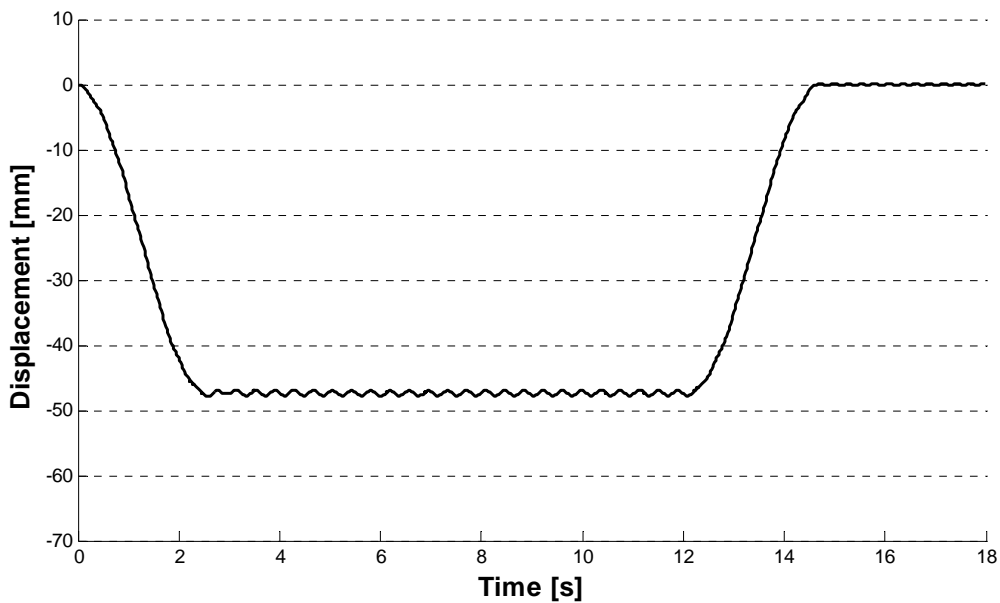


**Figure 7.20:** Mid span node displacement due to the passage of train type 5 using moving loads model.

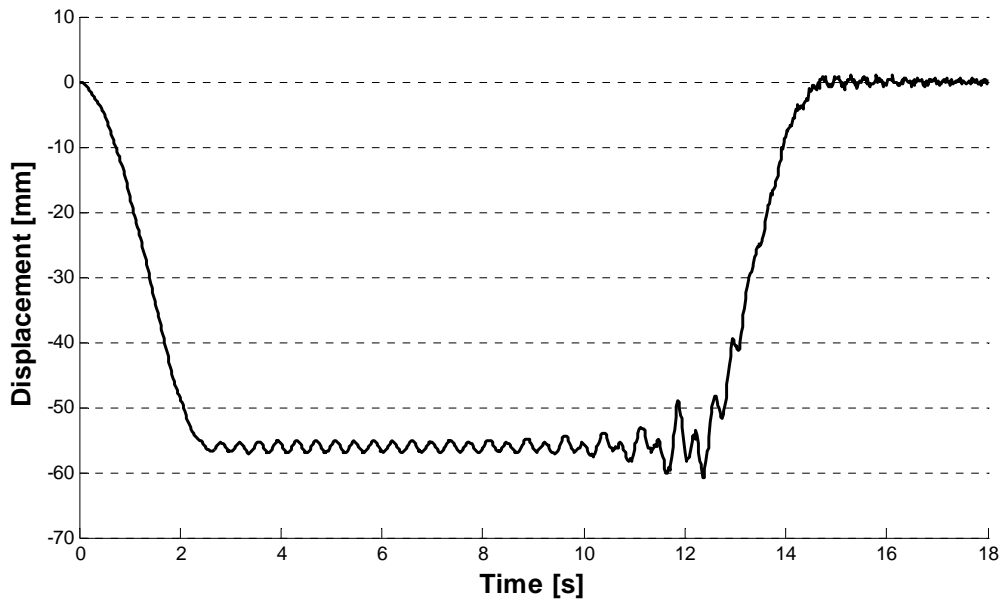


**Figure 7.21:** Mid span node displacement due to the passage of train type 5 using VBI model.

In this case the dynamic behavior of the bridge is different if moving loads or VBI model are considered, as it is possible to see better in figure (7.22). In fact very flat bridge behaviors without almost any oscillations are obtained for both the models, with the exception of the last portion of the VBI model in which little dynamic amplifications are kept, but the flat zones have two different displacement values. The moving loads model has the flat zone at about  $4.8\text{ mm}$  whereas the VBI at about  $5.6\text{ mm}$ , with a significant difference.

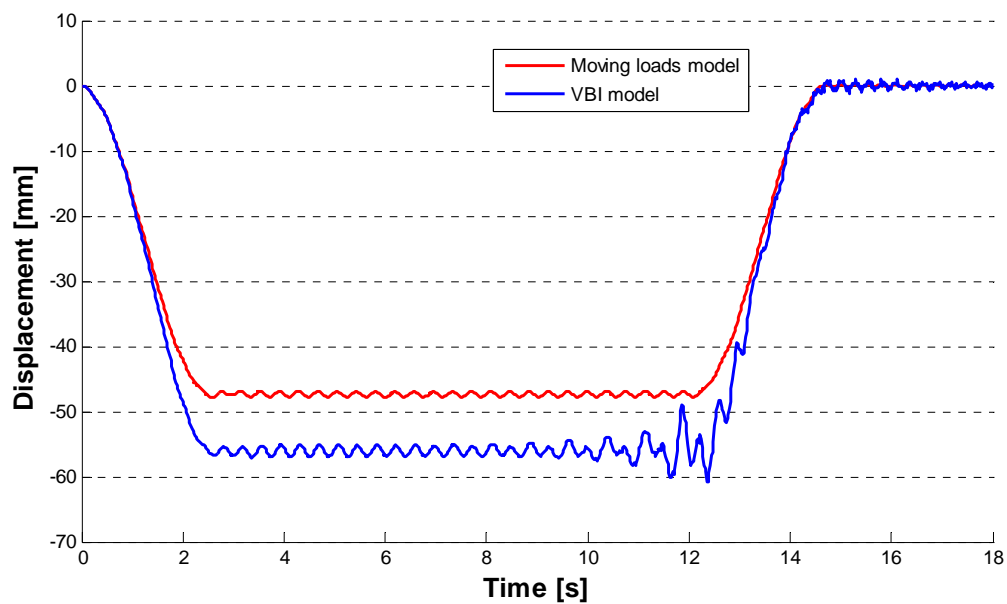


**Figure 7.22:** Comparison between moving loads and VBI models for train type 5.



Figures (7.25) (7.26) show the displacement in time of the mid span node due to the passage of the train type 7 using both moving loads and VBI models, respectively.

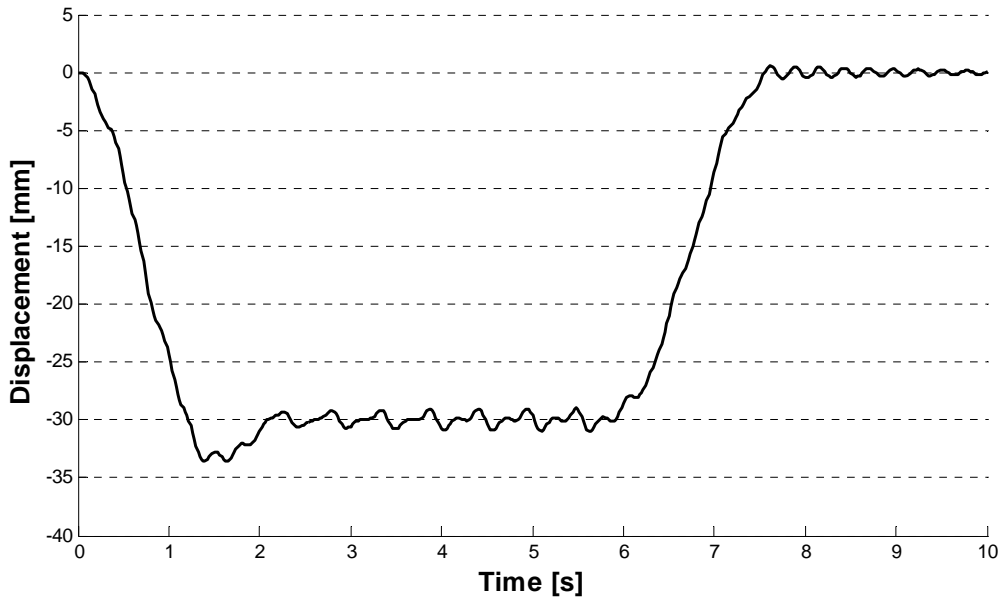


Figure 7.25: Mid span node displacement due to the passage of train type 7 using moving loads model.

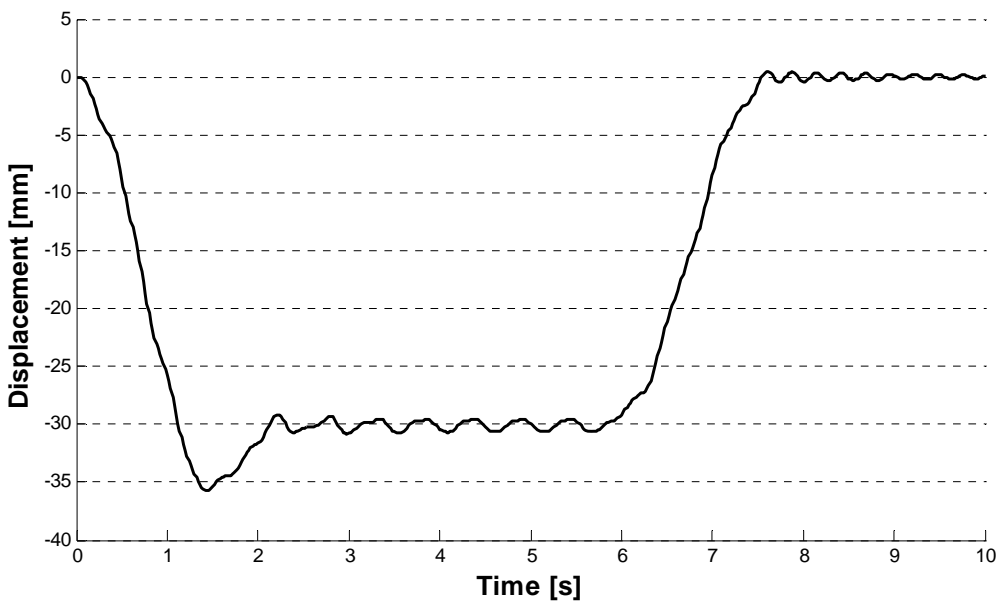


Figure 7.26: Mid span node displacement due to the passage of train type 7 using VBI model.

Also in this case the train used to perform the dynamic analysis is still a freight train, but now the dynamic interaction is lower in comparison to the previous case. In this case there is only a little amplification in the peak value in the initial part when considering VBI model. In fact the VBI plot has a maximum displacement that overcomes the threshold of 35 mm while this does not happen in the case of moving loads in which the maximum displacement is about 33 mm, see in figure (7.27).

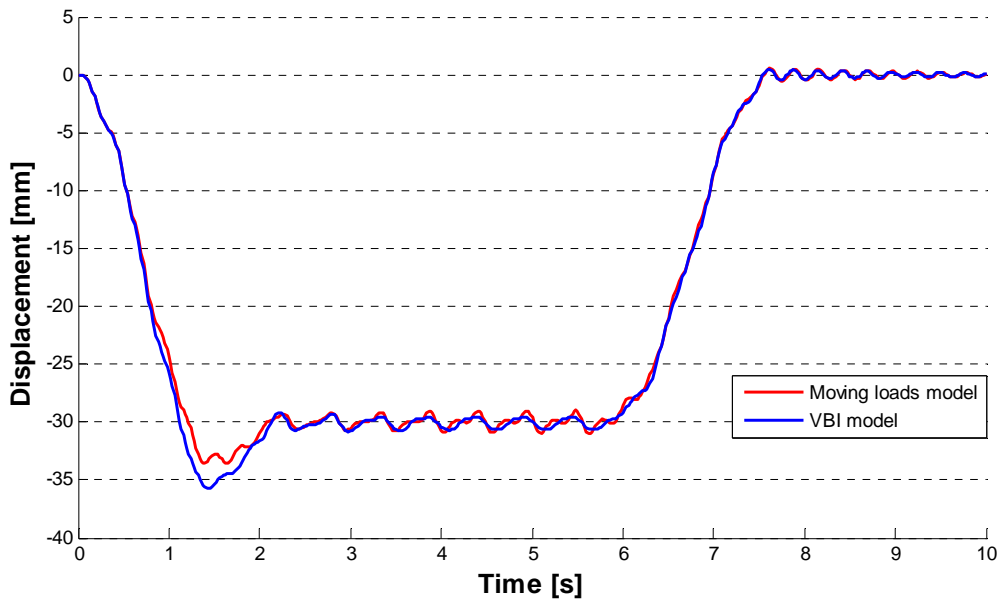


Figure 7.27: Comparison between moving loads and VBI models for train type 7.

As regards the train type 9, the force variation in time on the mid span node using both moving loads and VBI models are shown in figure (7.28)(7.29), respectively.

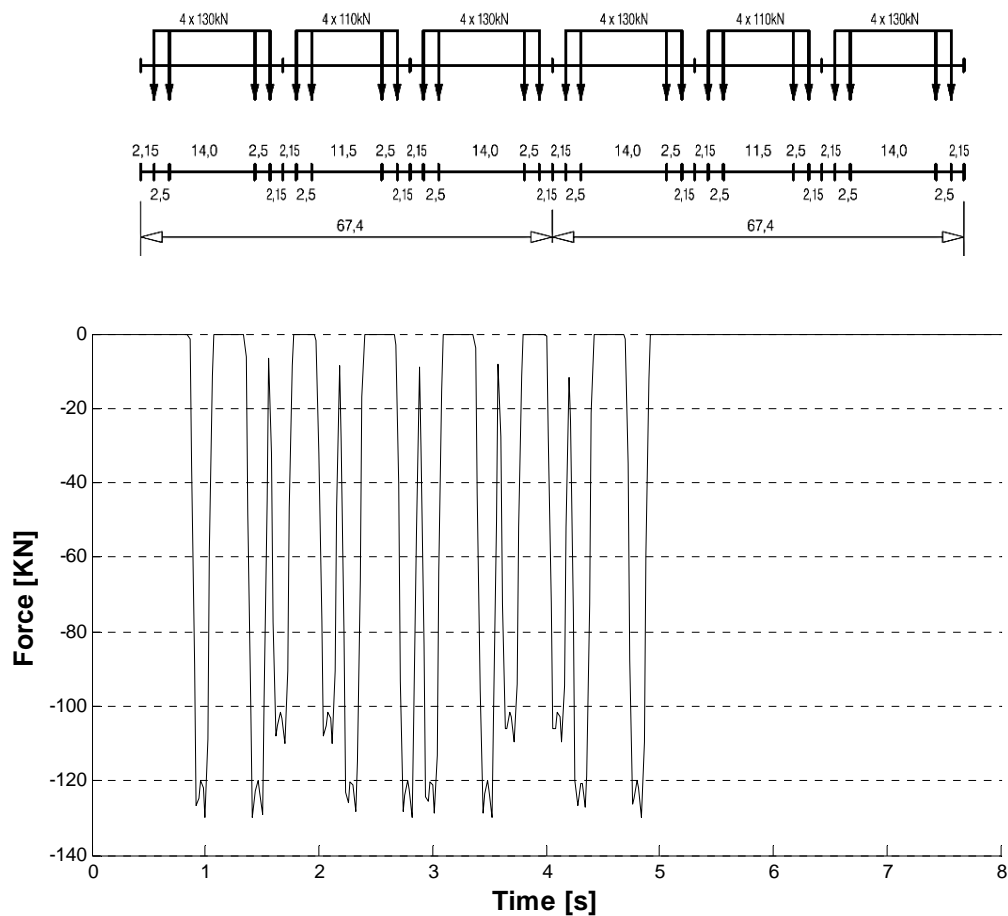
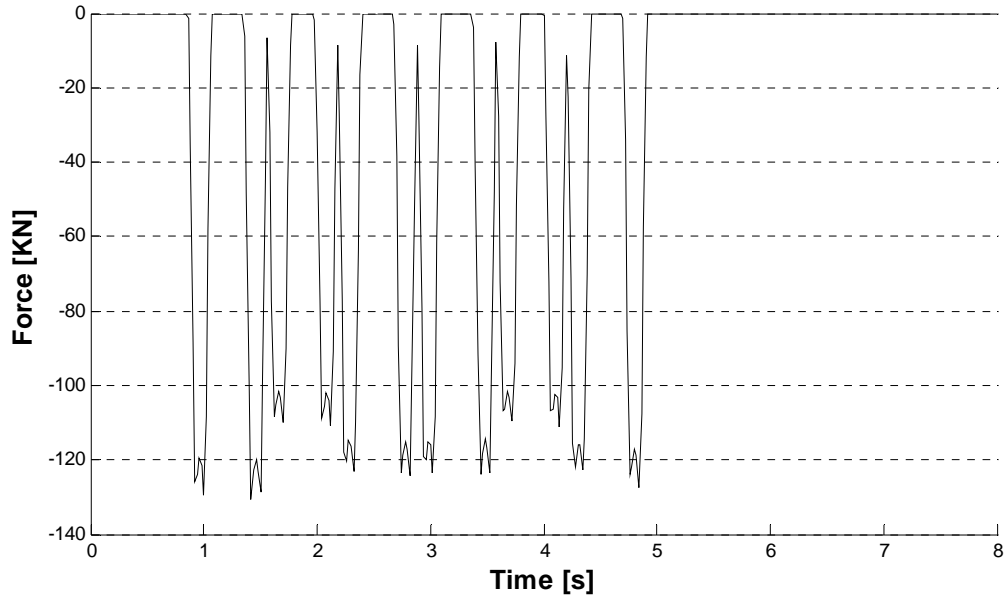


Figure 7.28: Mid span node force variation due to the passage of train type 9 using moving loads model.



**Figure 7.29:** Mid span node force variation due to the passage of train type 9 using VBI model.

The above figures show the effects caused by an underground on the mid span node, in terms of nodal forces. These are light trains, in fact the magnitude of the transmitted force are lower in comparison to the other cases. In most of those kinds of vehicles all the cars have more or less the same weight.

Figures (7.30) (7.31) show the displacement in time of the mid span node due to the passage of the train type 9 using both moving loads and VBI models, respectively.

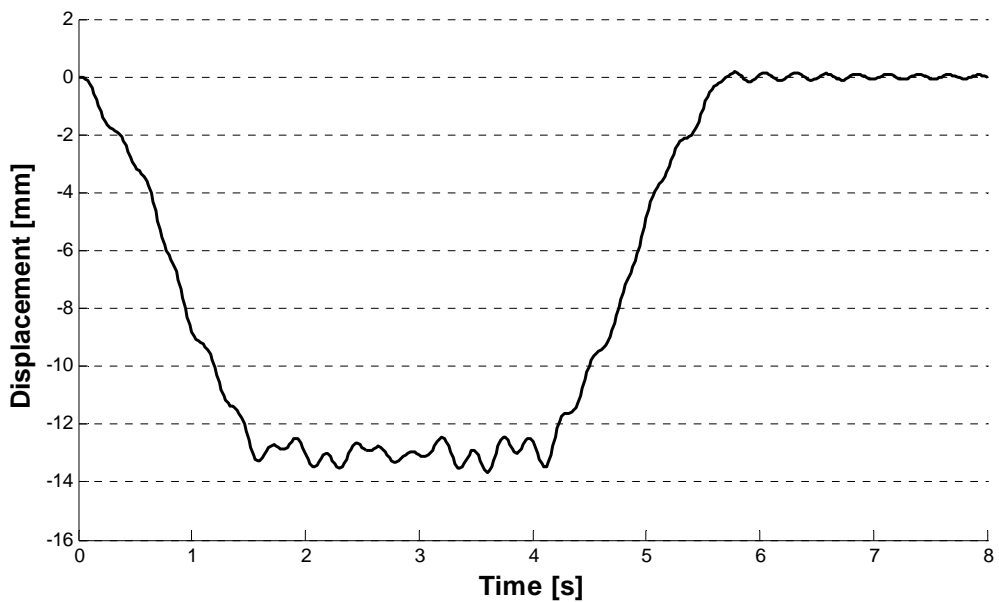


**Figure 7.30:** Mid span node displacement due to the passage of train type 9 using moving loads model.

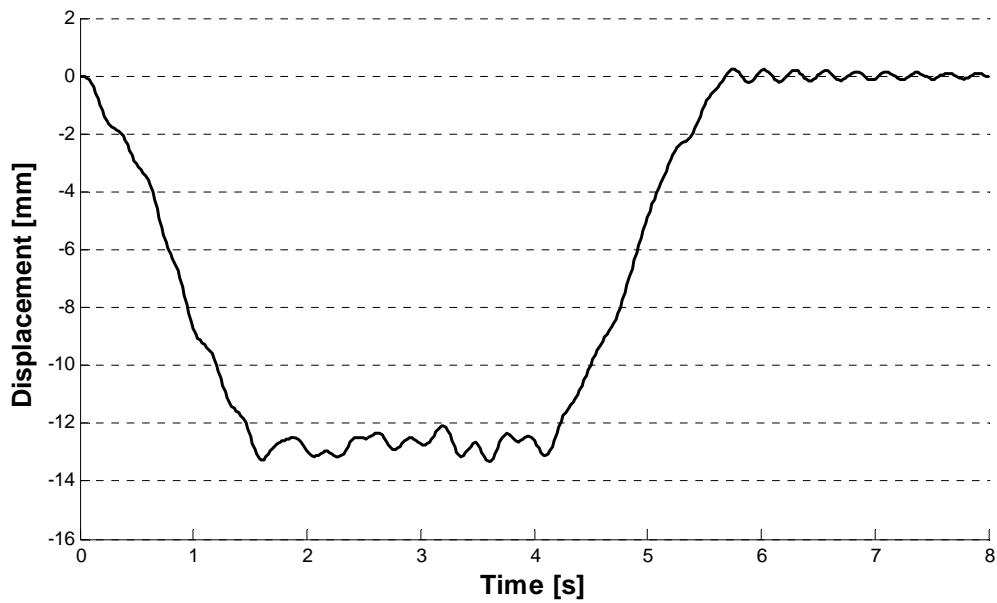


**Figure 7.31:** Mid span node displacement due to the passage of train type 9 using VBI model.

As shown by the above figures, for this suburban train, there aren't big differences between the moving loads and VBI models. The only difference is that in this case the moving load model exhibits a slightly higher values of the amplitude of the oscillations. In fact looking at figure (7.32) the red line that represents the moving load, in the central part always remains under the blue line that represents the VBI model. However the maximum displacement value is about  $1.4\text{ cm}$  for both the model.

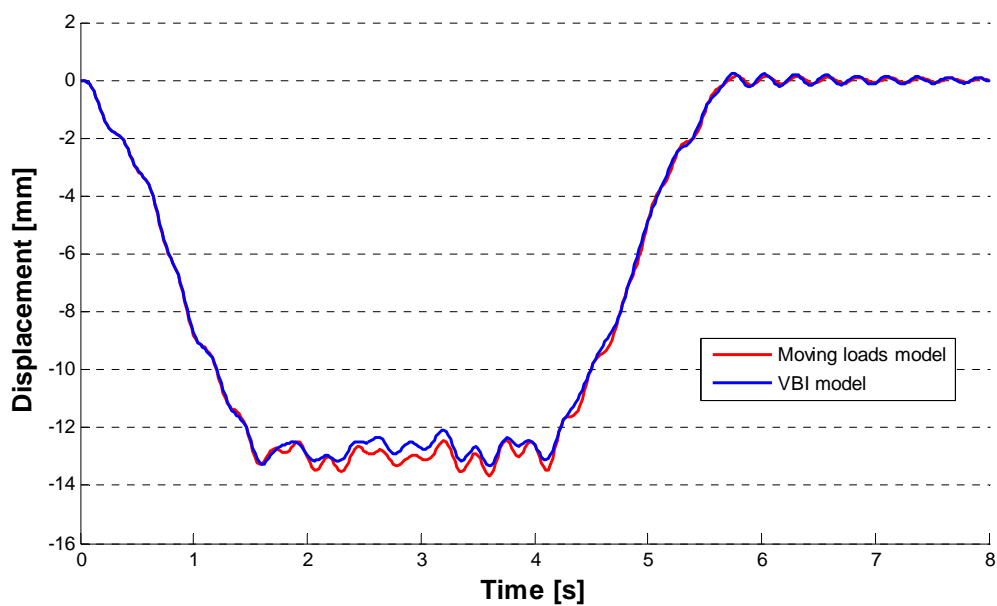


**Figure 7.32:** Comparison between moving loads and VBI models for train type 9.

Figures (7.33) (7.34) show the force variation in time on the mid span node due to the passage of the train type 10 using both moving loads and VBI models, respectively.

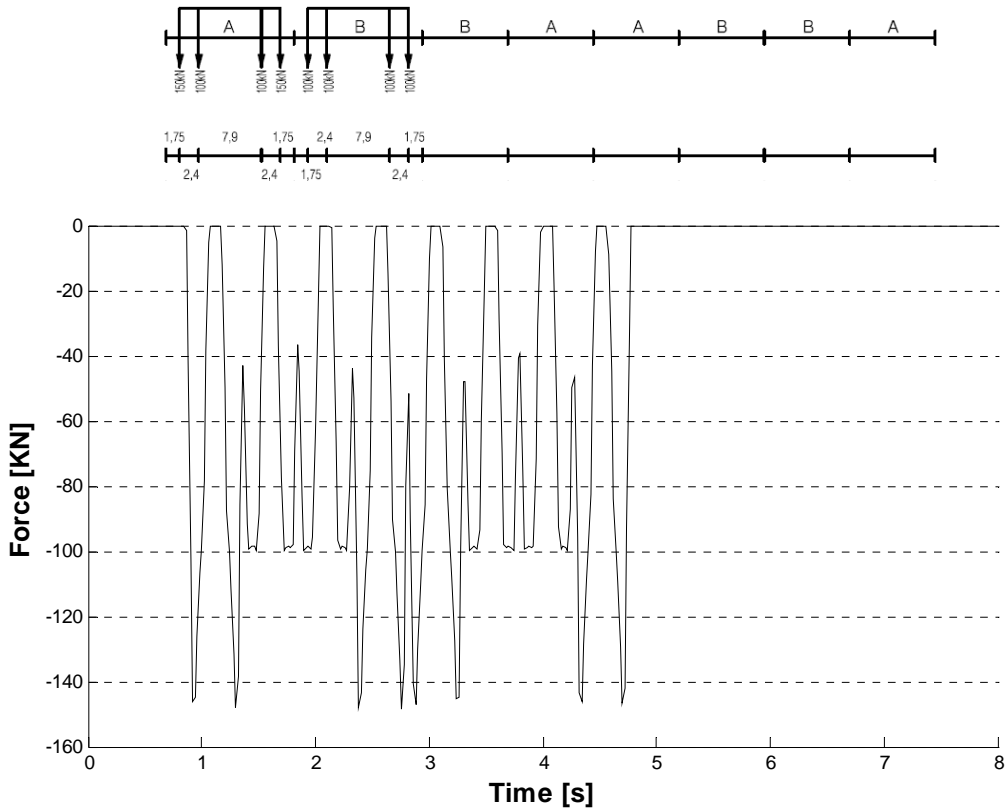


Figure 7.33: Force variation on the half span node due to the passage of train type 10 using moving loads model.

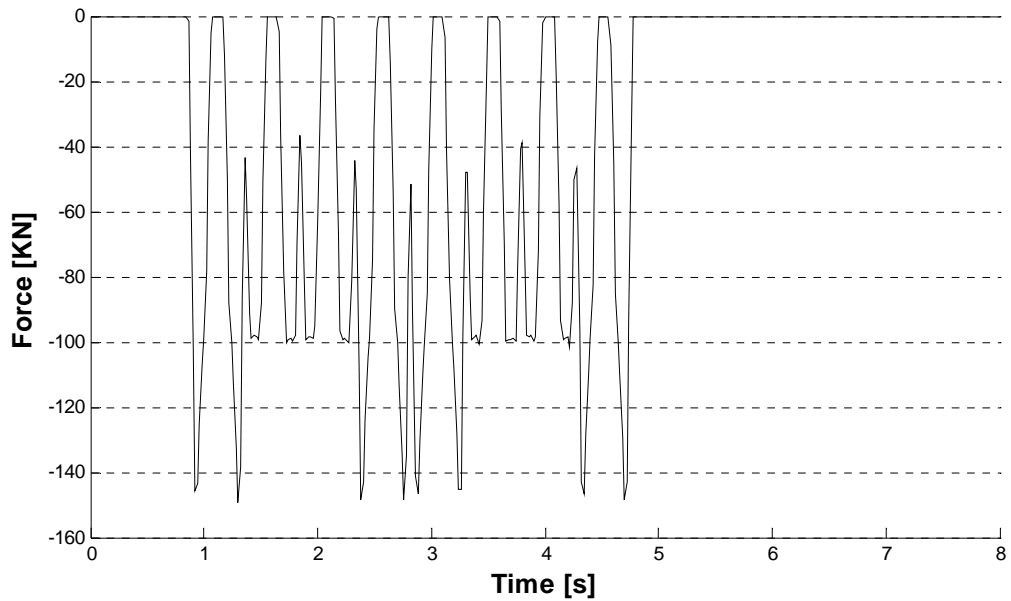


Figure 7.34: Force variation on the half span node due to the passage of train type 10 using VBI model.

Finally, figures (7.35) (7.36) show the displacement in time of the mid span node due to the passage of the train type 10 using both moving loads and VBI models, respectively.

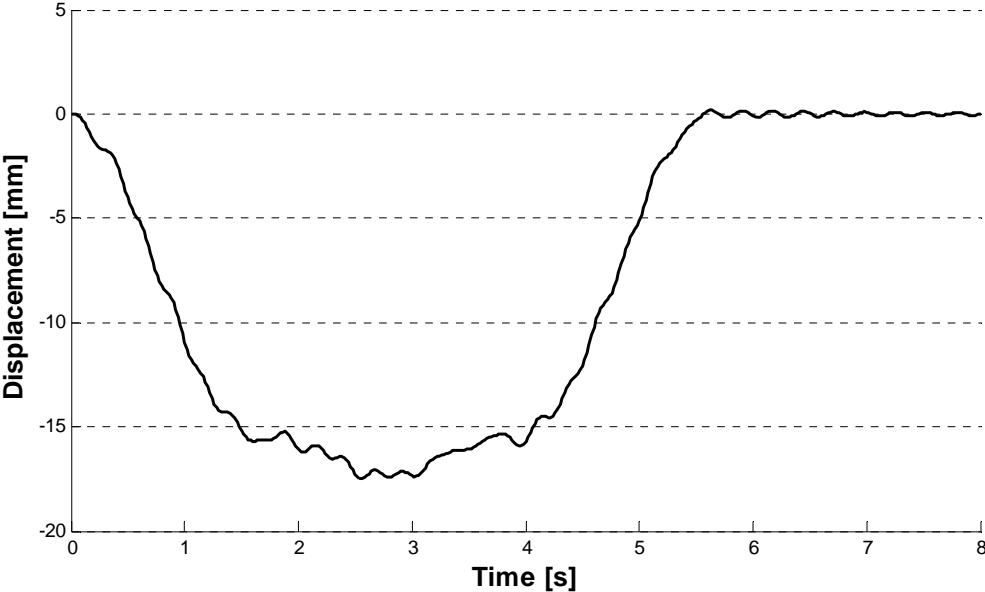


Figure 7.35: Mid span node displacement due to the passage of train type 10 using moving loads model.

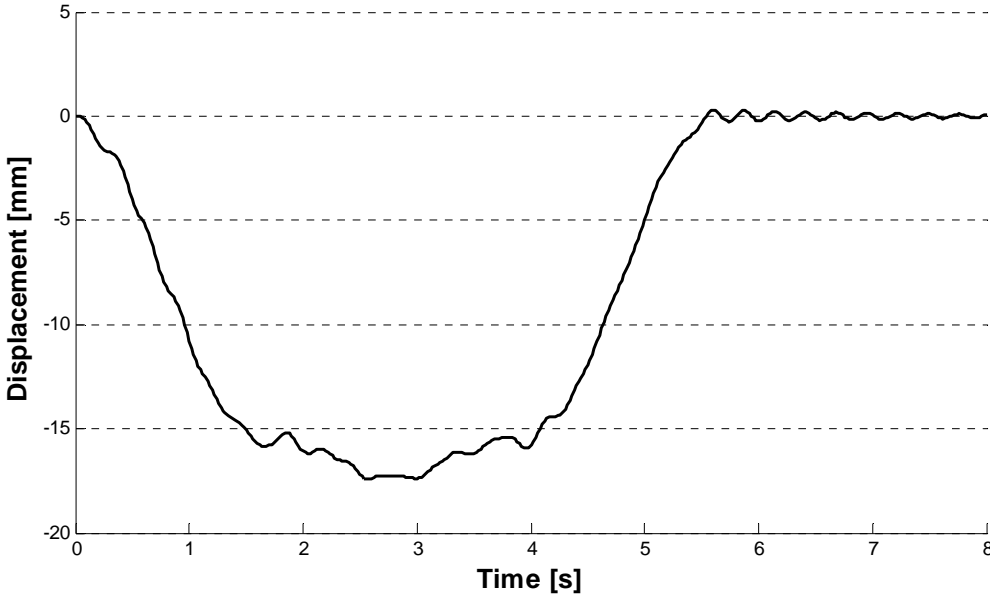


Figure 7.36: Mid span node displacement due to the passage of train type 10 using VBI model.

The above figures show the dynamic behavior of the bridge when an underground is passing. Also in this case the differences are minimal as it is possible to see also in figure (7.37). In fact the two models exhibit similar shape patterns and almost the same maximum displacement of about 1.7 cm.

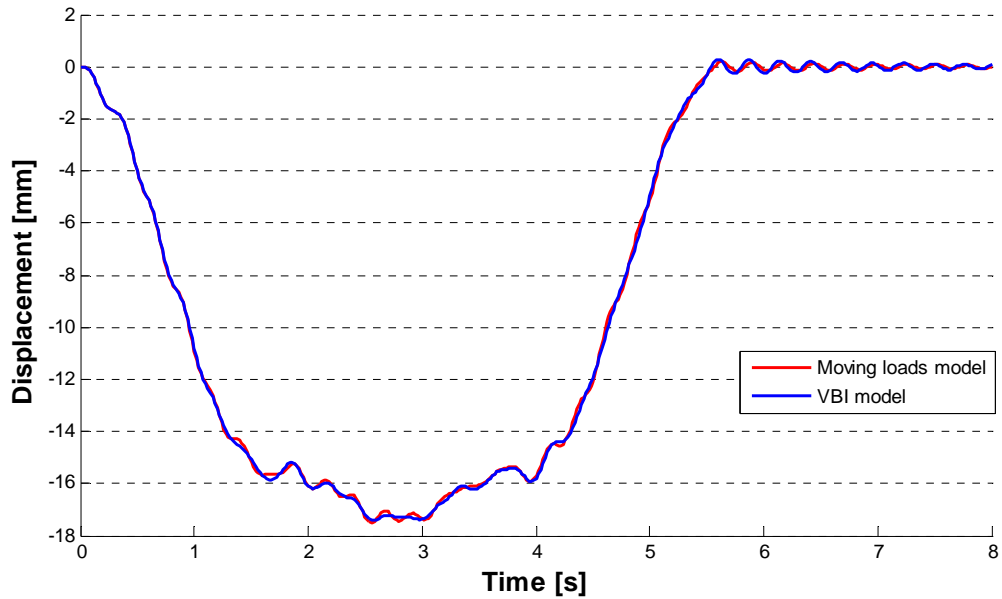


Figure 7.37: Comparison between moving loads and VBI models for train type 10.

At this point is interesting to compare the just obtained results to those obtained by R. Freddi [4]. In fact he had studied the fatigue life of the longer bridge typology as prescribed by the guidelines using the same trains given by the EC1. The two bridges described in *Section 6.1* are very similar, therefore similar behavior is expected. Actually he has carried out the dynamics analyses using the finite elements model of the bridge assigning the load history to each node of the model for each type of train. In the following are reported the results of the trains considered also in this paper, obtained by R. Freddi, see figure (7.38)-(7.44)

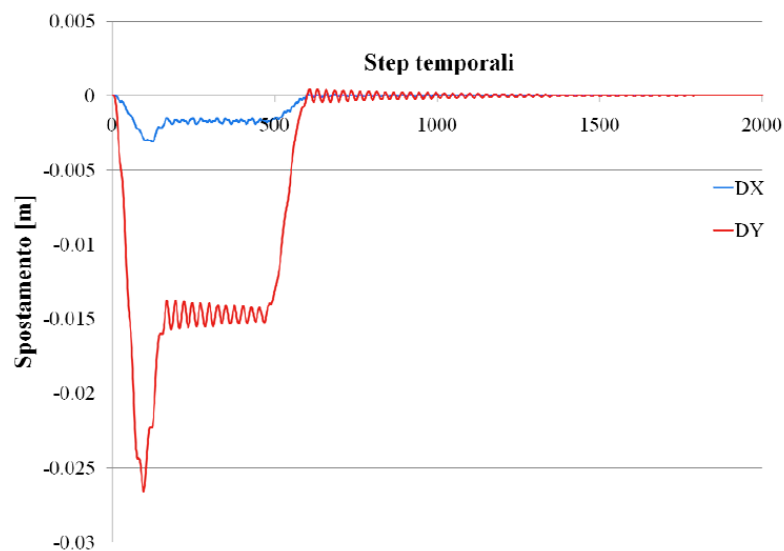
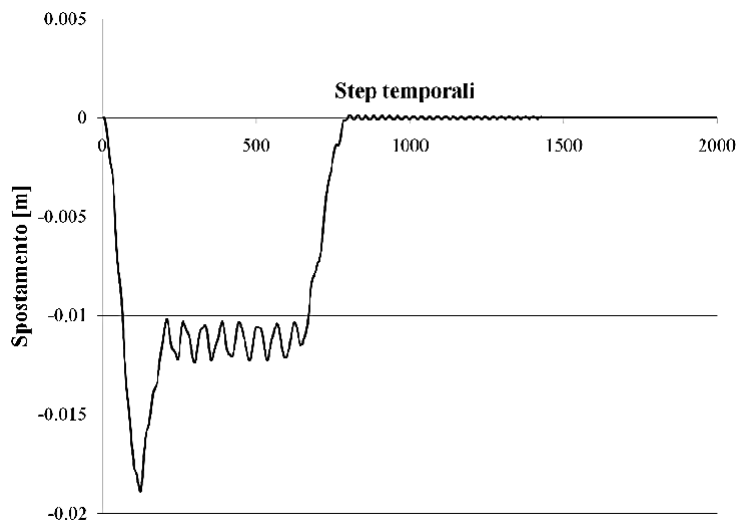
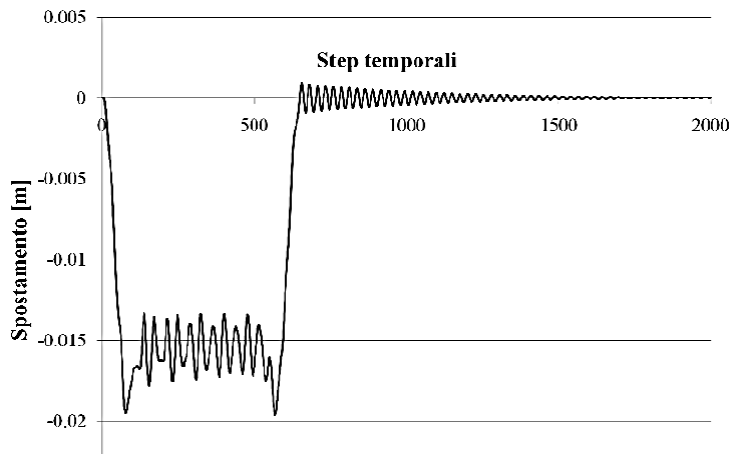


Figure 7.38: Results obtained in [10] for train type 1.



**Figure 7.39:** Results obtained in [10] for train type 2.



**Figure 7.40:** Results obtained in [10] for train type 3.

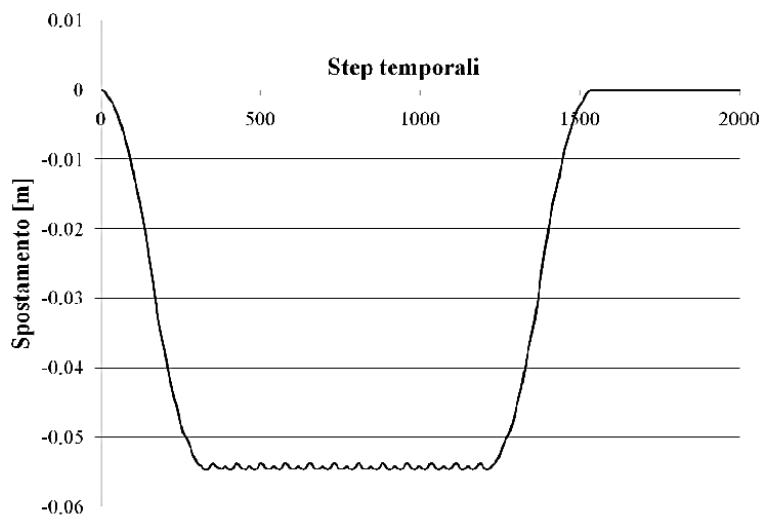


**Figure 7.41:** Results obtained in [10] for train type 5.

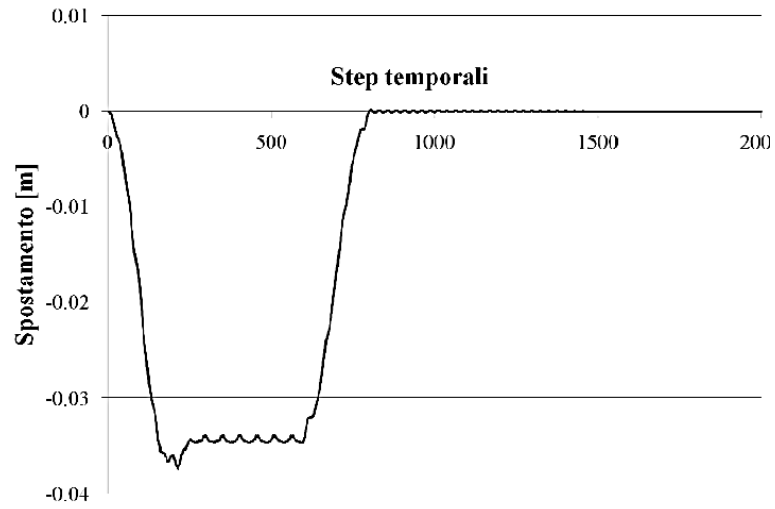


Figure 7.42: Results obtained in [10] for train type 7.

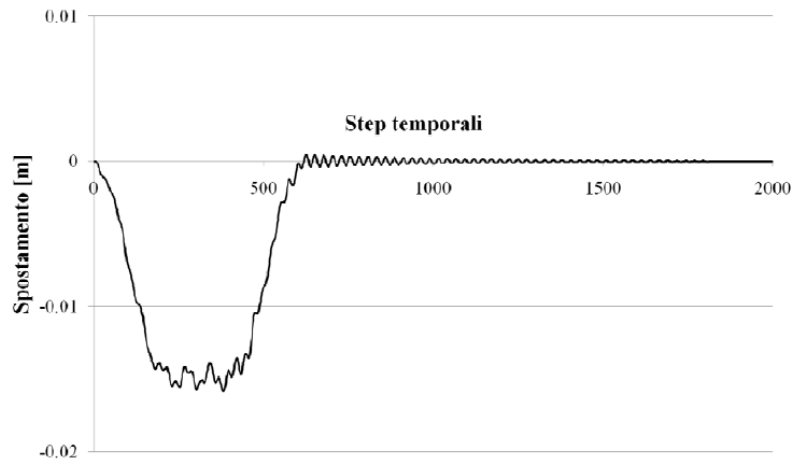


Figure 7.43: Results obtained in [10] for train type 9.

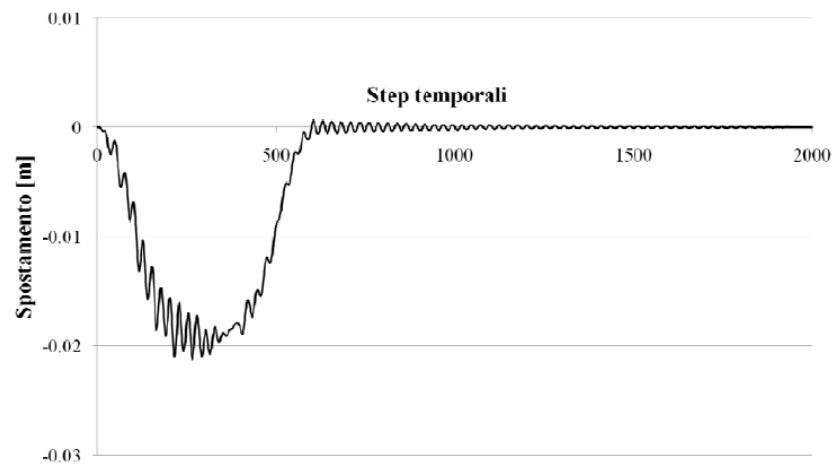


Figure 7.44: Results obtained in [10] for train type 10.

The graphs just presented are taken from [4], and refer to the displacement in time of the mid span node of the considered longer bridge. As it is possible to see the results obtained by R. Freddi and those obtained in this paper are very similar both in order of magnitude and shape patterns. In this way the two models confirm their validity each other since very close results are obtained.

However, apart little differences between the two models, the global dynamic behavior of the bridge is kept with both the models.

## 7.5 Parameters investigation

Up to now, some dynamic analyses of the bridge for some possible crossing trains, using two models for representing them, have been computed. Actually the bridge behavior is function of many parameters. Obviously, first of all, it depends on its own dynamic properties and so on its length, on its mass per unit length  $m$  and bending stiffness  $EI$ . In this way the bridge parameters have been changed accordingly to those given in [2] and [18], where a simply supported bridge with the following characteristics is considered. The bridge has a length  $L$  of 34 m, a mass per unit length of  $m = 11400 \text{ Kg/m}$  and bending stiffness  $EI = 9.92 \cdot 10^{10}$ . Then a Rayleigh damping of 2% for the first frequency and the last frequency of vibration has been assigned. The computed fundamental natural frequency of the bridge is now  $f = 4.01 \text{ Hz}$ . This means that this bridge is a little bit stiffer in respect to the one object of the present study which has fundamental natural frequency equal to 3.78 Hz.

The results obtained using moving loads model and VBI model are compared in figure (7.45), where the high-speed train type 1 is considered.

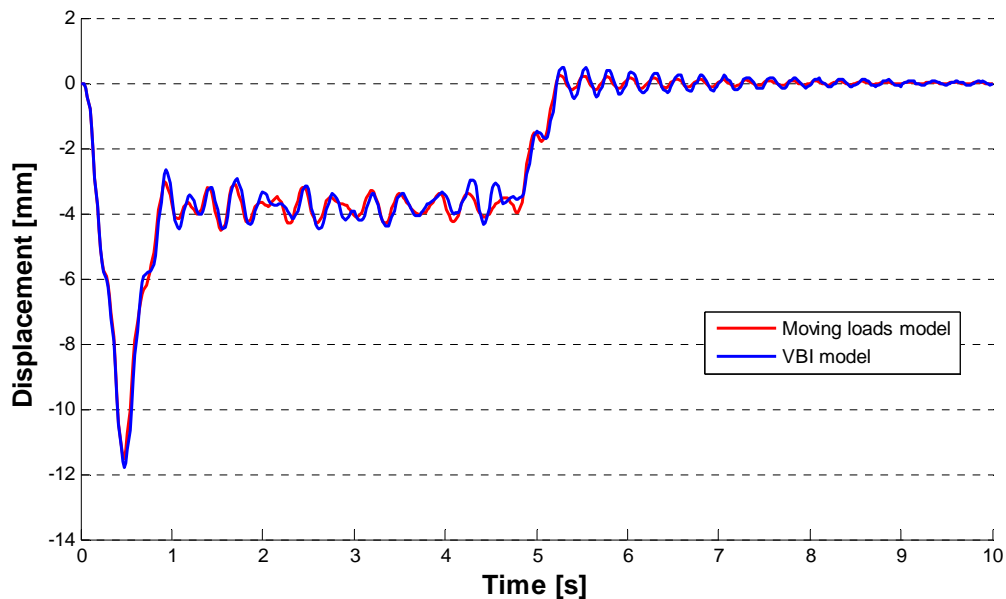


**Figure 7.45:** Mid span node displacement comparison between moving loads and VBI models for train type 1 using different bridge parameters.

As it is possible to see in the above plot, there isn't a strong dynamic interaction when VBI model is used. In fact the two shape patterns are very close each other without substantial differences, as instead happens in Pontelagoscuro bridge, see figure (7.7). In

this case the maximum displacement reached is about  $12\text{ mm}$  for both models. This value is lower in respect to the one obtained for Pontelagoscuro bridge that is about  $25\text{ mm}$  and  $27\text{ mm}$  for moving loads model and VBI model respectively. This result confirms that in general more flexible bridges experience more dynamic interactions in respect to stiffer bridges. In fact it may happen that a bending frequency of vibration of the bridge matches one vertical frequency of vibration of the vehicle causing a dynamic amplification effect.

Other important parameters that govern the problem are the weight of the trains and therefore the transmitted axles loads, the distances between them, as well as the traveling velocity. In fact going back to the dynamic analyses performed on the Pontelagoscuro bridge and changing the traveling velocity of the train type 5 from  $80\text{ Km/h}$  to  $90\text{ Km/h}$  a slightly different dynamic behavior of the structure is obtained. As showed in figure (7.46) at  $90\text{ Km/h}$ , the dynamic amplifications kept at velocity of  $80\text{ Km/h}$  there are no more exhibited.

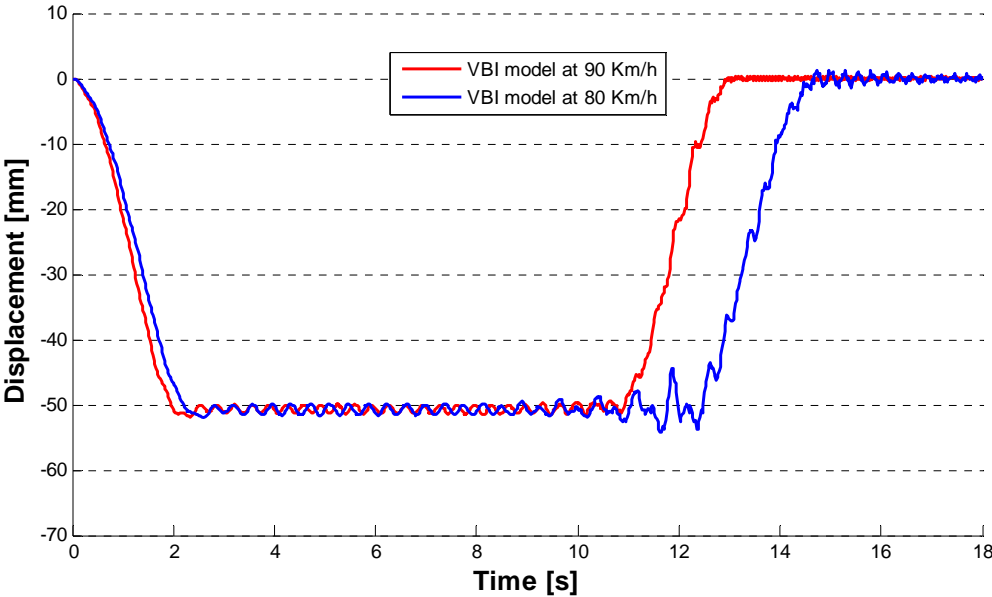


**Figure 7.46:**Mid span node displacement comparison between moving loads and VBI models for train type 5 changing the traveling velocity.

In this sense another attempt is done lowering the traveling velocity of the train type 1 from  $200\text{ Km/h}$  to  $100\text{ Km/h}$  contrarily to what has been done before for the train type 5 where the velocity has been increased. The results obtained are shown in figure (7.47). Also in this case there is a reduction in the amplitude of the oscillations, although small, in the central part of the plot.

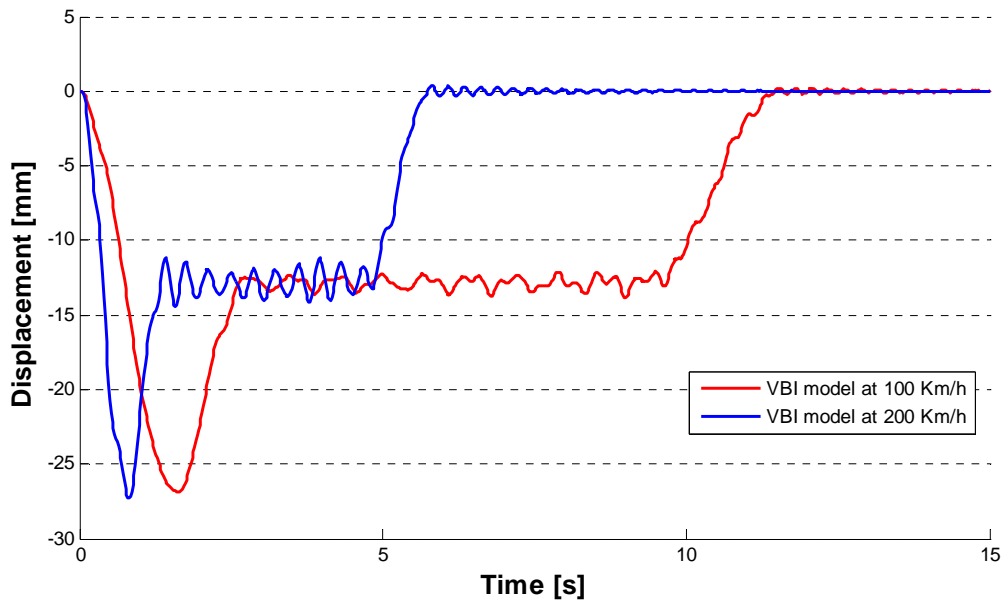


**Figure 7.47:** Mid span node displacement comparison between moving loads and VBI models for train type 1 changing the traveling velocity.

In the case of VBI model, as parameters of the problem there are also the values assigned to the suspension elements of the vehicle. In fact looking at Eq. (4.8) (4.12) the interaction forces transmitted depend strongly on the values of the stiffness and damping of those devices. For this reason a dynamic analysis has been performed doubling that values in the cars of the train type 5. The results obtained are shown in figure (7.48).

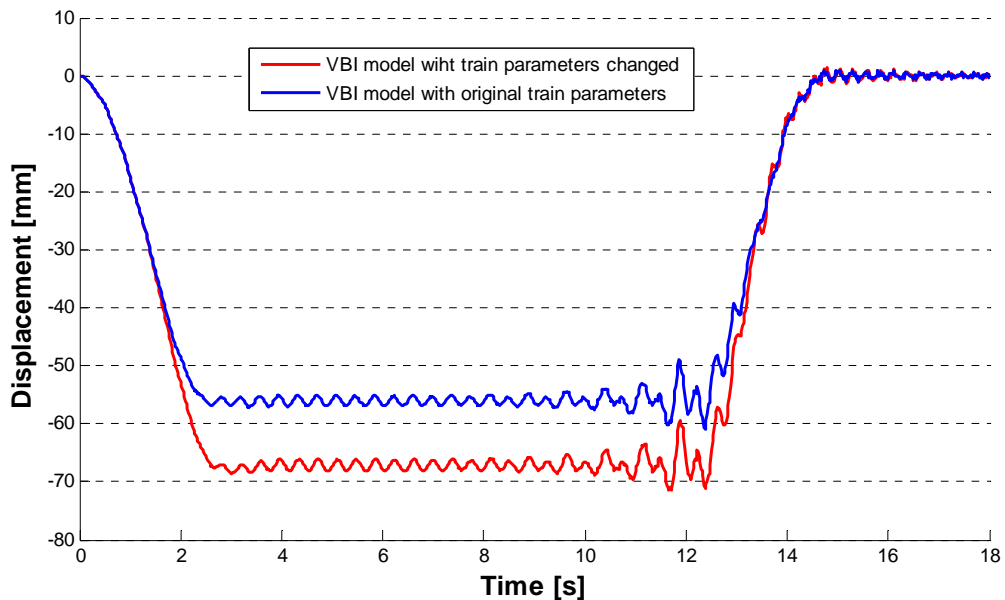


**Figure 7.48:** Mid span node displacement comparison between moving loads and VBI models for train type 5 changing the springs and dampers values of the vehicle.

Therefore increasing the values of the springs and dampers of the vehicle, there is a stronger dynamic interaction as is it possible to see in the above figure. In this case it has been obtained a maximum displacement higher of about  $1\text{ cm}$  for the modified parameters train in respect to the train with the original value parameters

In conclusion there are many parameters that have influence on the results. First of all there is the bridge with its properties. If the bridge is stiff then it will be subjected to very little displacements and so the vehicle will be not excited strongly and therefore little interaction forces will be exchanged. In this case moving loads model and VBI model will give approximately the same results. On the other hand flexible structure will be subjected to high interaction forces and so the two models could give very different results.

Finally there are not general rules to establish which parameters are critical in general, and each train has to be studied per for itself.

## 8. 3D VBI MODEL APPLICATION

### 8.1 Introduction

The aim of this section is to understand the effects of some crossing trains not only in the vertical direction, but including also lateral and torsional vibrations of the bridge performing three-dimensional vehicle bridge dynamic interaction analyses. Such analyses will provide an insight of what happens not only in the primary elements of the bridge that are designed for this purpose, but also on the secondary elements that could not be designed to face these effects, as for example the bracing systems. In fact there are very poor bracing elements in the bridge as shown in the picture in *Chapter 5.1*. This may be correlated to the fact that the structure is located in a not excessively windy area, and being the railway track centered in respect to the centroidal axis, not important torsional and lateral effects were expected.

In this chapter, in order to perform more accurate three-dimensional dynamic analyses of the bridge, it has been necessary to rewrite the equations of motion of the bridge in modal coordinates, taking into account only the main mode of vibrations of the structure. In this way some benefits are obtained; however more detail about this procedure will be given in the following.

## 8.2 Three-dimensional dynamic analyses

As already discussed in *Section 4* in order to perform VBI analysis the two sets of equations of motion of the bridge and of the vehicle are needed. As regards the bridge the equations of motion are represented by Eq. (4.13) rewritten in the following for clarity:

$$\mathbf{M}_b \ddot{\mathbf{V}}_b + \mathbf{C}_b \dot{\mathbf{V}}_b + \mathbf{K}_b \mathbf{V}_b = \mathbf{P}_b \quad (8.1)$$

with all the terms already specified.

Actually the finite elements model of the structure has more than 14000 nodes, and each of them has 6 degrees of freedom, resulting in a system of about 84000 equations. Moreover to obtain  $\mathbf{M}_b$ ,  $\mathbf{C}_b$  and  $\mathbf{K}_b$  of a structure like that is not an easy task. Nevertheless a big computational effort will be necessary to solve this kind of problem. To overcome these problems modal superposition method can be applied assuming that only the first  $N_0$  modes of the bridge are contributing to the response as already explained in *Chapter 4.3*. The equation of motion of the bridge can be rewritten accordingly to Eq. (4.14) as follows:

$$\ddot{\mathbf{q}} + \mathbf{C}_b^* \dot{\mathbf{q}} + \mathbf{K}_b^* \mathbf{q} = \mathbf{P}_b^* \quad (8.2)$$

where it has been assumed that the eigenvectors are normalized with respect to the mass matrix  $\mathbf{M}_b$ . Remembering that the vector  $\mathbf{q}$  collects the modal coordinates, and the matrices  $\mathbf{C}_b^*$ ,  $\mathbf{K}_b^*$  and the vector  $\mathbf{P}_b^*$  are defined as follows:

$$\mathbf{C}_b^* = 2\nu\mathbf{\Omega}$$

$$\mathbf{K}_b^* = \mathbf{\Omega}^2$$

$$\mathbf{P}_b^* = \mathbf{\Phi}^T \mathbf{P}_b$$

where  $\mathbf{\Phi}$  is the  $N_{DOF} \times N_0$  matrix of eigenvectors and  $\mathbf{\Omega}$  is the  $N_0 \times N_0$  diagonal matrix of eigenvalues of the considered modes. In this way a very reduced number of equations of motion are to be solved and all the terms are easily obtainable.

In this study only the first four fundamental modes are considered, which are the same used in the optimization process. Of these modes, the frequencies and the damping ratios are known experimentally, see table (5.2). Therefore the  $\mathbf{C}_b^*$  and  $\mathbf{K}_b^*$  can be obtained directly as:

$$\mathbf{C}_b^* = \begin{bmatrix} 0.1750 & 0 & 0 & 0 \\ 0 & 0.4217 & 0 & 0 \\ 0 & 0 & 0.2923 & 0 \\ 0 & 0 & 0 & 1.122 \end{bmatrix} \quad (8.3)$$

and

$$\mathbf{K}_b^* = \begin{bmatrix} 181.286 & 0 & 0 & 0 \\ 0 & 587.481 & 0 & 0 \\ 0 & 0 & 734.505 & 0 \\ 0 & 0 & 0 & 871.967 \end{bmatrix} \quad (8.4)$$

As regards  $\Phi$ , in this case, only the mode shapes of the nodes belonging to the internal longitudinal beams which support the sleepers with the railway track are needed, as points of applications of the forces transmitted by the train. Therefore computing a modal analysis with the finite elements program it has been possible to obtain the mode shape vector  $\phi$  of that points for each considered mode and so  $\Phi$ .

Therefore subdividing the length of the bridge into 133 couple of nodes, the  $\Phi$  matrix dimensions will be  $532 \times 4$ , because vertical and horizontal transversal displacements are taken into account. Transposing and multiplying it for the vector of the external forces  $532 \times 1$  matrix  $\mathbf{P}_b$ ,  $\mathbf{P}_b^*$  can be obtained, resulting in a  $4 \times 1$  matrix. As already said  $\mathbf{P}_b$  represents the nodal force vector caused by the wheel-rail interaction. It is determined by position, movement status and mass of the wheel sets. The horizontal, vertical and torsional forces produced by wheel set  $i$  of bogie  $j$  are computed from the equilibrium displacement of wheel, which in this case using the 3D vehicle model of figure (4.2) are:

$$\begin{cases} F_{YW1} = -M_{W1}\ddot{Y}_{W1} + 2C_H[\dot{Y}_1 + q\dot{R}_{z1} - h_3\dot{R}_{X1} - \dot{Y}_{W1}] + 2K_H[Y_1 + qR_{z1} - h_3R_{X1} - Y_{W1}] \\ F_{ZW1} = -M_{W1}\ddot{Z}_{W1} + 2C_V[\dot{Z}_1 + q\dot{R}_{Y1} - \dot{Z}_{W1}] + 2K_V[Z_1 + qR_{Y1} - Z_{W1}] + F_{G1} \\ F_{RXW1} = -I_{W1}\ddot{R}_{XW1} + 2C_VDb_1(\dot{R}_{X1} - \dot{R}_{XW1}) + 2K_VDb_1(R_{X1} - R_{XW1}) \end{cases}$$

$$\begin{cases} F_{YW2} = -M_{W2}\ddot{Y}_{W2} + 2C_H[\dot{Y}_1 + q\dot{R}_{z1} - h_3\dot{R}_{X1} - \dot{Y}_{W2}] + 2K_H[Y_1 + qR_{z1} - h_3R_{X1} - Y_{W2}] \\ F_{ZW2} = -M_{W2}\ddot{Z}_{W2} + 2C_V[\dot{Z}_1 + q\dot{R}_{Y1} - \dot{Z}_{W2}] + 2K_V[Z_1 + qR_{Y1} - Z_{W2}] + F_{G2} \\ F_{RXW2} = -I_{W2}\ddot{R}_{XW2} + 2C_VDb_1(\dot{R}_{X1} - \dot{R}_{XW2}) + 2K_VDb_1(R_{X1} - R_{XW2}) \end{cases} \quad (8.5)$$

$$\begin{cases} F_{YW3} = -M_{W3}\ddot{Y}_{W3} + 2C_H[\dot{Y}_3 + q\dot{R}_{z3} - h_3\dot{R}_{X3} - \dot{Y}_{W3}] + 2K_H[Y_3 + qR_{z3} - h_3R_{X3} - Y_{W3}] \\ F_{ZW3} = -M_{W3}\ddot{Z}_{W3} + 2C_V[\dot{Z}_3 + q\dot{R}_{Y3} - \dot{Z}_{W3}] + 2K_V[Z_3 + qR_{Y3} - Z_{W3}] + F_{G3} \\ F_{RXW3} = -I_{W3}\ddot{R}_{XW3} + 2C_VDb_1(\dot{R}_{X3} - \dot{R}_{XW3}) + 2K_VDb_1(R_{X3} - R_{XW3}) \end{cases}$$

$$\begin{cases} F_{YW4} = -M_{W4}\ddot{Y}_{W4} + 2C_H[\dot{Y}_3 + q\dot{R}_{z3} - h_3\dot{R}_{X3} - \dot{Y}_{W4}] + 2K_H[Y_3 + qR_{z3} - h_3R_{X3} - Y_{W4}] \\ F_{ZW4} = -M_{W4}\ddot{Z}_{W4} + 2C_V[\dot{Z}_3 + q\dot{R}_{Y3} - \dot{Z}_{W4}] + 2K_V[Z_3 + qR_{Y3} - Z_{W4}] + F_{G4} \\ F_{RXW4} = -I_{W4}\ddot{R}_{XW4} + 2C_VDb_1(\dot{R}_{X3} - \dot{R}_{XW4}) + 2K_VDb_1(R_{X3} - R_{XW4}) \end{cases}$$

where  $F_{YWi}$ ,  $F_{ZWi}$  and  $F_{RXWi}$  ( $i = 1,2,3,4$ ) represent the forces and the moment under the  $i^{th}$  wheel set.  $M_W$  is the mass of the wheel set,  $I_W$  is the inertia around the X-axis of the wheel set,  $F_G$

is the weight on the wheel and  $D$  is the gauge of the rail. The wheel-rail forces between nodes are transferred to the two neighboring rail nodes  $N_1$  and  $N_2$  using the following expression:

$$\begin{aligned} R_1 &= F \frac{b}{a+b} \\ R_2 &= F \frac{a}{a+b} \end{aligned} \quad (8.6)$$

with the meaning of the terms explained in next figure (9.1).

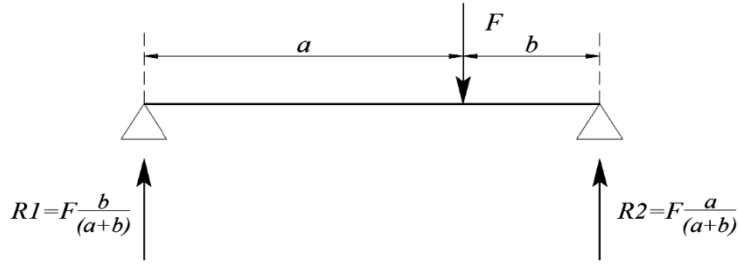


**Figure 8.1:** Scheme of the equivalent reaction forces.

As regards the vehicle its equations of motion are represented by the Eq. (4.1) rewritten in the following as:

$$\mathbf{M}_v \ddot{\mathbf{V}}_v + \mathbf{C}_v \dot{\mathbf{V}}_v + \mathbf{K}_v \mathbf{V}_v = \mathbf{P}_v \quad (8.7)$$

with the meaning of all the terms already specified in *Section 4.2*.

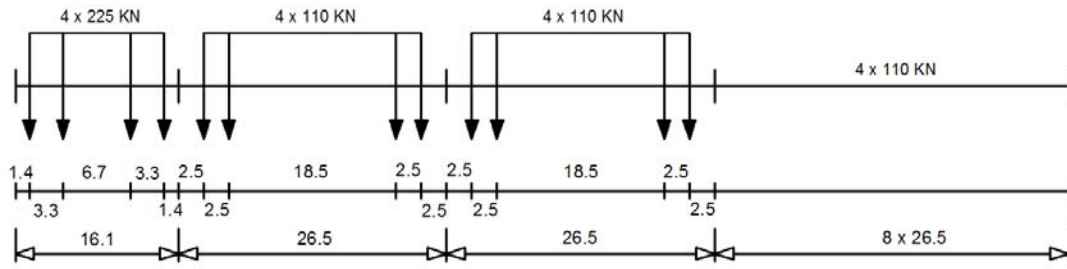
In order to carry out dynamic analyses of the Pontelagoscuro railway bridge the Italian high-speed train ETR500Y is considered as given in [3]. It is composed of a locomotive followed by eight passenger cars and another locomotive. The length of the locomotive is 19.7 m, while the length of the passenger car is 26.1 m. The average static axle loads for the locomotive and passenger cars are 176.4 KN and 112.9 KN, respectively, this train will be called in the following as “*train type B*”.

The vehicle system can be modeled as in figure (4.2) where each wagons is considered as an independent entity with one car body, two bogies and four wheel sets as already described in *chapter 4.2*.

Due to the lack of information about other trains that travel daily on the bridge, other three possible types of trains are considered. The four chosen trains with their characteristics are schematized in the following.

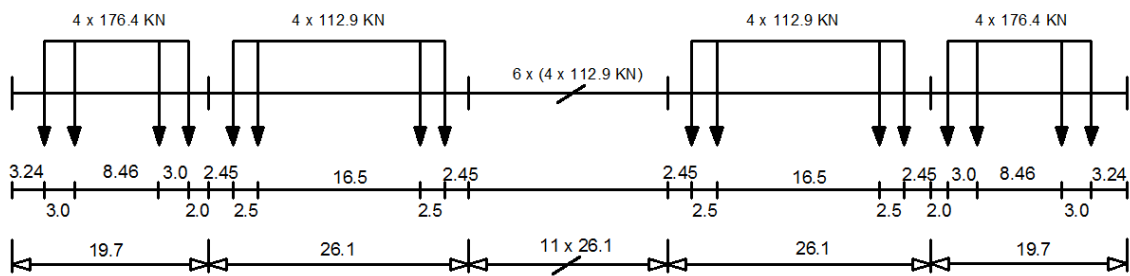
**Type A:** Locomotive-hauled passenger train

$\Sigma Q = 5300 \text{ KN}$      $v = 160 \text{ Km/h}$      $L = 281.10 \text{ m}$      $q = 18.9 \text{ KN/m}$



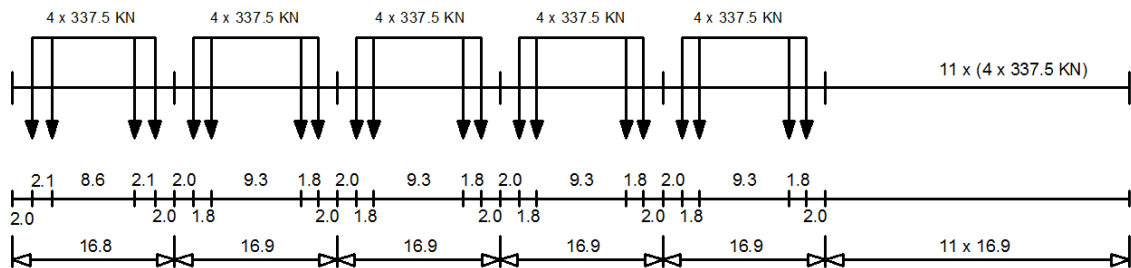
**Type B:** High speed passenger train

$\Sigma Q = 5024 \text{ KN}$      $v = 250 \text{ Km/h}$      $L = 248.20 \text{ m}$      $q = 20.24 \text{ KN/m}$



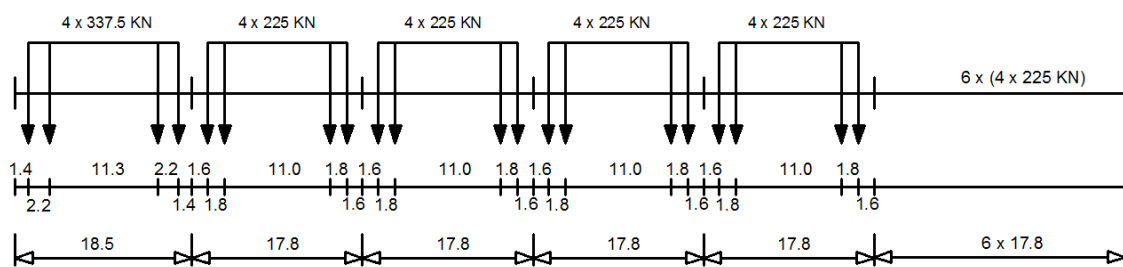
**Type C:** Locomotive-hauled freight train

$\Sigma Q = 21600 \text{ KN}$      $v = 80 \text{ Km/h}$      $L = 270.30 \text{ m}$      $q = 80.0 \text{ KN/m}$



**Type D:** Locomotive-hauled freight train

$\Sigma Q = 10350 \text{ KN}$      $v = 120 \text{ Km/h}$      $L = 196.50 \text{ m}$      $q = 52.70 \text{ KN/m}$



As shown in *Section 7.5* the vehicle's parameters, as the values of the springs and dampers of the suspension system have a very important role. Due to the absence of information about these data, in the next analyses those of the Italian ETR500Y high speed train given in [3] will be used for all the considered trains; the main characteristics are reported in table (8.1). Also in this case as already done in *chapter 7*, for passenger and high-speed trains will be used respectively the data for the locomotive and the cars, while for freight trains will be used only the data of the locomotive also for the other wagons.

Item	Unit	Locomotive	Passenger car
Mass of car body ( $M_2$ )	Kg	55976	34231
Mass moment of inertia of car body around $x$ -axis ( $I_{x2}$ )	Kg·m <sup>2</sup>	53366	54642
Mass moment of inertia of car body around $y$ -axis ( $I_{y2}$ )	Kg·m <sup>2</sup>	1643086	1821521
Mass moment of inertia of car body around $z$ -axis ( $I_{z2}$ )	Kg·m <sup>2</sup>	1630520	1760619
Mass of bogie ( $M_I$ )	Kg	3896	2760
Mass moment of inertia of bogie around $x$ -axis ( $I_{x1}$ )	Kg·m <sup>2</sup>	3115	2304
Mass moment of inertia of bogie around $y$ -axis ( $I_{y1}$ )	Kg·m <sup>2</sup>	2059	2504
Mass moment of inertia of bogie around $z$ -axis ( $I_{z1}$ )	Kg·m <sup>2</sup>	8107	4071
Mass of wheel set ( $M_w$ )	Kg	2059	1583
Mass moment of wheel set ( $I_w$ )	Kg·m <sup>2</sup>	1164	753
Lateral stiffness of the primary suspension system ( $K_H$ )	N/m	82821	3750
Vertical stiffness of the primary suspension system ( $H_V$ )	N/m	896100	404370
Lateral damping of the primary suspension system ( $C_H$ )	N·s/m	0	0
Vertical damping of the primary suspension system ( $C_V$ )	N·s/m	7625	3750
Vertical stiffness of the secondary suspension system ( $K_{HH}$ )	N/m	73035	32054
Vertical stiffness of the secondary suspension system ( $K_{VV}$ )	N/m	236030	90277
Lateral damping of the secondary suspension system ( $C_{HH}$ )	N·s/m	4625	5000
Vertical damping of the secondary suspension system ( $C_{VV}$ )	N·s/m	18125	8125
Half distance between two wheel-sets ( $q_0$ )	m	1.5	1.5
Half span of the primary suspension system ( $b_1$ )	m	1.115	0.965
Half span of the secondary suspension system ( $b_2$ )	m	1.0425	1.0825
Car body and the secondary suspension system distance ( $h_1$ )	m	0.915	0.7
Secondary suspension system and bogie distance ( $h_2$ )	m	0.098	0.12
Bogie and wheel sets distance ( $h_3$ )	m	0.087	0.13

**Table 8.1:** Characteristics of ETR500Y high-speed train.

Therefore assigning a time step  $\Delta t = 0.01$  s and knowing the velocity  $v$ , the weight and the relative distances of all the axles of each train, it has been possible to iteratively solve the vehicle-bridge dynamic interaction problem by means of the following coupled systems of equations as explained in *Chapter 4.4* and figure (4.4):

$$\begin{cases} \ddot{\mathbf{q}} + \mathbf{C}_b^* \dot{\mathbf{q}} + \mathbf{K}_b^* \mathbf{q} = \mathbf{P}_b^* \\ \mathbf{M}_v \ddot{\mathbf{V}}_v + \mathbf{C}_v \dot{\mathbf{V}}_v + \mathbf{K}_v \mathbf{V}_v = \mathbf{P}_v \end{cases} \quad (8.8)$$

Solving this problem, the interaction forces on the bridge and on the vehicle have been computed for each time step, and so nodal loads time history for each kind of train have been obtained. Furthermore accelerations, velocities and displacements time history for each degree of freedom both for bridge and vehicle have been calculated for all the possible train crossing.

Indeed the problem has been solved imposing an initial condition for the bridge, so that also the horizontal and torsional modes could be activate. In particular it has been thought to apply an initial moved position of the bridge accordingly to 0.6 times its first modal shape (that is the first lateral mode shape). This means to assume a very little initial displacement, in fact in this way the mid-span point is moved of about 1 mm in the horizontal direction, as the modal shapes are normalized in respect to the mass matrix.

Some representative obtained results are shown in the following for the four types of trains considered.

### *Analysis "A"*

In that analysis the train type A belonging to the passenger trains is considered. In figure (8.2) the displacement in time of the mid span node is plotted both for vertical and horizontal displacements.

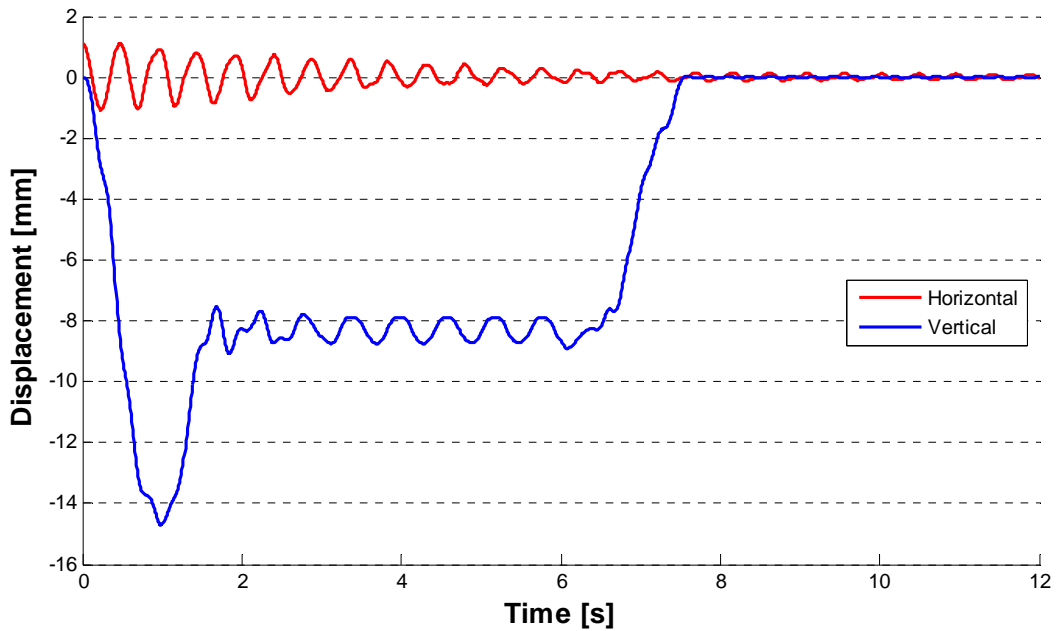


**Figure 8.2:** Mid span node displacements due to the passage of train type A.

The maximum vertical displacement is 15 mm at about 1 second, that is the moment in which the locomotive with its higher weight passes on the mid span point of the bridge. Then after 7.5 seconds the train left the bridge and very little remaining oscillations are observed. As regards the horizontal displacement, it seems that the imposed initial oscillation is not maintained or amplified, on the contrary there is a decline of the amplitude of the vibration, as it is possible to see in figure (8.3) where the horizontal displacement is plotted alone to better understand the trend.

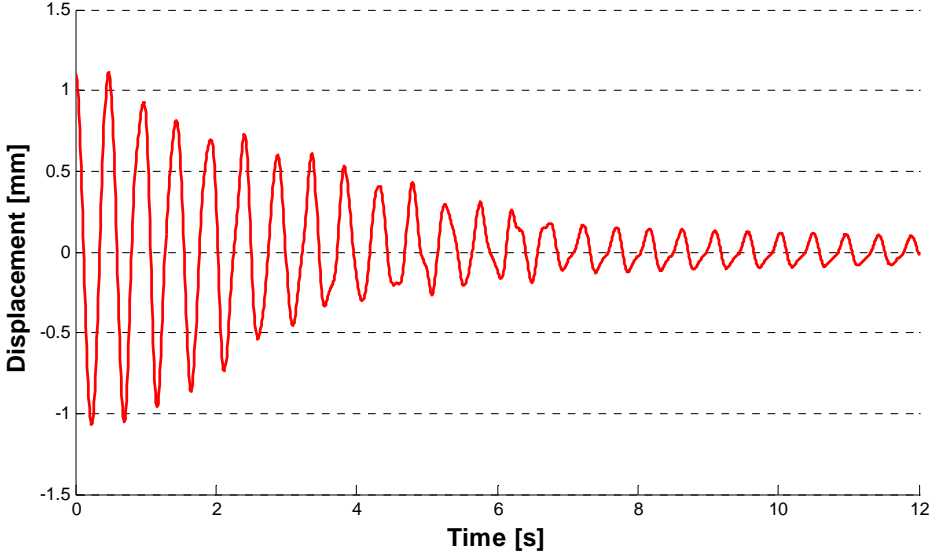


**Figure 8.3:** Mid span node horizontal displacement due to the passage of train type A.

It is also interesting to see the accelerations to which the bridge is subjected during the passing of the train, these quantities are plotted in the next figures (8.4) (8.5) for both horizontal and vertical directions, referred again to the mid span bottom node.

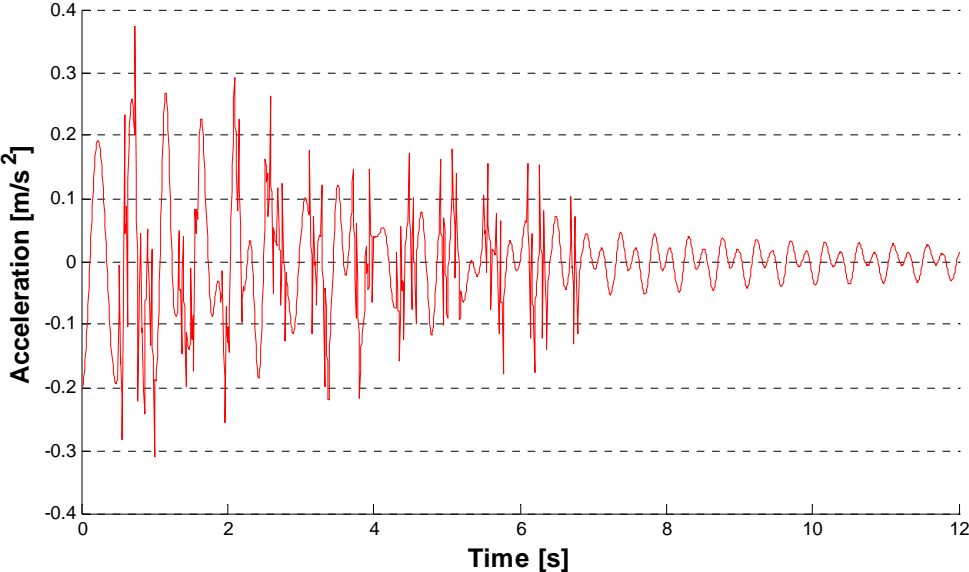


**Figure 8.4:** Mid span node horizontal acceleration due to the passage of train type A.

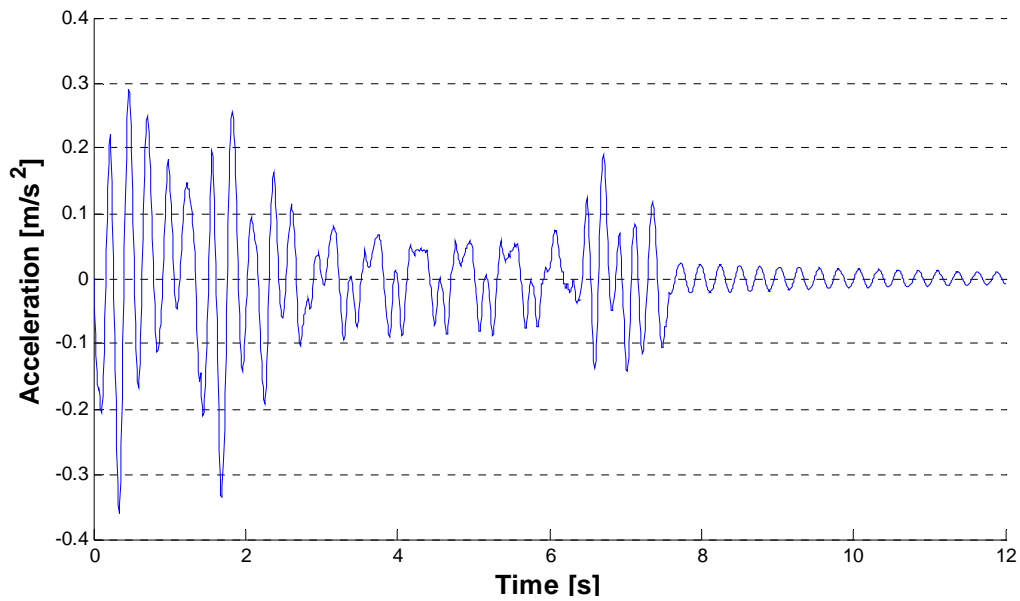


**Figure 8.5:** Mid span node vertical acceleration due to the passage of train type A.

Both accelerations in the two directions have the same order of magnitude and more precisely they are comprised between 0.3 and 0.4  $\text{m/s}^2$ .

Although it is not the aim of this research, it can be worth considering also the dynamic behavior of the vehicle during its motion on the bridge. Therefore in the following figures (8.6) and (8.7) the predicted displacement and acceleration time history of the vertical degree of freedom of the second car body (the first passenger car next to the locomotive) are shown. It is interesting to note that the obtained results are in agreement to those obtained in [3], since the order of magnitude and the period of the oscillations are very similar.

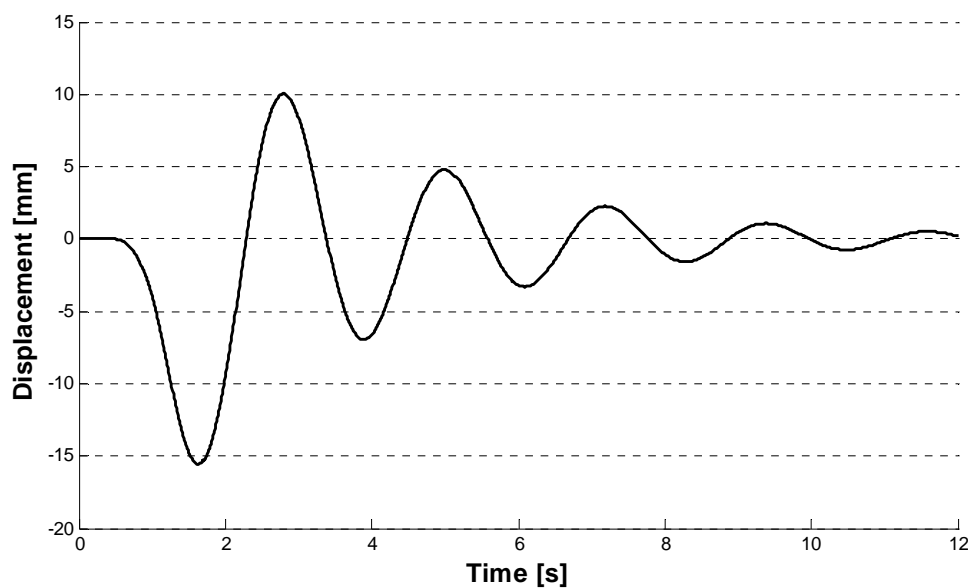


**Figure 8.6:** Vertical displacement of the car body type A.

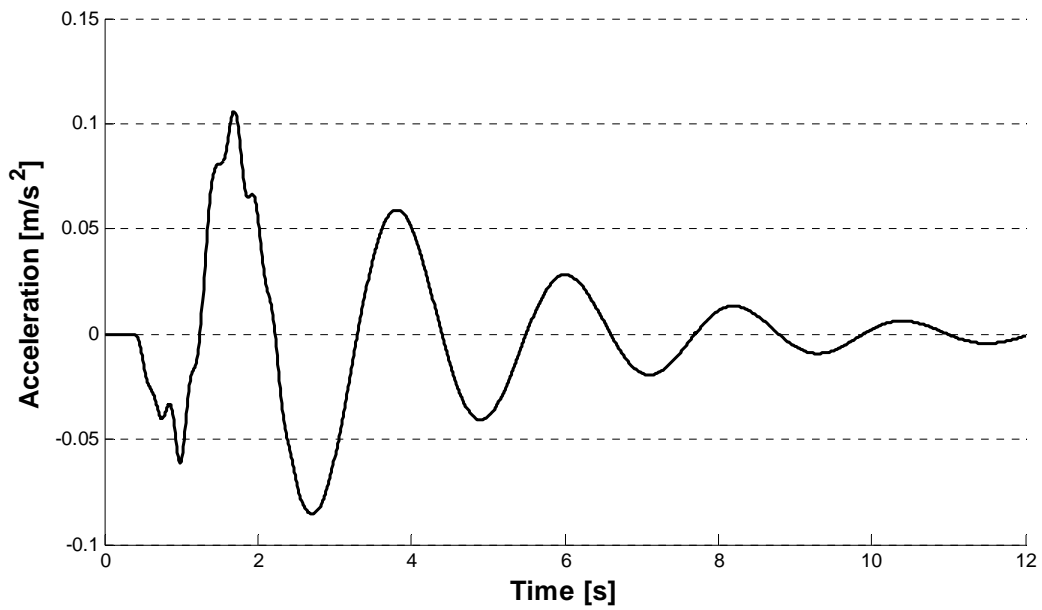


Figure 8.7: Vertical acceleration of the car body type A.

### Analysis “B”

In that analysis the train type B, that is the ETR500Y high speed train, is considered. In figure (8.8) the displacement in time of the mid span node is plotted both for vertical and horizontal displacements.

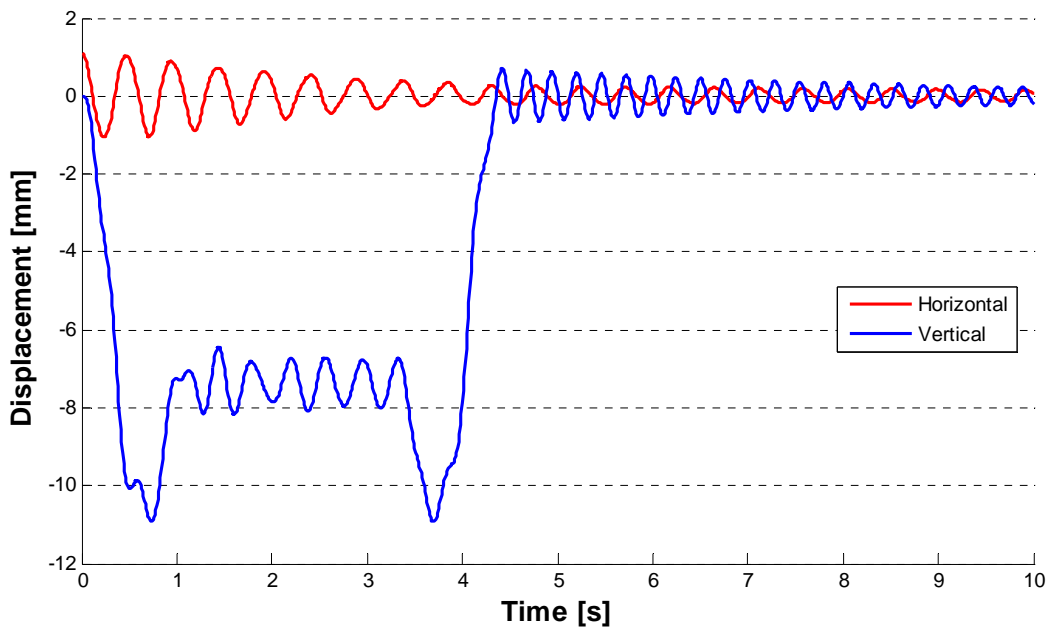
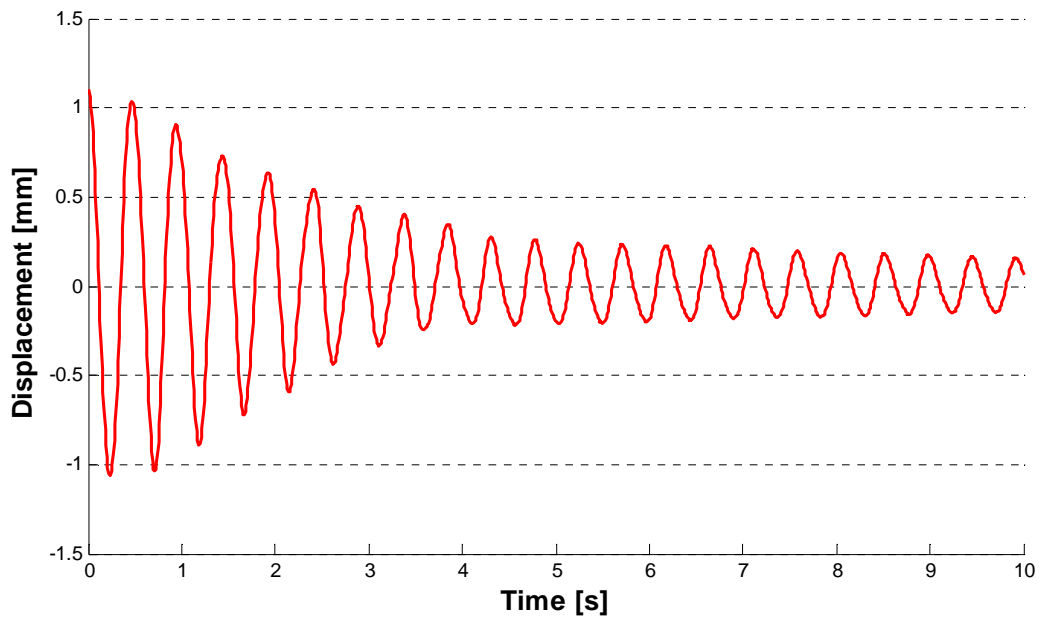


Figure 8.8: Mid span node displacements due to the passage of train type B.

The maximum vertical displacements are about 11 mm at 0.8 and 3.8 seconds, that also in this case represent the moment in which the initial and final locomotives with their higher weight pass on the mid span point of the bridge. Then after 4.6 seconds the train left the bridge and little remaining oscillations are observed. As regards the horizontal displacement, it seems that also in this case the imposed initial oscillation declines in time, as it is possible to see in figure (8.9) where the horizontal displacement is plotted alone.



**Figure 8.9:** Mid span node horizontal displacement due to the passage of train type B.

Also in this case it is interesting to see the accelerations referred to the mid span bottom node, see figures (8.10) (8.11).

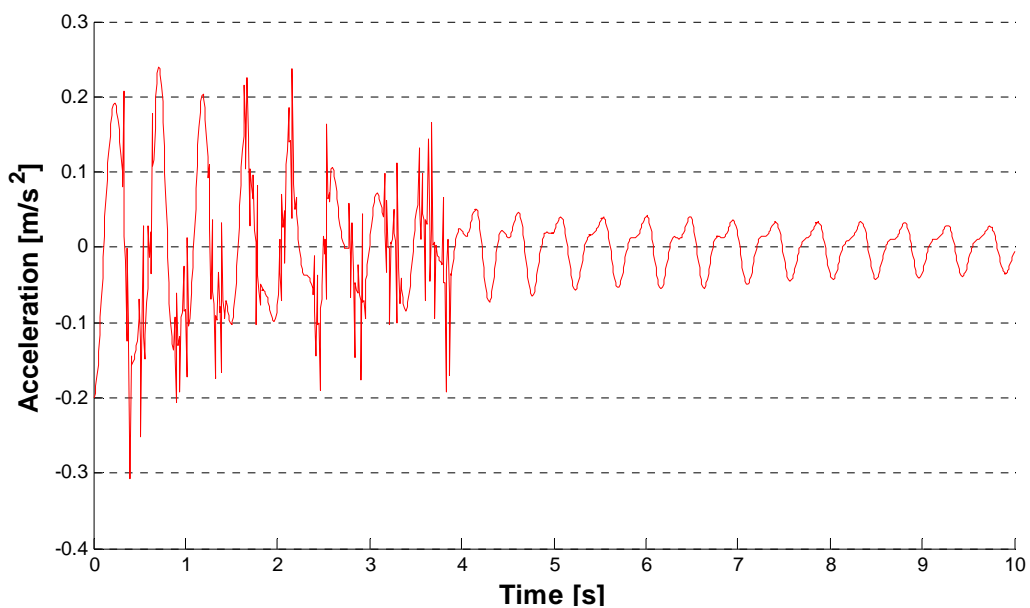


**Figure 8.10:** Mid span node horizontal acceleration due to the passage of train type B.

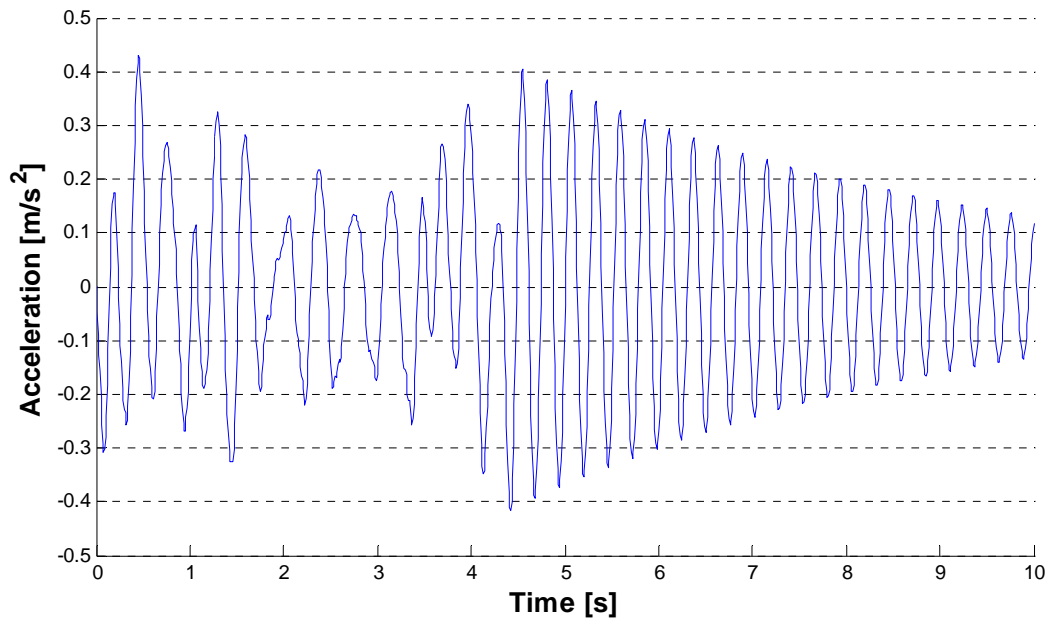


**Figure 8.11:** Mid span node vertical acceleration due to the passage of train type B.

The accelerations have similar order of magnitude in respect to the case A, and again they are comprised between 0.3 and 0.4  $\text{m/s}^2$ .

As regards the vehicle response, in the following figures (8.12) (8.13) the displacement and acceleration time history of the vertical degree of freedom of the second car body (the first passenger car next to the locomotive) are shown.

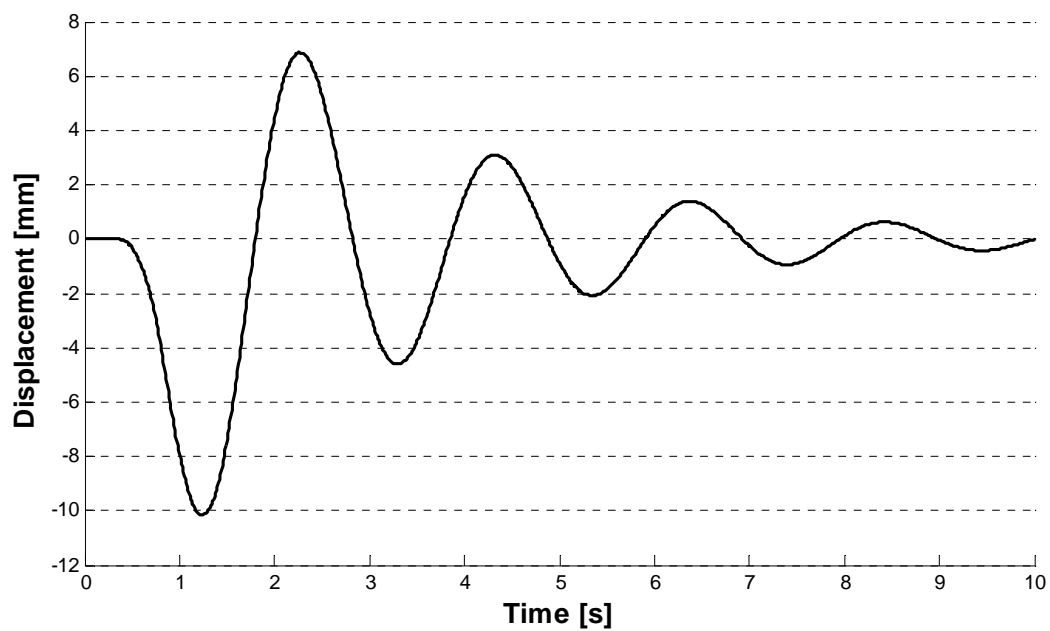


**Figure 8.12:** Vertical displacement of the car body type B.

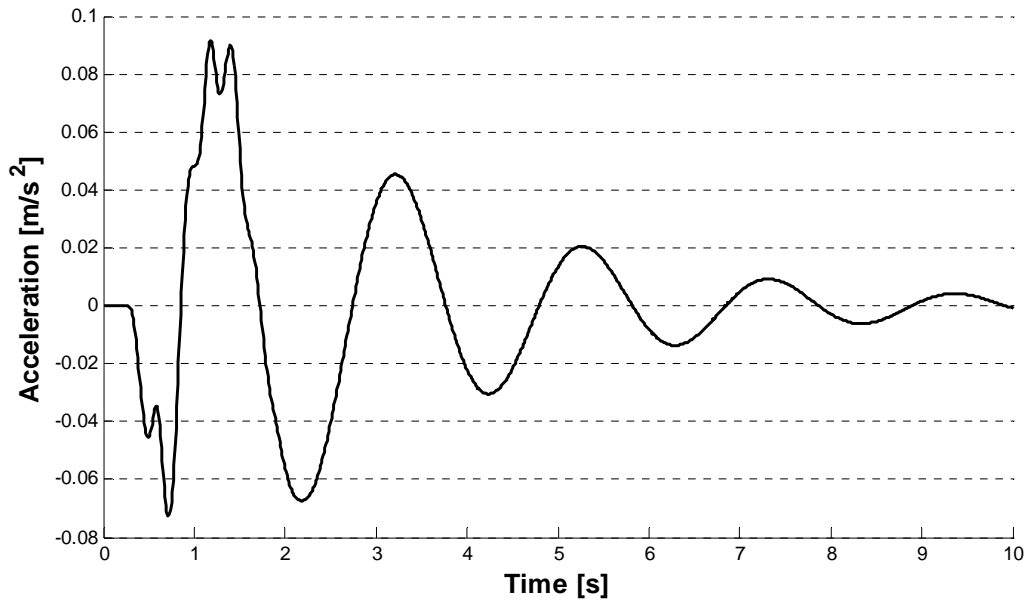


**Figure 8.13:** Vertical acceleration of the car body type B.

A vehicle behavior very similar to the previous case is obtained, and once again in agreement to the results of [3].

### *Analysis “C”*

In that analysis the train type C, belonging to the freight trains is considered. In figure (8.14) the displacement in time of the mid span node is plotted both for vertical and horizontal displacements.

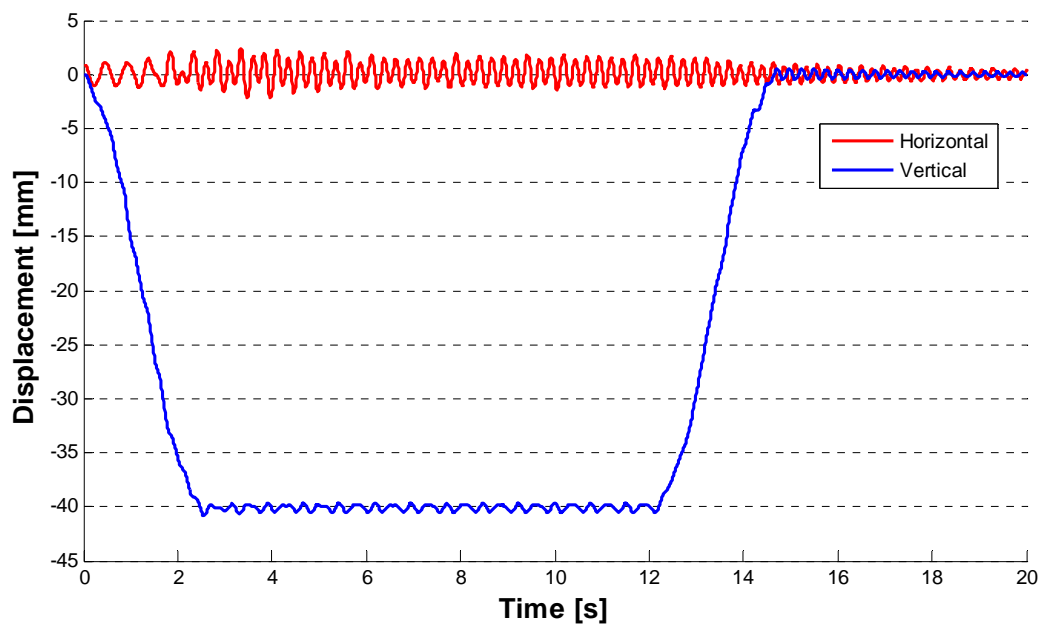


**Figure 8.14:** Mid span node displacements due to the passage of train type C.

This kind of train causes similar effects to those given by the train type 5 in the two-dimensional analyses of *chapter 7.4*. In fact at about 2.2 seconds the bridge reaches the maximum displacement of about 40 mm and then exhibits a flat behavior without hardly any oscillations until the train leaves the bridge. In this case the horizontal displacement does not decline with time but on the contrary it is a slightly amplified and maintained in time. Figure (8.14) shows more in detail the horizontal displacement of the mid span node of the bridge.

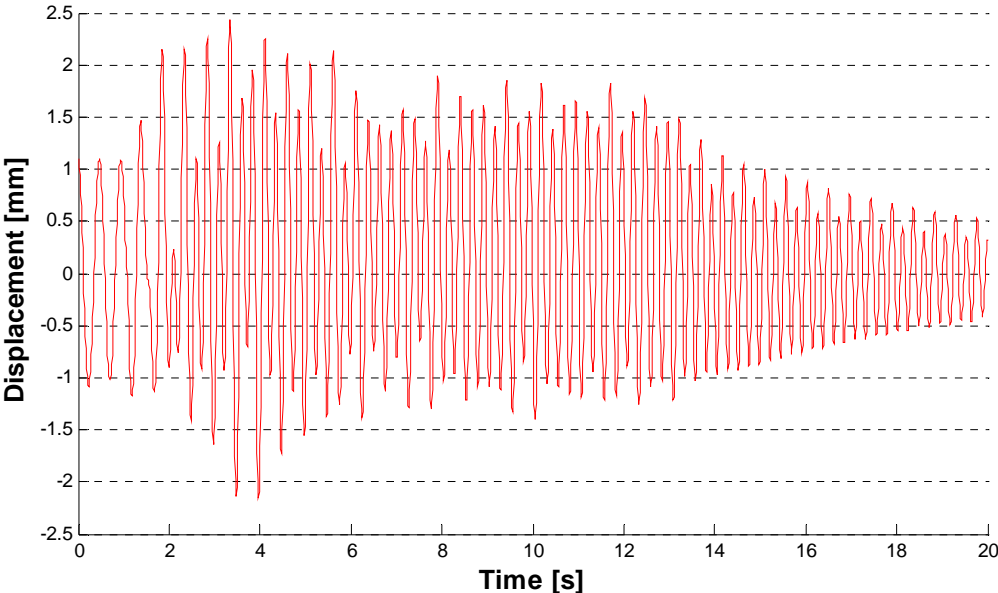


**Figure 8.14:** Mid span node horizontal displacement due to the passage of train type C.

Figures (8.15) (8.16) show the accelerations in both directions referred to the mid span.

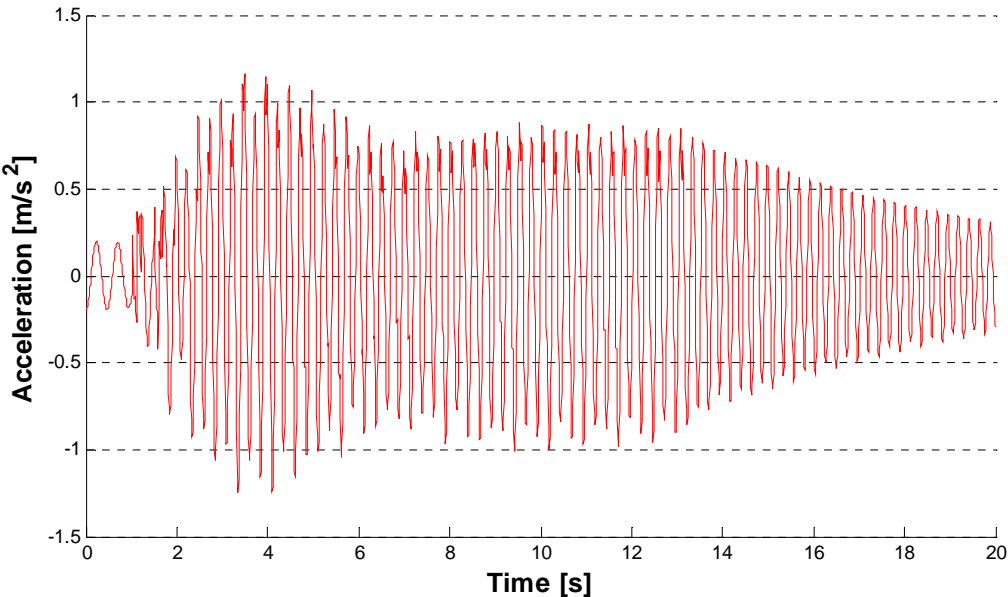


**Figure 8.15:** Mid span node horizontal acceleration due to the passage of train type C.

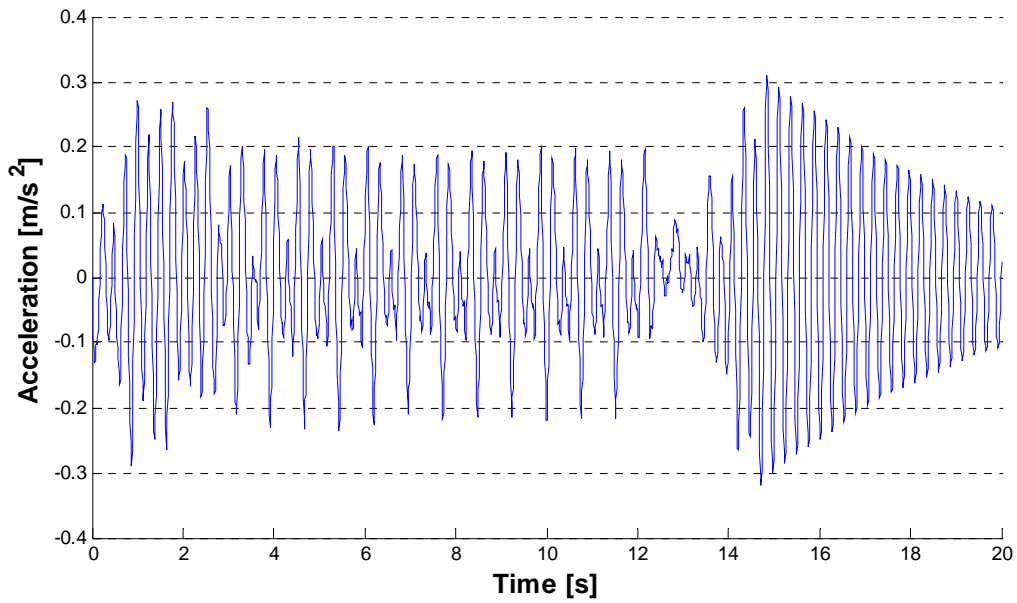


**Figure 8.16:** Mid span node vertical acceleration due to the passage of train type C.

On the vehicle side the computed displacement and acceleration time histories regarding the vertical degree of freedom of the first car body (the locomotive) are shown in the following figures (8.17) (8.18).

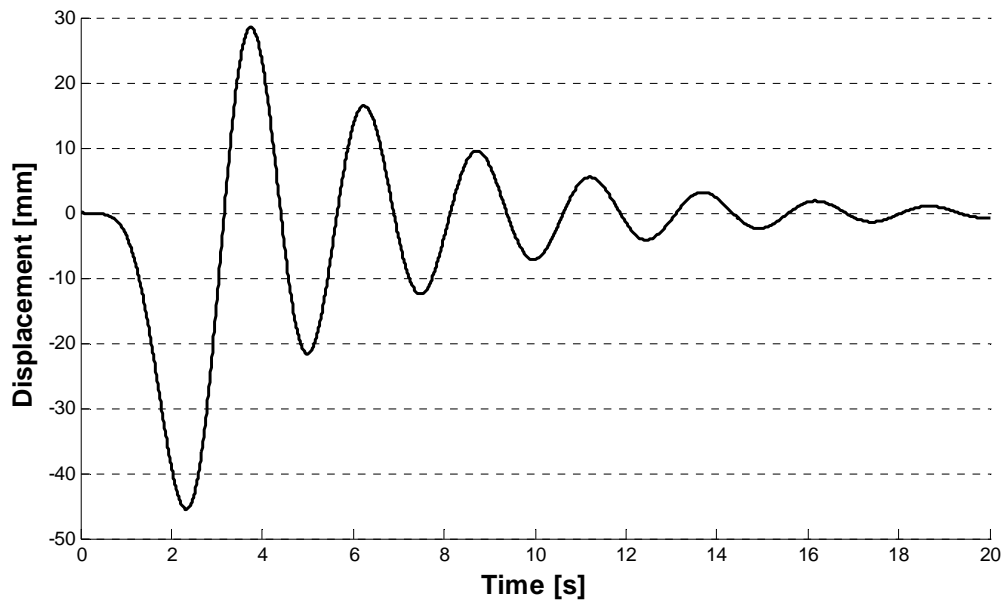


**Figure 8.17:** Vertical displacement of the car body type C.

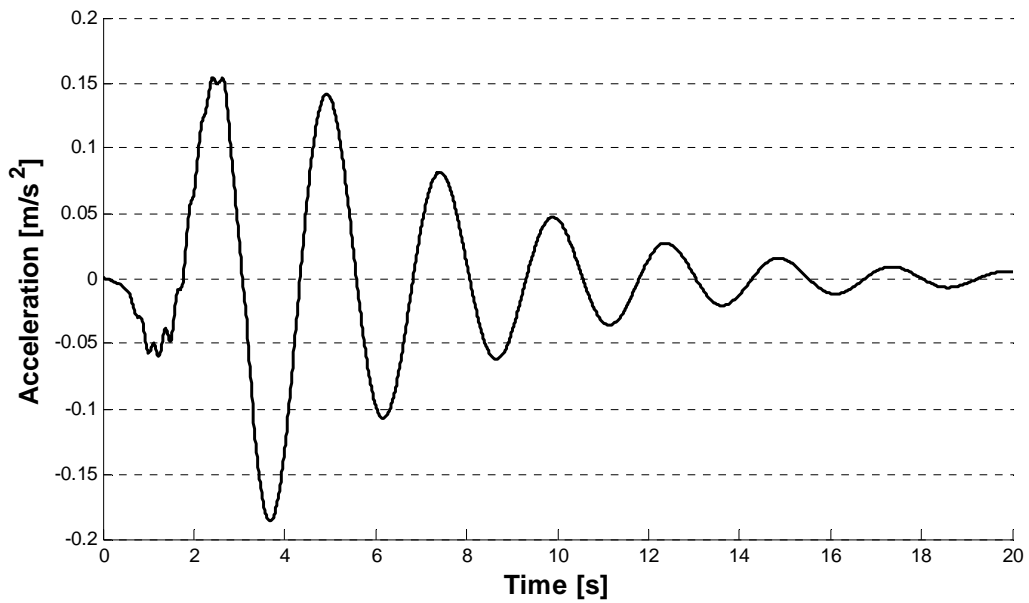


**Figure 8.18:** Vertical acceleration of the car body type C.

### *Analysis “D”*

In that analysis the train type D is considered, which, as in the previous case belongs to the freight trains. In figure (8.19) the displacement in time of the mid span node is plotted both for vertical and horizontal displacements.

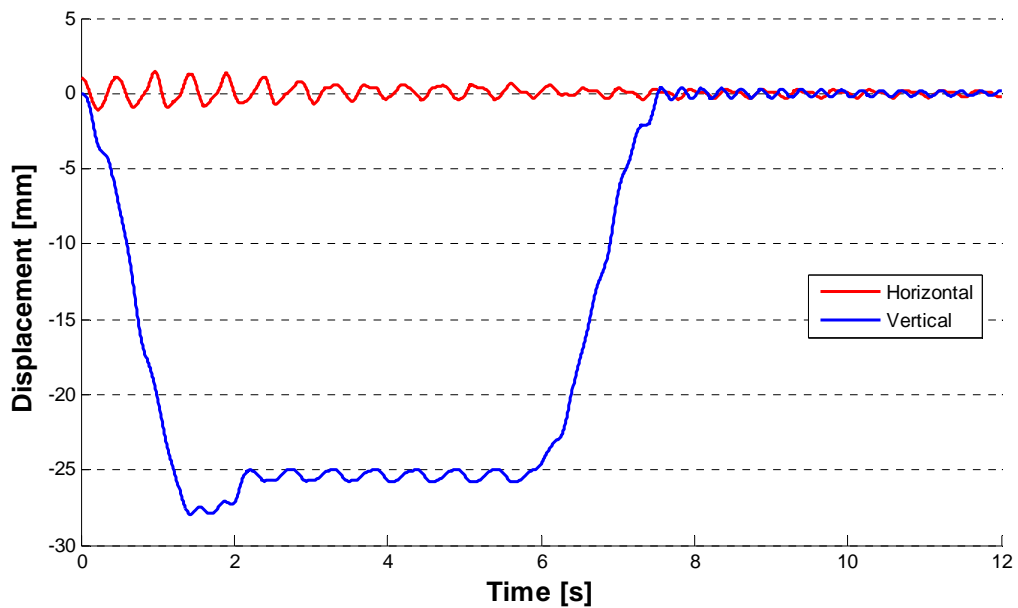


**Figure 8.19:** Mid span node displacements due to the passage of train type D.

The maximum vertical displacement is about 28 mm at 1.5 seconds, that also in this case represent the moment in which the locomotive with its higher weight passes on the mid span point of the bridge. After 7.5 seconds the train has passed the bridge and little remaining oscillations are observed. As regards the horizontal displacement for some seconds it is maintained and then it starts to decrease in time, as it is possible to see in figure (8.20) where the horizontal displacement is plotted alone.

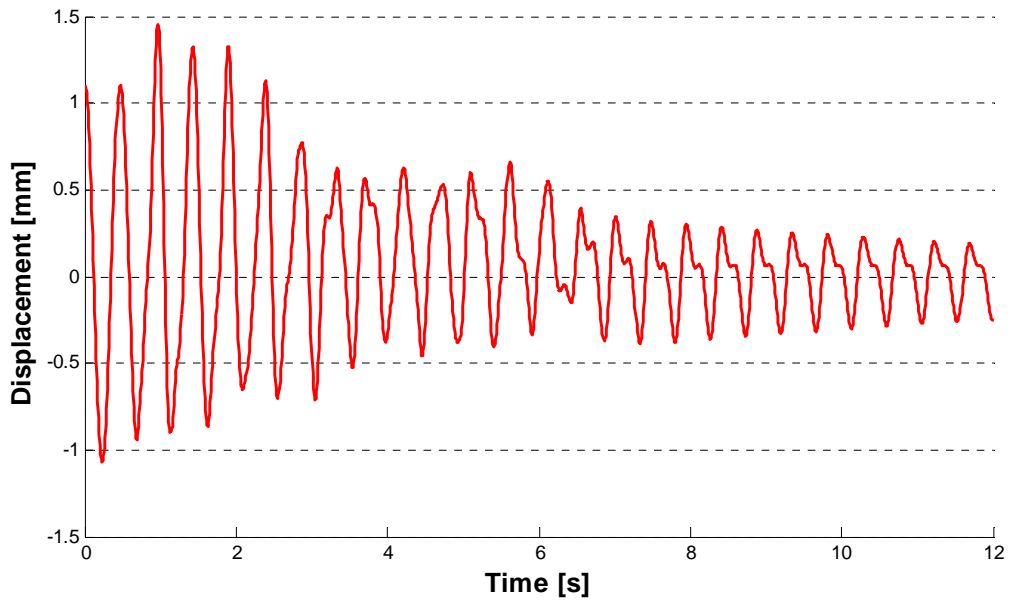


**Figure 8.20:** Mid span node horizontal displacement due to the passage of train type D.

As regards the horizontal and vertical accelerations referred to the mid span bottom node, they are plotted in figures (8.21) (8.22).

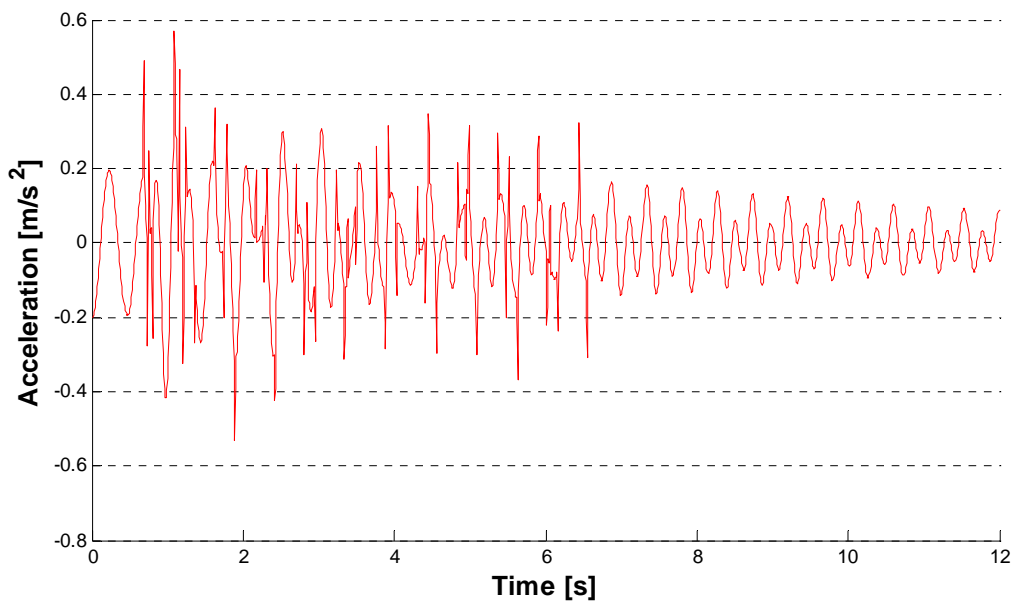


**Figure 8.21:** Mid span node horizontal acceleration due to the passage of train type D.

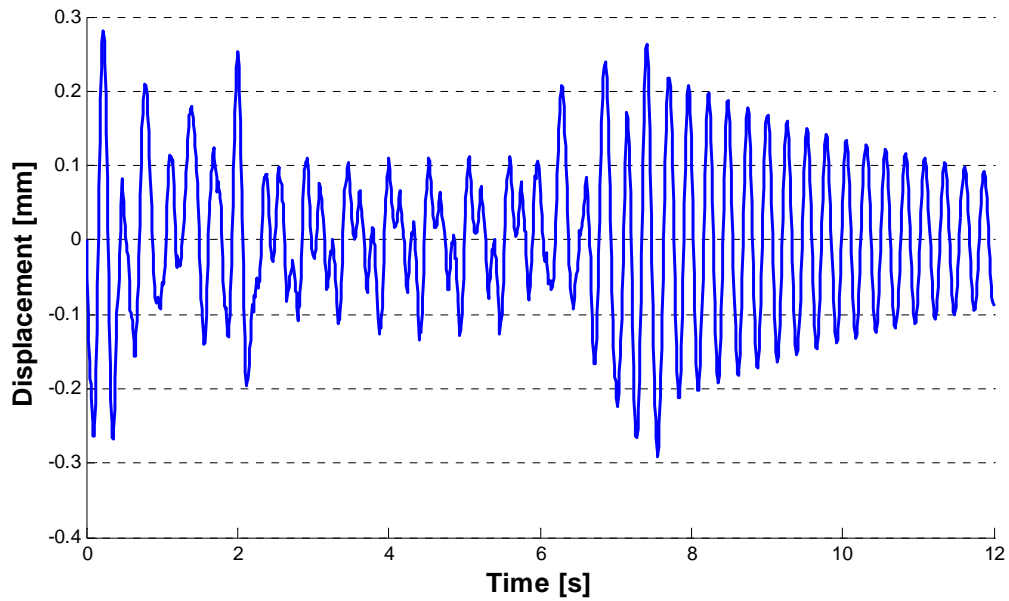


**Figure 8.22:** Mid span node vertical acceleration due to the passage of train type D.

Also in this case not relevant differences are obtained in terms of acceleration in respect to the previous cases.

Finally, the vehicle's computed displacement and acceleration time history regarding the vertical degree of freedom of the first car body (the locomotive) are shown in the following figures (8.23) (8.24).

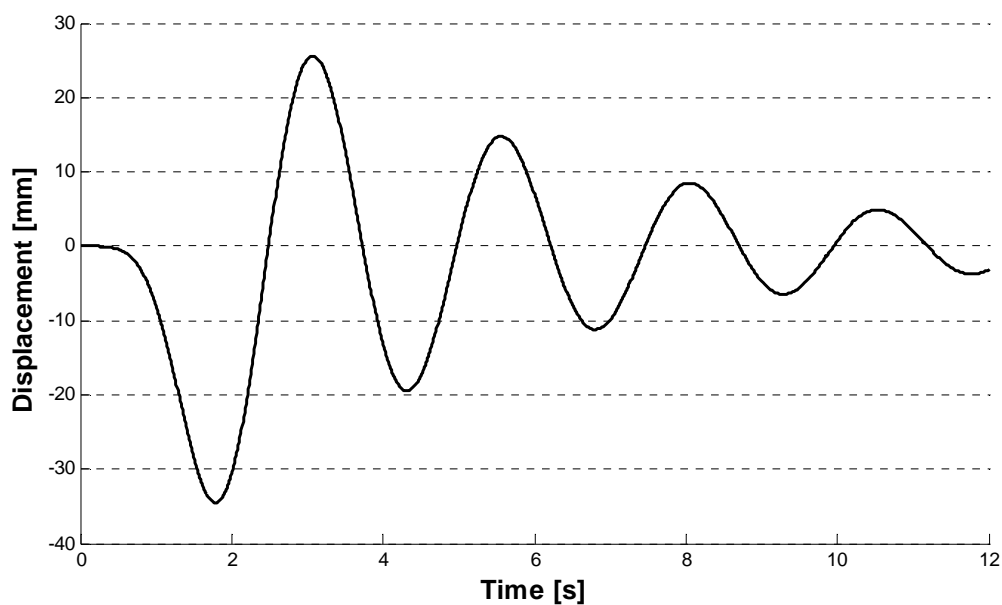


**Figure 8.23:** Vertical displacement of the car body type D.

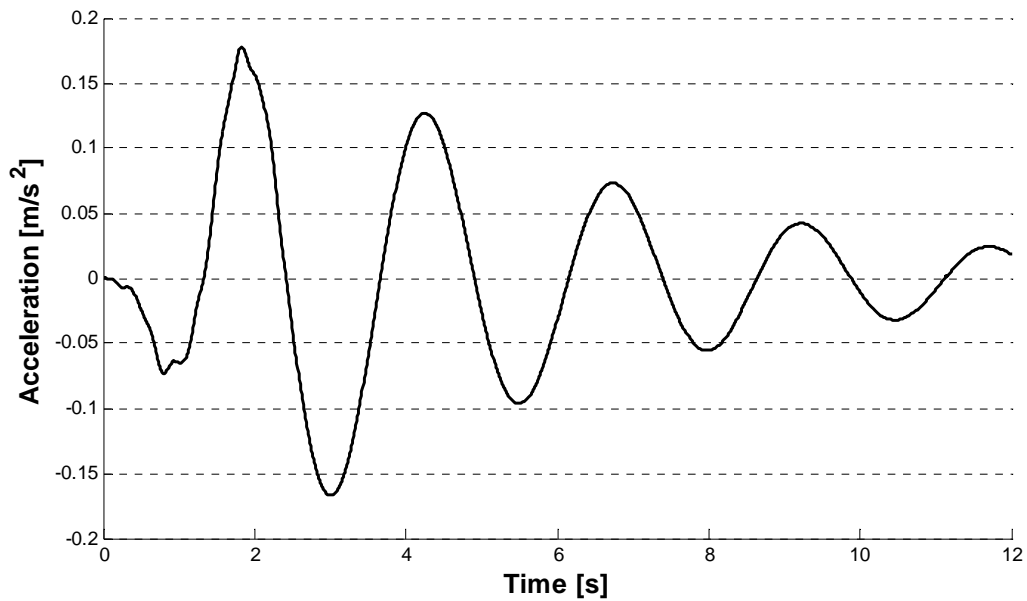


**Figure 8.24:** Vertical acceleration of the car body type D.

In this chapter dynamic analyses of the structure using vehicle-bridge interaction have been carried out, to obtain for each node the loading history both in vertical and horizontal directions. By applying these load histories to the structure model, and running dynamic analyses with the finite elements software, it will be possible to obtain the stresses load history in the elements of the bridge. In this way it will be possible to evaluate the fatigue life of the structure. Anyway more details about this procedure are given in the next section, *Chapter 9*.

Although it is not question of interest in the present study, it has been interesting to see also the dynamic behaviors of the vehicles, which had led to recognize, that with this method even the passengers' traveling comfort could be studied especially in the design phases of a new bridge construction.



## 9. FATIGUE ASSESSMENT

### 9.1 General

The aim of this chapter is to analyze and assess the fatigue life of Pontelagoscuro railway bridge, going to investigate the critical points in which the fatigue phenomena could appear.

*Fatigue* is the process of the progressive and localized structural damage occurring in a material when is subjected to cyclic loading. If the maximum stress in the specimen does not exceed the elastic limit of the material, the specimen returns to its initial condition when the load is removed. A given loading may be repeated many times, provided that the stresses remain in the elastic range, figure (9.1). However, when the loadings are repeated thousands or millions of times rupture will occur at a stress much lower than static breaking strength. This phenomenon is known as fatigue.

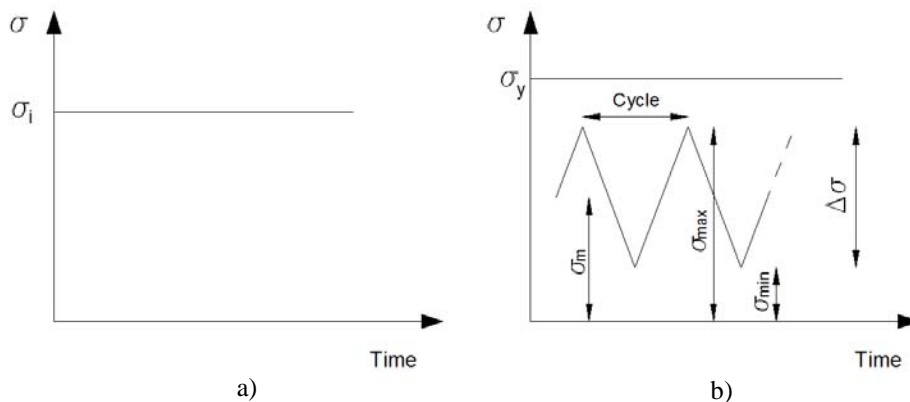


**Figure 9.1:** a) Static load; b) Cyclic load.

Fatigue is one of the observed modes of possible failure in practice. For this reason, fatigue becomes an obvious design consideration for many structures, such as bridges, aircraft, railroad cars, automotive suspensions and vehicle frames. For these structures, cyclic loads are identified that could cause fatigue failure if the design is not adequate.

For the fatigue design and verifications, several methods are available. All require similar types of information. These are the identifications of candidate locations for fatigue failure, the load spectrum for the structure or the element, the stresses or strains at the candidate locations resulting from the loads, the temperature, the corrosive environment, the material behavior, and a methodology that combines all these effects to give a life prediction. Prediction procedures are provided for estimating life using stress life (Stress vs Number of cycles curves), hot-spot stresses, strain life, and fracture mechanics.

The basis of the stress-life method is the S-N curve, that is a plot of alternating stress, S, versus cycles to failure, N. In fact since the well-known work of Wöhler in Germany starting in the 1850's, engineers have employed curves of stress versus cycles to fatigue failure, which are often called S-N curves (stress-number of cycles) or Wöhler's curve. S-N curves are derived from standardized tests on samples of the material to be characterized where a regular sinusoidal stress with a given amplitude is applied by a testing machine which also counts the number of cycles to failure. Each test generates a point on the log-log plot, with the actual S-N curve that approximates the data from several tests, see figure (9.2).

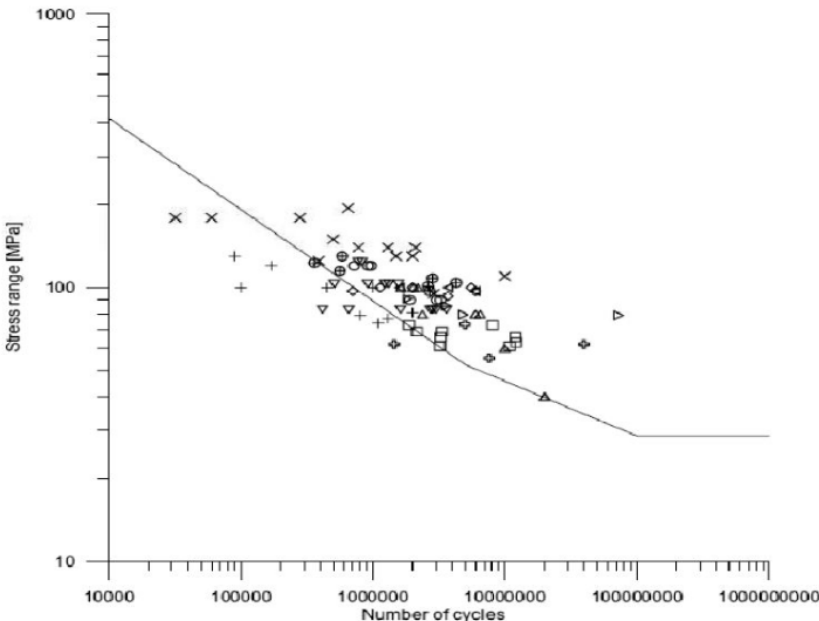


Figure 9.2: Experimental S-N curve.

Certain materials, as the steel, have a fatigue limit or *endurance limit* which represents a stress level below which the material does not fail and can be cycled infinitely. If the applied stress level is below the endurance limit of the material, the structure is said to have an *infinite life*.

Stress-life approach assumes that all stresses in the element stay below the elastic limit at all times. It is suitable when the applied stress is nominally within the elastic range of the material and the number of cycles to failure is large. The nominal stress approach is therefore best suited to problems that fall into the category known as high-cycle fatigue. High cycle fatigue is one of the two regimes of fatigue phenomenon that is generally considered for metals and alloys. It involves nominally linear elastic behavior and causes failure after more than about  $10^4$  to  $10^5$  cycles.

The stress-based approach continues to serve as a widespread used tool for the design and verifications of metal structures. Comparing the stress-time history at the chosen critical point with the S-N curve allows a life estimate for the element to be made.

Therefore for any fatigue analysis, the starting point is the element response in terms of stress time history. If the response time history is made up of constant amplitude stress cycles then the fatigue verification can be accomplished by referring to a typical S-N diagram. However, because real signals rarely confirm to this ideal constant amplitude situation, an empirical approach is used for calculating the damage caused by stress signals of variable amplitude. Despite its limitations, Palmgren-Miner rule is used for this purpose. This linear relationship assumes that the damage caused by parts of a stress signal with a particular range can be calculated and accumulated to the total damage separately from that caused by other ranges.

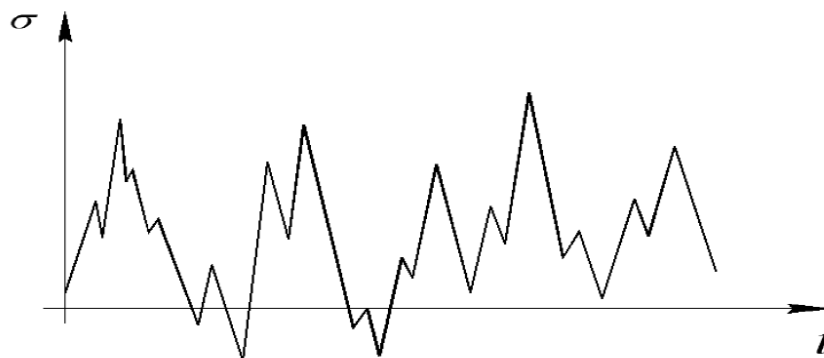


**Figure 9.3:** Irregular stress history.

When the response time history is irregular with time, as in figure (9.3), rainflow cycle counting is used to decompose the irregular time history into equivalent stress of block loading. The number of cycles in each block is usually recorded in a stress range histogram. This can be used in Palmgren-Miner calculation to obtain the fatigue life.

More details about the rainflow cycle counting and the Palmgren-Miner rule are given in *Section 9.2* and *9.3* respectively.

## 9.2 Rainflow cycle counting

The rainflow counting method is used in the analysis of fatigue data in order to reduce a spectrum of varying stress into a set of simple stress reversals. The algorithm was developed by Tatsuo Endo and M. Matsuishi in 1968, and it is the most popular method among the cycle-counting algorithms for such applications.

The origin of the name of rainflow counting method which is also called ‘Pagoda Roof Method’ derives from the fact that if the time axis is vertical then the random stress  $S(t)$  represents a series of roofs on which water falls.

The method procedure is illustrated in figure (9.4). First, the stress  $S(t)$  is transformed into a process of peaks and valleys. Then the time axis is rotated so that it points downward. At both peaks and valleys, water sources are considered. Water flows downward according to the following rules:

1. A rainflow path starting at a valley will continue down the “pagoda roofs”, until it encounters a valley that is more negative than the origin. From the figure, the path that starts at A will end at E.
2. A rainflow path is terminated when it encounters flow from a previous path. For example, the path that starts at C is terminated as shown.
3. A new path doesn’t start until the path under consideration has stopped.
4. Valley-generated half-cycles are defined for the entire record. For each cycle, the stress range  $S_i$  is the vertical excursion of a path. The mean  $\mu_{S_i}$  is the midpoint.
5. The process is repeated in reverse with peak-generated rainflow paths. For a sufficiently long record, each valley-generated half-cycle will match a peak-generated half-cycle to form a whole cycle.

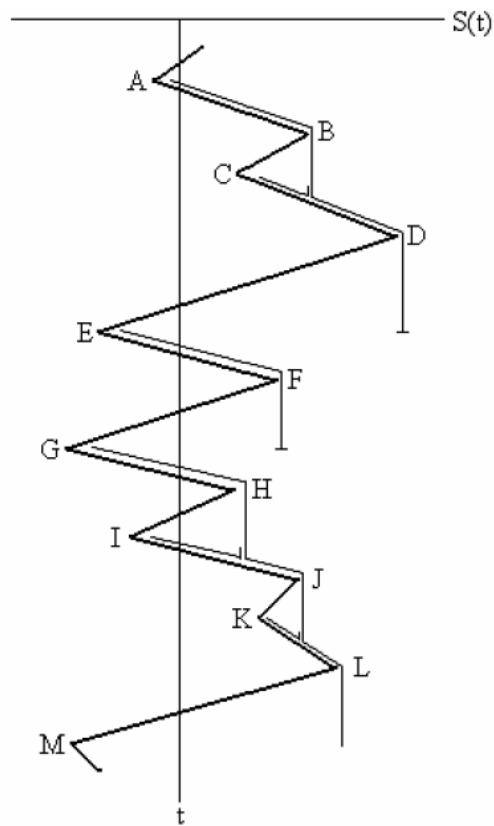
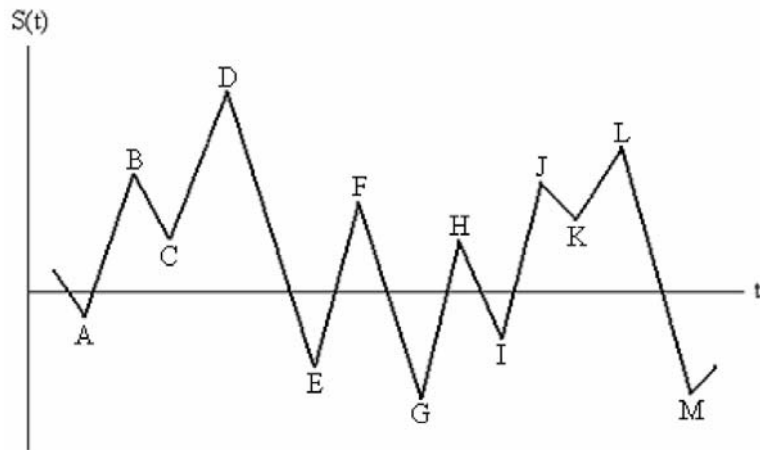


**Figure 9.3:** Rainflow cycle counting.

In this paper only the rainflow method is treated because it is used to carry out the fatigue analysis and verification. Actually other methods exist for such applications which are the reservoir method, level crossing cycle counting, peak-valley cycle counting and range counting. The reader who is interested in this methods is left to the literature and others books.

### 9.3 Palmgren-Miner rule

Almost all available fatigue data for design purposes are based on constant amplitude tests. However, in practice, the alternating stress amplitude may be expected to vary or change in some way during the service life when the fatigue failure is considered. The variations and changes in load amplitude, often referred to as spectrum loading, make the direct use of S-N curves inapplicable because these curves are developed and presented for constant stress amplitude operations. The key issue is how to use the mountains of available constant amplitude data to predict fatigue in a general element.

Many different cumulative damage theories have been proposed for the purposes of assessing fatigue damage and predict failure under conditions of spectrum loading. The most widely used model is the Palmgren-Miner rule or linear damage rule.

Life estimates may be made by employing Palmgren-Miner rule along with a cycle counting procedure. The target is to estimate how many of the blocks can be applied before failure occurs.

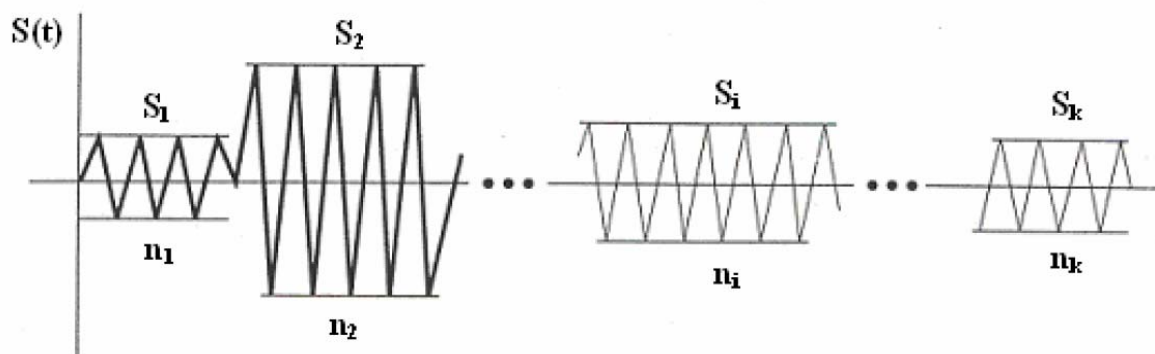


Figure 9.4: Rainflow cycle counting.

In figure (9.4), a spectrum of amplitudes of stress cycles is described as a sequence of constant amplitude blocks, each block having stress amplitude  $S_i$  and the total number of applied cycles  $n_i$ . The constant amplitude S-N curve is shown in figure (9.5).

By using the S-N data, number of cycles of  $S_1$  is found as  $N_1$  which would cause failure if no other stresses were present. Actually a stress amplitude  $S_1$  for a number of cycles  $n_1$  smaller than  $N_1$  produces a smaller fraction of damage which can be termed as  $D_1$ .

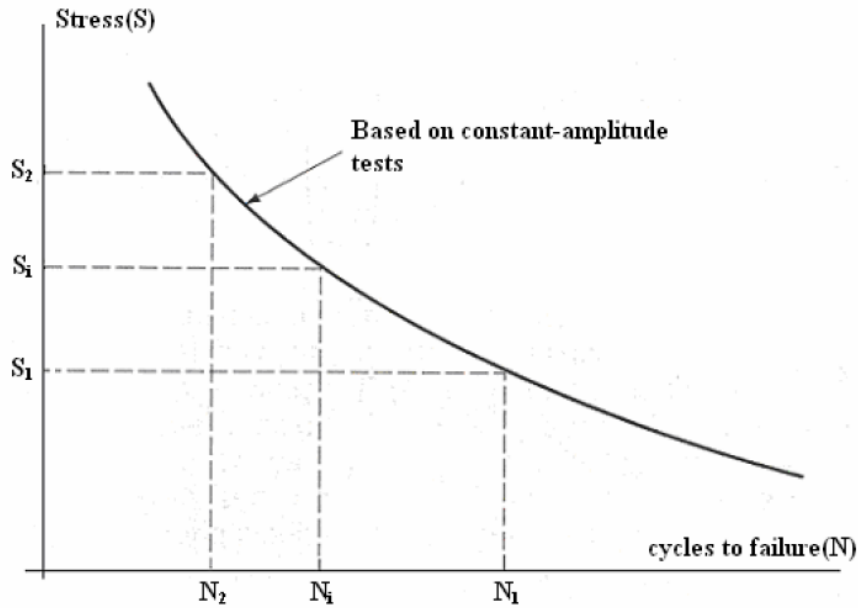


Figure 9.5: Constant amplitude S-N curve.

Operation over a spectrum of different stress levels results in a damage fraction  $D_i$  for each of the different stress levels  $S_i$  in the spectrum. It is clear that failure occurs if the fraction exceeds unity:

$$D_1 + D_2 + \dots + D_i + D_k \geq 1 \quad (9.1)$$

According to the Palmgren-Miner rule, the damage fraction at any stress level  $S_i$  is linearly proportional to the ratio of number of cycles of operation to the total number of cycles that produces failure at that stress level, that is

$$D_i = \frac{n_i}{N_i} \quad (9.2)$$

Then, a total damage can be defined as the sum of all the fractional damages over a total of  $k$  blocks,

$$D = \sum_{i=1}^k \frac{n_i}{N_i} \quad (9.3)$$

and the event of failure can be defined as

$$D \geq 1 \quad (9.4)$$

The limitations of the Palmgren-Miner rule can be summarized as follows:

- Linear: It assumes that all cycles of a given magnitude do the same amount of damage, whether they occur early or late in the life.

- Non-interactive (sequence effects): It assumes that the presence of  $S_2$  etc. does not affect the damage caused by  $S_1$ .
- Stress independent: It assumes that the rule governing the damage caused by  $S_1$  is the same as that governing the damage caused by  $S_2$ .

The assumptions are known to be faulty, however, Palmgren-Miner rule is still used widely in the applications of the fatigue life estimates.

## 9.4 Fatigue verification

The basic steps of the fatigue design and verification process as dictated also by the European guidelines are illustrated in figure (9.6).

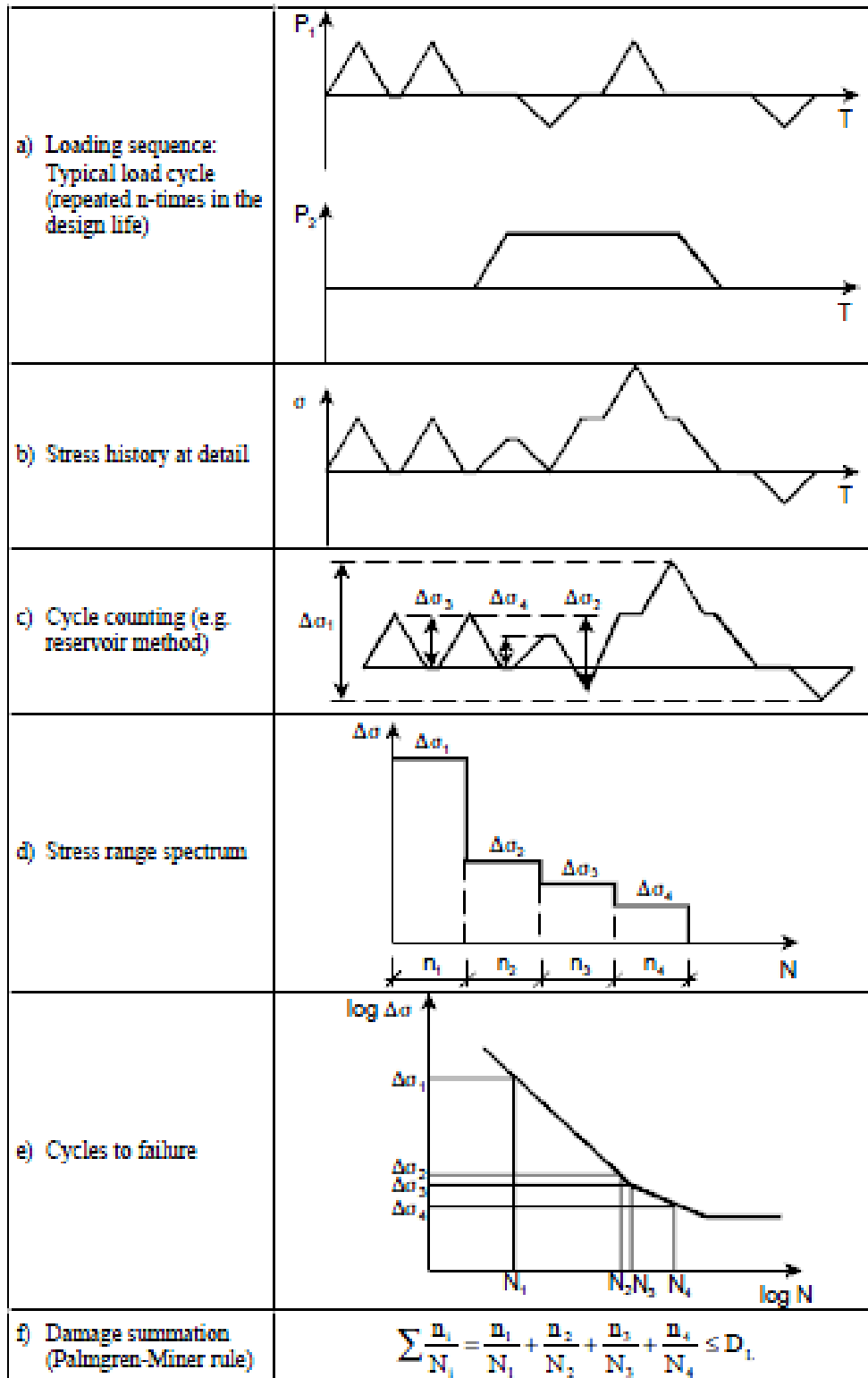


Figure 9.6: Cumulative damage method.

First of all a typical *loading sequence* that represents a credible estimate of all service load events expected during the fatigue life of the structure should be determined, see figure (9.6.a).

Then a *stress history* should be determined from the loading events to the structural detail under consideration., figure (9.6.b).

Once stress histories have been evaluated, a *cycle counting* method, as rainflow or reservoir method, is needed to determine stress ranges and their numbers of cycles, figure (9.6.c).

The stress range spectrum should be determined by presenting the stress ranges and the associated number of cycles in descending order, figure (9.6.d).

Finally, obtaining the *cycles to failure*  $N_{Ri}$  from the  $\Delta\sigma_c - N_R$  curve for each band of the spectrum  $\Delta\sigma_i$ , and knowing the number of cycles  $n_{Ei}$  associated with each stress rate  $\Delta\sigma_i$ , the damage  $D_d$  during the life should be calculated using the Palmgren-Miner rule:

$$D_d = \sum_i^n \frac{n_{Ei}}{N_{Ri}} \quad (9.5)$$

In this sense the exact traffic volume and the specific trains crossing the bridge are not known. Therefore using the trains presented in *chapter 8.2*, used to perform the dynamic analyses, along with the specifications gives by the Eurocode 1 that provides the load scenery, a possible traffic mix has been assumed, see figure (9.7).

<i>Standard traffic mix</i>		
Train type	Number of trains/day	
1	12	} 24 Train type "A"
2	12	
3	5	} 10 Train type "B"
4	5	
5	7	} 19 Train type "C"
6	12	
7	8	} 14 Train type "D"
8	6	

**Figure 9.7:** Assumed traffic mix.

Hence the assumed daily traffic mix is composed by 24 trains type “A”, 10 trains type “B”, 19 trains type “C” and 14 trains type “D”. Using each of these trains a dynamic analysis of the bridge has been computed as described and shown in *chapter 8.2*. As already said, performing these analyses it has been possible to obtain for each involved node of the bridge the load histories in both vertical and horizontal directions for each considered train. By applying the load histories to the nodes of the FEM model, and knowing the observation time and the time step, dynamic analyses of the bridge are carried out for each type of train.

These analyses are needed in order to identify the critical points in which higher stress are localized, and then to determine stress histories of the elements. In this regard, in figures (9.8) (9.9) are shown two plots of the Von Mises equivalent stresses in the bridge at 2 seconds of the dynamic analysis considering the train type “D”, where the unit of measure are in  $N/m^2$ , that is Pascal.

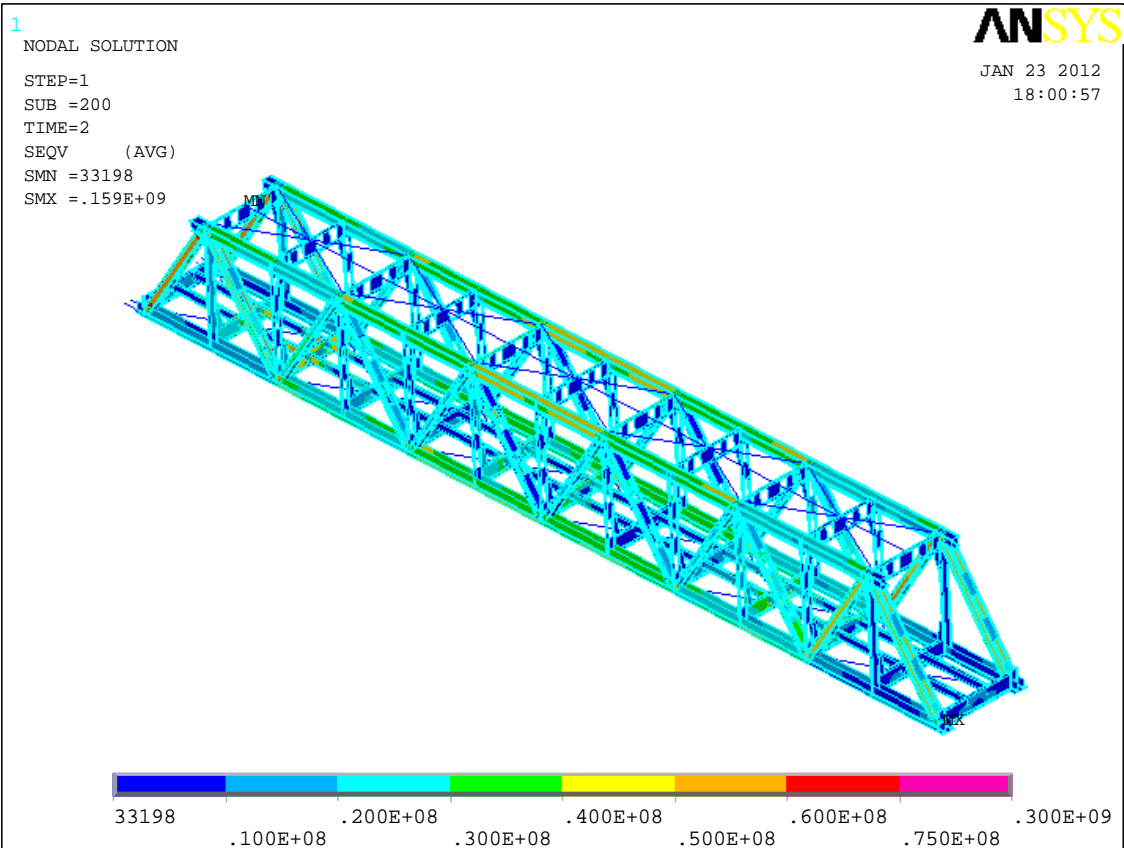


**Figure 9.8:** Von Mises stresses distribution in the bridge [Pa].

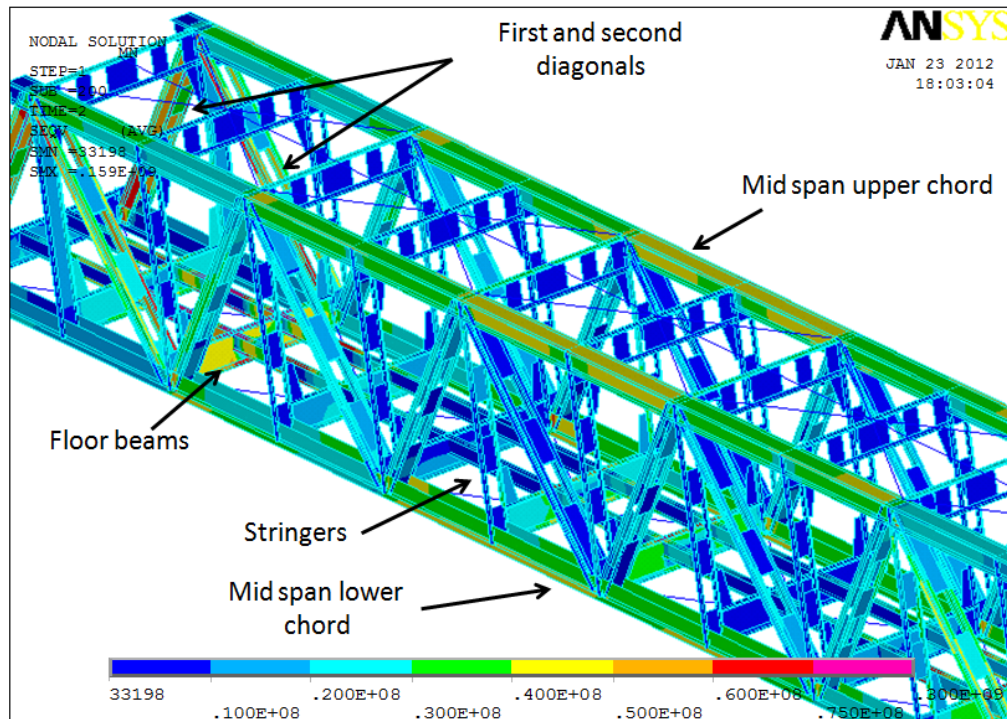


**Figure 9.9:** Bridge critical points where fatigue phenomena could arise.

In particular in figure (9.9) are highlighted the critical elements in which fatigue phenomena could appear as elements in which the stresses are higher. Therefore in addition to the bracing system elements, the fatigue life has been assessed in some points of those elements which are:

- Mid span upper chords
- Mid span lower chords
- Stringers
- Floor beams
- First and second diagonals

It is interesting to note that the above critical listed elements are in agreement to those found in its research by R. Freddi [4].

In order to perform a fatigue verification of those elements, stress time histories are needed at the considered points. In particular for each element the normal stress directed as the axial direction of the element itself is taken into account. In this way the stresses time histories of some points of the critical elements are shown in the following figure, regarding the passage of the train type “D”, remembering that in the same way have been obtained the stress histories for all the train types, *see Appendix*.

### *Mid span upper chord*

First of all the mid span upper chord investigated is put in evidence in figure (9.10), remembering that for symmetry the results obtained could be extended directly to the other three mid span similar elements.

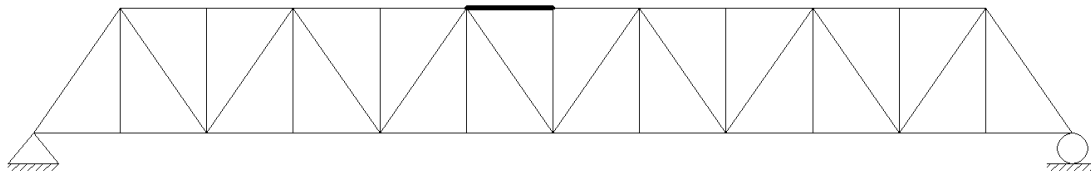


**Figure 9.10:** Mid span upper chord investigated.

Then in figure (9.11) the trend of the normal stress time history in a point of the element is plotted. This element, during the passage of the train type “D”, but in general during the passage of all the train types, is characterized mainly by a compressive state behavior. The maximum stress in this point reaches the value of about 50 Mpa at 1.4 seconds. It is also interesting to see how in this element the shape of the stress time history is similar to the plot of the displacement time history of the bridge shown in figure (8.19).

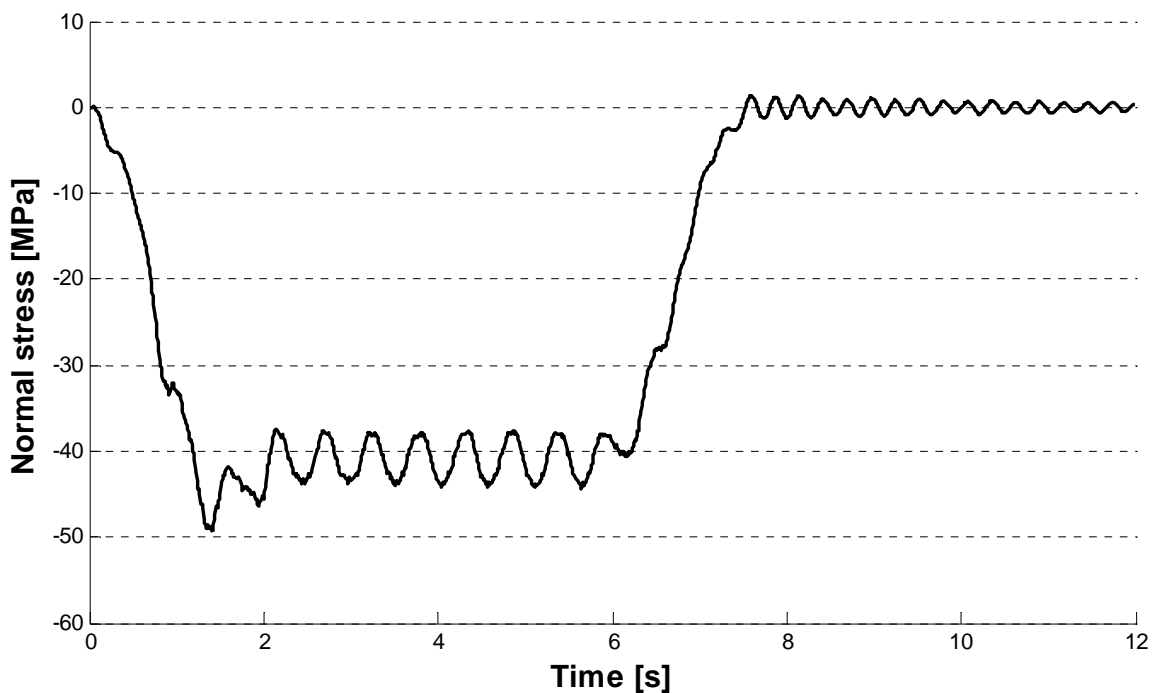


**Figure 9.11:** Stress time history in a point of the mid span upper chord.

### *Mid span lower chord*

In figure (9.12) the mid span lower chord considered for the fatigue verification is highlighted.

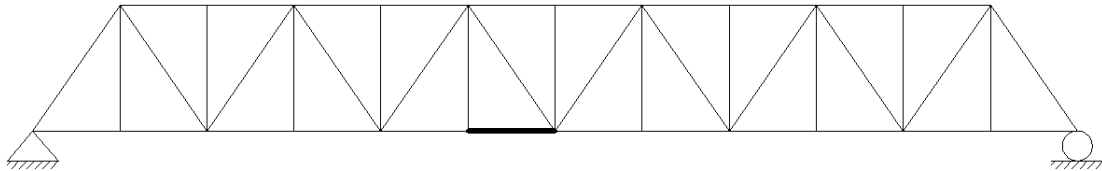


**Figure 9.12:** Mid span lower chord investigated.

The normal stress time history in a point of that element is represented in figure (9.13). The element during the passage of the trains exhibits mainly a traction behavior reaching a maximum value of about 45 MPa at 1.4 seconds. The shape of that plot is very similar to the opposite plot of the case before regarding the upper chord. Due to symmetry, also in this case the results obtained for this element can be extended to the other similar members.

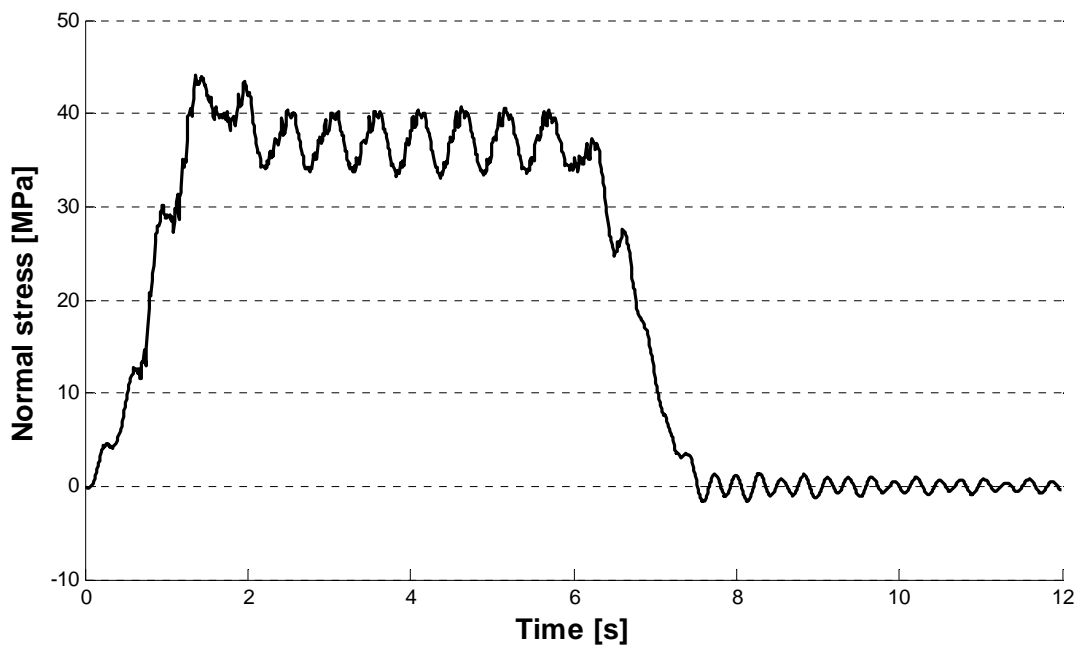


**Figure 9.13:** Stress time history in a point of the mid span lower chord.

### *Stringer*

In the following figure (9.14) the next element considered is highlighted. This element belongs to the stringers on which the sleepers and the railway tracks rest.

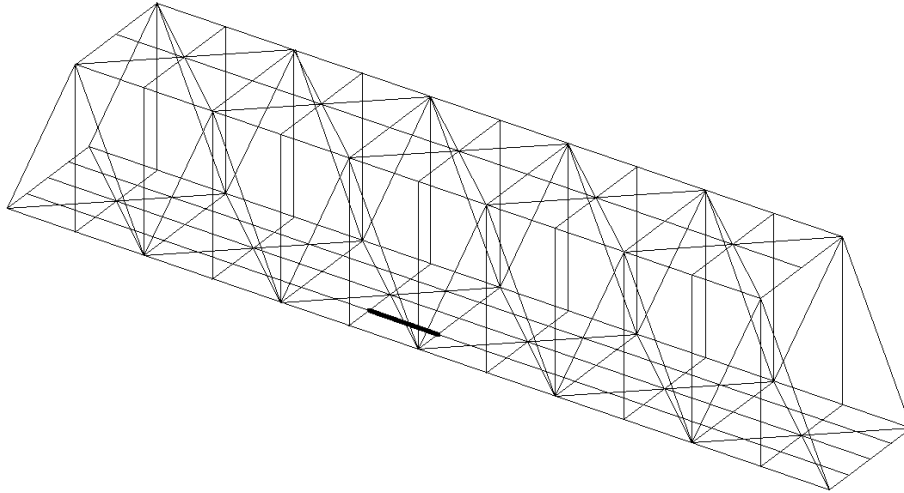


**Figure 9.14:** Longitudinal beam element investigated.

Figure (9.15) shows the trend of the normal stress in a point located at the bottom part of the element during the passage of the train type “D”. In general those elements are subjected to very high stresses, and in particular to high stress amplitude. In fact in this case one peak reaches the value of 140 MPa and some others reach value of 80-90 MPa.

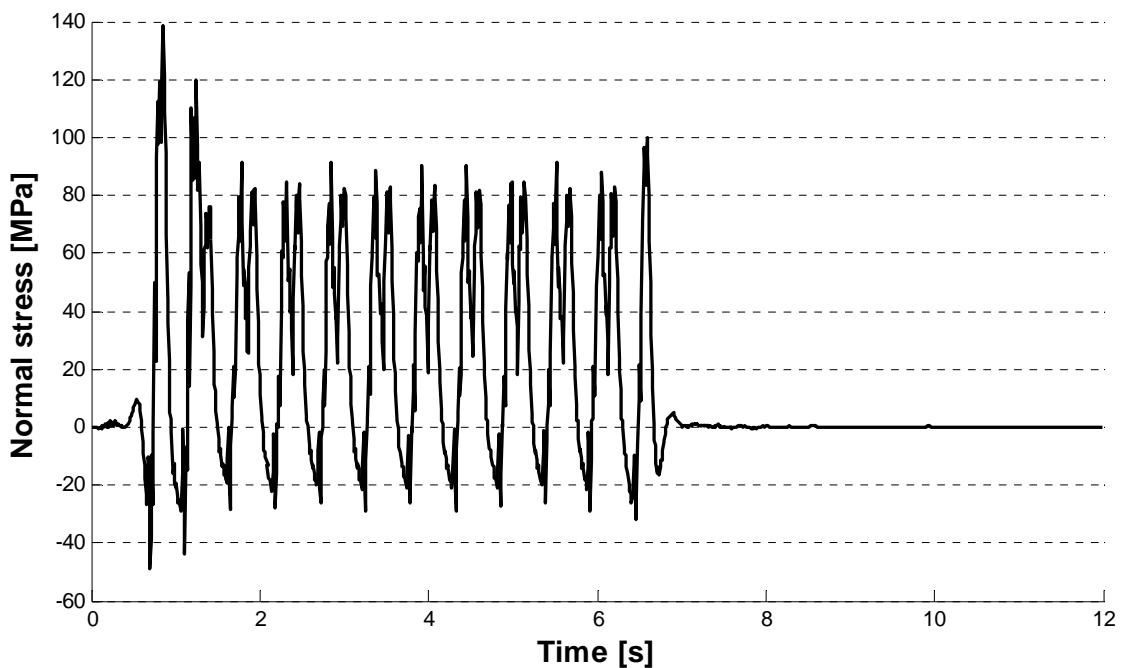


**Figure 9.15:** Stress time history in a point of the longitudinal beam element.

### *Floor beams*

Another category of elements investigated are the floor beams. In figure (9.16) one of these members is highlighted.

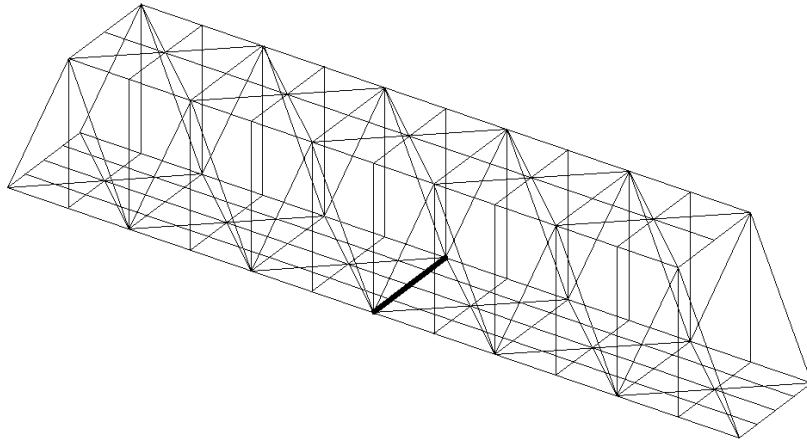


**Figure 9.16:** Floor beams investigated.

Those elements are mainly subjected to flexure state as their task is to support the stringers. Therefore in figure (9.17) the normal stress in a point located in the wings of that element is plotted. In this case the maxim value reached is about 65 MPa, and quite large amplitude cycles are recorded.

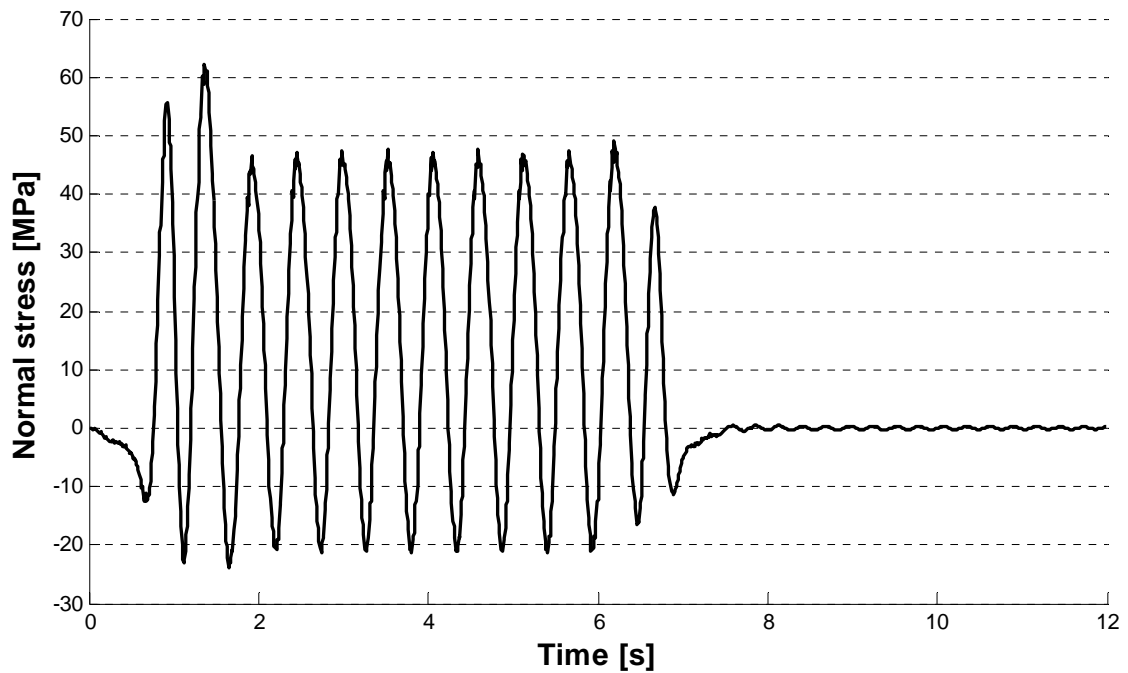


**Figure 9.17:** Stress time history in a point of the floor beams.

### ***First diagonal element***

In the following figure (9.18) the first diagonal element object of the fatigue analysis is highlighted.

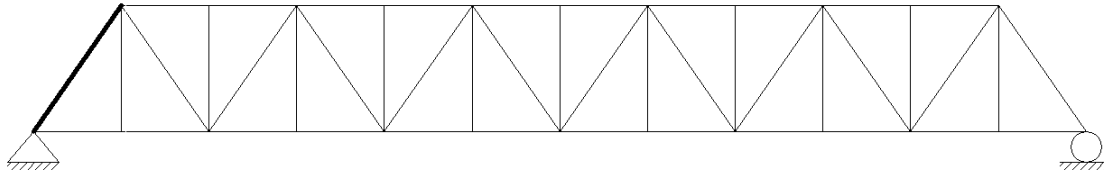


**Figure 9.18:** First diagonal element investigated.

This element, during the passage of the trains, is subjected mainly to compressive stress, see in figure (9.19). The maximum stress value reached due to the passage of the train type “D” is more or less 35 MPa. Similar behavior is however expected in the diagonal on the other side of the bridge, and the last two diagonals of the bridge.

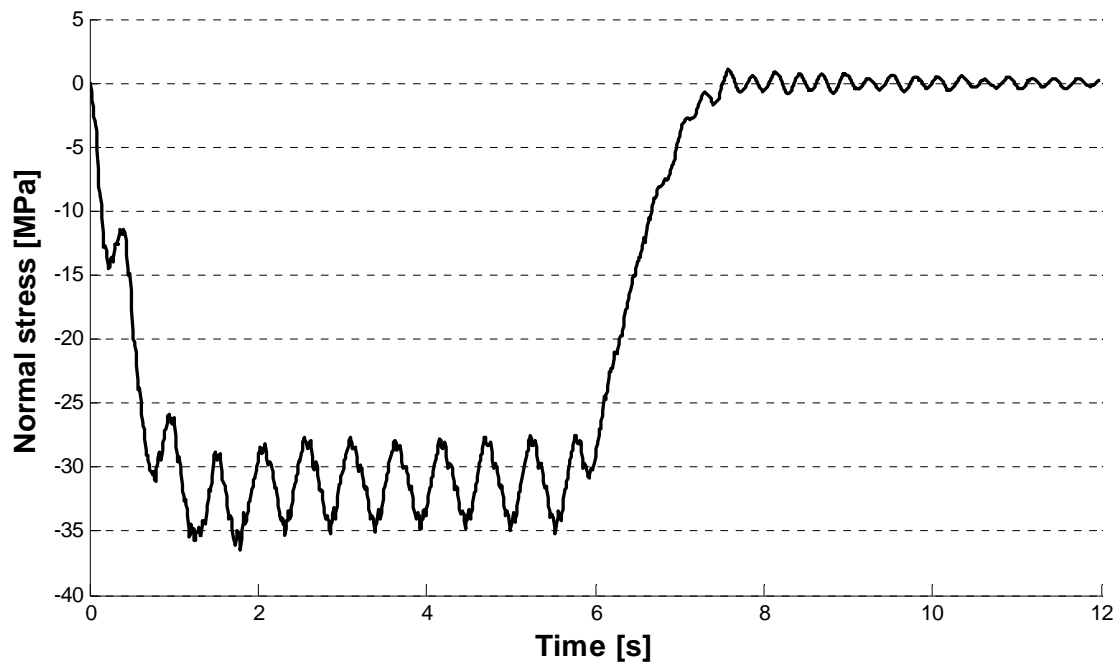


**Figure 9.19:** Stress time history in a point of the first diagonal element.

### *Second diagonal element*

As already said another critical element could be the second diagonal of the main truss of the bridge, highlighted in figure (9.20).

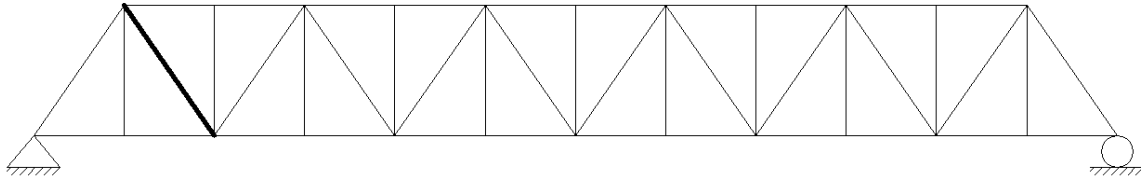


**Figure 9.20:** Second diagonal element investigated.

Contrary to the precedent case, in this element essentially compressive stress are developed when a train passes on the bridge as shown in figure (9.21). The maximum value reached is about 33 MPa and the plot shape is very similar to the mirrored previous plot.. Also in this case the results can be extended to the correspondent element in the bridge.

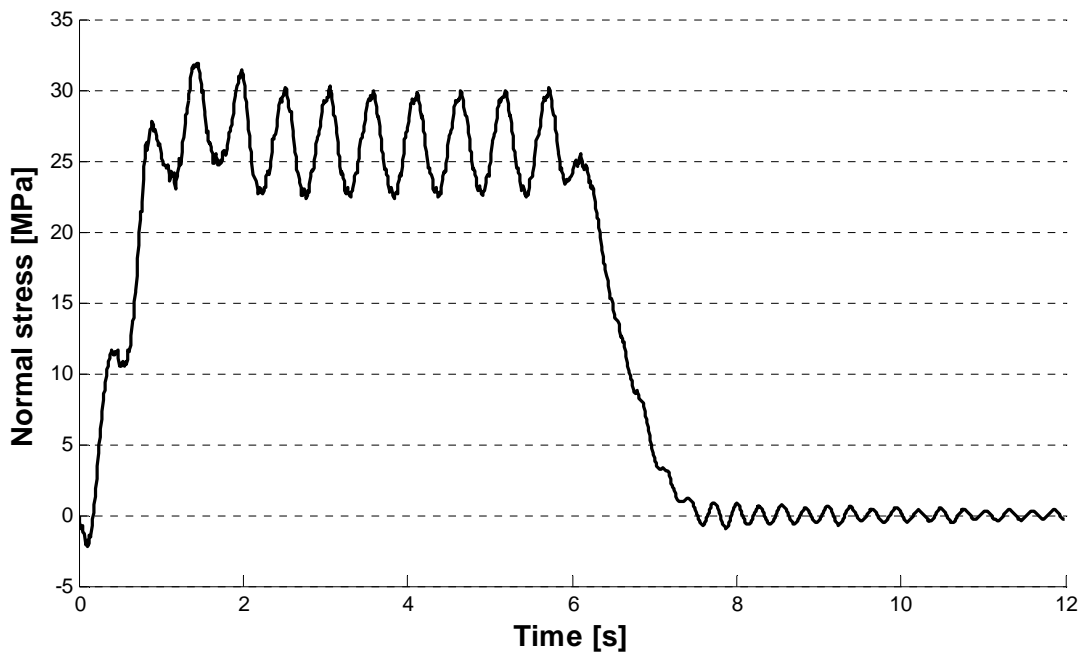


**Figure 9.21:** Stress time history in a point of the second diagonal element.

### ***Bracing system element***

Finally the last category of element investigated are those belonging to the bracing systems, as shown in figure (9.22).

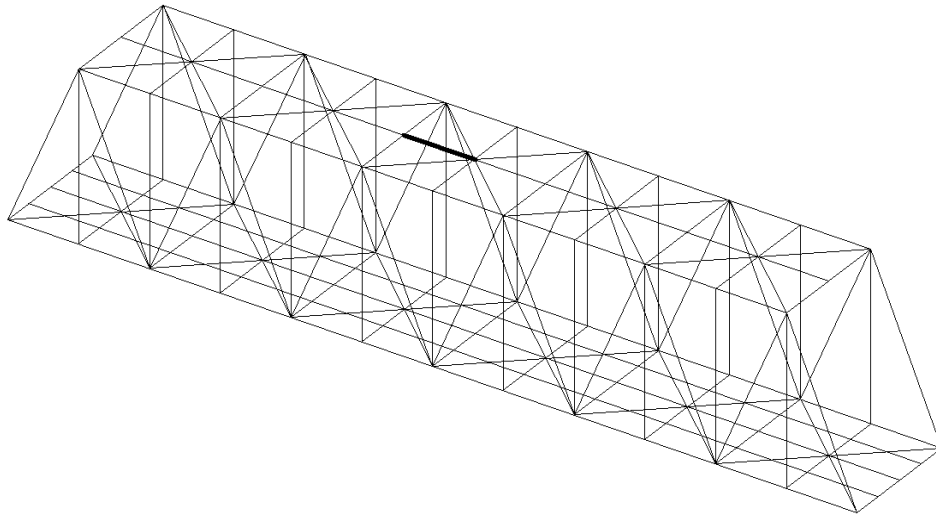


**Figure 9.22:** Bracing system elements.

In figure (9.23) the stress time history of a bracing element due to the passage of the train type “D” is shown. In particular the plot refers to an upper element of the system. For that reason an essentially compressive state of stress is observed in the element. The maximum value reached is about 43 MPa.

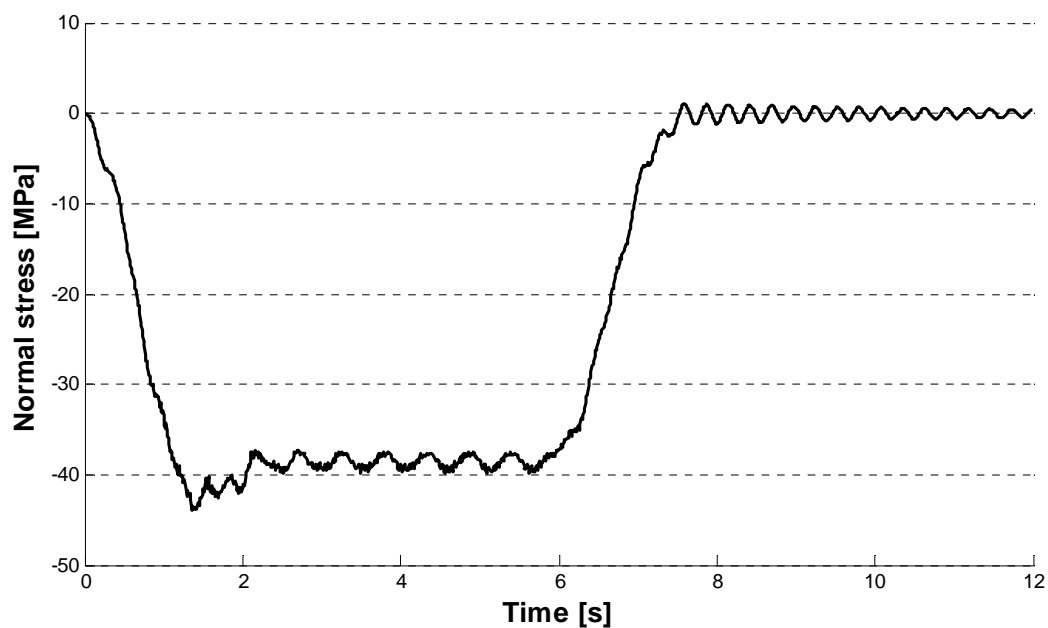


**Figure 9.23:** Stress time history in a bracing system element.

Once obtained the stress history in each considered point for each train crossing, then a cycle counting algorithm has been applied. In particular is has used a code, developed by [16] which deals with multi-axial fatigue phenomena and spectral methods for fatigue life assessment. The code has been written in according to the ASTM, and it is made available in a directory by Mathworks.

Therefore in this case giving as input the stress histories in matrix form, the algorithm first of all computes the “peak-valley” diagrams and then through the implemented rainflow method it performs the cycles counting. Finally at each stress amplitude range it associates the right number of cycles. This procedure has been done for all the trains types considered and for each investigated point. As example in the following plots are shown the histograms that collect the number of cycles for each stress range for the previously presented stress time histories regarding the train type “D”, see figures (9.24) to (9.30).

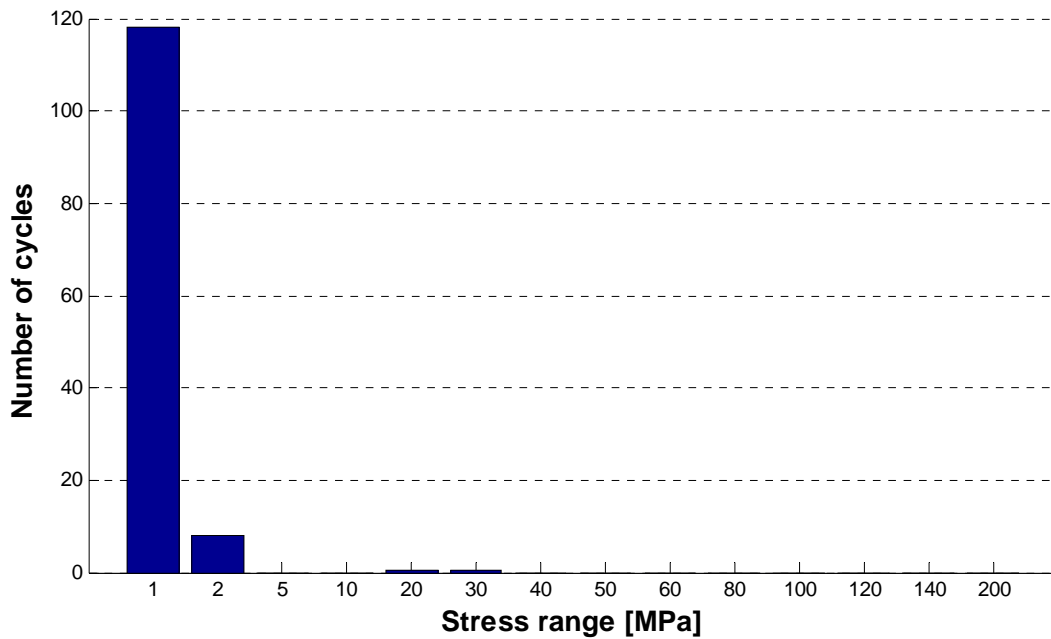


**Figure 9.24:** Histogram related to the stress time history of the mid span upper chord.

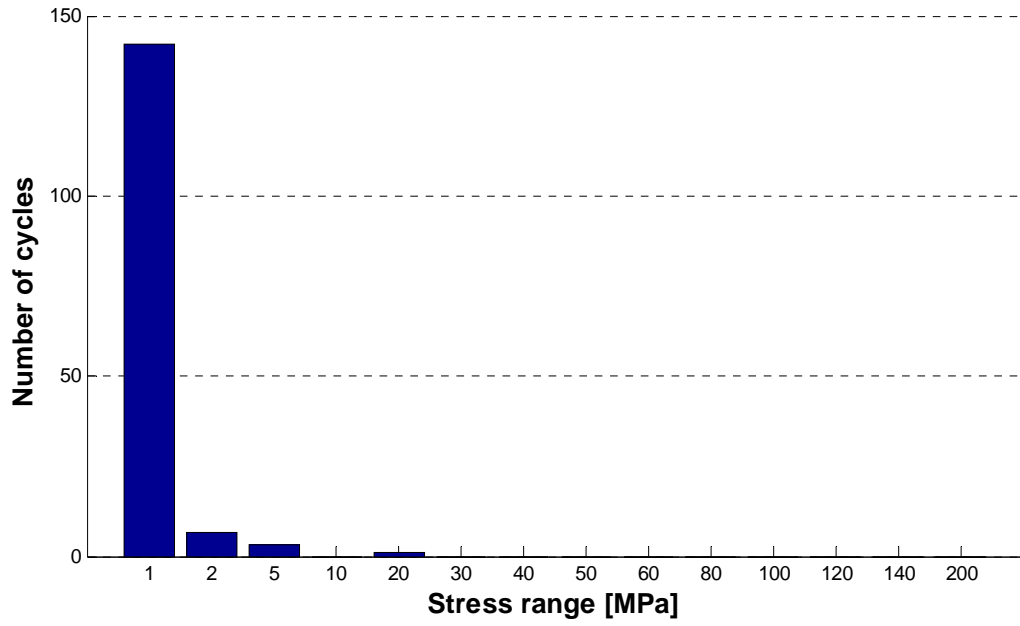


Figure 9.25: Histogram related to the stress time history of the mid span lower chord.

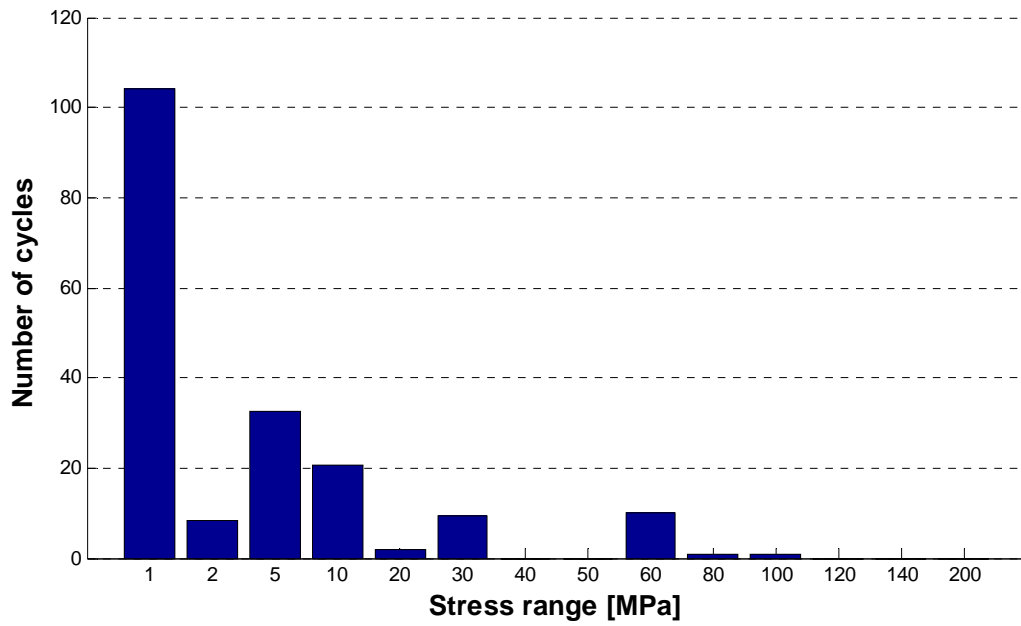


Figure 9.26: Histogram related to the stress time history of the stringer.

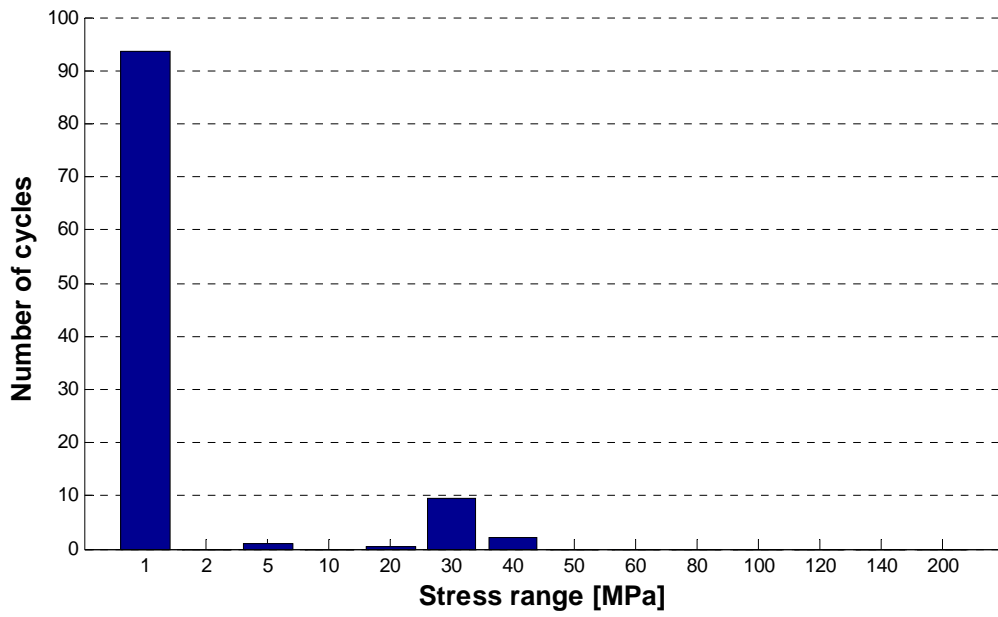


Figure 9.27: Histogram related to the stress time history of the floor beam.

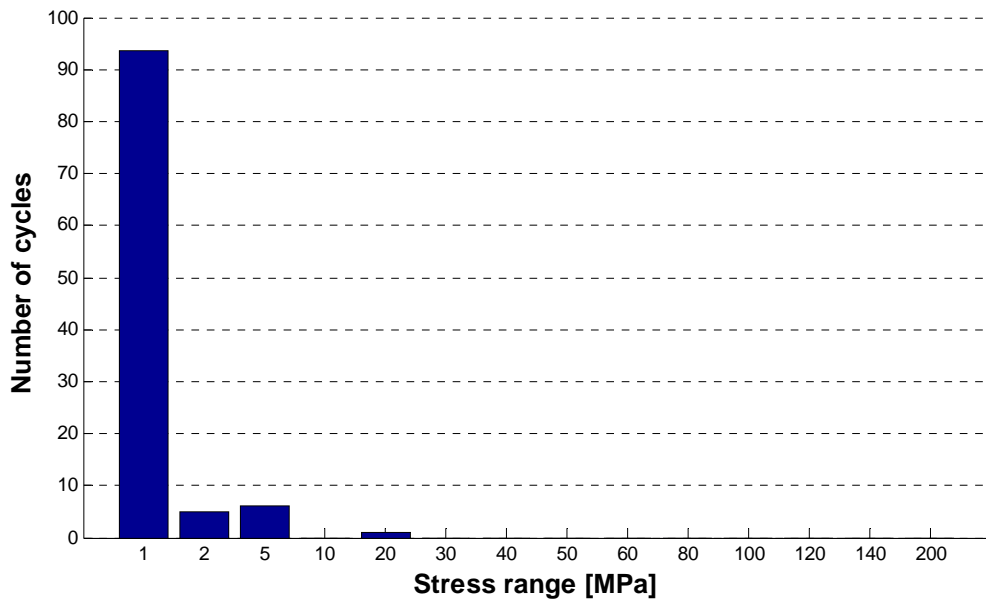


Figure 9.28: Histogram related to the stress time history of the first diagonal element.

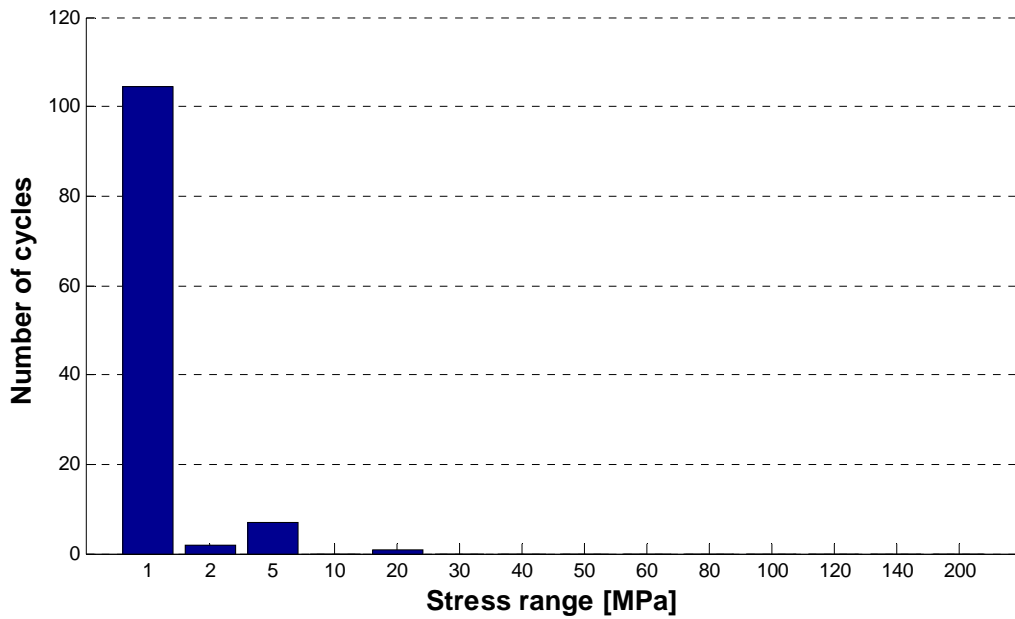


Figure 9.29: Histogram related to the stress time history of the second diagonal element.

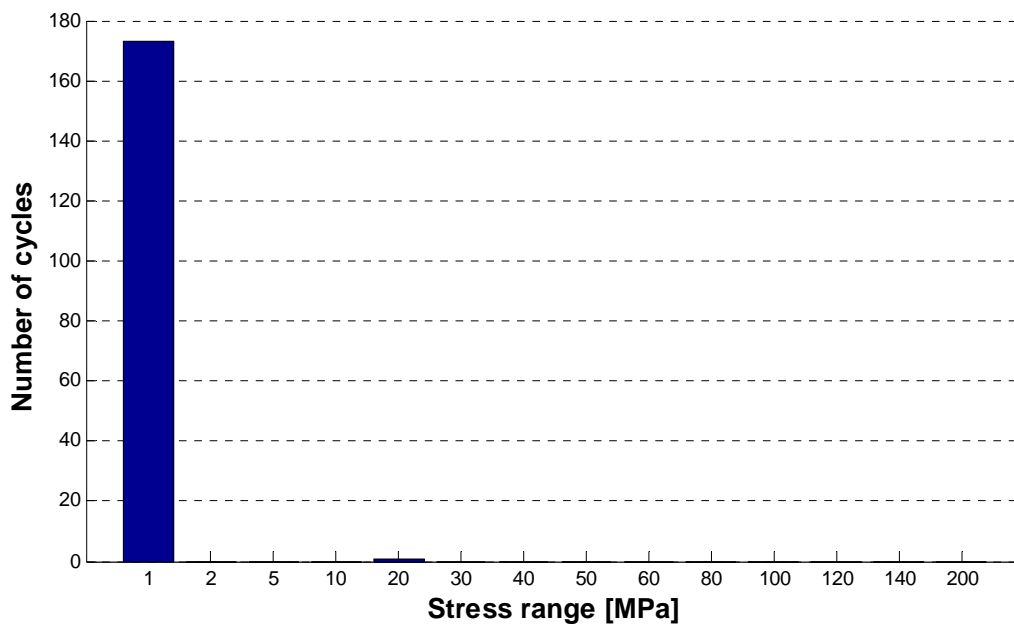
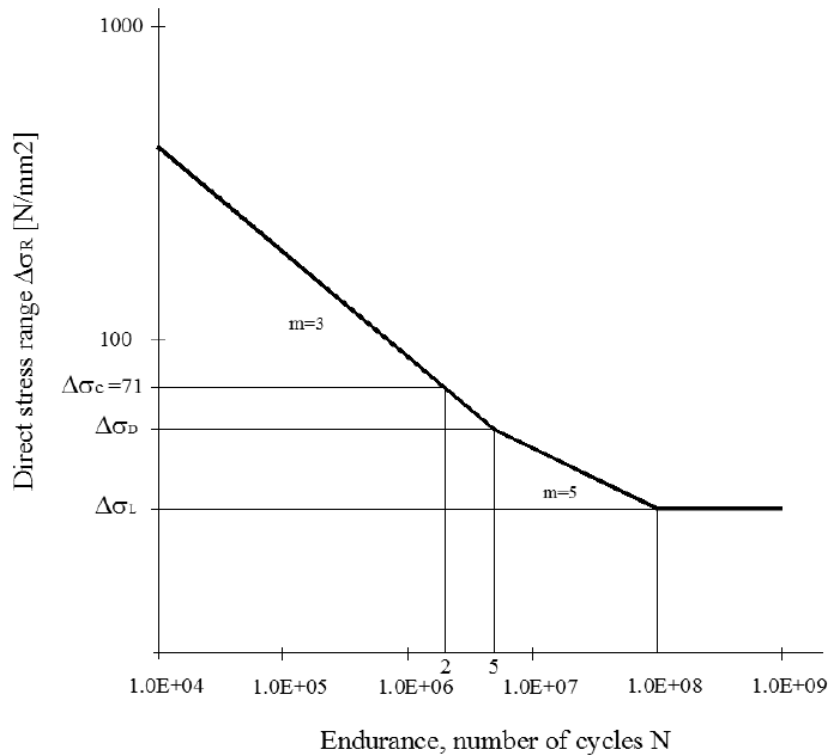


Figure 9.30: Histogram related to the stress time history of the bracing system element.

Having the stress histories and the correspondent number of cycles for each stress amplitude, a suitable S-N curve is needed. The elements are connected by means of rivets. Eurocode 3 does not provide any type of detail concerning riveted elements. Therefore two approaches are used.

The first approach is that given by the Italian Railway company, which impose the use of the detail category 71, figure (9.31).



**Figure 9.31:** Detail category 71 S-N curve.

For the detail category 71 curve, the reference fatigue limit at 2 millions of cycles is

$$\Delta\sigma_C = 71 \text{ MPa}$$

and the fatigue limit at constant amplitude at 5 millions of cycles is defined as

$$\Delta\sigma_D = \left(\frac{2}{5}\right)^{\frac{1}{3}} \Delta\sigma_C = 52.31 \text{ MPa}$$

and finally the cut-off limit is computed as

$$\Delta\sigma_L = \left(\frac{5}{100}\right)^{\frac{1}{5}} \Delta\sigma_D = 28.73 \text{ MPa}$$

Once defined the S-N curve it has been possible to determine for each stress range  $\Delta\sigma_i$  the correspondent number of cycles  $N_i$  needed to reach failure. Then by using Eq. (9.5) the damage index for the considered elements have been obtained considering a service time for the structure equal to 100 years.

The second approach is in accordance to what established in [6], which presents a different method for evaluating the fatigue life of riveted bridges. Usually only the stress range is assumed as the basic parameter for the evaluation of the fatigue strength. This is true for details with high stress concentration and residual stress levels, such as welded details, but it is very inaccurate for bolted and riveted details, where other factors have significant importance. Main factors determining the fatigue strength of a riveted detail may be specified as follows:

- Difference between maximum and minimum stress in the cycle, called stress range  $\Delta\sigma$ ;
- Ratio between minimum and maximum stress in the cycle called stress ratio  $R$ .

The influence of mean stresses and stress ratio on fatigue strength category is taken into account by function  $f(R)$  as follows:

$$\Delta\sigma_c(R) = f(R) \cdot \Delta\sigma_{c,0} \quad (9.6)$$

where  $\Delta\sigma_c(R)$  is the fatigue strength category for the considered detail as a function of the stress ratio;  $\Delta\sigma_{c,0}$  is the fatigue strength category for the considered detail for stress ratio  $R = 0$  (fatigue strength category is the stress range in [MPa] of a harmonic sinusoidal cyclic variable stresses leading to fatigue crack initiation in considered detail for exactly 2.10<sup>6</sup> load cycles); and  $f(R)$  is the correction function which for mild steels (low carbon steels with carbon level under 0,25%) is determined by the following formula:

$$f(R) = \begin{cases} \frac{1 - R}{1 - 0.6R} & \text{when } R > 0 \\ \frac{1 - R}{1 - 0.4R} & \text{when } -1 \leq R \leq 0 \end{cases} \quad (9.7)$$

Correction function  $f(R)$  is represented on Figure (9.32). It is seen that when stress ratio increases from -1 to 0 the correction function decreases from at about 1,4 to 1,0 which means decrease of fatigue strength category but it is still bigger than category, determined for stress ratio 0, see figure (9.33). When stress ratio increases from 0 there is a decrease of fatigue strength category in comparison with this determined for stress ratio 0.

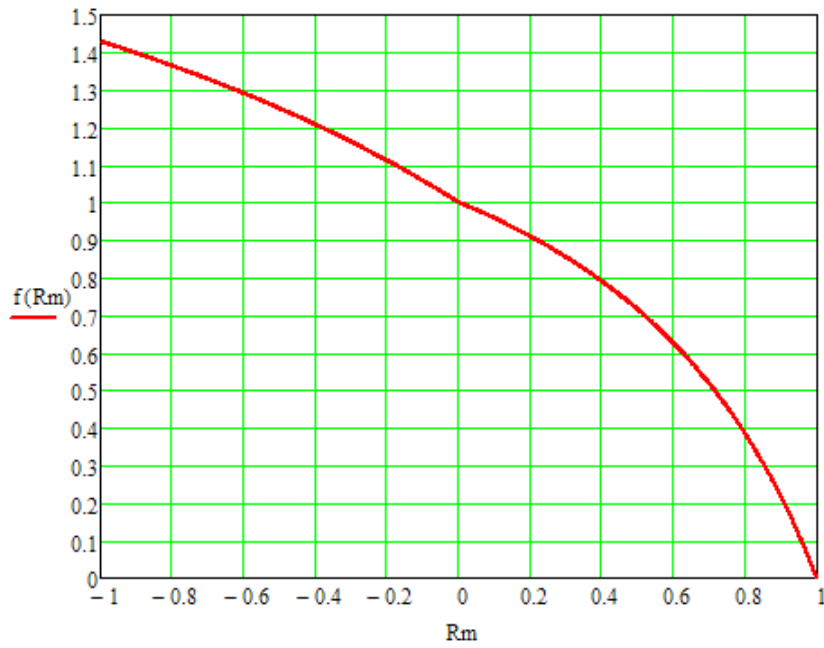


Figure 9.32: Correction function  $f(Rm)$  as a function of the stress ratio  $Rm$  [6].

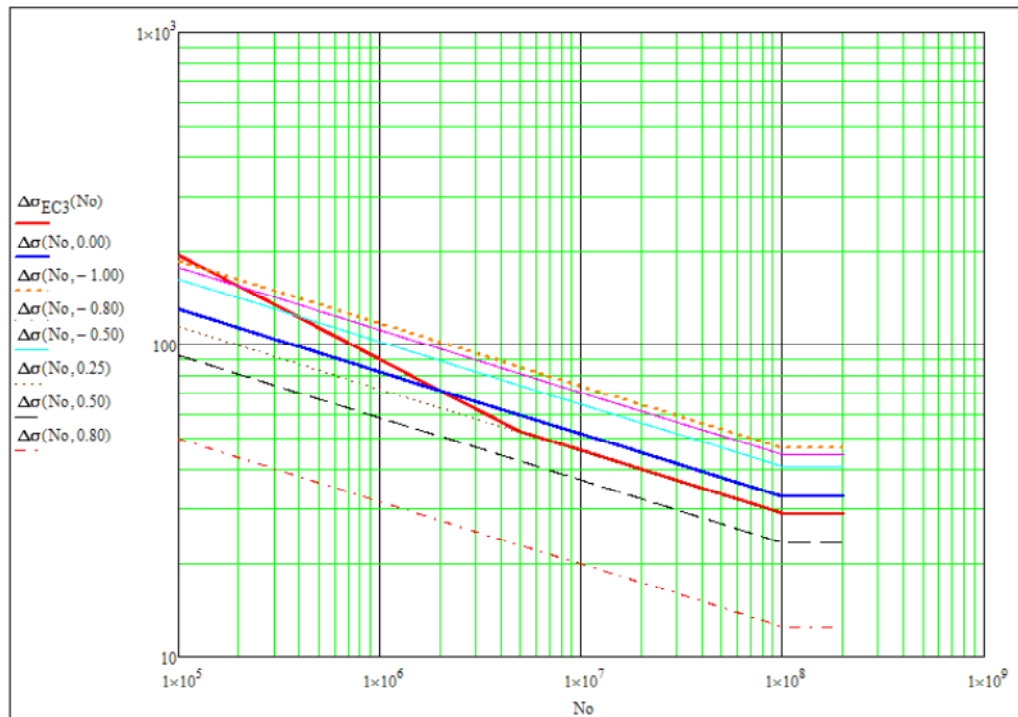


Figure 9.33: S-N curves for riveted connection discussed in accordance with Eurocode and with different  $R$  values [6].

Using Eurocode S-N line model and stress ratio correction just proposed, number of cycles to failure may be obtained as a function of stress range  $\Delta\sigma$  and stress ratio  $R$  as follows.

$$N(\Delta\sigma, R) = \begin{cases} \left( \frac{f(R) \cdot \Delta\sigma_{c,0}}{\Delta\sigma} \right)^5 \cdot 2 \cdot 10^6 & \text{for } \Delta\sigma > \Delta\sigma_{FL} \\ \infty & \text{for } \Delta\sigma \leq \Delta\sigma_{FL} \end{cases} \quad (9.8)$$

### *Mid span upper chord*

During the entire service period of structure, the mid span upper chord seems to have no fatigue problem, in fact the damage index is well below the 0.1 threshold, for both two approaches, as shown in figure (9.34), where five points along the element are investigated.

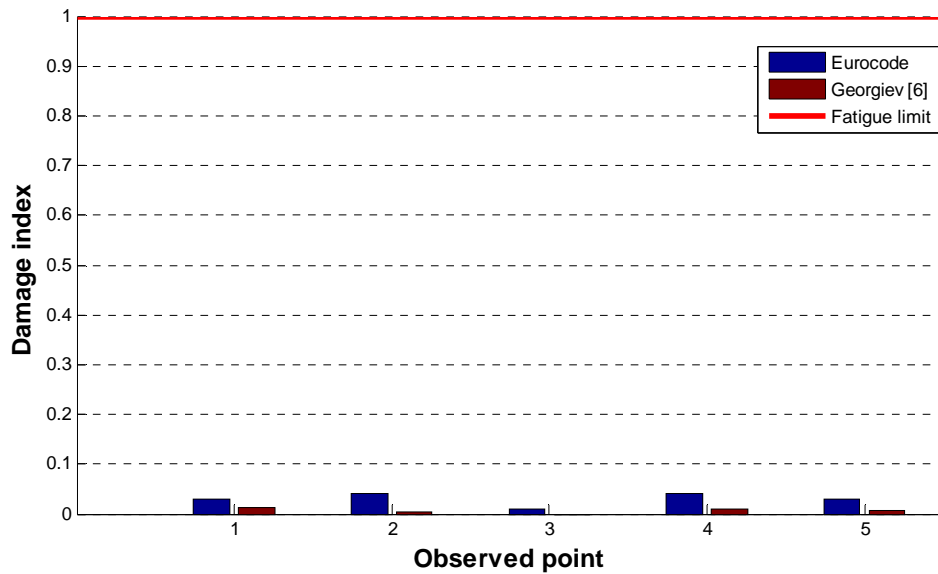


Figure 9.34: Mid span upper chord damage.

### *Mid span lower chord*

As in the previous case, also for this category of elements there are not fatigue problems. In fact as shown in figure (9.35) very low fatigue damage index are obtained, even below the 0.01 limit. For this reason this element of the bridge seems to be safe against a possible fatigue failure.

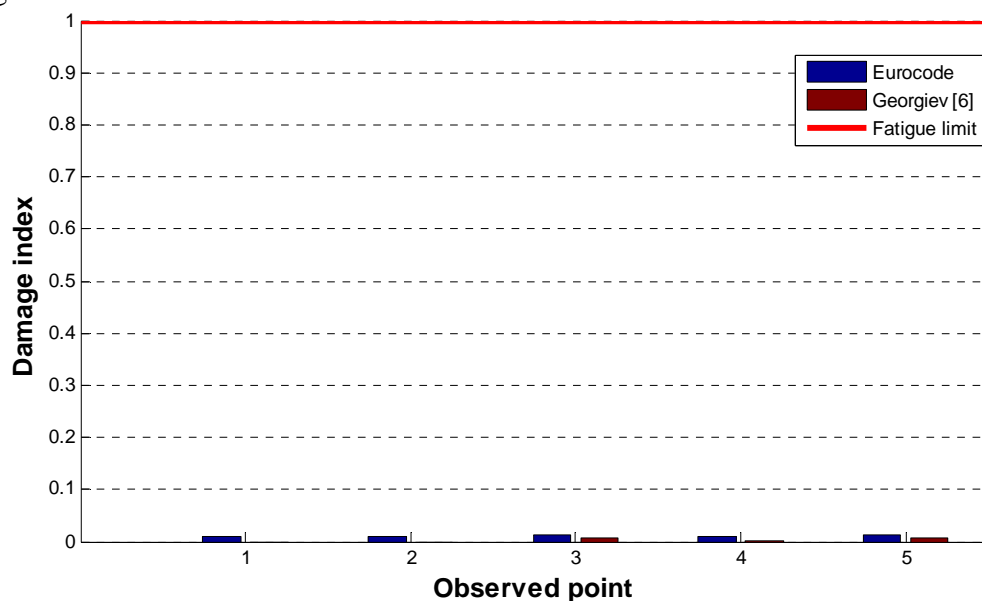


Figure 9.35: Mid span lower chord damage.

### Stringers

Looking at figure (9.36), appears very clear that these elements result to be critical since very high damage values are obtained, as expected. In fact these elements are essentially the points of application of the loads and indeed they are subjected to very high amplitude stress cycles, see figure (9.15). The damage index obtained in five points located at the bottom of one element reach the value of about 22 for the Eurocode approach and about 11 for the second approach [6]. So in these beams fatigue problems could arise.

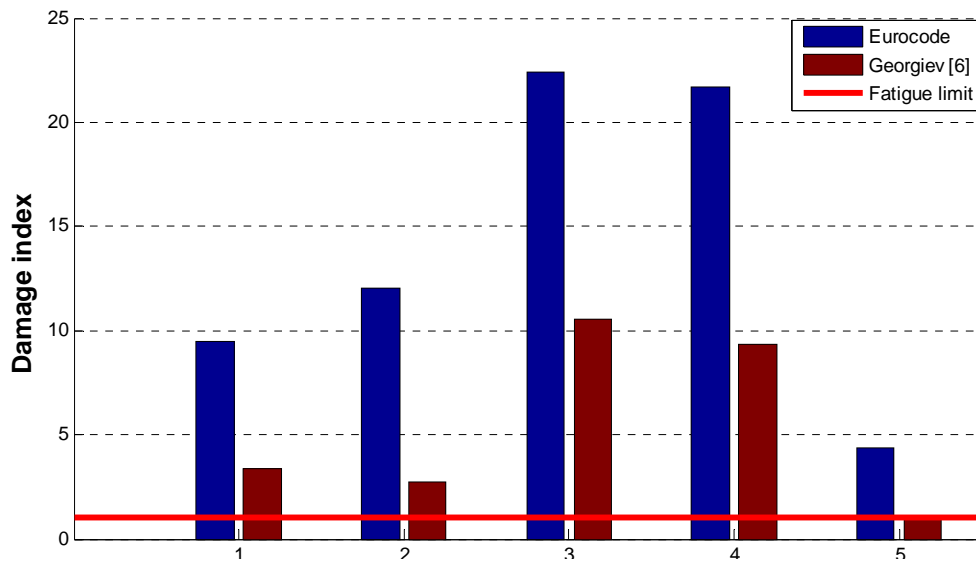


Figure 9.36: Stringer damage.

### Floor beam

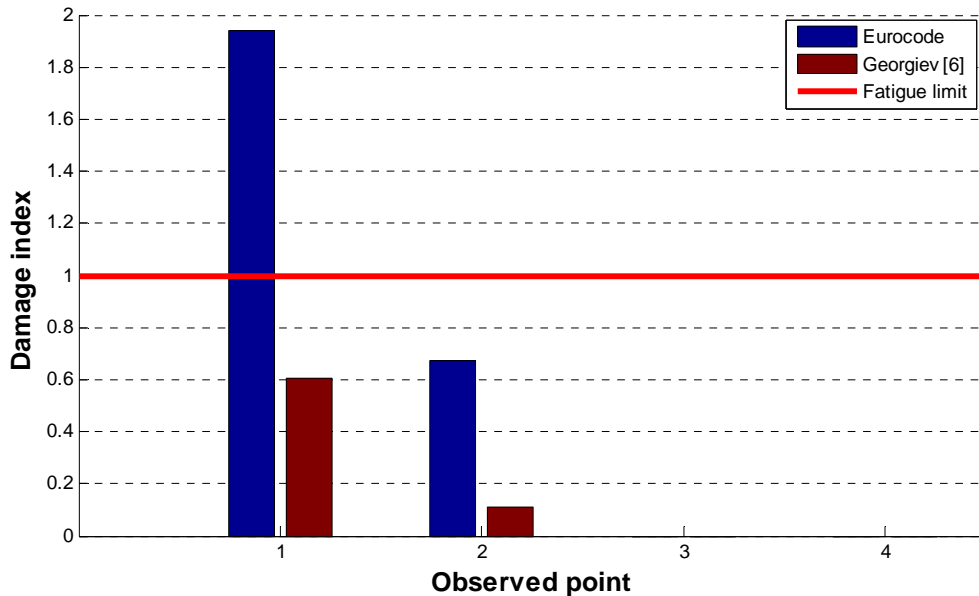


Figure 9.37: Floor beam damage.

As regards the floor beams, when using Eurocode approach, not verified results are obtained as shown in figure (9.37). In fact one of the four points investigated in the element, which is the point at the connection with the longitudinal beams, is above the safety limit. On the contrary using Georgiev theory [6] the results are verified. The other two zero value points are located in the two flanges on the side of the element near the stiffening plate, in this zone no fatigue problem is highlighted. Therefore as for the previous elements category an inspection and monitoring plan is strongly suggested for these elements.

**First and second diagonal elements**

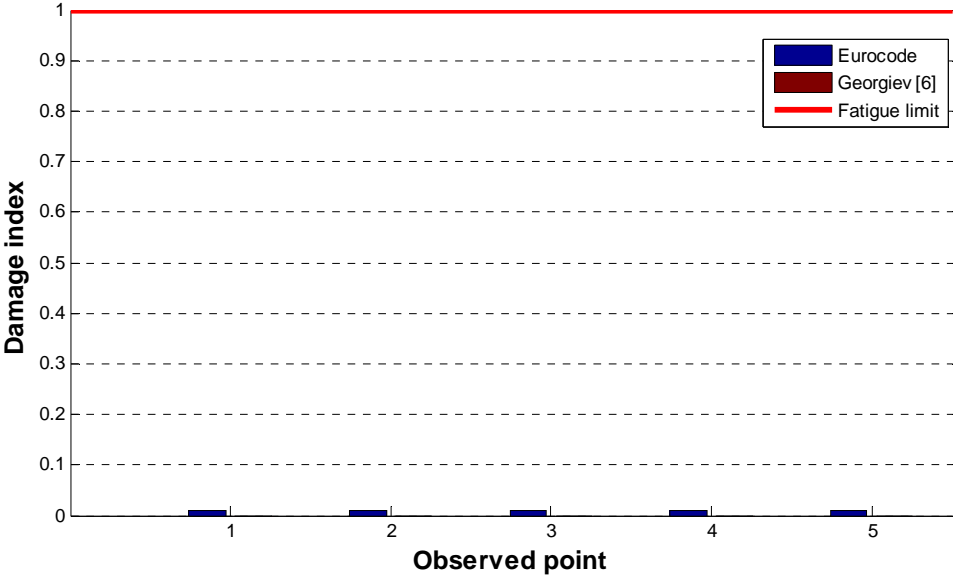


Figure 9.38: First diagonal element damage.

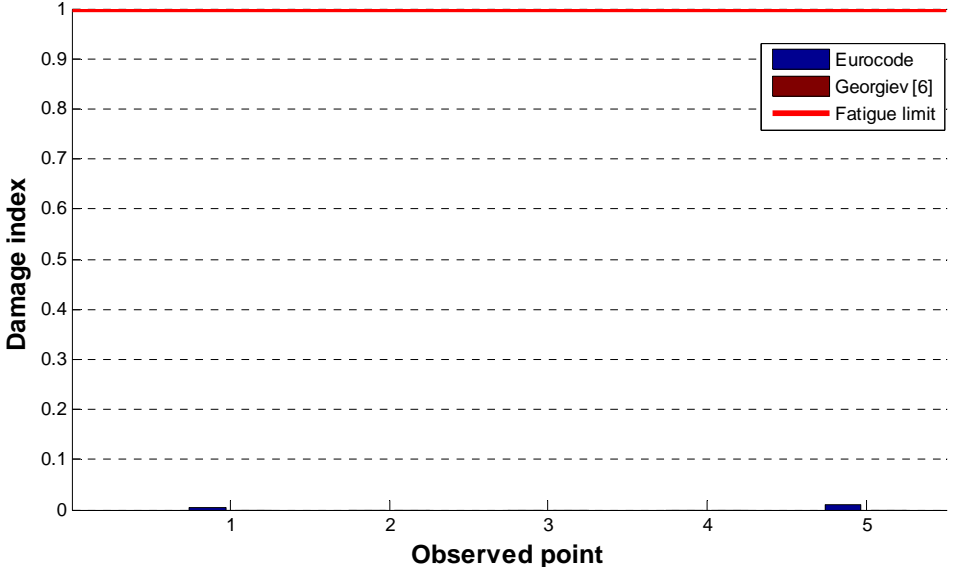
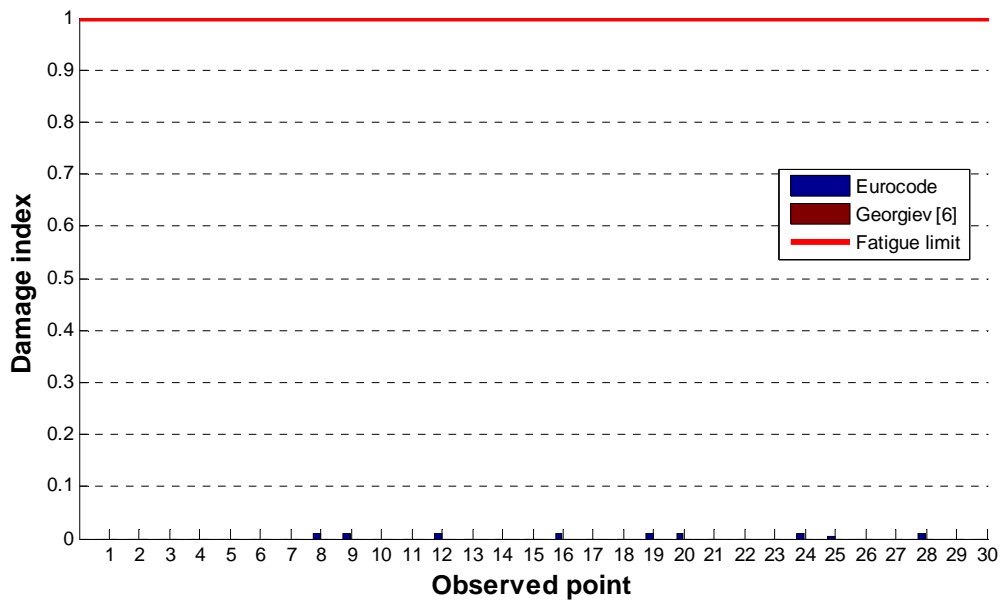


Figure 9.39: Second diagonal element damage.

For all the five points investigated for each of the two considered diagonal elements very low fatigue damage values are founded, meaning that these elements result safe over the entire service life of the bridge, figures (9.38) (9.39).

**Bracing system elements**

The upper and lower bracing system elements seem to be safe in respect to a possible fatigue failure, in fact very low values of accumulated damage is obtained as shown in figures (9.40) and (9.41), respectively.



**Figure 9.40:** Upper bracing system elements damage.

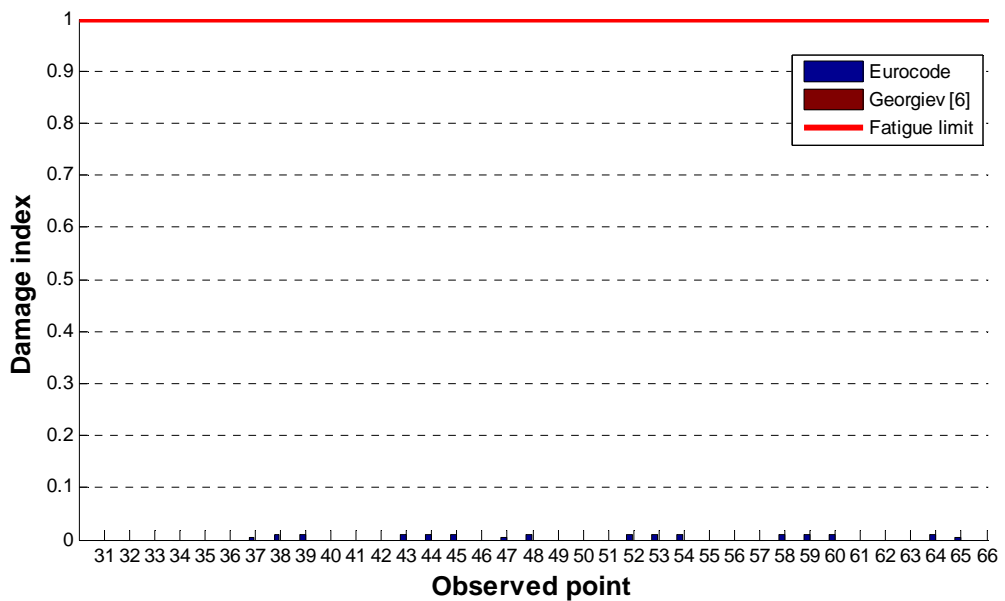


**Figure 9.41:** Lower bracing system elements damage.

Summarizing in the following table (9.1) for each element are shown the fatigue damages evaluated first over the entire service life (100 years), then over 65 years passed since the bridge was built and finally the remaining fatigue life evaluated as follows

$$RFL = \frac{1 - D_p}{D_{1f}} \quad (9.6)$$

where  $D_p$  is the accumulated damage in the considered element in the past periods of time and  $D_{1f}$  is the damage accumulated for one year of future exploitation.

<i>Fatigue assessment</i>						
Element	Eurocode			Georgiev [6]		
	Damage over 100 years	Damage over 65 years	RFL	Damage over 100 years	Damage over 65 years	RFL
Mid span upper chord	0.043	0.027	$2.28 \cdot 10^3$	0.013	0.0081	$9.75 \cdot 10^3$
Mid span lower chord	0.012	0.008	$8.43 \cdot 10^3$	0.0064	0.0041	$1.55 \cdot 10^4$
Stringer	22.396	14.652	0	10.552	6.753	0
Floor beam	1.938	1.260	0	0.603	0.386	101.88
First diagonal element	0.009	0.006	$1.16 \cdot 10^4$	0	0	Inf.
Second diagonal element	0.009	0.006	$1.16 \cdot 10^4$	0	0	Inf.
Bracing system elements	0.009	0.006	$1.16 \cdot 10^4$	0	0	Inf.

**Table 10.1:** Summarized fatigue results.

## *10. CONCLUSION AND FUTURE DEVELOPMENT*

The main objective of this paper was to assess the fatigue life of an old metallic railway bridge that crossing the Po river and connects Pontelagoscuro and Occhiobello near Ferrara and Rovigo, respectively. For this aim, to better represent the real situation of a crossing train, dynamic interaction model is used to perform dynamic analyses of the structure.

First of all in order to lead the reader through the arguments treated in this paper, brief dynamic notions are given. So in the first part of the elaborate SDOF and MDOF systems have been presented framing mainly the eigenvalue problem that allows to compute frequencies and modal shapes of an elastic system. After that two possible methods for solving the equations of motion have been presented; the first one is the classical modal analysis that can be used only when there is classical damping, and the second one is the Newmark's numerical time-step method that can be used directly to integrate the equations of motions.

Then some methods to model the vehicles, in this case trains, have been explained, starting by the classical way of representing the train crossing by means of moving loads, and going to more sophisticated methods that take into account the interaction between the vehicle and the bridge. These methods seen the vehicle as an elastic system, and so its

motion can be represented by a system of ordinary differential equations as done for the bridge. The two systems of equations, for the bridge and the vehicle, are coupled by each other due to the interaction between the two subsystems. So to solve this problem iterative and non-iterative procedures exist.

The structure investigated has been the Italian Pontelagoscuro railway bridge dating at the forties. In this way a three dimensional finite elements model of the structure has been implemented in a finite elements program. Then the model has been calibrated so that its own frequencies and eigenmodes were similar to those acquired experimentally by means of an optimization process using the so called *Differential Evolution algorithm*. In particular two unknown parameters were identified, which are the values of the equivalent material density of the lower and upper elements of the bridge.

Once obtained the model that well suited the real structure behavior, a comparison between the moving loads and VBI models, has been performed, carrying out some dynamic analyses on a 2D equivalent beam-bridge model of the structure solving the equation of motion written in real coordinates. The train used to perform the dynamics analyses are some of those given by the Eurocode 1 used for the fatigue verifications. As regard the dynamic parameters of the trains those relative to the Italian ETR 500Y are used since not data are available in literature and by the trains manufacturer.

Analyzing the obtained results the following conclusion can be done:

- for light, train moving loads and VBI models generally gives similar bridge dynamic responses;
- for freight trains VBI model gives accentuated values of the bridge displacement in time than the moving loads due to the higher counterthrust developed caused by the higher mass of the train itself;
- VBI models could catch effects of dynamic amplifications if the frequencies of the vehicle and the bridge are met.

Finally the results obtained are compared and validated with other results obtained by another author using a different procedure.

Once established the goodness and the benefits of the VBI model, an extension to a three dimensional model was done. In this way also lateral and torsional mode shapes of the bridge are involved and taken into account. Dealing with the 3D model of the bridge is been necessary to use the theorem of expansion of displacements to reduce the great number of equations of motion of the structure with few equations in terms of modal

coordinate including the first lateral, torsional and bending modes. With this procedure the interaction forces at the contact points are been computed and transformed to equivalent nodal loads, in this way by applying these loads to the finite element model, critical elements and stress time history in the considered points are computed. Then through the Rainflow cycles counting method along with the Miner's rule the fatigue assessment was performed. In this regard mainly two categories of elements are resulting critical and subjected to a possible fatigue damage, which are the stringers and the floor beams. Especially for the stringers very high values of the damage are founded, suggesting that the bridge could fails in every moment, while the bridge is still standing without any significant visible damage. However the results obtained are directly linked to the assumed traffic volume and vehicles characteristics and in particular to the trains weight. It can be shown that the biggest part of the damage index computed in *chapter 9* is mainly due to the passage of the train type "C" which is the heaviest one. Undoubtedly, the assumed traffic, results to be more severe than the traffic conditions to which the bridge is actually subjected and those at which has been subject in the last years. Furthermore now, reconstruct and go back to the past traffic history will be not an easy task.

However although overestimated damage values are obtained, remain the fact that stringers and floor beams are to be monitored and controlled as critical elements, while the other elements of the bridge seems to be safe against possible fatigue failures.

In order to obtain more reliable results it will be necessary to get at least the real traffic volume and the trains characteristics that travel daily on the bridge, along with their suspension systems values. After that, some improvements could be done upon the VBI model, including for example track irregularities that may occur as a result of initial installation errors, degradation of support materials and dislocation of track joints.



# APPENDIX

In the following the normal stress histories regarding the other type of trains in the considered elements identified for the fatigue analyses are shown.

## *Train type "A"*

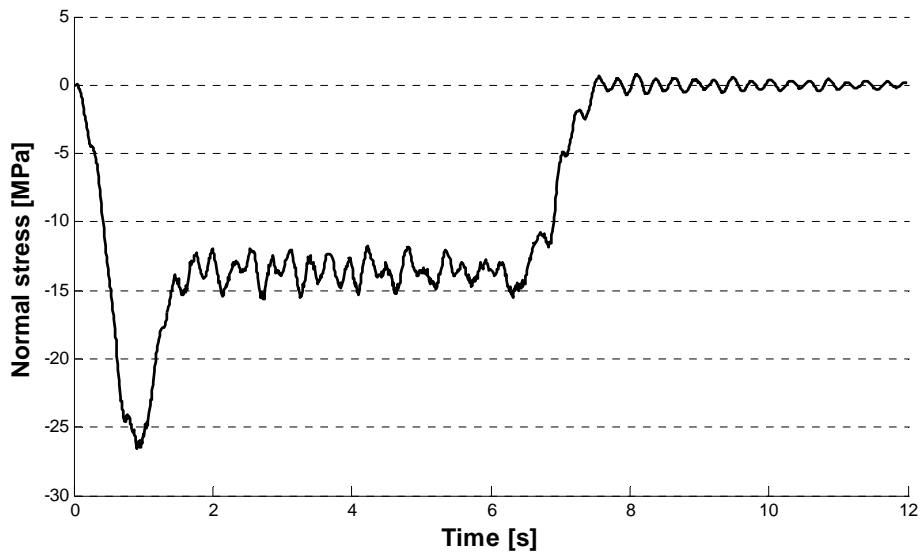


**Figure A.1:** Stress time history in a point of the mid span upper chord.

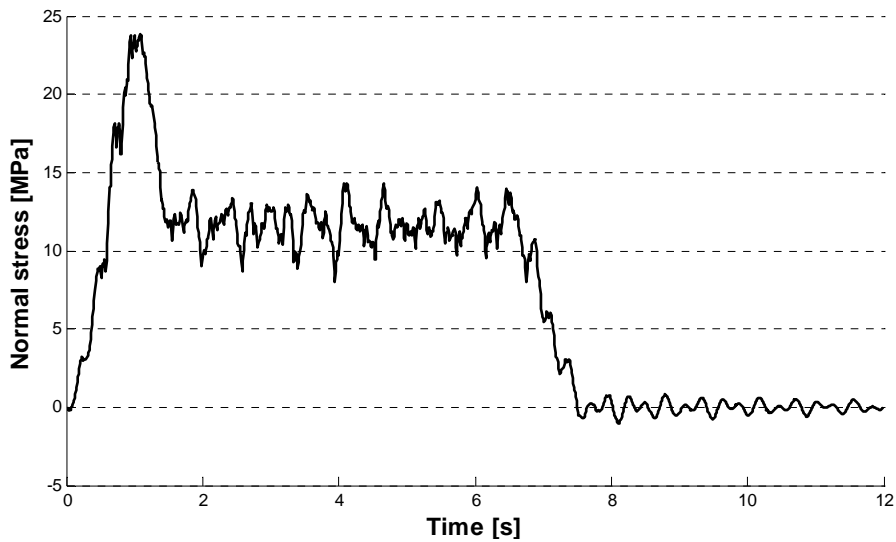


**Figure A.2:** Stress time history in a point of the mid span lower chord.

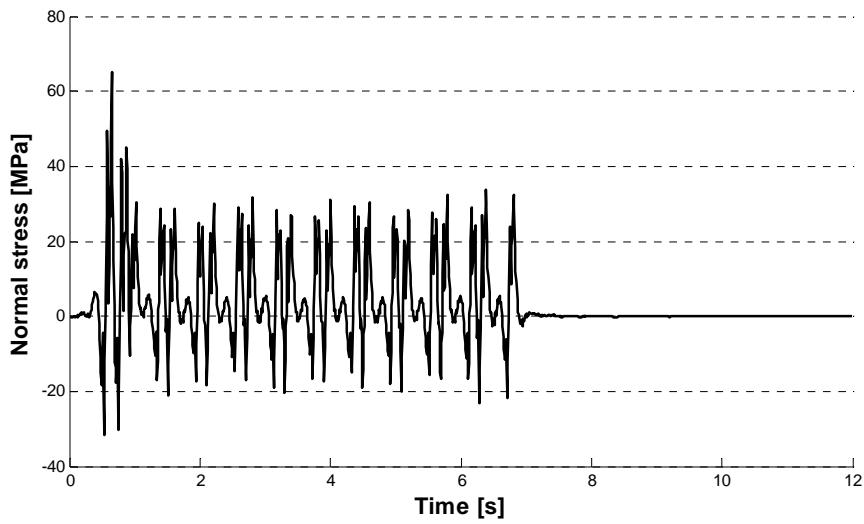


Figure A.3: Stress time history in a point of the stringer.

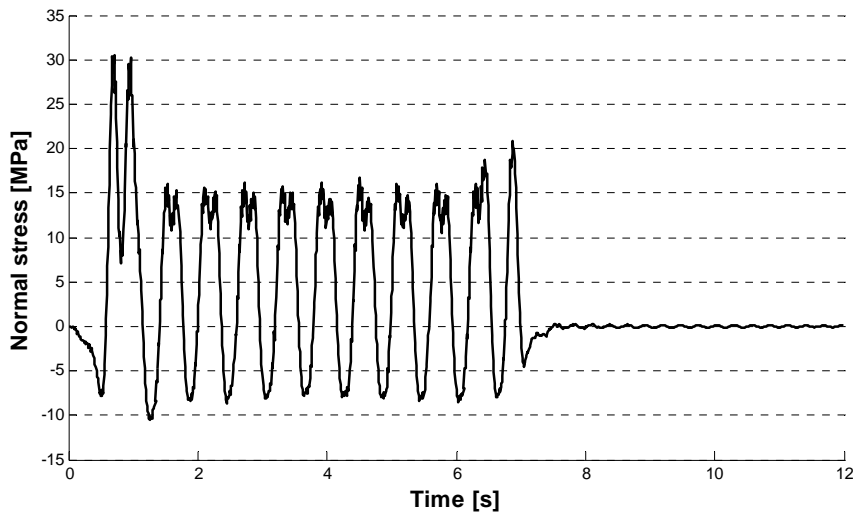


Figure A.4: Stress time history in a point of the floor beam.

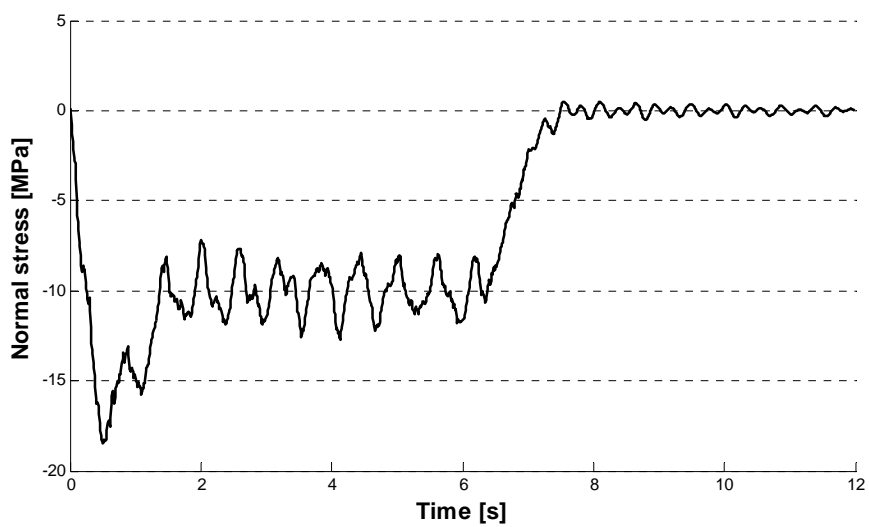
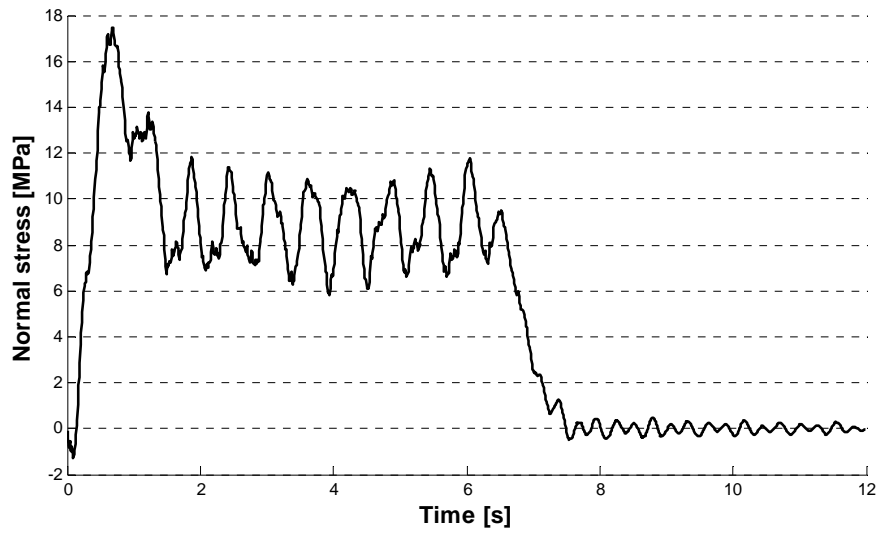
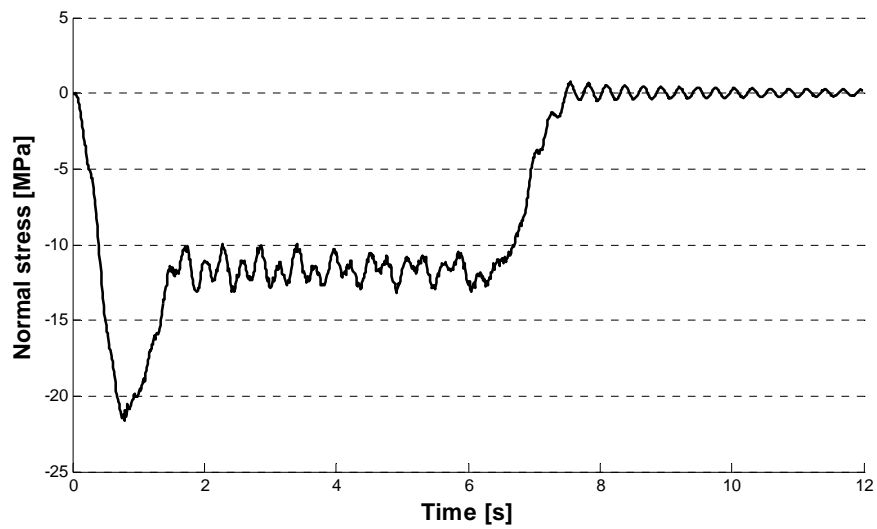


Figure A.5: Stress time history in a point of the first diagonal element.



**Figure A.6:** Stress time history in a point of the second diagonal element.



**Figure A.7:** Stress time history in a bracing system element.

*Train type "B"*

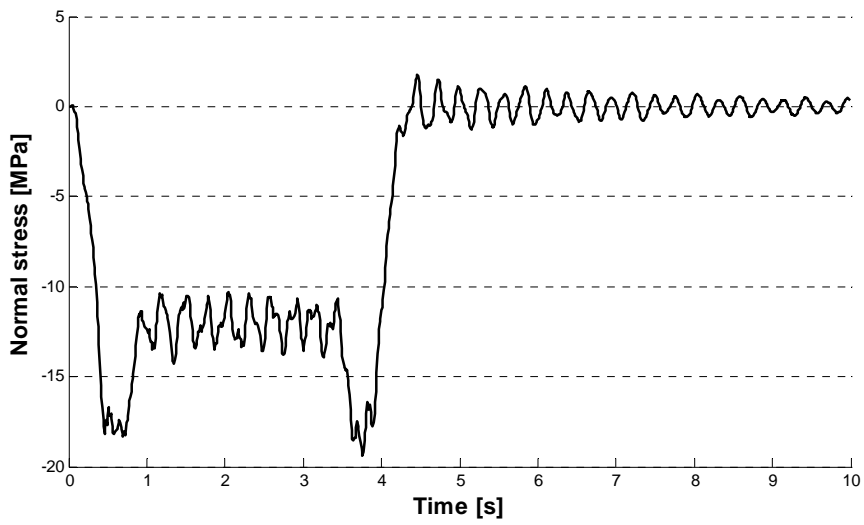


**Figure A.8:** Stress time history in a point of the mid span upper chord.

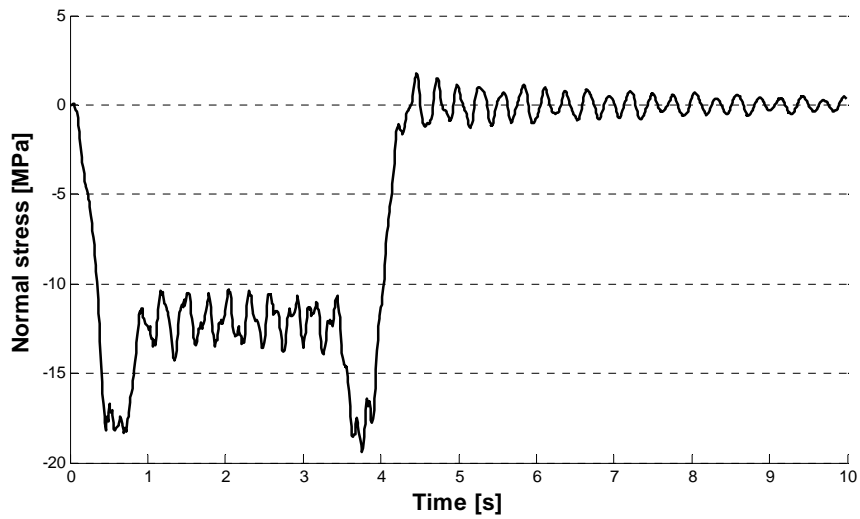


**Figure A.9:** Stress time history in a point of the mid span lower chord.

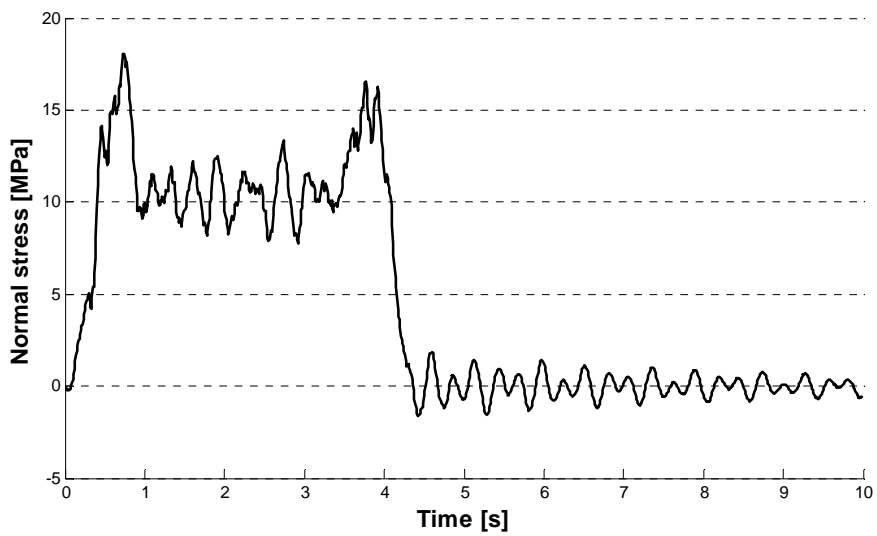


**Figure A.10:** Stress time history in a point of the stringer.

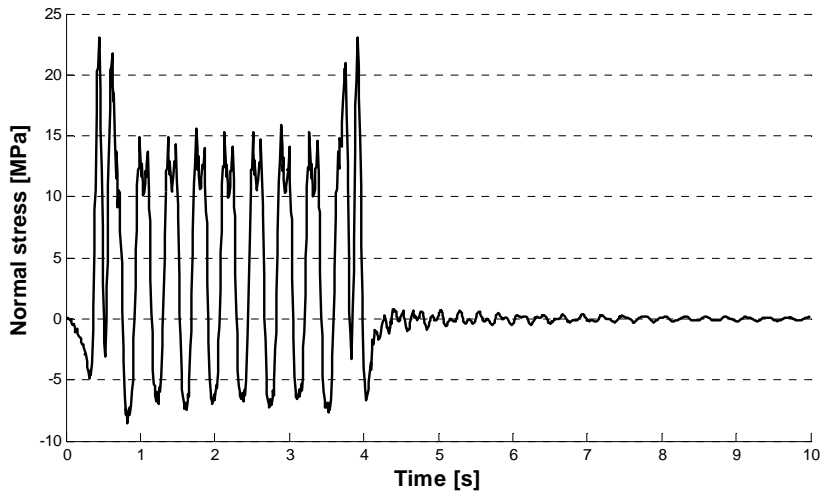


**Figure A.11:** Stress time history in a point of the floor beam.

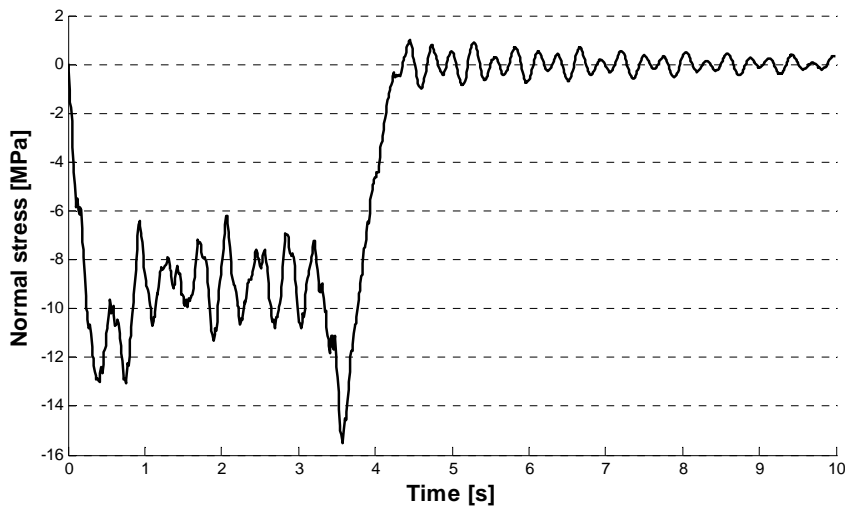


**Figure A.12:** Stress time history in a point of the first diagonal element.

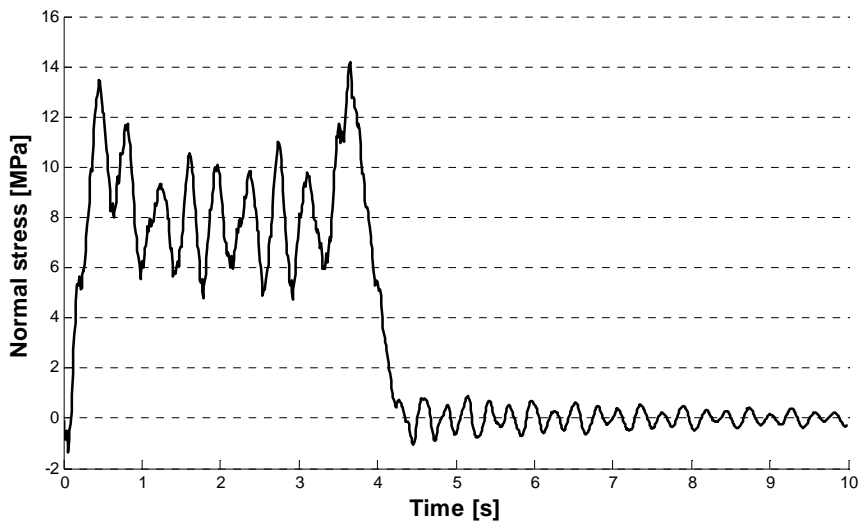


**Figure A.13:** Stress time history in a point of the second diagonal element.

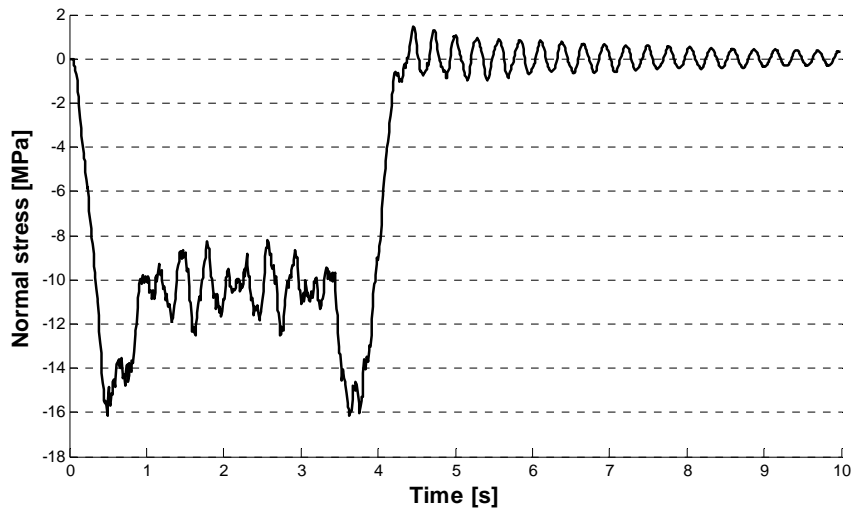


**Figure A.14:** Stress time history in a bracing system element.

*Train type "C"*

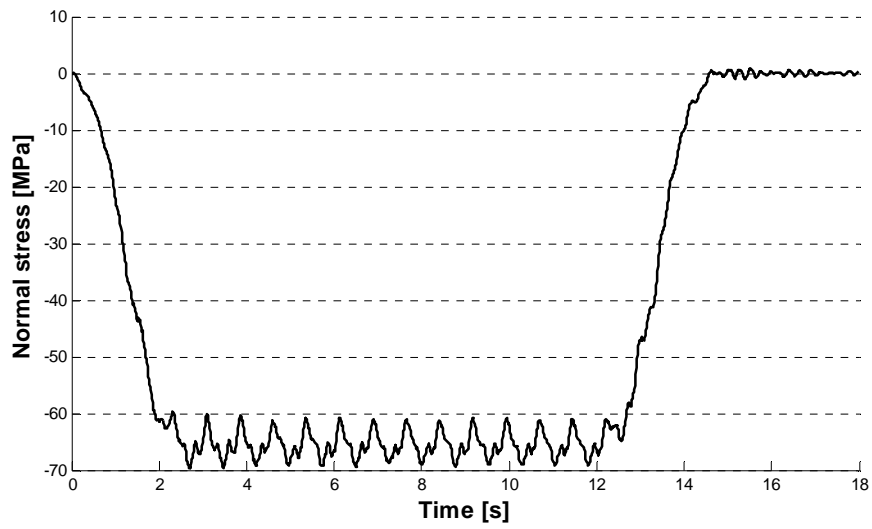


**Figure A.15:** Stress time history in a point of the mid span upper chord.

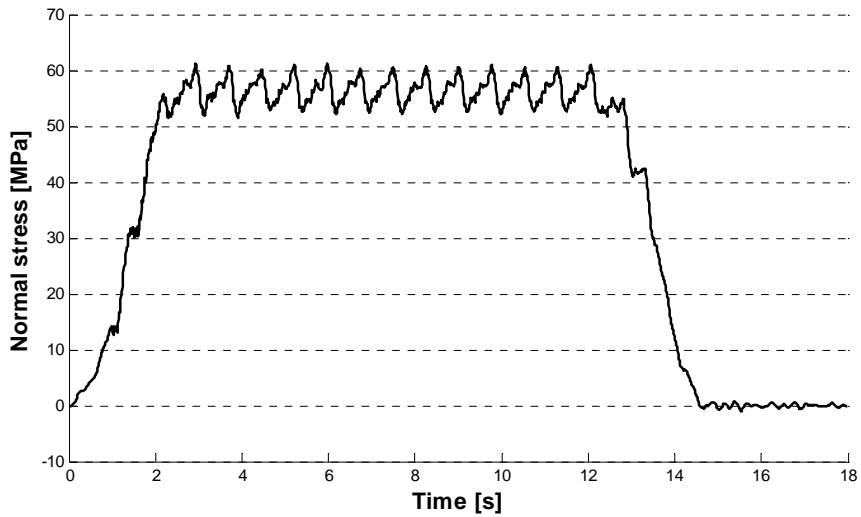


**Figure A.16:** Stress time history in a point of the mid span lower chord.

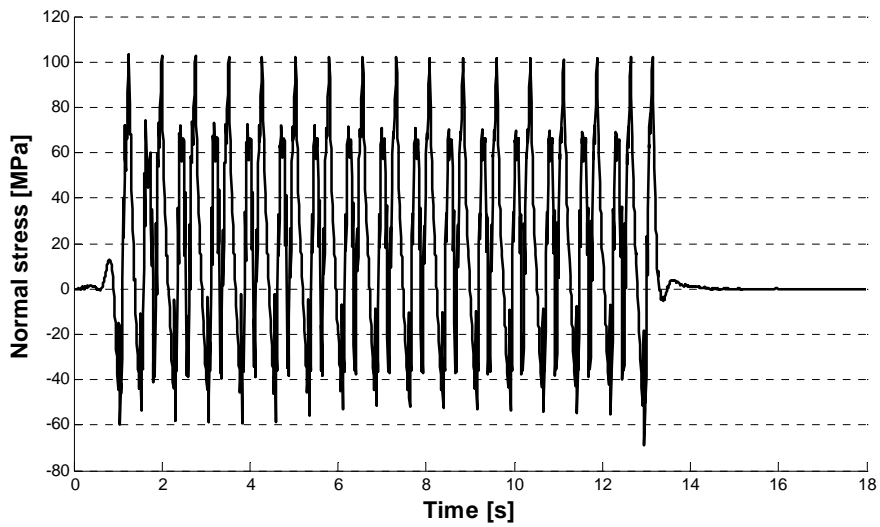


**Figure A.17:** Stress time history in a point of the stringer.

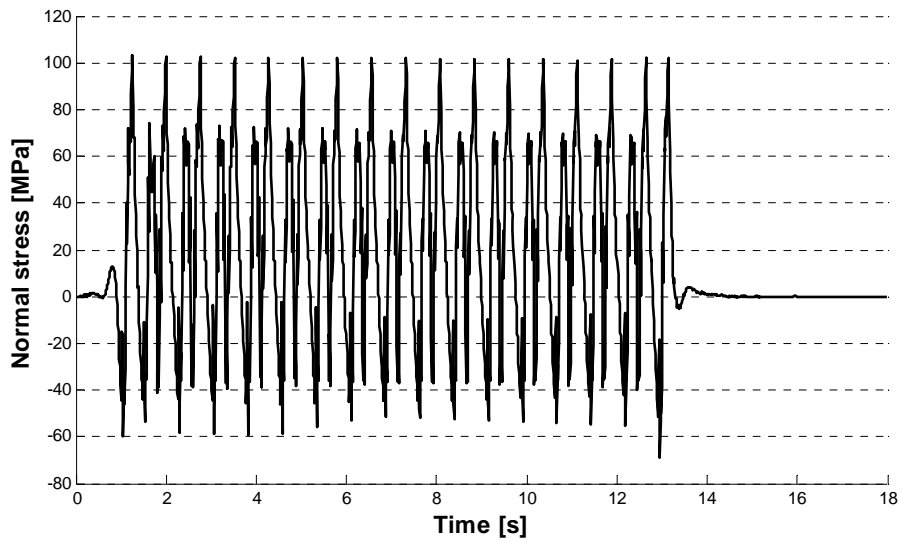


Figure A.18: Stress time history in a point of the floor beam.

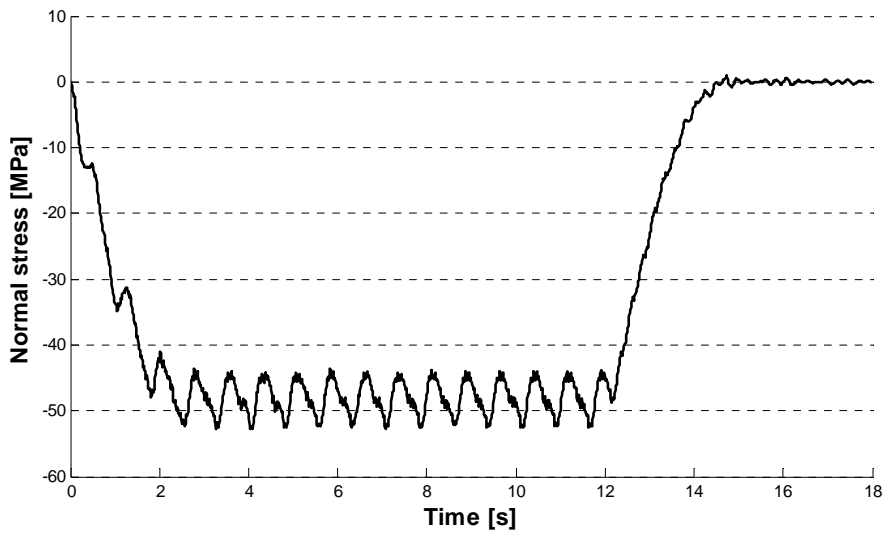


Figure A.19: Stress time history in a point of the first diagonal element.

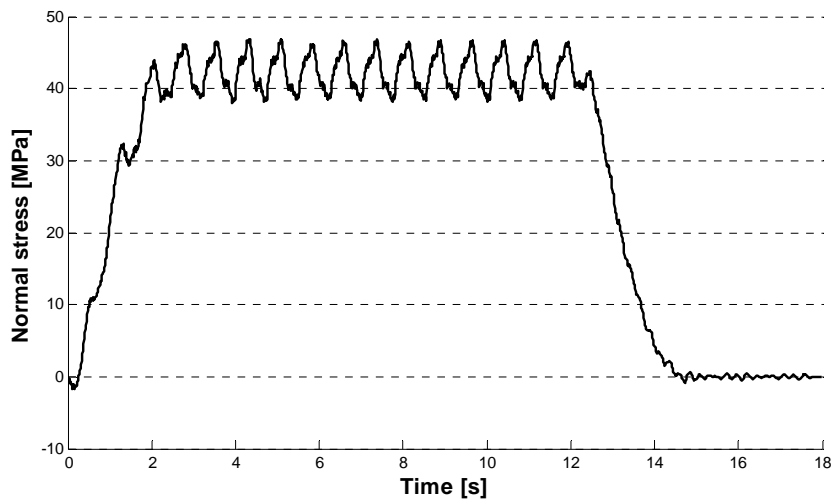


Figure A.20: Stress time history in a point of the second diagonal element.

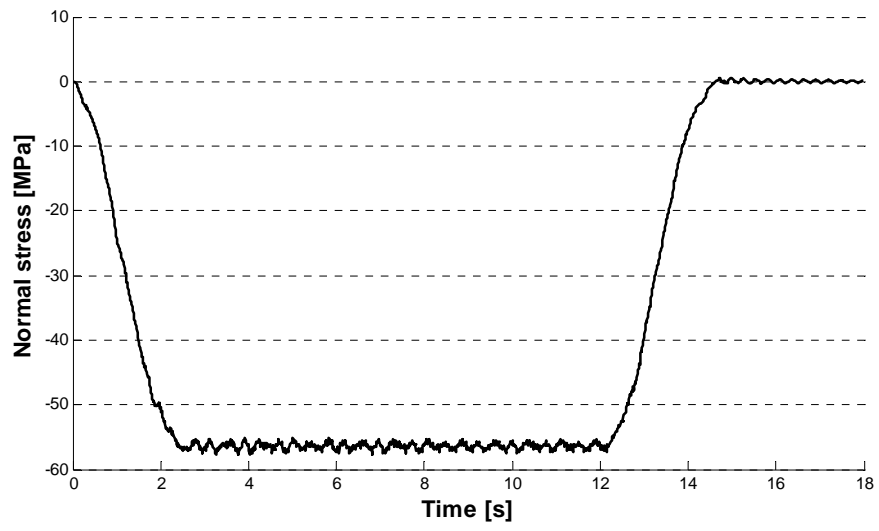


Figure A.21: Stress time history in a bracing system element.



# References

- [1] Eurocode 1: *Actions on structures – Part 2: Traffic loads on bridges*. European committee for standardization, BS EN 1991-2:2003.
- [2] K. Liu, G. De Roeck, G. Lombaert: *The effect of dynamic train-bridge interaction on the bridge response during a train passage*. Journal of Sound and Vibration 325, Elsevier, 2009.
- [3] K. Liu, E. Reynders, G. De Roeck, G. Lombaert: *Experimental and numerical analysis of a composite bridge for high-speed trains*. Journal of Sound and Vibration 320, Elsevier, 2008.
- [4] R. Freddi: *Verifica a fatica di un ponte ferroviario in acciaio*. Thesis in Civil Engineering, 2009/2010.
- [5] Eurocode 3: *Design of steel structures – Part 1.9: Fatigue*. European committee for standardization, prEN 1993-1-9:2003.
- [6] L. Georgiev: *Fatigue life analysis of an old riveted bridge based on S-N lines*. 7<sup>th</sup> International Conference on Bridges across the Danube 2010, Sofia, Bulgaria.
- [7] S. Timoshenko: *Vibration problems in engineering*. D. Van Nostran Company Inc., New York.
- [8] L. Fryba: *Dynamics of railway bridges*. Co-published with Thomas Telford Ltd, London, 1996.
- [9] Y. B. Yang, J. D. Yau, Y. S. Wu: *Vehicle-Bridge Interaction Dynamics – with applications to high-speed railways*. World Scientific Publishing Co. Pte. Ltd., 2004.
- [10] K. Liu, E. Reynders, G. De Roeck: *Experimental validation of the dynamic interaction analysis between high-speed trains and the Sesia viaduct*. Leuven University, Belgium.

- [11] A. Gonzalez: *Vehicle-Bridge Dynamic Interaction Using Finite Element Modelling*. University College Dublin, Ireland.
- [12] H. Xia, N. Zhang: *Dynamic analysis of railway bridge under high-speed trains*. Computer and Structures 83, Elsevier, 2005.
- [13] M. Savoia, L. Vincenzi: *Differential evolution algorithm for dynamic structural identification*. Journal of Earthquake Engineering, 12:800-821, 2008.
- [14] L. Vincenzi, M. Savoia: *Improving the speed performance of an evolutionary algorithm by second-order cost function approximation*. 2<sup>nd</sup> International Conference on Engineering Optimization, September 6-9, 2010, Lisbon, Portugal.
- [15] S. Rebecchi: *Identificazione dei parametri meccanici del ponte metallico ferroviario a Pontelagoscuro attraverso un algoritmo di ottimizzazione di tipo evolutivo*. Tesi di Laurea di Ingegneria Civile, Bologna, 2010.
- [16] A. Nieslony. *Determination of fragments of multiaxial service loading strongly influencing the fatigue of machine components*. Mechanical Systems and Signal Processing. 2009;23(8):2712–2721.
- [17] A. Khuri and J.A. Cornell: *Response Surfaces. Designs and Analyses*. Marcel Dekker Inc., New York, 1996.
- [18] R. Karoumi: *Response of a cable-stayed and suspension bridges to moving vehicles*. Ph.D. Thesis, 1998.